TAMPEREEN TEKNILLINEN YLIOPISTO
TAMPERE UNIVERSITY OF TECHNOLOGY

Hannu Teisala

Multifunctional Superhydrophobic Nanoparticle Coatings for Cellulose-based Substrates by Liquid Flame Spray

Julkaisu 1169 • Publication 1169

Tampere 2013

Tampereen teknillinen yliopisto. Julkaisu 1169
Tampere University of Technology. Publication 1169

Hannu Teisala

Multifunctional Superhydrophobic Nanoparticle Coatings for Cellulose-based Substrates by Liquid Flame Spray

Thesis for the degree of Doctor of Science in Technology to be presented with due permission for public examination and criticism in Konetalo Building, Auditorium K1702, at Tampere University of Technology, on the 1st of November 2013, at 12 noon.

Tampereen teknillinen yliopisto - Tampere University of Technology
Tampere 2013

ISBN 978-952-15-3172-9 (printed)
ISBN 978-952-15-3183-5 (PDF)
ISSN 1459-2045

Abstract

Wettability of a solid surface by a liquid plays an important role in several phenomena and applications, for example in adhesion, printing, and coating. Especially, wetting of rough surfaces has attracted a great scientific interest in recent decades. Superhydrophobic surfaces, which possess extraordinary water repellency properties due to their low surface energy chemistry and specific nano- and microscale roughness, are of particular interest due to the great variety of potential applications ranging from self-cleaning surfaces to microfluidic devices. Another driving force for the extensive scientific work on superhydrophobicity has been a desire for detailed understanding of wetting phenomena on different types of superhydrophobic surfaces, for example on natural superhydrophobic surfaces of lotus leaves where easy mobility of water droplets results in self-cleaning effect, rose petals where water droplets firmly adhere to the surface, and butterfly wings which possess directional water droplet adhesion.

This thesis work reviews recent aspects on different modes of superhydrophobicity and explores a variety of functional anti-wetting/wetting properties on both natural and artificial superhydrophobic surfaces. In addition, fabrication techniques, properties, and potential applications of superhydrophobic surfaces and coatings are examined with focus on cellulose-based substrate materials on which an extensive literature survey is executed. In recent years, a great number of different approaches ranging from simple one-step methods to sophisticated multi-step procedures to fabricate superhydrophobic coatings on cellulose-based substrate materials such as cotton or paper have been reported. Potential applications for the cellulose-based superhydrophobic materials vary from water- and stain-repellent, self-cleaning and breathable clothing to cheap and disposable lab-on-a-chip devices.

The experimental section of this work focuses on fabrication of functional superhydrophobic and superhydrophilic nanoparticle coatings on cellulose-based substrate materials by liquid flame spray (LFS) and examination of the coating properties. LFS proved itself straightforward and versatile one-step method to fabricate broad range of functional nanoparticle coatings on various substrate materials in an atmospheric roll-to-roll process. It has established itself among the most potential candidates for large-scale production of superhydrophobic coatings on affordable cellulose-based substrates.

Preface

This thesis work was carried out at Tampere University of Technology, Paper Converting and Packaging Technology during 2009–2013. The Finnish Funding Agency for Technology and Innovation, Tekes, is gratefully acknowledged for the financial support of the work. The experimental work for the thesis was performed in two Tekes-funded projects, “Nanorata” and “Nanorata 2”. The International Doctoral Programme in Pulp and Paper Science and Technology, PaPSaT, and Suomen Pakkausyhdistys are acknowledged for their financial support. Beneq Oy, Stora Enso Oyj, UPM Kymmene Oyj, and Kemira Oyj are acknowledged for their supportive role in the work.

I am very grateful to my supervisor Professor Jurkka Kuusipalo for offering me a possibility to work in the field I really enjoy. I also want to thank him for the relaxed atmosphere and the freedom to work on the topics I found the most interesting. It has been vital for my personal motivation and ability to carry out the work. I am also very grateful to Dr. Mikko Tuominen for his help and support during the whole work. His personal guidance and motivating attitude has been crucial, especially in the beginning of the work, and has influenced me a lot. I also want to thank the pre-examiners of the work, Professor Olli Ikkala and Professor Lars Wågberg, for their contributions and valuable comments. In addition, I want to thank the opponents, Professor Hans-Jürgen Butt and Professor Robin Ras.

I also want to thank all my co-authors. It has been good to work with you. Especially, I want to thank the Aerosol Physics people, Professor Jyrki M. Mäkelä, Dr. Mikko Aromaa, and M.Sc. Janne Haapanen, for our close and fruitful cooperation. Your contribution to this work has been significant. I also wish to express my gratitude to Dr. Mari Honkanen for her contributions. In addition, I want to thank all the people working at the Paper Converting and Packaging Technology for the company and help in any matter. Especially, I want to thank Mr. Alvi Sivula for kindly building up the equipment for the trials and for fixing everything from my bicycle to the experimental equipment I have needed.

Finally, I want to thank my parents, siblings, friends, and family for being there and supporting me. Thanks for mom and dad for the love, support, and guidance you have always given to me. Jussi, Antti, and Tiina, it has been good to grow up with you. Nothing has changed, you are very important to me, and it is always a pleasure to spend time with you. Thanks for all my friends. Our common passion for cross-country skiing and other activities with you give so much energy and good mood. Especially, Aki and Niina, I and Sini are lucky to have you. We are like a family with you and your lovely children. For you Sini, my wife, I want to say that I feel privileged to live my life with you and with our two lovely sons. You have given me more than I could ever imagine.

Tampere, October 2013

Hannu Teisala

Table of contents

List of original publications

[P1] Teisala, H.; Tuominen, M.; Aromaa, M.; Mäkelä, J. M.; Stepien, M.; Saarinen, J. J.; Toivakka, M.; Kuusipalo, J. Development of superhydrophobic coating on paperboard surface using the Liquid Flame Spray. *Surf. Coat. Technol.* **2010**, 205, 436–445, DOI: 10.1016/j.surfcoat.2010.07.003

[P2] Teisala, H.; Tuominen, M.; Aromaa, M.; Stepien, M.; Mäkelä, J. M.; Saarinen, J. J.; Toivakka, M.; Kuusipalo, J. Nanoparticle Deposition on Packaging Materials by Liquid Flame Spray – Generation of Superhydrophilic and Superhydrophobic Coatings. In: Gutowski, W. and Dodiuk, H. (eds.) *Recent Advances in Adhesion Science and Technology in Honor of Dr. Kash Mittal*, Taylor & Francis, In press.

[P3] Teisala, H.; Tuominen, M.; Aromaa, M.; Stepien, M.; Mäkelä, J. M.; Saarinen, J. J.; Toivakka, M.; Kuusipalo, J. Nanostructures Increase Water Droplet Adhesion on Hierarchically Rough Superhydrophobic Surfaces. *Langmuir* **2012**, 28, 3138–3145, DOI: dx.doi.org/10.1021/la203155d

[P4] Teisala, H.; Tuominen, M.; Aromaa, M.; Stepien, M.; Mäkelä, J. M.; Saarinen, J. J.; Toivakka, M.; Kuusipalo, J. High- and low-adhesive superhydrophobicity on the liquid flame spray-coated board and paper: structural effects on surface wetting and transition between the low- and high-adhesive states. *Colloid Polym. Sci.* **2013**, 291, 447–455, DOI: 10.1007/s00396-012-2833-5

[P5] Teisala, H.; Tuominen, M.; Stepien, M.; Haapanen, J.; Mäkelä, J. M.; Saarinen, J. J.; Toivakka, M.; Kuusipalo, J. Wettability conversion on the liquid flame spray generated superhydrophobic TiO_2 nanoparticle coating on paper and board by photocatalytic decomposition of spontaneously accumulated carbonaceous overlayer. *Cellulose* **2013**, 20, 391–408, DOI: 10.1007/s10570-012-9825-y

Author's contribution to original publications

[P1] The author prepared the samples and planned the experiments together with the co-authors. All the experiments were carried out by the author, excluding the high-speed video imaging, microscopy, and XPS experiments. The author wrote the manuscript as a corresponding author.

[P2] The author prepared the samples and planned the experiments together with the co-authors. All the contact angle experiments were carried out by the author. The author wrote the manuscript as a corresponding author.

[P3] The original idea of the article was the work of the author. The author prepared the samples and planned the article together with the co-authors. All the experiments, excluding the SEM imaging, were carried out by the author. The author wrote the manuscript as a corresponding author.

[P4] The original idea and planning of the article were the work of the author. The author prepared the samples together with the co-authors. All the experiments were carried out by the author. The author wrote the manuscript as a corresponding author.

[P5] The author prepared the samples and planned the experiments together with the co-authors. All the experiments, excluding the SEM, XPS, and roughness measurements, were carried out by the author. The author wrote the manuscript as a corresponding author.

Related publications

[R1] Teisala, H.; Tuominen, M.; Kuusipalo, J. Adhesion mechanism of water droplets on hierarchically rough superhydrophobic rose petal surface. *J. Nanomater.* **2011**, DOI: 10.1155/2011/818707

[R2] Stepien, M.; Saarinen, J. J.; Teisala, H.; Tuominen, M.; Aromaa, M.; Kuusipalo, J.; Mäkelä, J. M.; Toivakka, M. Adjustable wettability of paperboard by liquid flame spray nanoparticle deposition. *Appl. Surf. Sci.* **2011**, 257, 1911–1917.

[R3] Mäkelä, J. M.; Aromaa, M.; Teisala, H.; Tuominen, M.; Stepien, M.; Saarinen, J. J.; Toivakka, M.; Kuusipalo, J. Nanoparticle deposition from liquid flame spray onto moving roll-to-roll paperboard material. *Aerosol Sci. Technol.* **2011**, 45, 827–837.

[R4] Stepien, M.; Saarinen, J. J.; Teisala, H.; Tuominen, M.; Aromaa, M.; Kuusipalo, J.; Mäkelä, J. M.; Toivakka, M. Surface chemical characterization of nanoparticle coated paperboard. *Appl. Surf. Sci.* **2012**, 258, 3119–3125.

[R5] Aromaa, M.; Arffman, A.; Suhonen, H.; Haapanen, J.; Keskinen, J.; Honkanen, M.; Nikkanen, J.-P.; Levänen, E.; Messing, M. E.; Deppert, K.; Teisala, H.; Tuominen, M.; Kuusipalo, J.; Stepien, M.; Saarinen, J. J.; Toivakka, M.; Mäkelä, J. M. Atmospheric synthesis of superhydrophobic TiO_2 nanoparticle deposits in a single step using liquid flame spray. *J. Aerosol Sci.* **2012**, 52, 57–68.

[R6] Stepien, M.; Saarinen, J. J.; Teisala, H.; Tuominen, M.; Aromaa, M.; Kuusipalo, J.; Mäkelä, J. M.; Toivakka, M. Surface chemical analysis of photocatalytic wettability conversion of TiO_2 nanoparticle coating. *Surf. Coat. Technol.* **2012**, DOI: 10.1016/j.surfcoat.2012.08.008

[R7] Tuominen, M.; Teisala, H.; Aromaa, M.; Stepien, M.; Mäkelä, J. M.; Saarinen, J. J.; Toivakka, M.; Kuusipalo, J. Superhydrophilic Surface for Paper and Board. *J. Adhes. Sci. Technol.* **2012**, DOI: 10.1080/01694243.2012.697744

Abbreviations and symbols

AKD	alkyl ketene dimer
ALD	atomic layer deposition
ATRP	atom transfer radical polymerization
CA	contact angle
$CaCl_2$	calcium chloride
CAH	contact angle hysteresis
CeO_2	cerium dioxide
CNT	carbon nanotube
CO_2	carbon dioxide
CVD	chemical vapor deposition
DFTMS	dodecafluoroheptyl-propyl-trimethoxylsilane
DTMS	n-dodecyltrimethoxysilane
ECA	ethyl-2-cyanoacrylate
Fe_3O_4	iron oxide
FEG-SEM	field emission gun scanning electron microscope
FOTS	(tridecafluoro-1,1,2,2-tetrahydrooctyl)trichlorosilane
GMA	glycidyl methacrylate
GPTMS	3-glycidoxypropyltrimethoxysilane
H_2SO_4	sulfuric acid
HDTMS	hexadecyltrimethoxysilane
HMDSO	hexamethyldisiloxane
IR	infrared
LbL	layer by layer
LDPE	low-density polyethylene
LFS	liquid flame spray
LOC	lab-on-a-chip
MPS	3-(trimethoxysilyl) propyl methacrylate
MTCS	methyltrichlorosilane
NaOH	sodium hydroxide
ODP	octadodecylphosphonic acid
OH	hydroxyl
OTS	octadecyltrichlorosilane
PANI	polyaniline
PCC	precipitated calcium carbonate
PCPT	Paper Converting and Packaging Technology
PDDA	poly(diallyldimethylammonium chloride)
PDMS	polydimethylsiloxane
PDVB	polydivinylbenzene
PECVD	plasma-enhanced chemical vapor deposition
PET	poly(ethylene terephthalate)
PFE	pentafluoroethane
PMS	potassium methyl siliconate

POTS	perfluorooctyltriethoxysilane
PP	polypropylene
PS	polystyrene
PTFE	poly(tetrafluoroethylene)
PVA	poly(vinyl alcohol)
RESS	rapid expansion of supercritical solution
RH	relative humidity
SA	sliding angle
SEM	scanning electron microscope
SiO_2	silicon dioxide
SLIPS	slippery liquid-infused porous surfaces
SS	sodium silicate
TCMS	trichloromethylsilane
TEM	transmission electron microscopy
TEOS	tetraethyl orthosilicate
TiO_2	titanium dioxide
TTIP	titanium tetraisopropoxide
TUT	Tampere University of Technology
UV	ultraviolet
XPS	X-ray photoelectron spectroscopy
ZnO	zinc oxide
ZrO_2	zirconium dioxide
f	fraction of the projected area of the surface that is wetted by the liquid
r	actual area divided by the projected area of the surface
r_f	actual wetted area divided by the projected wetted area of the surface
γ_{LV}	interfacial tension between liquid and vapor
γ_{SL}	interfacial tension between solid and liquid
γ_{SV}	interfacial tension between solid and vapor
θ_{CB}	Cassie–Baxter's contact angle
θ_W	Wenzel's contact angle
θ_Y	Young's contact angle

1. Literature review

1.1. Introduction

Various techniques based on plasma deposition [1], chemical vapor deposition (CVD) [2], atomic layer deposition (ALD) [3], nanoparticle deposition [4], and sol–gels [5, 6] among others, have been introduced to create nanoscale coatings that can improve material properties and bring functionality for the surfaces. One of the important material properties is wettability of a solid surface by a liquid. Surface wetting is a relevant characteristic for various materials, including cellulose-based materials such as paper and cotton fabrics, as it plays an important role in the field of printing, coating, and adhesion among others. In addition to creation of a new coating layer onto a material surface, wettability and other properties of the material can be affected by activation methods such as flame, corona, and plasma treatments. However, the effect of activation methods on surface wetting is typically not a permanent characteristic [7][R7].

In addition to the many industrial applications, wetting of solid surfaces is closely related to our daily life. For example, detergents are needed to lower the surface tension of water and thus to enable its penetration below the dirt, or rain droplets on a window may hinder the view. Surface wetting also plays an important role in the function of waterproof breathable clothing, or in the phenomena such as fogging and icing of windows, windscreens, eyeglasses, and metal surfaces among others. Evidently, the ability to control wettability of solid surfaces is of high interest.

Smooth surfaces
Chemistry of a solid surface determines whether the surface has a tendency to repel or get wetted by a liquid. Wetting of ideal, chemically homogeneous and smooth, surface can be evaluated by the Young equation [8]:

$$\cos\theta_Y = \frac{\gamma_{SV} - \gamma_{SL}}{\gamma_{LV}} \qquad (1)$$

where θ_Y is the contact angle (CA) of the liquid on the solid surface, and γ_{SV}, γ_{SL}, and γ_{LV} are the interfacial tensions between the solid and vapor, solid and liquid, and liquid and vapor, respectively (Figure 1).

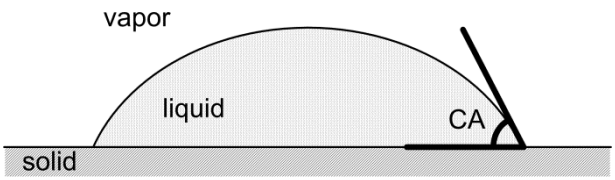

Figure 1. Determination of CA on solid surface.

In the case that water droplet CA on a surface is < 90º, *i.e.*, water has a tendency to spread over the surface, the surface is termed hydrophilic. In contrast, if water CA is > 90º, and the surface thus repels spreading of water, the surface is termed hydrophobic.

Rough surfaces

Real surfaces are rarely completely smooth. Even though a surface may appear macroscopically smooth, there typically exists micro-, nano-, and molecular scale roughness. Wetting of rough surfaces has attracted appreciable attention ever since Wenzel [9] and Cassie and Baxter [10] introduced their wetting theories for rough surfaces. Wenzel and Cassie and Baxter describe two opposite wetting states (Figure 2), *i.e.*, the state where the surface is completely wetted by a liquid (Wenzel state) and the state where air gets entrapped in the roughness of the substrate and only top areas of the surface are wetted (Cassie state). Wenzel and Cassie–Baxter wetting theories are still very useful in modeling and perceiving wetting phenomena on rough surfaces. The Wenzel equation describes complete wetting state on a rough surface and is written as:

$$\cos\theta_W = r\cos\theta_Y \qquad (2)$$

where θ_W is the Wenzel's CA on the rough surface, r is the actual area divided by the projected area of the surface, and θ_Y is the Young's CA on the smooth surface of the same material. Partial wetting of a rough surface can be evaluated by the Cassie–Baxter equation:

$$\cos\theta_{CB} = r_f f\cos\theta_Y + f - 1 \qquad (3)$$

where θ_{CB} is the Cassie–Baxter CA on the rough surface, r_f is the actual wetted area divided by the projected wetted area of the surface, and f is the fraction of the projected area of the surface that is wetted by the liquid.

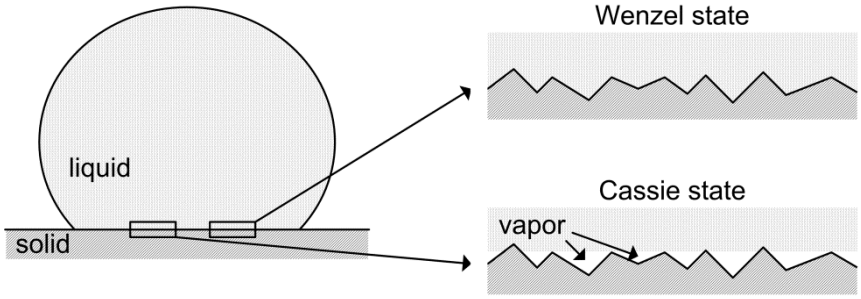

Figure 2. Illustration of the Wenzel and Cassie wetting states on rough surface.

Roughness of a solid surface can enhance the surface wettability or repellency against liquid, depending on the chemical composition of the surface and the properties of the liquid. The effect of roughness on wetting of a solid surface is well illustrated by the Kao experiment [11, 12]. Onda *et al.* [11] from the Kao Corporation executed CA measurements on rough and smooth surfaces of the same material using liquids that vary in surface tension: from the curvature of the graph shown in Figure 3 it is easy to see that roughness of the solid has a drastic effect on wetting both in wettable ($\cos\theta > 0$) and repellent ($\cos\theta < 0$) domains.

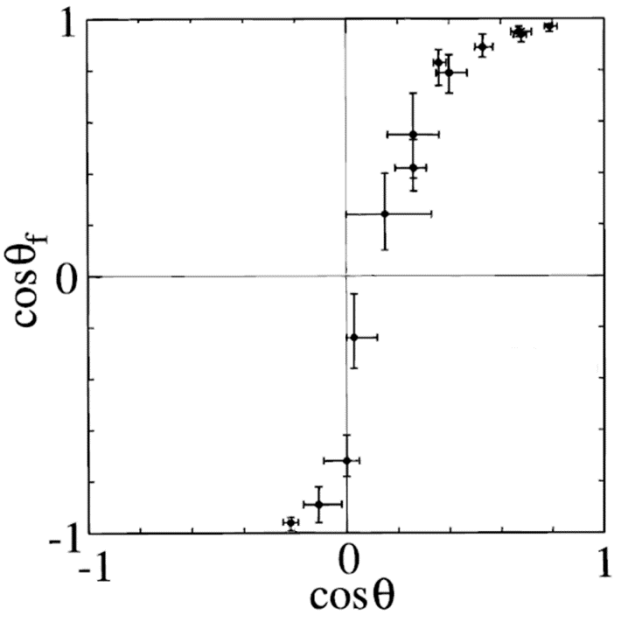

Figure 3. CA on rough surface (θ_f) as a function of CA on smooth surface (θ) of the same material. Cosine θ_f and cosine $\theta > 0$ correspond to wettable domains (CA < 90º), while cosine θ_f and cosine $\theta < 0$ correspond to repellent domains (CA > 90º) [11].

In the case that water CA on a hydrophilic surface is < 10º, and thus water spreads almost perfectly over the solid, the surface is often termed superhydrophilic. In the opposite situation, if water CA on a hydrophobic surface is > 150º, and the droplet thus takes a spherical shape on the solid, the surface is often termed superhydrophobic. This work focuses on superhydrophobic surfaces. Other terminology that is used to describe superhydrophobicity include absolutely hydrophobic, ultrahydrophobic, and highly hydrophobic [13, 14].

1.2. Superhydrophobic surfaces

1.2.1. Wetting of superhydrophobic surfaces

Water CA on smooth solids cannot exceed approximately 120°, which is thus the limit for chemical hydrophobicity. Therefore, superhydrophobic solids always possess appropriate surface roughness at micrometer scale and below to obtain CAs greater than 150º. Superhydrophobic surfaces have attracted considerable scientific interest in the past decade, which becomes evident in the huge number of research papers published on superhydrophobicity [13, 15-17]. The phenomenon of superhydrophobicity and related wetting mechanisms are attractive scientifically, but also from the industrial point of view, because extreme water repellency is desired in several applications. In addition to practical experiments on superhydrophobic surfaces, which is the focus of this work, lot of theoretical study have been executed on superhydrophobicity, *e.g.* related to the transitions between the Cassie and Wenzel wetting states [18-24].

Characterization of superhydrophobic surfaces

Although superhydrophobic surfaces have in common the high static and high advancing water CA, the receding CA and droplet adhesion can vary a lot depending on the chemical and physical nature of the surface. Therefore, in addition to the static CA, contact angle hysteresis (CAH) and sliding angle (SA) are commonly used to characterize anti-wetting properties of superhydrophobic surfaces. CAH is determined as the difference between advancing and receding contact angles of a droplet, whereas SA is the tilt angle of the substrate at which the droplet starts to slide or roll off the surface. Low CAH and SA on a superhydrophobic surface indicate that water does not penetrate into the surface roughness at large extent, but water droplets sit on the asperities of the surface with small liquid–solid contact area and low adhesion, *i.e.*, the droplets reside in the Cassie state. In contrast, large CAH and SA indicate that water has, at least partially, penetrated into the roughness of the surface, and thus the droplet resides in the Wenzel state. In such case, droplet can adhere tightly to the surface due to the large liquid–solid contact area, where the electrostatic forces such as van der Waals interactions govern the high droplet adhesion.

Measuring of CAH, however, can be challenging. This was recently pointed out by Korhonen *et al.* [25], who demonstrated that reliable determination of the receding CA may require surprisingly large initial droplet volume. At the moment, there are not any generally accepted procedures to execute the CAH or SA measurements, but the used methods and droplet volumes *etc*. vary a lot. Therefore, it is important to bear in mind that direct comparison between different studies and surfaces is not valid if the experimental procedures vary from one to the other, because the experimental differences between the studies can result in great differences in the observed CAH and SA results.

Many scientists have proposed that in addition to the static CA greater than 150°, another criterion for superhydrophobicity should be low CAH or low SA. On the other hand, it is commonly accepted that superhydrophobic surfaces can create high adhesion to water droplets. In such cases, the words “sticky” [13, 14, 26] or “high-adhesion” [27, 28] are typically used to describe the high-adhesive nature of the superhydrophobic surfaces. To clarify the used terminology in the field, Marmur *et al.* [29] proposed a 3-layer methodology to be used with hydrophobic surfaces, according which superhydrophobic solid surfaces, which do not have a very low CAH, should be termed as parahydrophobic surfaces. In this work, the static CA greater than 150° is considered as a sole criterion for superhydrophobicity, and CAH and SA values are reported to emphasize differences in the anti-wetting properties between the surfaces.

Functional wettability and modes of wetting

Throughout history, humans have learned from nature. There are several natural examples of different types of superhydrophobic surfaces on plants, insects, and animals [30-35]. Self-cleaning of lotus leaves (Figure 4a) [33, 36], high water adhesion on rose petals (Figure 4b) [28][R1], and the ability of water striders to walk on water [37] are just few examples of functional superhydrophobicity that can be found from nature.

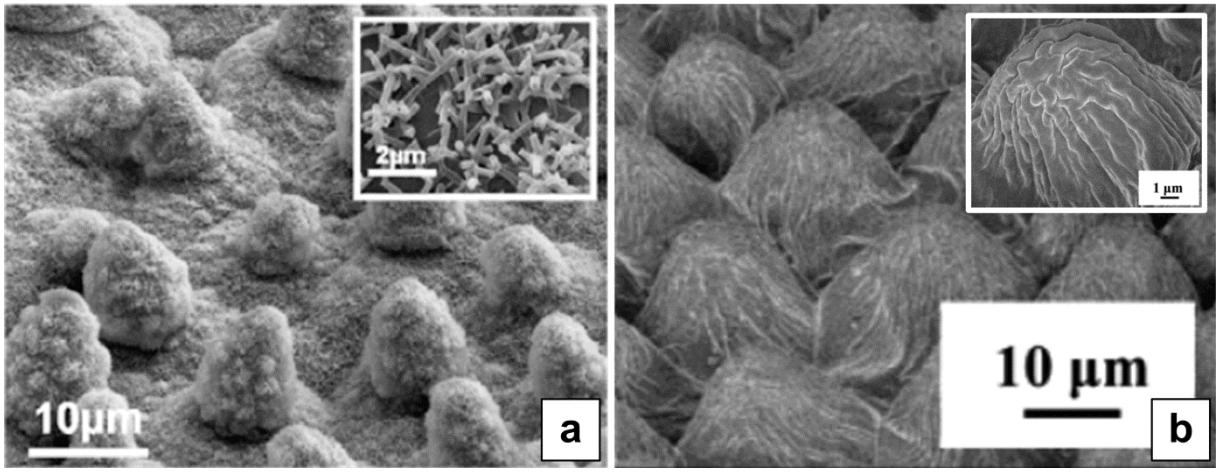

Figure 4. Scanning electron microscope (SEM) images of hierarchically structured functional superhydrophobic surfaces of (a) lotus leaf [33] and (b) rose petal [28]. Insets show the wax tubules and cuticular folding on the epidermal cells of the lotus and rose surfaces, respectively.

The most famous example of superhydrophobic surface is the lotus leaf (*Nelumbo nucifera*). The dual-scale roughness of the waxy surface of lotus leaf (Figure 4a) is the basis for its superhydrophobic character with an extremely low water adhesion. Water CAs greater than 160º and CAH and SA less than 5º have been reported on lotus surface [30, 33, 36]. That is, water droplets reside in the Cassie state on the lotus surface, and the easy mobility of the droplets is because of the small contact area between the droplets and solid surface. Rolling droplets, for example rain water, can easily collect contaminating particles from the plant leaf keeping the surface clean. The self-cleaning effect, also referred to as the lotus-effect, has been demonstrated on various superhydrophobic plant leaves by Barthlott and Neinhuis [36, 38], who firstly reported on the self-cleaning effect of lotus leaves as well.

Another type of superhydrophobicity takes place on petals of many roses (Figure 4b). The superhydrophobic rose petals can create high adhesion to water droplets. The high-adhesive superhydrophobicity on red rose petal (*rosea Rehd*) was firstly characterized by Feng *et al.* [28], who reported that water droplets as large as 10 μl were able to remain on the petal surface when tilted upside down. They suggested that the high adhesive force on the petal surface was due to a sort of combined wetting state between the Cassie and Wenzel states, where water was able to fill the large micrometer scale cavities on the rough surface, while the smaller cavities could entrap air and remain in the Cassie state (Cassie impregnating wetting state, Figure 5). Direct experimental observation in a later study [R1] revealed that the micrometer scale cavities on rose petal surface entrapped large amount of air, and thus the high adhesion of water was caused by the round and grooved fine structure on top of the micrometer scale epidermal cells (Figure 6). The grooved fine structure on the superhydrophobic rose petal surface, completely different from the tubular fine structure on lotus surface, can provide sufficiently large liquid–solid contact area for the high water droplet adhesion.

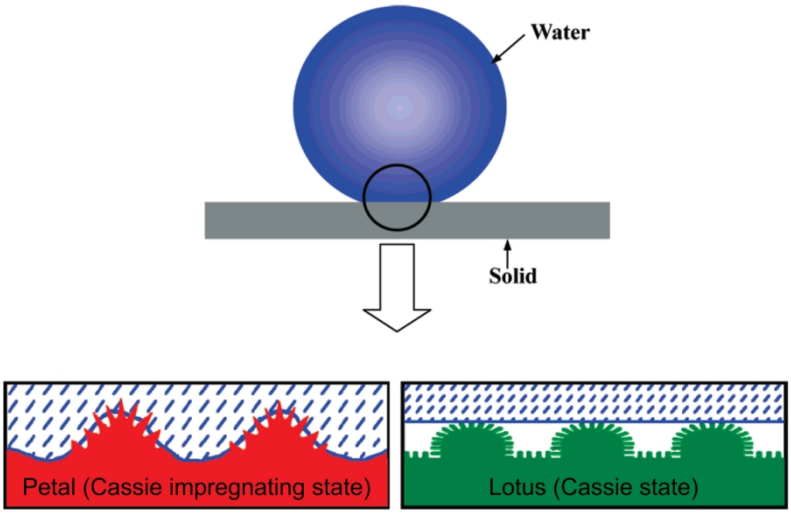

Figure 5. Schematic drawing of wetting states on rose petal and lotus surfaces by Feng *et al.* [28].

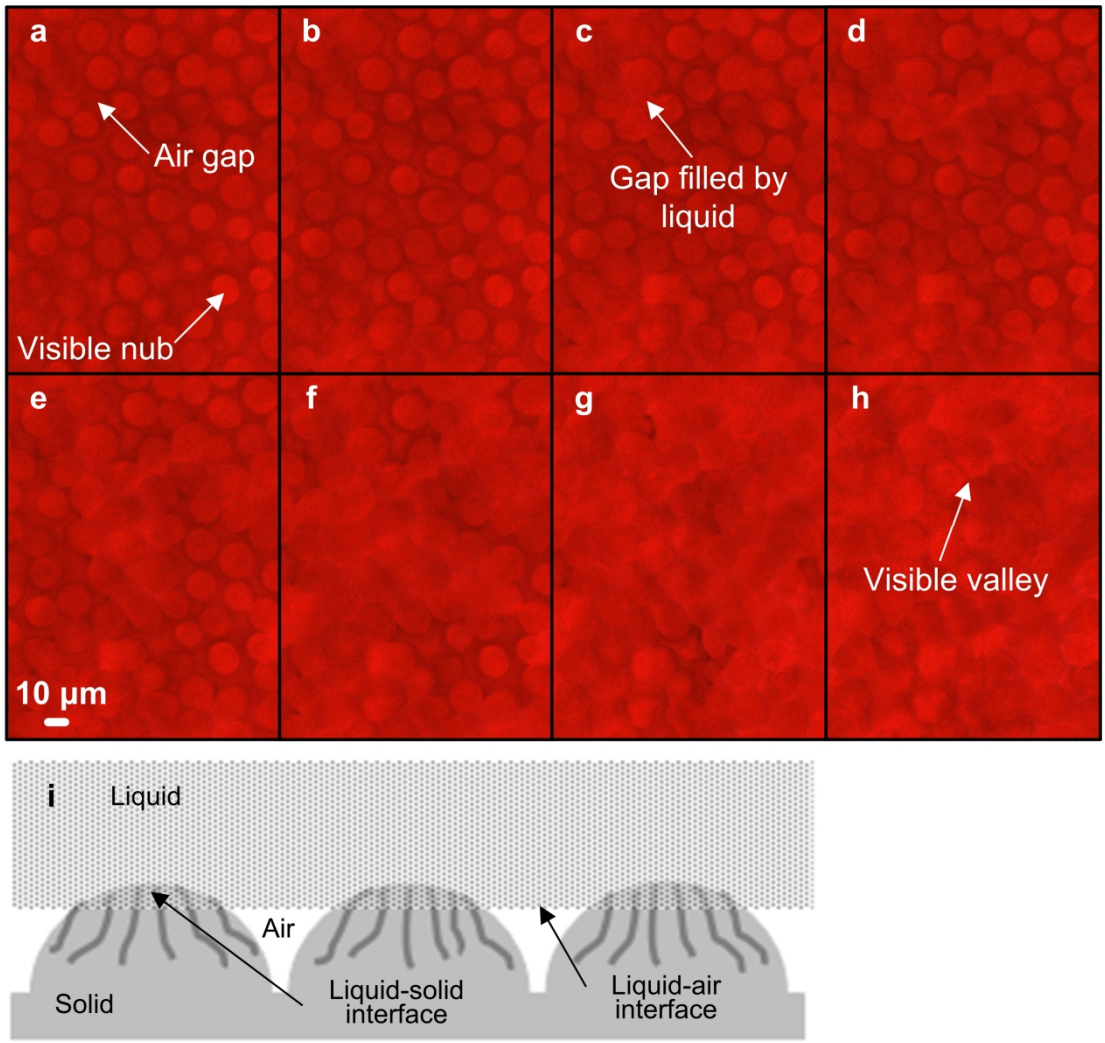

Figure 6. Wetting of high-adhesive superhydrophobic rose petal surface. Optical microscope images (top view) reveal that (a) air pockets remain on the surface between the epidermal cells under the film of pure water, and (b–h) the air pockets disappear one after the other when the

surface tension of liquid is decreased by adding ethanol in the film of water. (i) A schematic drawing of the petal wetting by water [R1].

In addition to the functional wetting of lotus leaf and rose petal, there are several other interesting examples of both natural and artificial superhydrophobicity. To name a few, Jin *et al.* [27] prepared high-adhesive superhydrophobic aligned polystyrene (PS) nanotube films (CA = 162º) inspired by the feet of gecko. The dense array of nanotubes (about 6.76 x 10^6 nanotubes mm^{-2}) resulted in a high van der Waals' force and strong adhesion of water on the surface (Figure 7a). Feng *et al.* [30] reported anisotropic dewetting on a rice leaf (*Oryza sativa*, Figure 7b), where SAs of 3–5º and 9–15º were measured in the parallel and perpendicular directions of the leaf, respectively. In addition, they fabricated biomimicked aligned carbon nanotube (CNT) film inspired by the anisotropic rice leaf (Figure 7c). Zheng *et al.* [32] characterized hierarchical structure and directional water adhesion on a butterfly wing (*Morpho aega*, Figure 7d). Water droplets were not able to roll towards the body of the insect, but in the opposite direction, away from the body, the SA was only 9º. Gao and Jiang [37] studied legs of water strider (*Gerris remigis*, Figure 7e). The non-wetting legs of the insect enable its floating and easy moving on water. The maximal supporting force of a single leg of water strider is about 15 times the total body weight of the insect. Watson *et al.* [34] demonstrated the anti-wetting mechanism on a hierarchically structured wing of a termite (*Nasutiterems walkeri*, Figure 7f). Microscale droplets are able to deposit on the superhydrophobic wing surface, while the water-repellent hairs on the wing can carry larger droplets or bulk water above the wing surface. The microdroplets can be absorbed by the above larger droplets, which are then removed from the wing surface *via* the hair arrays.

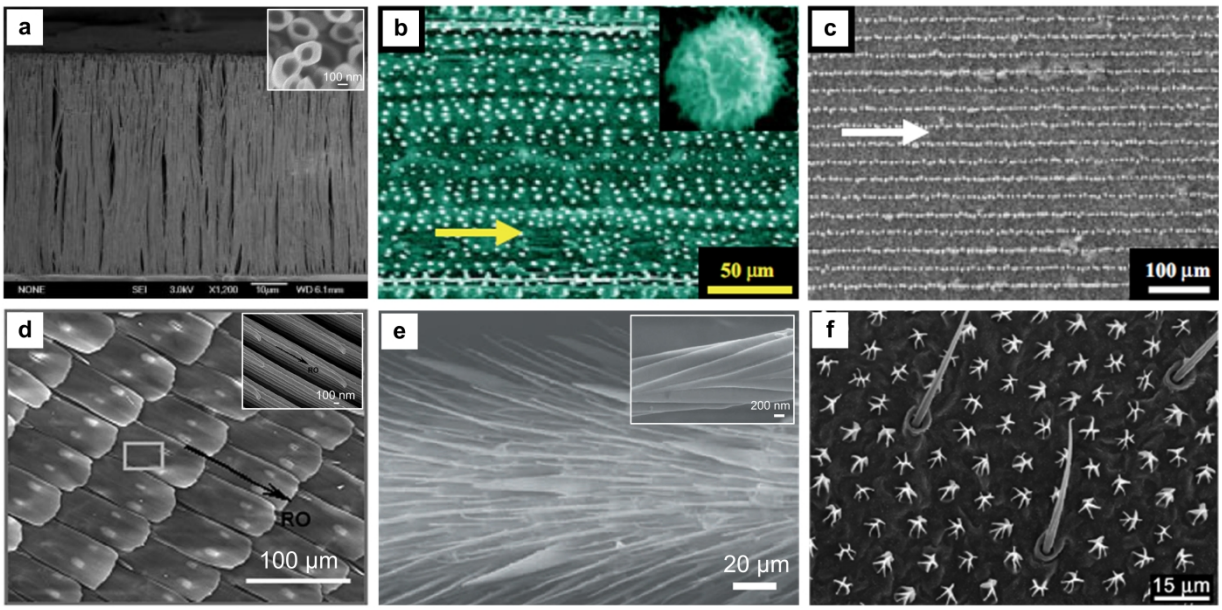

Figure 7. SEM micrographs of biomimicked and natural superhydrophobic surfaces. (a) Side view (inset: top view) of PS nanotube film mimicked from gecko feet [27] and top views of (b) natural rice leaf and (c) biomimicked CNT film [30], (d) butterfly wing [32], (e) water strider leg [37], and (f) termite wing [34].

The broad range of natural examples has helped scientists to understand the wetting phenomena on various superhydrophobic surfaces. By mimicking natural surfaces, different types of artificial superhydrophobic surfaces have been successfully prepared for various applications.

1.2.2. Fabrication of superhydrophobic surfaces

A great variety of methods to fabricate superhydrophobic surfaces on different substrates have been introduced in recent years. A typical approach to create a superhydrophobic surface is either to pattern a hydrophilic material and coat the surface afterwards with a thin layer of hydrophobic material, or to pattern some inherently hydrophobic material. Low surface energy materials such as siloxanes or fluoropolymers are typically used to obtain the hydrophobic chemistry on artificial superhydrophobic surfaces. However, the extremely low energy surface chemistry is not a necessary condition for superhydrophobicity, because natural superhydrophobic surfaces, which can have extremely high CAs and low SAs, possess only moderately low energy chemistry on their waxy surface.

Almost any solid material, *e.g.* hard solids such as metals and metal oxides, elastic and flexible polymers, and fiber-based materials such as paper and textiles, can be used as a substrate for a superhydrophobic surface. Among others, plasma, laser, and chemical etching can be used to roughen solid substrates in order to fabricate a superhydrophobic surface. Photolithography is a common way to create well-defined silicon micropillar arrays for superhydrophobic surfaces. Other frequently used methods to fabricate superhydrophobic surfaces include the use of different templates, electrospinning of nanofibers, evaporation of polymer solutions, sol–gel coatings, and various spraying techniques *e.g.* using nanoparticle suspensions [13, 15, 17].

Roughening of hydrophilic materials

Fabrication of superhydrophobic surfaces from hydrophilic materials, such as metals and metal oxides, involve two steps: (i) roughening of the solid and (ii) introduction of hydrophobic surface chemistry. Zhang *et al.* [39] roughened titanium dioxide (TiO_2) film using CF_4 plasma and hydrophobized the roughened surface with an octadodecylphosphonic acid (ODP) monolayer (Figure 8a). Water CA on the resulted superhydrophobic surface was as high as 168º and CAH was measured to be 0º. Prior to the ODP modification, water CA on the roughened TiO_2 film was close to 0º due to the high roughness and intrinsic hydrophilic nature of the surface. Gao *et al.* [40] used a facile laser-etching method to fabricate anisotropic microstructures and rugged nanoprotrusions on a silicon wafer (Figure 8b). After modification with fluoroalkylsilane, the surface showed perfect isotropic superhydrophobicity (CA ~180º) without any apparent CAH, water adhesion, or drag resistance. Öner and McCarthy [41] prepared well-defined silicon micropillars with various dimensions by the means of photolithography (Figure 8c–e) and modified the surfaces with hydrophobic compounds in order to execute fundamental superhydrophobicity studies. Micropillars with closely controlled dimensions are very useful, for example, in combining the theoretical and practical understanding of superhydrophobicity.

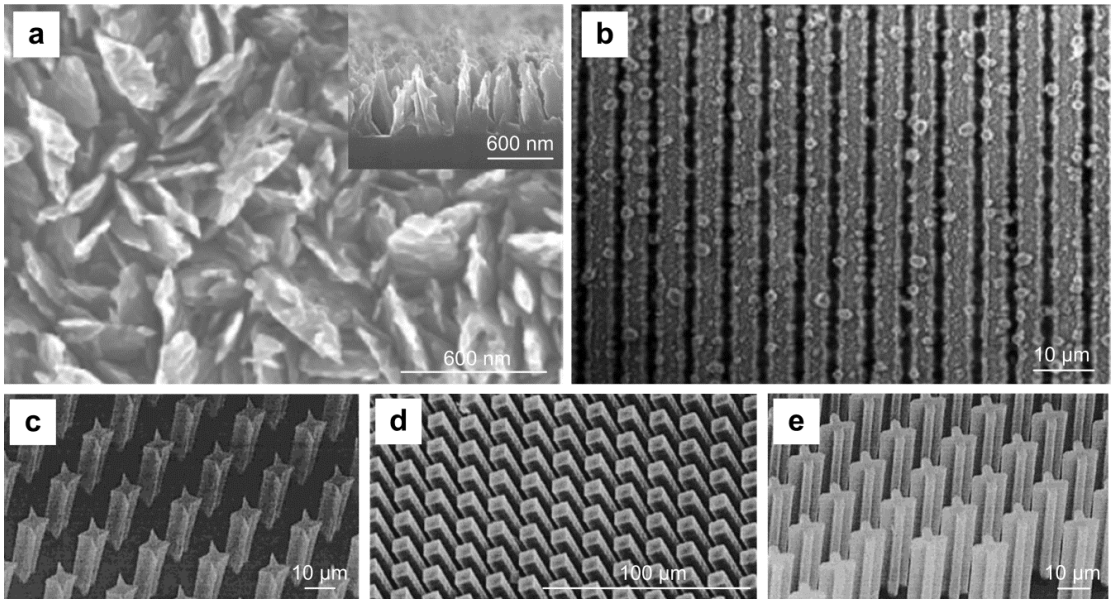

Figure 8. SEM micrographs of superhydrophobic surfaces fabricated by roughening and subsequent chemical modification of inherently hydrophilic materials. Top views of (a) plasma-etched TiO_2 surface (inset: side view) [39] and (b) laser-etched silicon surface [40], and (c–e) tilted views of silicon micropillar arrays fabricated by photolithography [41].

Fabrication of rough surfaces from hydrophobic materials

When a superhydrophobic surface is made by roughening intrinsically hydrophobic material, further hydrophobization steps are not needed. Feng *et al.* [30] fabricated the superhydrophobic anisotropic CNT film shown in Figure 7c by local growth of packed aligned CNTs. Jin *et al.* [27] prepared the high-adhesive superhydrophobic PS nanotube film shown in Figure 7a using porous alumina membrane as a template. The use of polymeric templates, *e.g.* polydimethylsiloxane (PDMS) or poly(vinyl alcohol) (PVA), is an effective way to mimic natural surfaces with high level of details, as was shown by Sun *et al.* [42] and Feng *et al.* [28], who replicated superhydrophobic surfaces of lotus leaf and rose petal, respectively. Water CA on the PDMS replica of lotus surface was 160º and SA for a droplet with a radius of 1 mm was less than 2º, while the PS replica of rose petal did show similar high-adhesive superhydrophobicity (CA = 155º, droplets were pinned to the surface) that was observed on the natural petal surface. Zhu *et al.* [43] prepared a lotus-leaf-like conductive polyaniline (PANI)/PS composite film by electrospinning method (Figure 9a). The superhydrophobic film showed CA of 166.5º for 4 µl water droplets, and the SA was measured to be < 5º. Erbil *et al.* [44] prepared a porous superhydrophobic polypropylene (PP) coating (Figure 9b), on which water CA was 160º, by evaporating a mixture of PP, xylene, and methyl ethyl ketone. Similar approach was later adapted by Lu *et al.* [45] for preparation of superhydrophobic low-density polyethylene (LDPE) coating, on which water CA as high as 173º and SA of only 1.9º were measured. Shirtcliffe *et al.* [46] prepared superhydrophobic and highly porous organosilica sol–gel foam (Figure 9c), on which the advancing water CA and CAH were 155º and 6º, respectively. Kulinich and Farzaneh [47] sprayed zirconium dioxide (ZrO_2) nanoparticle

containing fluoropolymer solution on aluminum plate to produce a high-adhesive superhydrophobic surface (Figure 9d), where water CA was 152º and CAH was > 70º.

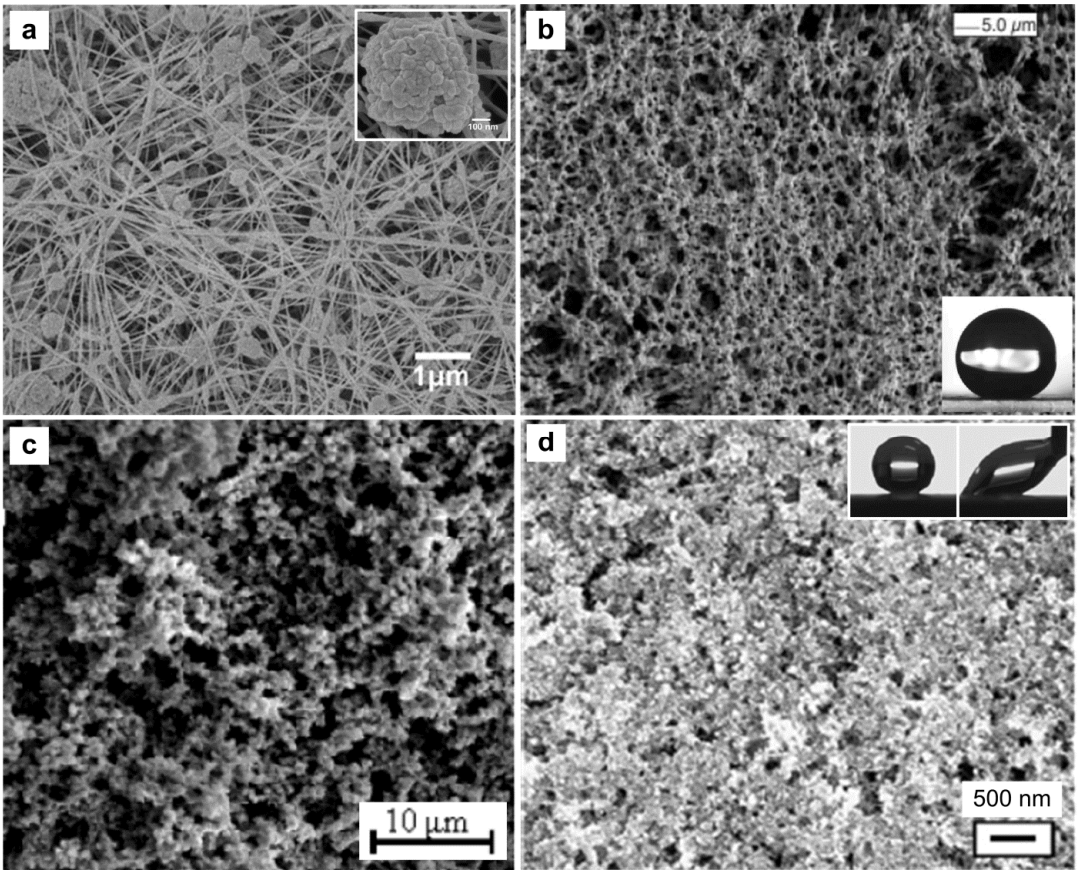

Figure 9. Superhydrophobic surfaces fabricated from hydrophobic materials. SEM micrographs (top views) of (a) electrospun lotus-like PANI/PS fiber mat [43], (b) porous PP film prepared by evaporating the polymer solution [44], (c) organosilica sol–gel foam [46], and (d) spray-coated fluoropolymer nanoparticle suspension [47].

Many of the techniques that are used to fabricate superhydrophobic surfaces or coatings are multi-step and time consuming, and may require special equipment or conditions, *e.g.* low-pressure vacuum chambers. However, there are also very simple approaches to create superhydrophobic surfaces. For example, Onda *et al.* [11] fabricated the surface used in the Kao experiment (Figure 3) by letting melted alkyl ketene dimer (AKD) solidify at room temperature in the ambience of dry nitrogen gas. Water CA on the resulted fractal AKD surface was as high as 174º. Zhang *et al.* [48] achieved a superhydrophobic surface simply by extending a Teflon® (poly(tetrafluoroethylene), PTFE) film. The CA increment from 118º to 165º was due to the changed microstructure on the surface and the increased fraction of air between the fibrous PTFE crystals. Xu *et al.* [49] demonstrated a simple laminating templating method, which appears to be suitable for large-scale fabrication of robust superhydrophobic surfaces on polymers. They laminated different types of woven meshes on LDPE under heat and pressure. After cooling, the meshes were peeled off leaving behind highly textured polymer surfaces (Figure 10), on which water CAs ~160º were measured, and CAH and SA for 10 μl droplets were in the range of 5–8º and 3–5º, respectively. In fact, a superhydrophobic coating can be

fabricated, as simply as, by collecting a layer of soot from a candle flame on, for example, metal or glass plate.

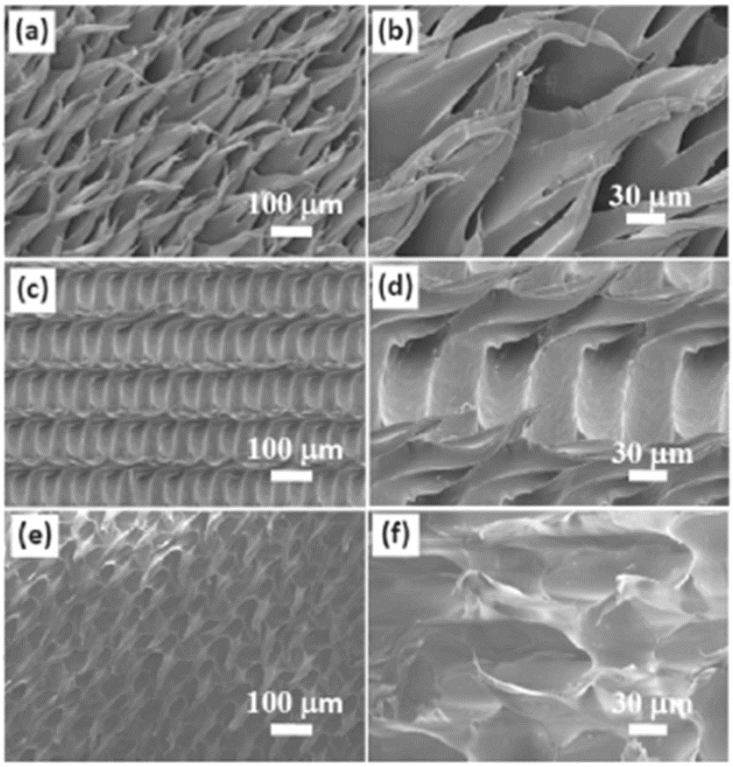

Figure 10. SEM images of superhydrophobic LDPE surfaces fabricated by laminating templating method using different types of woven mesh templates. Images b, d, and f are magnifications from images a, c, and e, respectively [49].

1.2.3. Wettability switching

As it is clear by now, surface roughness can support either hydrophobicity or hydrophilicity depending on the surface chemistry. Therefore, it is easy to execute a superhydrophobicity–superhydrophilicity conversion on a textured surface simply by changing its chemistry. Wettability alteration on superhydrophobic surfaces has attracted great scientific interest due to its many potential applications, *e.g.* in the field of microfluidic devices. Various external stimuli, including electric-field, heating and cooling, extension, solvent treatments, plasma treatments, self-assembly, and illumination, can be used to realize the wettability conversion on different types of superhydrophobic surfaces. Moreover, typically the wettability switching can be done repeatedly using one stimuli to induce the hydrophilicity conversion and another to return the hydrophobicity [50, 51].

Photo-induced wettability changes on photoactive inorganic materials such as TiO_2 and zinc oxide (ZnO) have been of particular interest in recent years both because of their potential practical applications and the lack of fundamental understanding of the phenomena. Both TiO_2 and ZnO can decompose organic material from their surface under exposure to UV-illumination. For example, Zhang *et al.* [39] executed superhydrophilicity conversion on TiO_2

surface shown in Figure 8a by degrading the hydrophobic ODP monolayer from the photocatalyst surface by UV-illumination. However, there has been a debate whether the hydrophilicity conversion on photocatalyst surfaces, particularly on TiO_2, occurs solely because of the removal of hydrophobic molecule layer from the surface, or do the structural changes on the photocatalyst surface, namely formation of oxygen vacancies and increment of hydroxyl (OH) groups, also play a role in the hydrophilicity conversion [52-54].

Benefit of the photocatalytic wettability switching is that it enables the control of surface properties with high level of details. By illuminating the sample through a photomask, micrometer scale surface energy patterns can be fabricated on, for example, TiO_2 to control its surface wettability. Zhang *et al.* [55] demonstrated fabrication of 50 µm wide superhydrophilic stripes on a superhydrophobic ODP-modified TiO_2 surface, which were able to guide water condensation and deposition of PS microspheres from aqueous suspension (Figure 11). Surface energy patterning can improve for example printability, especially in the field of printed electronics, were strict control of patterns and line widths is necessary [56].

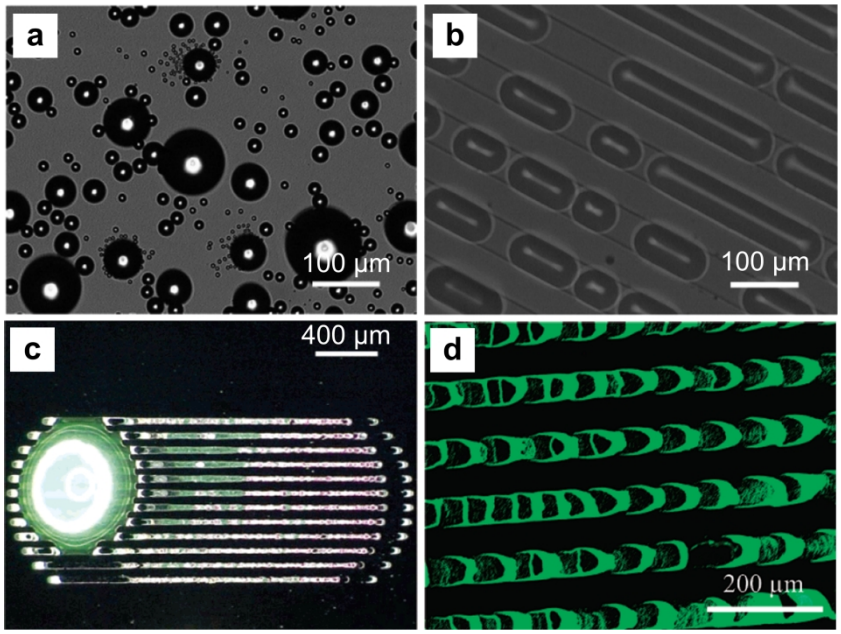

Figure 11. Wetting of photopatterned superhydrophobic ODP-modified TiO_2 surface. Optical micrographs of water condensation on the surface (a) before and (b) after the creation of superhydrophilic patterns by illumination. (c) Optical micrograph of deposition of PS microspheres from evaporating water droplet and (d) fluorescence micrograph of the PS microsphere stain on the surface [55].

1.2.4. Superamphiphobic surfaces

Because of the high surface tension of water, fabrication of superhydrophobic surfaces is relatively easy. Natural superhydrophobic surfaces have shown that extremely low surface energy materials are not needed to obtain high CA, low SA, and low CAH for water. Neither are the requirements for the physical structure of the surface especially strict, but superhydrophobicity can be obtained, for example, on simple micropillar surfaces. When the

target is to achieve repellency against liquids of significantly lower surface tension than water, requirements for both the chemistry and physical structure of the surface are much stricter. In recent years, interest towards superamphiphobic surfaces, which repel both water and oils, has grown increasingly. The number of potential applications for superamphiphobic surfaces is greater compared to superhydrophobic surfaces which can repel solely water. However, because of the strict requirements for the chemistry and physical structure, superamphiphobic surfaces are rare.

Superamphiphobicity can be obtained for example with fluorinated T-letter shaped or mushroom-like micropillar surfaces, where re-entrant curvature plays a critical role in the non-wetting properties (Figure 12) as was shown by Tuteja *et al.* [57, 58]. However, it is not necessary to use carefully designed re-entrant curved structures to obtain superamphiphobicity. For example, Deng *et al.* [59] applied a simple method to fabricate a robust superamphiphobic coating that could repel a variety of low surface tension liquids (Figure 13). They collected candle soot on a glass slide, and used the soot layer as a template to produce a porous silica network. After coating the silica layer with a semi-fluorinated silane, the surface showed excellent superamphiphobic properties, *e.g.* CA and SA for water (surface tension of 72.1 mN/m) were 165° and 1°, respectively, and the corresponding values for hexadecane (surface tension of 27.5 mN/m) were 156° and 5°, respectively.

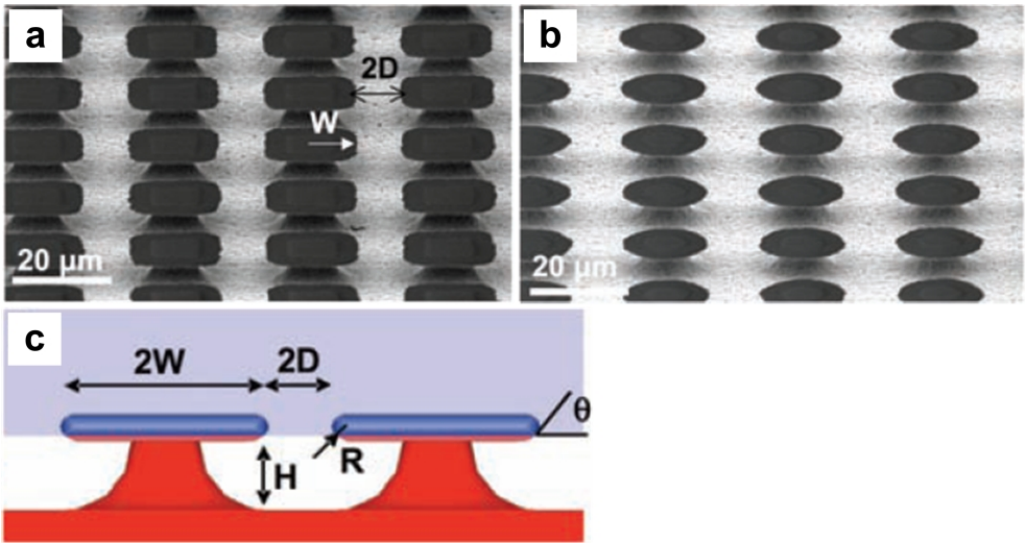

Figure 12. Superamphiphobic surfaces with re-entrant curvature. (a–b) SEM micrographs of the micropillar surfaces with re-entrant topography and (c) a cartoon highlighting the formation of a liquid–solid–air composite interface on the re-entrant curved surface [57].

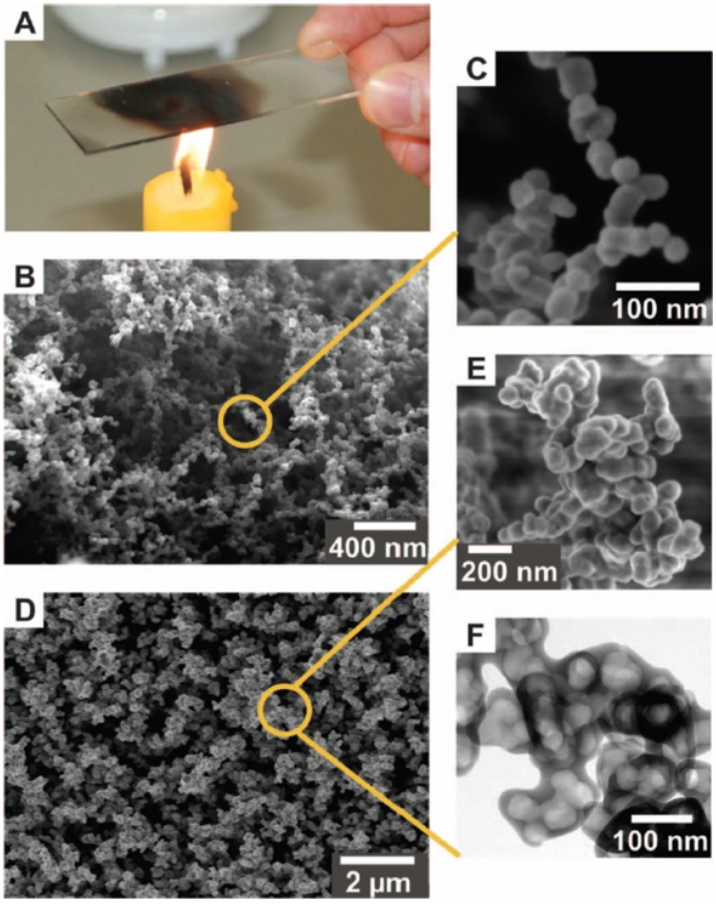

Figure 13. Fabrication of a superamphiphobic coating using candle soot as a template. (a) Photograph shows the collection of a soot layer on a glass slide. (b–c) SEM micrographs of the soot layer and (d–e) the silica shell deposited on the soot. (f) Transmission electron microscope (TEM) image reveals the hollow structure of the silica shell after calcination [59].

Recently, Wong *et al.* [60] introduced a new approach to create slippery surfaces with pressure-stable omniphobicity and self-healing properties. The idea is that a porous substrate, similar to many superhydrophobic surfaces, is infused with a lubricating fluid. While the substrate resembles superhydrophobic surfaces, the strategy to create slippery surfaces using lubricating fluids is very different from superhydrophobicity, because the lubricating fluid (*e.g.* perfluorinated liquid), which is locked in place by a nano/microporous substrate, creates a smooth and slippery surface for both high- and low surface tension liquids. The as-prepared slippery liquid-infused porous surfaces (SLIPS) had minimal adhesion to variety of liquids, *e.g.* liquids with low surface tension such as hexane (surface tension of 18.6 mN/m). Droplets of various liquids could easily slide on the surface without leaving any stain: the measured CAH values were < 2.5° and SAs were ~5° at the maximum. Once again, inspiration for the surface design was found from nature, from the *Nepenthes* pitcher plants [61].

1.2.5. Applications

Superhydrophobic surfaces and coatings can potentially be utilized in variety of applications including self-cleaning, stain-resistant, anti-icing, and anti-fogging surfaces; wind screens;

waterproof breathable clothing and coatings; anti-biofouling and anti-corrosion coatings; fog-harvesting; oil separation from water; microfluidics; drag reduction; and liquid transportation. In addition to the special wettability, many other useful properties have been typically incorporated into superhydrophobic coatings, for example transparency, structural color, gas permeability, and flexibility [13, 15-17].

Even though many promising applications for superhydrophobicity have been identified, and there are several facile methods to fabricate superhydrophobic surfaces and coatings, the large-scale utilization of superhydrophobic surfaces is limited. This is mainly due to the poor wear resistance, which is a common problem with superhydrophobic surfaces [13, 16]. The fragile micrometer and submicrometer scale surface structures are easily damaged in daily use, for example, due to abrasion. Artificial superhydrophobic surfaces cannot renew and heal the damages similarly to natural surfaces. Fabrication of robust surfaces, which can maintain their functionalities also in wearing conditions, is one of the major issues to be resolved with superhydrophobic and other functional surfaces.

However, major progress in fabrication of robust superhydrophobic surfaces has been achieved in recent years. For example, the superamphiphobic coating introduced by Deng *et al.* [59] could maintain its liquid-repellent properties even when the topmost surface layer was worn out or peeled off using adhesive tape. Zhao *et al.* [62] fabricated a grooved surface with re-entrant curvature to obtain directional superamphiphobicity and mechanical robustness, and Zhou *et al.* [63] applied a highly durable superhydrophobic silicone rubber/nanoparticle composite coating on fabrics, which was capable of withstanding 500 laundering cycles without any significant change in its wetting properties. Recently, also self-healing functions have been successfully incorporated into superhydrophobic surfaces [64-66]. Apparently, the first self-healing superhydrophobic coating was introduced by Li *et al.* [64]. Their porous micro-/nanostructured fluoro-modified polymer coating could preserve healing agent units of reacted fluoroalkylsilane, and the preserved healing agents could migrate to the coating surface to heal its chemistry after the original fluoroalkylsilane layer was decomposed by an oxygen plasma treatment. However, so far there are no artificial superhydrophobic surfaces which are capable of healing physical damages similar to SLIPS [60] or natural superhydrophobic surfaces.

Although many natural superhydrophobic surfaces possess a dual-scale roughness that contributes to easy mobility of water droplets and self-cleaning properties, by now it is clear that hierarchical surface roughness is not a necessary condition for superhydrophobicity with low droplet adhesion and self-cleaning properties, but similar superhydrophobic properties can be achieved with a single-scale submicrometric surface roughness. It seems reasonable that one important reason why nature has chosen dual-scale hierarchical roughness for many of its superhydrophobic surfaces, *e.g.* lotus leaf, is the enhanced wear resistance of the fragile surfaces [24, 67].

1.3. Superhydrophobic coatings on cellulose-based substrates

1.3.1. Cellulose as a substrate material

Cellulose is an abundant biopolymer, which is commonly used as a raw material for paper products and cotton fabrics. Cellulose chemistry includes a great number of surface OH-groups, which readily create hydrogen bonds with water molecules enabling water to spread over the surface. Cellulose is also capable of absorbing water. That is, cellulose is a hydrophilic and hygroscopic material by nature. Water CAs reported on smooth cellulose films vary between 17° and 47° [68, 69]. The rough and porous surface structure of paper and cotton fabrics further enhance spreading and absorption of water by capillary action between the cellulose fibers. The capillary driven liquid transportation is utilized, for example, in paper-based microfluidic devices [70].

In order to fabricate hydrophobic paper or cotton, sort of hydrophobization treatment needs to be carried out. Although cellulose fibers create a rough surface structure, for example on paper, typically water CAs greater than 150° are not reached on paper surface after hydrophobization treatments. Even with low surface energy fluorine coatings the CAs typically remain below 150°, and water droplets firmly adhere to the surface. For example, Mukhopadhyay *et al.* [71] used four types of plasmas from different fluorine-containing monomers to coat filter paper. Already, a very thin layer of fluorocoating (thickness less than 1–2 nm) turned the initially hydrophilic surface hydrophobic: CAs on the plasma coated surfaces varied between 141° and 146°. However, increment in the coating thickness did not further increase the CAs. Balu *et al.* [26] deposited thin fluorocarbon films on commercial copy-grade paper and hand-made sheets using plasma-enhanced chemical vapor deposition (PECVD). After the plasma coating, both surfaces showed high CAs between 140° and 145° and large CAHs between 60° and 110°.

When looking at the fiber structure of paper surface, it is not surprising that after hydrophobization treatment the surface becomes nearly superhydrophobic, but water droplets still adhere firmly to the surface, because paper surface resembles, to some extent, the high-adhesive surface of rose petals [28][R1]. That is, although air gets entrapped between the cellulose fibers on a hydrophobic paper surface creating a liquid–solid–air composite interface, the round and grooved structure of the fiber surface enables large liquid–solid contact area and high adhesion of water droplets. In order to fabricate a superhydrophobic surface on paper or cotton, chemical modification alone is not enough, but in most cases the surface roughness needs to be modified as well.

Fabrication of superhydrophobic surface on cellulose-based substrates such as paper, board, and cotton fabrics has recently attracted appreciable attention of scientists. These versatile and economically viable materials, made of renewable and biodegradable cellulose fibers, have many profitable properties such as affordability, recyclability, flexibility, and mechanical strength. Superhydrophobic surface properties on paper and cotton can further broaden their exploitation potential and open new possibilities, for example, in the fields of printing,

diagnostics, and microfluidics. However, fabrication of superhydrophobic surface on cellulose-based materials can be challenging because of the complex surface structure and limited thermal and chemical resistance of the substrate material. Therefore, suitable methods to fabricate a superhydrophobic surface on paper and cotton are limited. Apparently, Lin *et al.* [72] carried out the first study where a superhydrophobic coating was applied on cotton in 2005 by spray-coating the substrate with TiO_2 nanoparticle containing fluoro-copolymer solution, while Nyström *et al.* [73] firstly reported on fabrication of superhydrophobic paper in 2006 *via* tailored grafting architecture. Since then, the number of research papers published on fabrication of superhydrophobic cotton or paper has exploded.

As was discussed earlier, one of the major challenges with superhydrophobic surfaces is the long-term durability and wear resistance. Indeed, durability is one of the key issues with superhydrophobic cotton clothes which need to stand abrasion and repeated washing cycles. However, the applications of paper products are typically quite different from the applications of cotton fabrics. Paper products are typically cheap and disposable, and they are produced in high volumes for short-term applications. Therefore, because of the nature of the substrate material, with paper it is even more important to seek new methods suitable for low-cost roll-to-roll mass production of superhydrophobic surfaces than focus on surface durability. In the following sections, different approaches to fabricate superhydrophobic surfaces on cellulose-based materials are explored and properties of the surfaces are discussed.

1.3.2. Fabrication by wet-chemical methods

Dip-coating

Li *et al.* [74] dip-coated cotton fabrics in silica hydrosols, and subsequently hydrophobized the samples through self-assembly of hexadecyltrimethoxysilane (HDTMS) in ethanol solution. Additional steps of the coating procedure included padding of the samples, drying, and curing for 1 h in an oven at 120°C. The best hydrophobic properties with water CA of 151° were achieved on the coating which composed of silica particles with an average diameter of 21 nm.

Wang *et al.* [75] prepared a sol solution which contained silica nanoparticles with an average size of ~50–150 nm by co-hydrolysis and condensation of two silane precursors, tetraethyl orthosilicate (TEOS) and tridecafluorooctyl triethoxysilane. The solution could be applied on various substrates, including textiles and filter paper, by dipping, spin-coating, or spraying. Because the solution itself contained a fluorocompound, any separate hydrophobization treatment was not needed to obtain the transparent and superhydrophobic coating, on which water CAs greater than 170° and SAs lower than 7° were measured. This was apparently the first so-called one-step approach to fabricate a superhydrophobic coating on paper, *i.e.*, any separate hydrophobic modification was not needed to bring the low surface energy chemistry for the coating. However, after application of the coating solution, two additional steps, *i.e.*, drying at room temperature and curing for 1 h at 110°C, were still needed to finalize the superhydrophobic coating.

Arbatan *et al.* [76] fabricated a superhydrophobic coating on filter paper (Figure 14) by dip-coating the paper samples in an aqueous suspension of precipitated calcium carbonate (PCC) pigments and cellulose nanofibers, after which the samples were dried between two sheets of blotting paper in a drum dryer at 112°C for 18 min. After the dip-coating procedure, the samples were hydrophobized in a solution of AKD in *n*-heptane and cured in an oven at 105°C for 30 min. Water CA on the coated filter paper was measured to be 160°, and 5 µl water droplets instantly rolled off the surface when placed on the sample which was inclined at 5°. The cellulose nanofibers had a critical role in the formation of the hierarchically structured coating layer as they acted as binding agents between the PCC particles and the substrate.

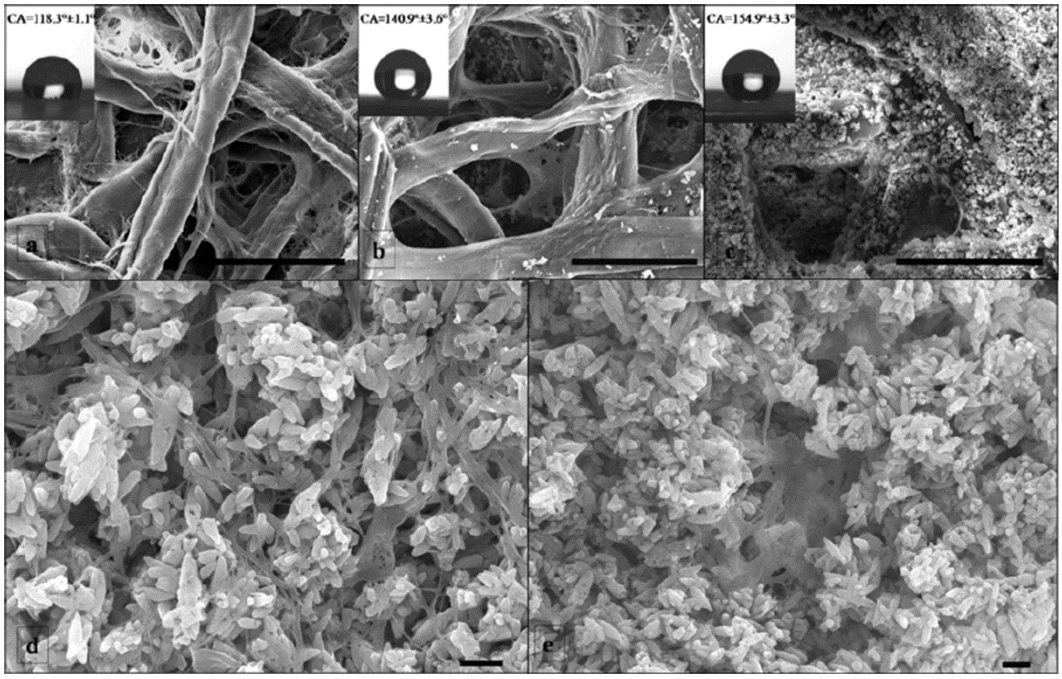

Figure 14. SEM images of PCC pigment/cellulose nanofiber coating. (a) Filter paper sized with AKD, (b) filter paper dipped in an aqueous suspension of PCC and subsequently sized with AKD, and (c) filter paper dipped in an aqueous suspension of PCC and cellulose nanofibers and subsequently sized with AKD (scale bars correspond to 50 µm). (d–e) High-magnification images of the PCC/nanofiber coating on a glass slide (scale bars correspond to 1 µm) [76].

Gao *et al.* [77] fabricated superhydrophobic cotton by dip-coating the fabrics in different silica sols formed by hydrolysis and condensation of tetraethoxysilane under alkaline conditions. After coating the cotton fabric with silica sol, which contained silica particles of ~52 nm in diameter, the sample was padded, dried, and modified in a solution of hydrolyzed HDTMS. Finally, the coating was cured at 120°C for 1 h to obtain a superhydrophobic surface with water CA of 155°. Physical properties of the superhydrophobic cotton were compared to the properties of unmodified cotton. The comparison revealed a slight decrement in the tensile strength of the coated cotton (< 10%). Changes in the whiteness and air permeability of the cotton were negligible. Laundering test revealed that the superhydrophobic coating could not withstand multiple washing cycles, because after 5 cycles water CA on the coated cotton had decreased to ~125°, and after 30 cycles to ~95°.

Wang *et al.* [78] synthesized particle-containing silica sols by co-hydrolysis and co-condensation of different silane precursors to fabricate superhydrophobic coatings on fabrics. The fabrics were dip-coated in the silica sol and padded, after which the samples were dried at room temperature and cured at 110°C for 1 h to finish the coating. The authors highlighted that the sols could potentially be applied on the substrates with several other methods as well, *e.g.* by spray-coating. The effect of different sol recipes on the particle size, hydrophobicity, and durability of the coating were examined. When an epoxide group containing silane, 3-glycidoxypropyltrimethoxysilane (GPTMS), was added in the sol, hydrophobicity of the coating slightly decreased, but its laundering durability improved significantly. Water CA and SA for a 4 µl droplet on the cotton fabric coated with the GPTMS containing sol were ~170° and < 10°, respectively, and after 50 washing cycles, the corresponding values remained at ~160° and < 30°, respectively.

Zhou *et al.* [63] fabricated an extremely durable superhydrophobic tridecafluorooctyl triethoxysilane modified PDMS/silica nanoparticle composite coating to be used on different fabrics (Figure 15). An inspiration for the robust composite coating was obtained from tyres, a classic and highly durable nanocomposite material, where the main components are natural rubber and carbon black. The coating dispersion was applied on the fabrics by dip-coating, after which the samples were dried at room temperature and cured at 135°C for 30 min. The authors highlighted that other coating techniques, *e.g.* spray-coating and padding, could be used as well. The coating showed excellent mechanical and chemical durability. For example, CA and SA for a 5 µl water droplet on pristine coated cotton were 170° and 3°, respectively, and after 500 wash cycles the corresponding values were nearly unchanged, 165° and 6°, respectively. Similar results were also obtained after treatments with boiling water and acid or base solutions. In addition to the durable superhydrophobicity, the coated fabrics showed good stain resistance and maintained their inherent good air permeability.

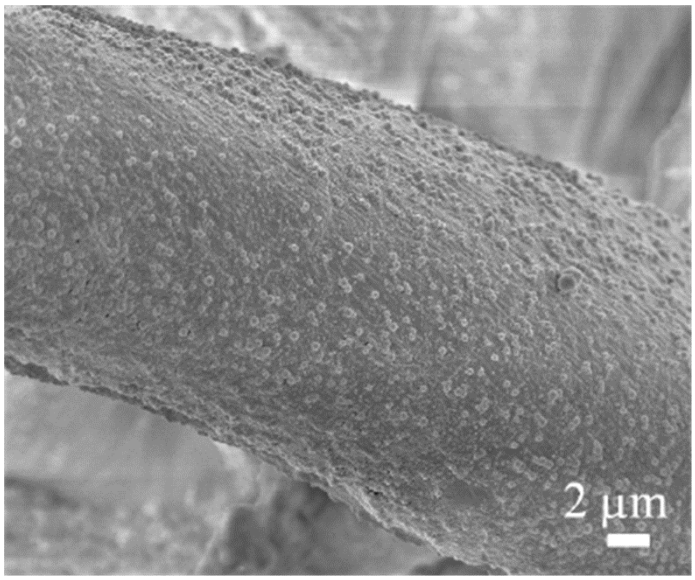

Figure 15. SEM image of PDMS/silica nanoparticle coated cotton [63].

Duan *et al.* [79] treated cotton fabrics with cerium dioxide (CeO_2) sol using a dip–pad–cure process. The curing was carried out at 170°C for 3 min. The whole coating procedure was repeated three times to obtain a dense film of CeO_2 coating on cotton. After subsequent modification of the samples in a solution of ethanol and hydrolyzed dodecafluoroheptyl-propyl-trimethoxylsilane (DFTMS), drying, and curing at 120°C for 1 h, the cotton fabrics showed superhydrophobic properties with water CA of 158° and SA of 14° for 5 µl droplets. After 30 laundering cycles, the CA on the treated cotton still remained greater than 150°. In addition to the superhydrophobicity, the coating showed good UV-shielding properties due to the presence of aggregated CeO_2 nanoparticles (average size ~15 nm).

Li *et al.* [80] used an industrial waterproof reagent, potassium methyl siliconate (PMS), as a starting material to fabricate superhydrophobic surfaces on paper and cotton through a simple solution-immersion method. An aqueous solution of PMS was reacted with carbon dioxide (CO_2) at room temperature to prepare the silanol solution, where the polymethylsilsesquioxane coatings were formed on the substrates as a result of polycondensation process and hydrogen bond interactions between the OH-groups of cellulose molecules and silanols. To obtain a dense coating, the samples were cured in a vacuum oven at 120°C for 30 min. Water CAs on the modified cotton and filter paper were measured to be 158° and 157°, respectively. The coating layer appeared transparent and showed satisfactory mechanical and chemical durability as the superhydrophobic character of the coated cotton textile remained after 20 washing cycles and the coating could withstand treatments with aqueous solutions over wide pH range.

Wang *et al.* [81] treated filter paper with a mixture of PDMS-modified silica nanoparticles (average particle size of 14 nm) and PS solution in toluene to obtain superhydrophobic and superoleophilic filters to be used in selective absorption and separation of liquids that differ in surface tension (Figure 16). The treatment was carried out by dip-coating the paper in the coating solution for approximately 15 s, after which the paper was dried in an oven at 60°C for several hours. The treated filter paper showed good superhydrophobic properties with water CA of 158° and SA of 4° for 8 µl droplets, and fully absorbed organic liquids such as diesel oil, hexane, octane, and dodecane. Chemical stability of the coating was evaluated by exposing the sample to aqueous solutions of varying pH between 1 and 14. The coating showed good tolerance to both acidic and basic conditions as the water CAs on the surface remained greater than 150°.

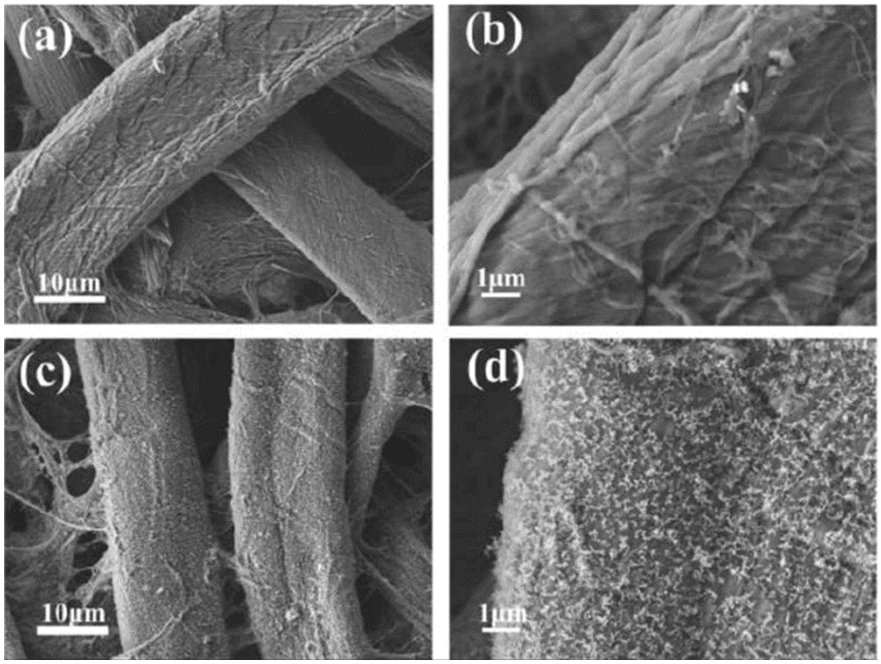

Figure 16. SEM images of filter paper surface (a–b) before and (c–d) after coating with superhydrophobic PS/silica nanoparticle layer [81].

Bayer *et al.* [82] fabricated superhydrophobic cellulose sheets by dip-coating the samples in a suspension of submicrometer scale PTFE particles (~150 nm) and ethyl-2-cyanoacrylate (ECA) monomer solution. One of the fascinating properties of ECA is that it starts cross-linking around cellulose fibers instantly after solvent evaporation due to the native OH-groups on cellulose and the moisture that has adsorbed to the surface. After dipping the cellulose sheets in the coating solution, the samples were left to dry and polymerize under ambient conditions overnight. The highest water CAs on the as-prepared surfaces were measured to be around 160°, and the coatings showed low adhesion to water droplets with CAH around 10°.

Huang *et al.* [83] impregnated filter paper with fluorinated waterborne epoxy emulsion to render the paper surface superhydrophobic. The coating was cured in an infrared (IR)-oven at 120°C for 30 min. Water CA on the treated paper was 152° and the surface showed sticky properties as 5 μl droplets remained on the surface when tilted upside down. CAH on the surface was measured to be 34°. The treated paper showed potential for oil filtration from water emulsions due to its superoleophilic properties (CA for hexadecane = 0°) and good oil permeability.

Zhou *et al.* [66] fabricated a highly durable superamphiphobic coating with self-healing properties on polyester, wool, and cotton fabrics. The fabrics were coated *via* a two-step dip-coating method. In the first step, the substrate was immersed in a suspension of fluoroalkyl silane modified silica particles (average diameter ~150 nm) in ethanol for 1 min, after which the sample was dried at room temperature for 10 min. In the second step, the sample was immersed in a fluoro-polymer/fluoroalkyl silane containing solution for 1 min and dried at 130°C for 1 h. The coated fabrics showed great CAs and low SAs for both water and hexadecane. For example, the coated cotton showed CAs of 171° and 158° and SAs of 3° and 7° for water and hexadecane, respectively. Most of the experiments were performed using polyester fabrics as a

substrate material, on which the coating could withstand at least 600 laundry cycles and several thousands of abrasion cycles without apparent change in its wetting properties. That is, both water and hexadecane CA and SA remained > 150° and < 10°, respectively, after the durability experiments. In addition, the coating was stable to strong acid/base, boiling, and ozone treatments, and showed very little influence on the air permeability of the fabrics. After the coating chemistry was artificially damaged by oxidizing the surface with a vacuum plasma treatment, the coating lost its super liquid-repellent properties and showed CAs of 0° for both water and hexadecane. However, the superamphiphobic properties of the coating were healed by ageing the plasma treated sample at room temperature for several hours or by a 5 min heat treatment at 130°C. Durable superamphiphobic properties with self-healing capability, which were demonstrated using polyester fabric as a substrate material, were reported also on the coated wool and cotton fabrics.

Spray-coating

Lin *et al.* [72] fabricated superhydrophobic TiO_2 nanoparticle containing fluoromethylic copolymer coatings on different substrates by spray-coating. They sprayed solution of nanoparticles mixed with perfluoroalkyl methacrylic copolymer and distilled water on the substrates by a specific nozzle and dried the coating in an oven at 85°C for 12 h. Different coating parameter combinations were examined using cement plates as a substrate material, and the effects of different parameters were evaluated statistically by the analysis of variance and Taguchi methodologies. The solid ratio of nanoparticles in the precursor solution was concluded to be the most important single factor in preparation of the superhydrophobic coatings. The optimal parameter combination, which contained 3 layers of the coating on the substrate, resulted in oleophobic and superhydrophobic properties of the coating with water CA of 161°. The authors demonstrated fabrication of the superhydrophobic coating also on cotton fabric using the determined optimal parameter settings.

Bayer *et al.* [84] spray-coated paper and fabrics with an emulsion of surface functionalized silver flakes and colloidal copolymer blend. The first component of the blend, vinyl copolymer, was used to enable good dispersion of the silver flakes in the emulsion and to obtain good adhesion to different substrates, while the other, perfluoroethylacrylate/*n*-alkyl acrylate copolymer, was used to induce hydrophobic chemistry for the composite coating. Prior to the spray-deposition of the coating, a paraffin wax-based film was melted on the substrates. The spray-coating was carried out while the wax-based film was still molten at 60°C to ensure mechanical interlocking between the coating and the melt. After 15 min of thermosetting, the coating was cooled down to room temperature. Water CA on the superhydrophobic coating was measured to be 164°, and both SA and CAH were around 5°. The coating showed good thermal stability as the SA and CAH remained below 10° after the coated paper was exposed to 80°C for 15 h in an oven.

Ogihara *et al.* [85] demonstrated a simple spray-coating method to fabricate transparent superhydrophobic coating on paper and cotton (Figure 17). Dodecyltrichlorosilane modified SiO_2 nanoparticles (average size 25 nm) in different alcohol suspensions were manually sprayed over the substrates, after which the samples were dried at room temperature overnight.

Aggregation state of the particles, and thus hydrophobicity of the coating, could be controlled by the choice of the alcohol in the nanoparticle suspension. Ethanol suspension gave the best hydrophobicity of the coating with water CA of 155° and SA of 7° for 3 µl droplets. Robustness of the coating was tested by pressing the surface with a bare finger, after which the CA and SA were measured to be 153° and 10°, respectively. The authors reported that superhydrophobicity of the coated paper was also maintained after folding the sample.

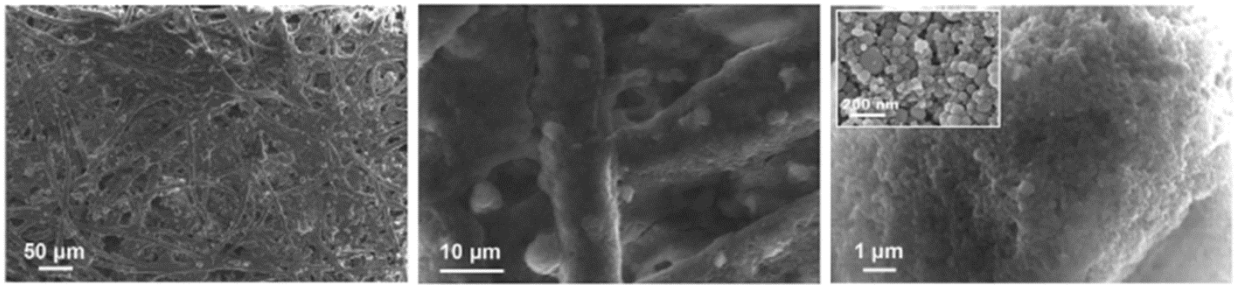

Figure 17. SEM images of different magnifications of spray-deposited SiO_2 nanoparticle coating on paper [85].

Mertaniemi *et al.* [86] used spray-dried nanofibrillated cellulose microparticles to fabricate a lotus-like hierarchically structured superhydrophobic surface (Figure 18). The dispersion of cellulose microparticles in ethanol was sprayed on a glass surface and dried in ambient conditions to form a semi-transparent coating. Hydrophobic chemistry for the coating was achieved by fluoro-modifying the cellulose microparticles with (tridecafluoro-1,1,2,2-tetrahydrooctyl)trichlorosilane (FOTS). Two types of approaches were used in the surface modification: in the first approach the modification was accomplished after the spray-coating by CVD at 90°C for 8 h, and in the second approach the modification was carried out prior to the spray-coating in toluene dispersion. In both cases, the coating appeared as low-adhesive superhydrophobic surface on which the advancing CAs for water were > 160° and droplets readily rolled off the surfaces at SAs < 5°. CAHs were measured to be 17° and 8° on the CVD-modified and dispersion-modified surfaces, respectively. Robustness of the coating was evaluated by droplet impingement test: over 100 droplets dropped on the same spot could bounce off the surface without leaving a residue. The authors reported, however, that the coating could be damaged by mechanical abrasion.

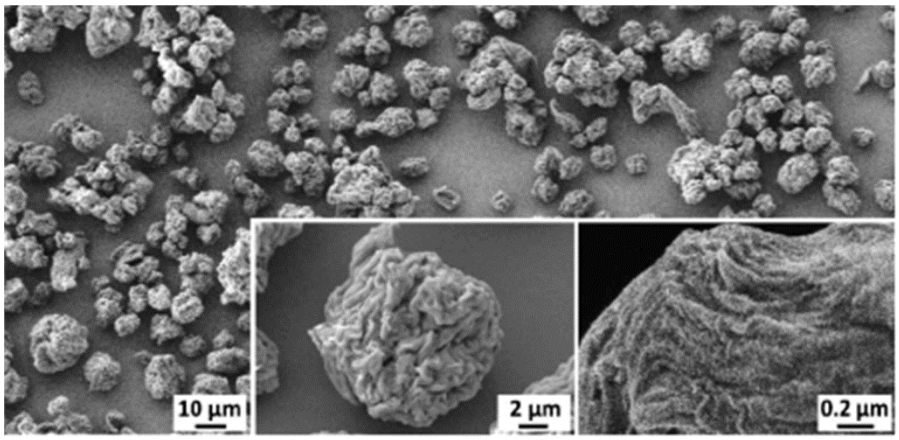

Figure 18. SEM images of spray-dried cellulose microparticles sprayed on glass substrate [86].

Barona and Amirfazli [87] fabricated superhydrophobic polymer–nanoclay composite film on paper by spray-coating. The coating recipe contained montmorillonite clay, adhesive, and water dispersed fluoro-methacrylic latex as a hydrophobization agent. Advancing water CA of 159° and CAH of only 2° were measured on the paper sample coated with the 25 µm thick nanocomposite film. Wetting properties of the coated paper samples were manipulated by printing solid grey patterns of different intensities on the superhydrophobic substrate. The superhydrophobic coating could withstand running through an ink-jet printer without any significant damage: after running the coated paper sample through the printer, the high advancing CA was maintained but the CAH suffered a slight increment to 14°.

Li *et al.* [88] sprayed octadecyltrichlorosilane (OTS) modified SiO_2 nanoparticles (particle size ~50 nm) in ethanol suspension on paper to obtain a transparent superhydrophobic coating. The spray-coating was repeated 10–20 times repeatedly, after which the coating was dried at room temperature for 1 h. Water CA and SA for 5 µl droplets on the as-prepared superhydrophobic coating were measured to be 163° and 3°, respectively.

Polymerization techniques

Nyström *et al.* [73] modified filter paper surface by atom transfer radical polymerization (ATRP) of glycidyl methacrylate (GMA) using a branched "graft-on-graft" architecture. They used a sophisticated multi-step chemical procedure, where GMA polymer grafts were grown on the cellulose surface. After the grafting, the surface was fluorinated using pentadecafluorooctanoyl chloride. The as-prepared surface showed water CA as high as 172°. In addition, the self-cleaning ability, well known from the lotus leaves, was demonstrated on the surface. In another study, Nyström *et al.* [89] used different types of hydrophobic modifications on the ATRP "graft-on-graft" treated filter paper. Water CAs on the surfaces modified with PDMS, perfluorinated chains, or alkyl chains varied between 162° and 172°. All the modified surfaces had low CAH values ranging from 5° to 10°. Moreover, the fluorinated surfaces showed oleophobic properties with sunflower oil CAs of 124° and 144°.

Deng *et al.* [90] fabricated superhydrophobic cotton with good laundering durability by radiation-induced graft polymerization of fluorinated acrylate monomer, 1H,1H,2H,2H-

nonafluorohexyl-1-acrylate. The radiation by γ-rays for 6 h at room temperature caused formation of radicals on the cotton substrate and in the monomer solution to undergo both the "grafting from" and "grafting to" mechanisms. Water CA on the as-prepared covalently bonded fluoropolymer coating was around 160°, and the droplets firmly attached to the surface: 10 μl droplets could not roll off the surface even when tilted upside down. The coating showed good chemical stability over the entire pH range from 0 to 14. In addition, the surface remained superhydrophobic after overnight immersion in 10% sulfuric acid (H_2SO_4) at room temperature and after treatments with hot solvents such as butane or water. After 50 accelerated laundering cycles, which is equivalent to 250 commercial launderings, hydrophobicity of the modified cotton had slightly decreased, but water CA on the sample was still measured to be greater than 140°. After the laundering, superhydrophobicity of the treated cotton could be easily recovered by extracting the sample in deionized water.

In-situ nanorod/particle growth

Hoefnagels *et al.* [91] formed covalently bonded silica microparticles on cotton textiles by *in-situ* growth process, where the cotton textiles were stirred in the reaction mixture for 6 h at room temperature. Subsequently, the textiles were PDMS-modified or fluorinated using perfluoroalkyl silane to obtain superhydrophobic properties. Water CA and SA for 10 μl droplet on the PDMS-modified surface were measured to be 155° and 15°, respectively. Larger droplets showed smaller SAs, and for *e.g.* 500 μl droplet the SA was less than 2°. The particle adhesion to the cotton substrate was tested by sonicating the sample in an ethanol bath. Any significant changes in the surface wettability were not observed after the sonication treatment, which indicated a good adhesion between the silica particles and cotton fibers. The fluorinated surface showed similar water CA to the PDMS-modified surface, however, in contrast to the PDMS-modified surface, the fluorinated surface also showed oleophobic properties. Sunflower oil CA on the fluorinated surface was 140°, and the oil droplets of 15 μl rolled off the surface at SA of 24°. Hexadecane CA on the fluorinated surface was measured to be 135°, but the droplets were firmly attached to the surface and remained stuck even when tilted upside down.

Xu and Cai [92] coated cotton fabrics with ZnO nanocrystals using a dip–pad–cure process. The curing was carried out at 170°C for 3 min. The dip–pad–cure procedure was repeated three times to obtain a dense film of the nanocrystal seeds on cotton, on which ZnO nanorod array was then hydrothermally grown by immersing the sample in the reagent solution at 90°C for 3 h. After drying at 70°C for 20 min, the ZnO nanorod coated fabric was modified by self-assembled monolayer of n-dodecyltrimethoxysilane (DTMS) to obtain the hydrophobic chemistry. After washing and drying, the sample was finally cured at 120°C for 1 h. Water CA on the as-prepared superhydrophobic surface was measured to be 161° and SA for a 40 μl droplet was 9°.

Leng *et al.* [93] fabricated superamphiphobic cotton textiles based on a multilength-scale roughness from the woven structure of the substrate and two additional layers of micro and nanosized silica particles (Figure 19). The silica microparticles were *in-situ* synthesized on cotton from a solution of TEOS for 6 h at room temperature, and the subsequent silica nanoparticle deposition was carried out in isopropanol dispersion by electrostatic attraction. The

nanoparticle deposition was executed 1–3 times repeatedly, and after each cycle the sample was treated with silicon tetrachloride–toluene solution to improve mechanical robustness of the surface by forming cross-links among the silica particles and cotton substrate. Finally, the surface was modified using perfluoroalkyl silane to obtain the low surface energy chemistry. CAs for 5 μl water and hexadecane droplets on the modified fabrics were measured to be ~160° and ~152°, respectively. In addition, both water and hexadecane droplets easily rolled off the modified fabric surface: SAs for 5 μl, 10 μl, and 20 μl water droplets were around 15°, 10°, and 7°, respectively, while the corresponding values for hexadecane droplets were around 30°, 15°, and 10°, respectively. Mechanical robustness of the modified cotton was evaluated by sonication treatment in ethanol bath, which the sample seemed to tolerate relatively well without any significant changes in its anti-wetting properties.

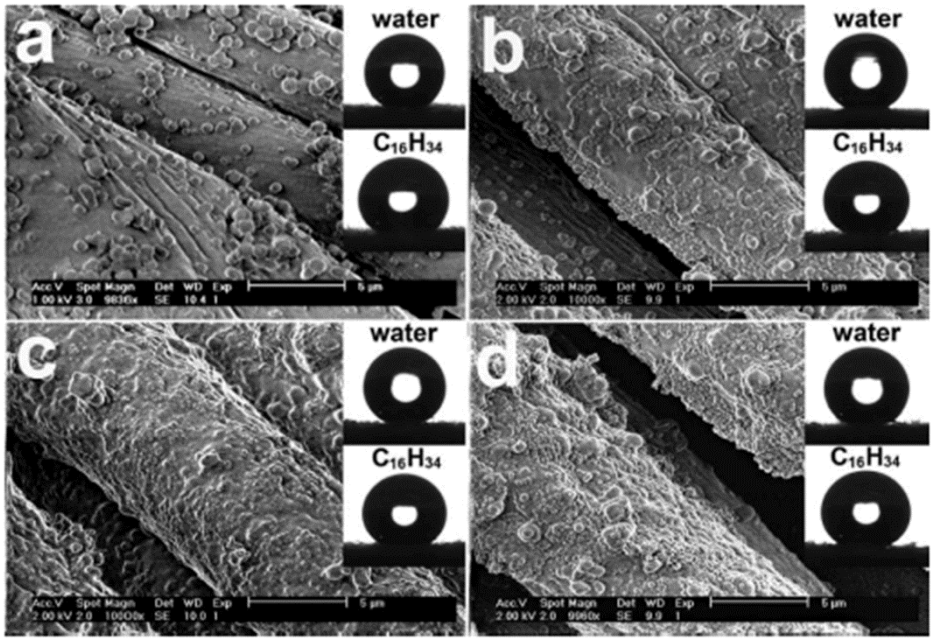

Figure 19. SEM images of superamphiphobic cotton fabrics. (a) Fabric coated with *in-situ* synthesized silica microparticles, and (b) the microparticle coated fabric after 1 cycle of 220 nm silica nanoparticle deposition, (c) after 2 nanoparticle deposition cycles, and (d) after 3 nanoparticle deposition cycles. Insets display shapes of water and hexadecane droplets on the corresponding surfaces [93].

Kivotidi *et al.* [94] fabricated flame-retarded superhydrophobic cellulose-based materials, *e.g.* filter paper and cotton fabrics, by treating the samples with aqueous solutions and supercritical CO_2. In the first step, the samples were immersed in an aqueous solution of calcium chloride ($CaCl_2$) for 40 min, after which the samples were immersed and reacted in an aqueous solution of sodium hydroxide (NaOH) for another 40 min. Followed by the treatments in the aqueous solutions, the samples were exposed to supercritical CO_2 atmosphere at high pressure for 40 min and dried under vacuum. During the multi-step treatment procedure, various salts were produced *in-situ* on the cellulose substrates to form micro-sized particles. The salts contributed to the flame-retardancy of the treated materials by different mechanisms, but, in addition, they increased surface roughness of the substrate materials, which contributed to enhanced water repellency after hydrophobic modification. The hydrophobic surface chemistry was achieved by

dip-coating the samples in a silane–siloxane monomer containing solution for 20 min, after which the samples were left in air atmosphere overnight and dried under vacuum to form a thin silicon-based polymer film on the surface. The as-treated filter paper showed water CAs around 145–154°, and the authors reported easy mobility of the droplets on the surface.

Shateri-Khalilabad and Yazdanshenas [95] fabricated a superhydrophobic and electroconductive graphene–polymethylsiloxane composite coating on cotton. In the first step of the coating procedure, graphene oxide sheets in an aqueous dispersion were deposited on cotton by dip-coating the substrate in the dispersion for 10 min, after which the sample was padded. The dip-coating and padding were repeated three times repeatedly, after which the sample was dried at 70–80°C for 60 min. In the next step, the graphene oxide was chemically reduced to graphene by immersing the sample into a solution of ascorbic acid at 95°C for 60 min, after which the sample was rinsed with water and dried in an oven at 70–80°C for 60 min. The as-prepared graphene coated cotton showed near-superhydrophobic properties with water CA of 143°. In addition, another type of method, so called water shedding angle, was used to characterize wetting properties of the surface. The shedding angle was determined as the smallest inclination of the substrate where water droplets of 10 μl dropped from the needle-to-substrate distance of 2 mm completely rolled off the surface. The shedding angle on the graphene coated cotton fabric was measured to be 41°. Water repellency of the treated fabric could further be improved by growing a layer of polymethylsiloxane nanofilaments (diameter ~30–90 nm) on the sample surface during 15 min of immersion in a solution of methyltrichlorosilane (MTCS) in hexane, after which the sample was washed and dried/cured in an oven at 110°C for 60 min. Water CA and shedding angle on the graphene/nanofilament coated cotton fabric were measured to be 163° and 7°, respectively.

Other methods

Gonçalves *et al.* [96] reported on fabrication of superhydrophobic coating on filter paper using a multi-step nanoengineering process. In the first stage, the surface roughness of paper was increased by depositing amorphous silica particles (~800 nm in diameter) on the surface of cellulose fibers in an aqueous suspension. After the particle deposition, the surface roughness and stability were further enhanced by layer by layer (LbL) deposition of poly(diallyldimethylammonium chloride) (PDDA) and sodium silicate (SS). The LbL deposition was accomplished by immersing the sample 5 times repeatedly in PDDA and SS solutions for 15 min. After each step, the sample was washed and dried in a nitrogen flow. Finally, the surface was modified with fluorosiloxane in ethanol solution, dried, and cured at 120°C for 2 h. Two different types of fluorosiloxanes were used in the surface modification, 3,3,3-trifluoropropyl trimethoxysilane and 1H,1H,2H,2H-perfluorooctyl triethoxysilane, from which the latter gave better hydrophobic properties for the surface with water CA of 147°. That is, the surface showed near-superhydrophobic properties according to the classical definition of superhydrophobicity. Interestingly, the study revealed that when small silica particles of ~100 nm or ~300 nm in diameter were used instead of the large particles of ~600 nm and ~800 nm in diameter, any increment in the hydrophobicity of the modified cotton was not observed compared to a sample modified solely with the fluorosiloxane without the presence of any silica particles.

Georgakilas *et al.* [97] described a procedure to prepare perfluorinated CNTs to be used in superhydrophobic coatings. The authors demonstrated a fabrication of superhydrophobic CNT coating on cotton by adding droplets of the fluoro-modified CNTs dispersed in hexafluoro-isopropanol on the fabric, after which the sample was dried overnight at 80°C. Water CA and SA on the CNT coated cotton were reported to be 170° and < 5°, respectively.

Yang and Deng [98] applied multilayer deposition of silica particles on paper substrate by dipping the sample repeatedly in aqueous suspensions of polydiallyldimethylammonium chloride and silica particles for 20 min and 10 min, respectively. Chemical modification of the silica coated paper sample was carried out by CVD of perfluorooctyltriethoxysilane (POTS) at 125°C for 2.5 h, after which the sample was treated another 2.5 h at 150°C to volatilize the unreacted POTS molecules from the surface. Water CA and SA of 155° and < 5°, respectively, were measured on the silica coated paper surface. The CA remained above 150° even after the specimen was kept fully immersed in water for 72 h. Unlike uncoated paper, the superhydrophobic paper could maintain its tensile strength also in humid conditions. In addition, the authors reported reduced contamination of bacteria from an aqueous solution on the superhydrophobic surface.

Hu *et al.* [99] used commercial PCC particles, hydrophobic stearic acid, and polymer latex particles to fabricate superhydrophobic coating on linerboard paper. Application of the coating slurry was carried out by a simple rod wire coater, after which the sample was dried for 3 min by heating with an IR lamp. The optimized ratios of different compounds in the coating led in decent hydrophobicity with water CAs close to 150°. However, in order to reach CAs greater than 150°, the coated paper was further dipped in potassium stearate, rinsed with water, and dried. In addition to the increased CA, the dipping treatment remarkably decreased water absorption (Cobb value) of the coated paper.

Huang *et al.* [100] fabricated superhydrophobic paper using TiO_2 nanoparticles (10–20 nm in diameter) modified with 3-(trimethoxysilyl) propyl methacrylate (MPS). Cellulose fibers were treated with the modified nanoparticles already in the pulp, and thus any type of further treatments were not needed after preparation of the paper handsheets. This was apparently the first study, where a superhydrophobic modification was applied to cellulose fibers prior to the papermaking process. Water CA, CAH, and SA of 154°, 4°, and < 3°, respectively, were measured on the as-prepared paper. In addition to the enhanced water repellency, the nanoparticle modification improved opacity of the paper, but, on the other hand, decreased its tensile strength.

Stanssens *et al.* [101] synthesized organic nanoparticles by imidization of poly(styrene-maleic anhydride) copolymers in aqueous dispersion or in presence of palm oil and applied them as hydrophobic coatings on papers by a standard rod-coater. The coatings were dried at 100°C for 2 min and subsequently stabilized for at least one day. The nanoparticles synthesized in presence of palm oil gave more continuous coating, lower water absorption rate, and greater

hydrophobicity compared to the particles synthesized in aqueous solution. The authors reported near-superhydrophobic water CA of 148° on the nanoparticle/oil coated tissue paper.

Fang *et al.* [102] fabricated superhydrophobic coatings on various substrates, including filter paper and cotton fabric, using a magnet-assembly technique. Hydrophobic iron oxide (Fe_3O_4) nanoparticles synthesized and functionalized with tridecafluorooctyl triethoxysilane in aqueous solution were deposited on the substrates under a magnetic field. After removal of the solvent by drying in atmospheric conditions, the nanoparticle coating appeared as a hierarchically structured surface composing of aggregated particles of about 10 nm in diameter. Water CAs on the as-prepared coating on filter paper and cotton fabric were measured to be 171° and 165°, respectively. When the nanoparticle coating was deposited without the magnetic field, the particles were distributed more homogenously on the substrate, and thus the superhydrophobic properties were not achieved due to reduced hierarchical roughness of the surface.

Zhao *et al.* [103] coated cotton fabrics using LbL assembly of azido-functionalized silica nanoparticles (~70 nm in diameter) and azido-grafted poly(allylamine hydrochloride). The fabrics were sequentially dipped in the aqueous reagent solutions for 5 min and washed with water. UV-irradiation was used to improve coating durability by inducing covalent cross-linking within the photoreactive coating layers and the substrate. Hydrophobic chemistry for the coating was obtained by treating the sample with a solution of tridecafluorooctyl triethoxysilane in hexane for 1 h, after which the coating was dried at 100°C for 30 min. Water CA on the multilayer coated fabric was measured to be 158°, and the coating showed good chemical resistance against various organic solvents and aqueous solutions of wide range of pHs. In addition, the coating could withstand several washing cycles, which was demonstrated by the high water CA of > 150° after 50 washing cycles and low CAH of < 10° after 25 washing cycles.

Zhang *et al.* [104] fabricated an OTS-modified silica particles (mean particle diameter ~243 nm) containing PS solution to form a superhydrophobic coating on filter paper. The coating mixture was applied on the paper substrate by dropping several droplets of the solution on the sample surface, after which the sample was dried at 75°C for about 20 min. The coating solution which had the mass ratio of the modified silica particles to PS of 2:1 resulted in the best hydrophobic properties of the coating with water CA of 156°. In addition to the good water repellency, the coating showed good repellency for aqueous solutions of wide pH range with CAs greater than 140°.

1.3.3. Fabrication by dry methods

Plasma processing

Balu *et al.* [26] fabricated a superhydrophobic surface on commercial copy-grade paper and hand-made sheets by the means of plasma etching and plasma deposition. In the first step of the procedure, amorphous areas of the cellulose fibers were etched by low-pressure oxygen plasma for 30 min to modify the surface roughness, and in the second step, to obtain a thin low surface energy fluorocarbon layer on the etched substrates, the samples were coated in vacuum by

PECVD for 2 min using pentafluoroethane (PFE) as a precursor. After the plasma modification, both paper grades were superhydrophobic with water CAs > 160° and CAHs < 10°. The PFE-film adhesion to the substrate was evaluated by a standard tape test, which caused cohesive failure in the paper substrate and thus indicated a good adhesion between the PFE-film and cellulose fibers. In addition, robustness of the superhydrophobic surface was evaluated by pressing the paper sample by a bare finger, which caused a slight decrement in the superhydrophobic properties of the surface as the CA on the handsheet paper decreased from 167° to 157° and CAH increased from 3° to 21°. In another study, Balu *et al.* [14] demonstrated that the hysteresis behavior of the modified paper surface could be drastically altered by affecting the hierarchical structure of the substrate by the plasma etching (Figure 20). Droplet adhesion to the modified paper could be altered between the sticky and roll-off states, and CAH on the surface could be tuned between 150° and 3.5° by simply adjusting the plasma etching time.

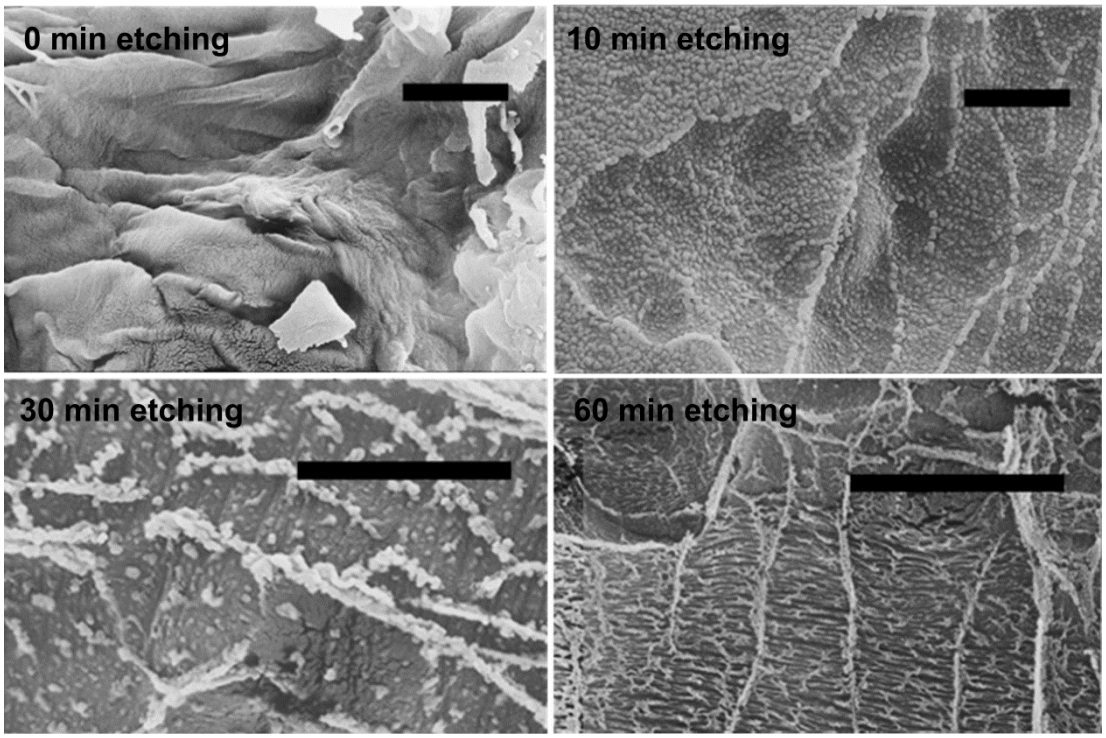

Figure 20. SEM images of paper surface after different periods of oxygen plasma etching and PFE plasma deposition of 2 min. The scale bars correspond to 2 μm [14].

Cho *et al.* [105] treated filter paper and cotton fabrics by low-pressure hexamethyldisiloxane (HMDSO)/toluene plasma to render them superhydrophobic. The plasma treatment time was fixed at 30 s. The study revealed that HMDSO/toluene mixing ratio of 3:1 increased surface hydrophobicity more efficiently than other mixture ratios. The plasma-modified paper and cotton surfaces showed superhydrophobic properties with water CAs of 157° and 173°, respectively.

CVD and nanofilament growth

Artus and Zimmermann *et al.* [106, 107] applied a transparent and superhydrophobic silicone nanofilament coating on cotton and other types of fabrics (Figure 21). A dense layer of polyalkylsilsesquioxane filaments was grown on the surface of individual fibers in one-step process in gas phase under ambient pressure and temperature. To form the coating, the substrates were placed in a sealed chamber for 12 h to react with trichloromethylsilane (TCMS) precursor and water vapor. Water CA and SA for 10 µl droplets on coated cotton were measured to be > 150° and < 30°, respectively. However, difficulties in determination of the baseline on the uneven substrates and individual sticking fibers hinder reliability of the traditional CA and SA measurements, and therefore, wetting properties of the coated samples were studied also by water shedding angle (13 µl droplets were dropped from the height of 1 cm). The shedding angles of the coated cotton samples varied between 25° and 35°, depending on the type of the cotton substrate. As a drawback, the authors reported that the coating treatment dramatically reduced tensile strength of cotton, which limits its use in any real applications. Similar weakening effect, which was observed on coated cotton fabrics, did not occur on coated poly(ethylene terephthalate) (PET) fabrics, on which extensive durability experiments, *e.g.* abrasion and laundering tests, were performed and material properties were carefully evaluated.

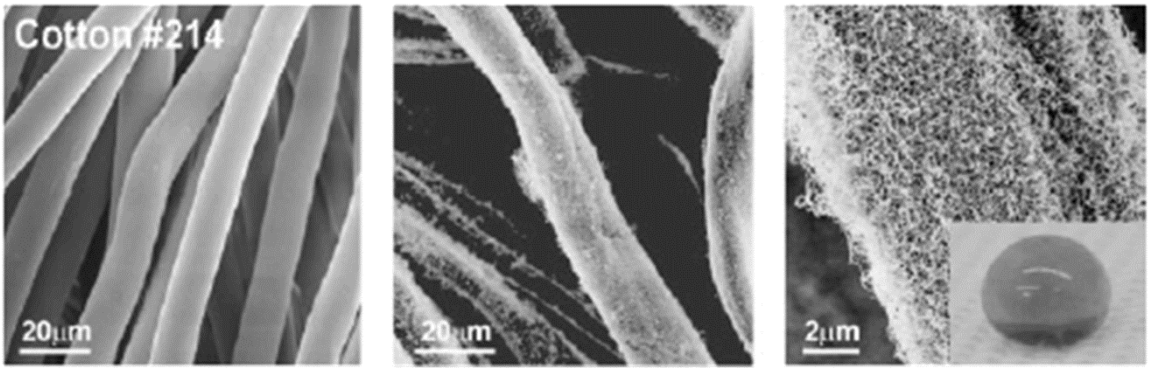

Figure 21. SEM images of cotton fabrics: left: uncoated fabric; middle and right: silicone nanofilament coated fabric. Inset shows water droplet on the coated fabric [107].

Jin *et al.* [108] fabricated nanocellulose aerogels consisting of fibrillar networks and structures at different length scales by freeze-drying the hydrogel in vacuum. To obtain superhydrophobic and superoleophobic properties, the aerogel membranes were fluorinated by CVD of FOTS at 70°C for 2 h. Water CA on the fluorinated membrane was 160° and the surface showed high-adhesive properties as 10 µl water droplet could remain on the surface when tilted upside down. In addition, the surface showed good oleophobicity as the CAs of 153° and 158° were measured for paraffin oil and mineral oil, respectively. Similar to water, the oil droplets were firmly attached to the surface. The authors highlighted the aerogel made of nanocellulose as particularly simple and scalable approach to fabricate overhang structures, which are known to promote superoleophobicity. Plastron layer, *i.e.*, the layer of entrapped air on the surface, could be seen even after 1 week of immersion of the fluorinated aerogel both in water and oil.

Cervin *et al.* [109] freeze-dried aqueous dispersions of nanocellulose in vacuum to obtain highly porous aerogels (porosity > 99%) to be used in oil/water separation (Figure 22). To obtain the

hydrophobic surface chemistry, the aerogels were treated by vapor deposition of octyltrichlorosilane for 30 min. After the silanization, the surface showed superhydrophobicity with water CA of approximately 150° and superoleophilicity with hexadecane CA of 0°. The authors did not give exact values, but reported that water droplets easily rolled off the aerogels when slightly inclined.

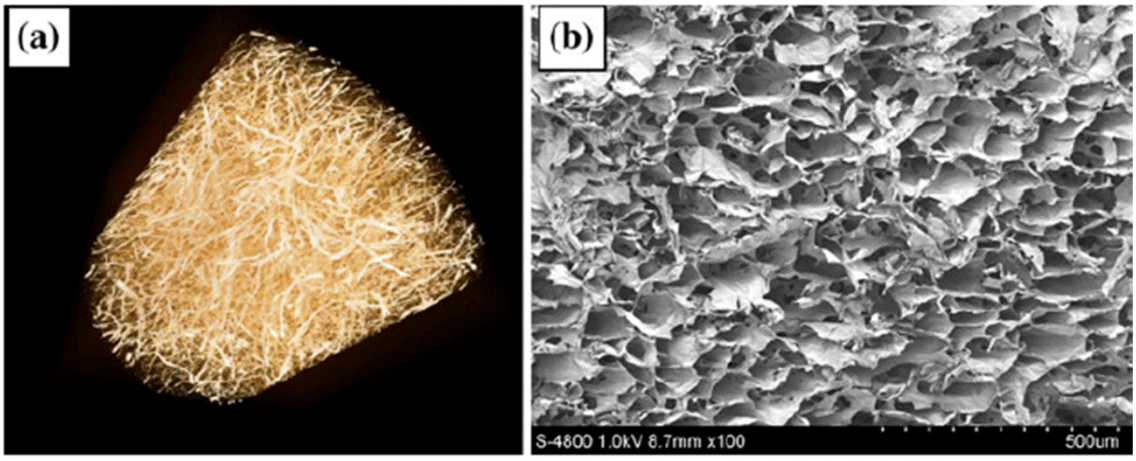

Figure 22. (a) 3-D microtomography image and (b) SEM image of nanofibrillated cellulose aerogel [109].

Other methods

Daoud *et al.* [110] utilized pulsed laser deposition to fabricate thin PTFE films on cotton fabrics. The film deposition was carried out in vacuum at room temperature, and the deposition time was about 3 min. The PTFE coated fabrics showed superhydrophobic properties with water CA of 151°. SEM imaging revealed that the PTFE film on cotton had a granular surface structure where the grain size was about 50–70 nm in diameter. This was apparently the first straightforward one-step approach to fabricate a superhydrophobic coating on cotton. That is, any type of chemical modification, drying, or curing steps were not needed after application of the coating.

Quan *et al.* [111] used a rapid expansion of supercritical CO_2 solution (RESS) process to fabricate fractal AKD coatings on paper. The flake-like AKD particles with an average size of 1–2 μm were formed as a result of an extremely fast phase transfer when the solution expanded from the supercritical to the gas-like state when sprayed on the substrates in atmospheric conditions. Water CA on paper coated with AKD flakes was 153°. In the case that paper surface was roughened with an emery cloth prior to the AKD coating, the CA was measured to be as high as 172°. Apparently, this was the first study where a superhydrophobic coating was fabricated on paper by straightforward one-step method without any additional steps. In another study [112], the same group examined hysteresis properties of the AKD coated paper surfaces. The advancing contact angles on the surfaces varied between 150° and 160°, while the receding contact angles were between 110° and 130°. The lowest CAH values were measured to be approximately 30° on the AKD coated surfaces.

Zhang *et al.* [113] presented a solvothermal synthesis of nanoporous polydivinylbenzene (PDVB) powder and demonstrated an innovative approach to apply the superhydrophobic nanopowder coating on various substrates. The as-prepared PDVB powder took a form of a solid monolith, by which the substrates were simply wiped to paint the superhydrophobic and transparent nanoporous polymer coating. Attachment of the polymer powder on the rough paper surface occurred by the electrostatic interaction, and average thickness of the coating was estimated to be ~10 μm. Water CA on the polymer coated paper was 157° and droplets could roll off the surface at SA of 6°. The superhydrophobic properties of the coating remained stable during the long-term follow-up period of a single water droplet as the CA decreased only 3° in 24 h. In addition, the superhydrophobic properties of the coating were reported to remain stable also in humid conditions.

1.3.4. Potential applications

A superhydrophobic coating on paper or cotton textiles brings new properties and functionalities for the materials and widens their utilization potential in new application areas. Superhydrophobic paper can find use, for example, in water-repellent packaging materials, *e.g.* food and beverages, in self-cleaning labels, cartons, and boards, or as membranes with low degree of surface fouling [14, 26, 89]. Applications for superhydrophobic cotton include liquid- and dirt-repellent, breathable, and self-cleaning clothes and textiles. In addition, superhydrophobic paper and cotton have good utilization potential in some other important applications such as cheap and disposable microfluidic devices for, for example, point-of-care diagnostics [26, 70, 114].

Balu *et al.* [115] fabricated two-dimensional paper-based lab-on-a-chip (LOC) microfluidic devices by printing high surface energy black ink patterns on superhydrophobic paper substrate. The ink patterns provide local control over droplet adhesion on the superhydrophobic paper, and thus enable storage, transport, mixing, sampling, and splitting of droplets of test liquids on the surface. Barona and Amirfazli [87] demonstrated a simple way to control water droplet mobility and hysteresis on paper-based LOC devices by printing solid grey patterns of different intensities on superhydrophobic paper surface. Li *et al.* [116] demonstrated how test liquids could be sampled in a controlled manner by printing high hysteresis wax islands onto low hysteresis superhydrophobic paper. The volume of the sampled droplets could be controlled by the choice of the wax type, and by the surface roughness and size of the wax islands. The authors highlighted point-of-care biomedical testing as a potential application for the paper-based LOC devices, and demonstrated a colorimetric glucose test performed with the high hysteresis islands on superhydrophobic paper.

Another suitable application for superhydrophobic paper is oil separation from water. For instance, Huang *et al.* [83] suggested that superhydrophobic paper could be used in automobile oil filters. Wang *et al.* [81] fabricated superhydrophobic filter paper capable of selectively absorb and separate liquids that differ in surface tension. The modified filter paper could absorb diesel oil and organic solvents floating on water up to 3.4 times of its own weight. By removing the absorbed oil or organic solvent from the filter paper by drying it in an oven at 80°C, the

filter paper could be reused several times and the absorption capacity and water CA on the surface remained nearly unchanged. The modified filter paper could efficiently separate oil/water mixtures of different volume ratios by letting oil permeate through the paper while water remained on the surface. Interestingly, the modified filter paper could also be used to extract ethanol from homogeneous aqueous solutions. Cervin *et al.* [109] utilized superhydrophobic ultra-porous nanocellulose aerogels as separation medium for oil/water mixtures. The aerogels had porosity greater than 99%, and their absorption capacity of hexadecane was up to 45 times of the aerogel weight. The aerogels could be reused several times as they did not show significant change in volume upon sorption/desorption cycles.

Jin *et al.* [108] fabricated superhydrophobic and superoleophobic nanocellulose aerogel membranes to be used as bioinspired cargo carriers on water and oil. On water, the aerogel was capable of supporting a load over 500 times its own weight. On oil, the aerogel could support a load over 300 times its own weight. The authors envisaged the aerogel membranes as foul-resistant and gas permeable carriers and coatings for miniaturized robots or environmental gas sensors floating on practical liquids.

2. Aims of the study

The purpose of this work is to examine suitability of thermal nanoparticle synthesis method called liquid flame spray (LFS) in roll-to-roll coating of cellulose-based materials such as paper, pigment coated board, and extrusion-coated paper. Suitable LFS processing parameters for roll-to-roll coating of various types of cellulose-based substrates are explored, and properties and functionalities of the novel nanoparticle coatings are studied with focus on surface wettability, especially on superhydrophobicity. In addition, potential applications for the LFS-coated cellulose-based materials in the field of surface wetting are explored.

The main research topics in the original publications were as follows:

In publication 1, LFS roll-to-roll nanoparticle coating method was introduced and effects of the processing parameters in fabrication of superhydrophobic TiO_2 coating on paperboard substrate were examined. In addition, an overview of the coating structure and properties was given. Publication 2 focused on finding suitable processing parameters to fabricate superhydrophilic and superhydrophobic SiO_2 and TiO_2 coatings, respectively, on different cellulose-based substrate materials. In addition, phenomena related to different wettability of the coatings were examined. In publication 3, hierarchically structured superhydrophobic TiO_2 coatings were examined, and the effect of different structural dimensions on water droplet adhesion and hysteresis on the coatings was studied. In publication 4, liquid-repellency of different hierarchical coatings on paper and board using water–ethanol solution as a probe liquid was examined. Publication 5 focused on photocatalytic self-cleaning effect and the related reversible wettability conversion on superhydrophobic TiO_2 coating.

3. Materials and methods

LFS-coating procedure

The LFS-coating was carried out roll-to-roll in ambient conditions at the Tampere University of Technology (TUT) on the Paper Converting and Packaging Technology (PCPT) pilot line. Pigment coated board (200 g/m^2, Stora Enso), machine glossed paper (83 g/m^2, UPM), and LDPE extrusion-coated paper (15 g/m^2 of LDPE on the machine glossed paper) were used as substrate materials for the nanoparticle coatings. The SiO_2 and TiO_2 nanoparticle coatings studied in this work were fabricated using the fixed parameter combinations presented in Table 1.

Table 1. Fixed parameter combinations used in the LFS-coating.

parameter set	precursor feed rate (ml/min)	burner-to-substrate distance (cm)	line speed (m/min)
1	32	15	50
2	12	15	50
3	12	6	50

Tetraethyl orthosilicate (TEOS, 98% pure, Aldrich) and titanium tetraisopropoxide (TTIP, 97% pure, Aldrich) diluted in isopropanol with the concentration of 50 mg (atomic metal)/ml were used as the precursors for the SiO_2 and TiO_2 coatings, respectively. Hydrogen and oxygen with the flow-ratio of 50/15 l/min were used as the combustion gases in the coating process. The aerosol synthesized TiO_2 nanoparticles made by LFS are mainly of anatase crystal structure [117][R5].

Water contact angle

Water CA measurements were performed in a conditioned room in ambient conditions of 23ºC/50% relative humidity (RH) using distilled water and KSV CAM200 equipment (KSV Instruments Oy, Finland). CA was determined 3 seconds after the droplet placement onto the sample. Unless mentioned otherwise, the droplet volume of 2 µl was used in this study, and the given CAs are average values measured from 5 droplets. The given error margins indicate standard deviation. During ageing the samples were stored in the dark in a conditioned room at 23ºC/50% RH.

FEG-SEM

Zeiss ULTRAplus field emission gun scanning electron microscope (FEG-SEM) was used for imaging the nanoparticle coatings. The samples were sputter coated with thin gold or carbon films prior to the FEG-SEM imaging to obtain conductivity.

TEM

Transmission electron microscopy (TEM) of TiO_2 nanoparticles was performed with JEOL JEM-2010 instrument. TEM grid (lacey carbon film on copper grid, Agar) was attached on the board substrate with a staple aligned with the moving direction of the web, and the TiO_2

particles were collected on the grid during the normal on-line coating procedure of the board substrate.

XPS

X-ray photoelectron spectroscopy (XPS) experiments were performed by PHI Quantum 2000 instrument (Physical Electronics Instruments, USA) equipped with a monochromatic Al Kα X-ray source and operated at 25 W. The charge compensation was enhanced by combination of electron flood and ion bombarding. The take-off angle was 45º in relation to the sample surface. The survey spectra were recorded with the pass energy of 184 eV from 3 different points with diameter of approximately 100 µm. Pressure in the main chamber was maintained at 2×10^{-7} Torr during spectra acquisition.

UV-illumination

UV-illumination was carried out with a lamp (Bluepoint 4 ecocure, Hönle UV Technology, Germany) providing the central wavelength of 365 nm with the filter of 320–390 nm. Illumination intensity was 50 mW/cm^2. The artificial daylight illumination was accomplished by GTI MiniMatcher illumination system (model MM-1UV/65, GTI Graphic Technology Inc., USA). Both illuminations were carried out in ambient conditions. The subsequent XPS and CA experiments were performed instantly after removing the samples from the illumination to minimize the surface contamination and other possible changes occurring after the illumination.

Heat treatment

Heat treatment of the samples was carried out in Firlabo Air Concept oven equipped with fan circulation. After placing the samples in the oven the real temperature in the oven decreased momentarily below the set value, but was rapidly restored within approximately 1 min. The CA measurements on the heat treated samples were carried out as soon as the sample had cooled down to room temperature.

4. Results and discussion

4.1. Fabrication of superhydrophilic and superhydrophobic coatings

In the LFS process, liquid precursor is fed together with the combustion gases (hydrogen and oxygen) into a specially designed spray gun to form solid nanoparticles. Instantly after exiting the burner nozzle, the precursor solution is atomized to micrometer-sized droplets by the high-velocity hydrogen flow. Liquid droplets evaporate in a hot and turbulent flame, and subsequent reactions in the precursor vapor lead to formation of nanoparticles and nanoparticle aggregates of desired material by nucleation, condensation, coagulation, coalescence, and agglomeration [117-121]. Adaptability and simplicity are among the greatest benefits of the LFS coating method. Thus, different types of substrates can be coated with wide selection of materials and compositions of the coatings. Typically, metal salts or organometallic compounds diluted in water or organic solvents such as isopropanol or xylene are used as precursors in the LFS process to form metal, oxide, and composite nanoparticles of size varying from 2 to 200 nm. The particle size can be controlled by the processing parameters, for example through feed rate of the precursor material. As is demonstrated in Figure 23, the greater feed rate of the precursor material and longer burner-to-substrate distance of the processing parameter set 1 (see Table 1) yield to greater average size of the produced TiO_2 particles compared to the particles produced with the parameter set 3.

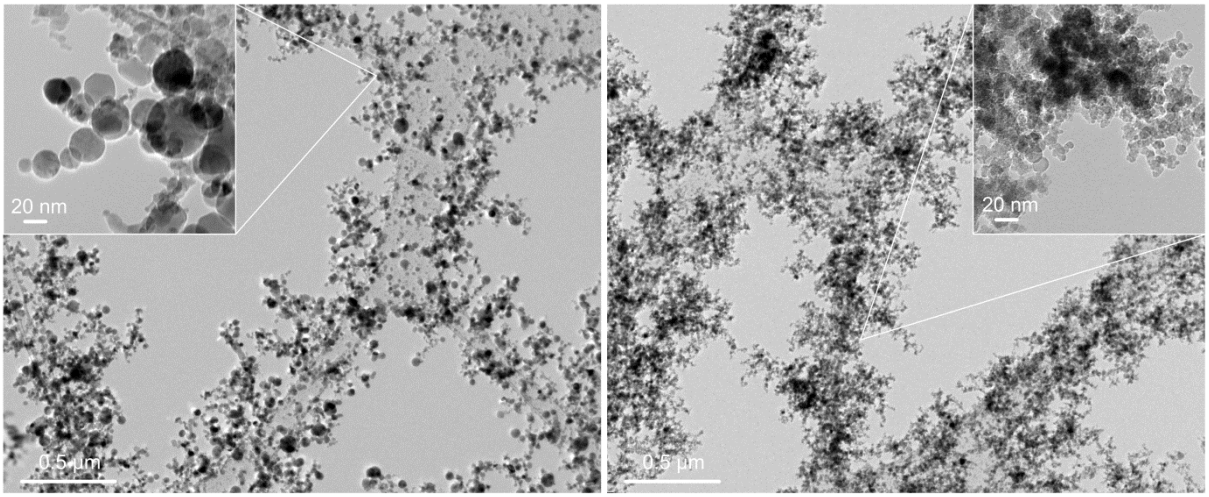

Figure 23. TEM micrographs of TiO_2 particles collected during the LFS on-line coating procedure. The effect of processing parameters on the produced particle size is clearly visible (left: parameter set 1, right: parameter set 3 [P5]).

In the LFS roll-to-roll coating procedure (Figure 24), flame synthesized nanoparticles are directly deposited on the substrate in ambient conditions to form a highly porous coating layer composed of nanoparticles and nanoparticle aggregates [P1, R2, R3]. Instead of impaction, which is typical for conventional spray-coating techniques where droplet or particle size is in the range of micrometers, in the LFS-coating the nanoparticle deposition on the substrate occurs by thermophoresis and diffusion [R3]. Adjustable processing parameters in the LFS roll-to-roll coating procedure include flow rates of the combustion gases, concentration and feed rate of the

precursor solution, burner-to-substrate distance, and line speed [P1]. Typical coating thickness is < 1 µm, the amount of coating is < 100 mg/m^2, and the estimated yield of the process, *i.e.*, the number of deposited nanoparticles, is ~7–23% depending on the substrate and the processing parameters [P1, P2, R3]. Any type of additional chemical modification, drying, or curing steps are not needed to obtain nanoparticle coatings with functionalities such as permanent superhydrophilicity or superhydrophobicity. Such straightforward one-step methods to fabricate superhydrophobic surfaces are extremely rare. In this section, selected results of the thesis work are presented and discussed. More comprehensive results and detailed discussions can be found from the attached publications [P1-P5].

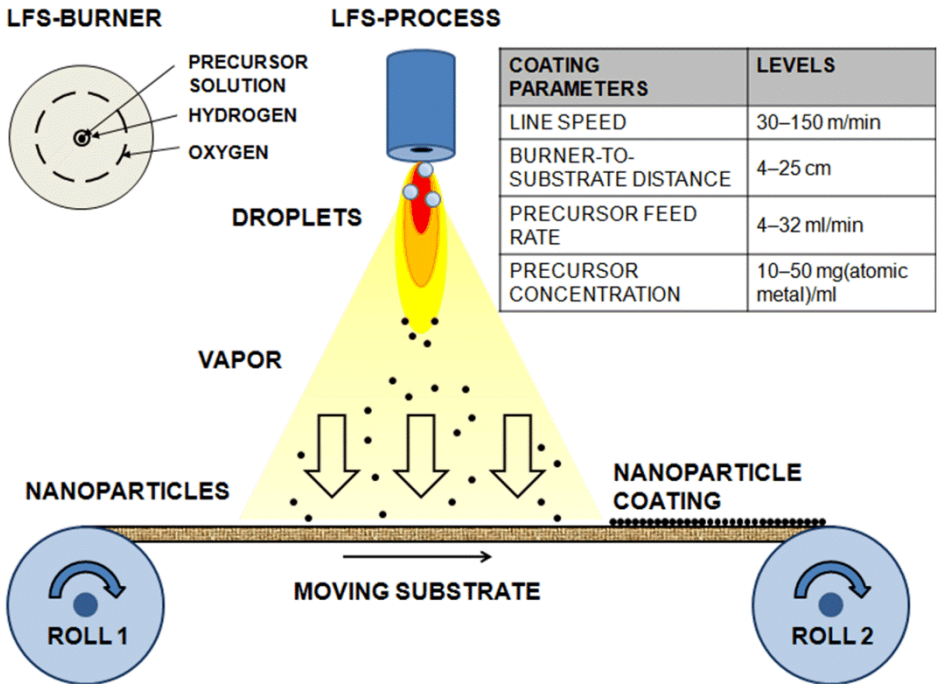

COATING PARAMETERS	LEVELS
LINE SPEED	30–150 m/min
BURNER-TO-SUBSTRATE DISTANCE	4–25 cm
PRECURSOR FEED RATE	4–32 ml/min
PRECURSOR CONCENTRATION	10–50 mg(atomic metal)/ml

Figure 24. LFS roll-to-roll coating procedure and typical parameters [P1].

While this work focuses on wettability manipulation of cellulose-based substrate materials by SiO_2 and TiO_2 coatings and reviews only some wettability related functionalities, at this point it is worth emphasizing that LFS has strong potential to introduce several other functionalities for cellulose-based and other materials. These include many well-known effects such as self-cleaning, anti-fogging, anti-icing, and anti-biofouling which are related to surface wettability [13, 15-17], and other functionalities such as anti-bacterial properties with silver and TiO_2 [82, 122], UV-barrier with TiO_2 and CeO_2 [79, 123], magnetic properties with iron oxide [102, 124], and several catalytic properties with, for example, TiO_2, gold, palladium, and platinum [125-127].

Figures 25–27 show some representative SEM micrographs of cellulose-based substrates coated with the different LFS parameter combinations (parameter sets 1–3). From these images it can be seen that the hierarchical coating structure is composed of (i) individual nanoparticles which create the finest roughness-scale for the coatings; (ii) particle aggregates; and (iii) roughness of the substrate. Figure 25 shows that the SiO_2 and TiO_2 nanoparticle coatings fabricated with the

same processing parameters (parameter set 1) appear very similar and, in both cases, fully cover the pigment coated board substrate. Water CAs on the corresponding SiO_2 and TiO_2 coatings were measured to be 12° and 156°, respectively [P2].

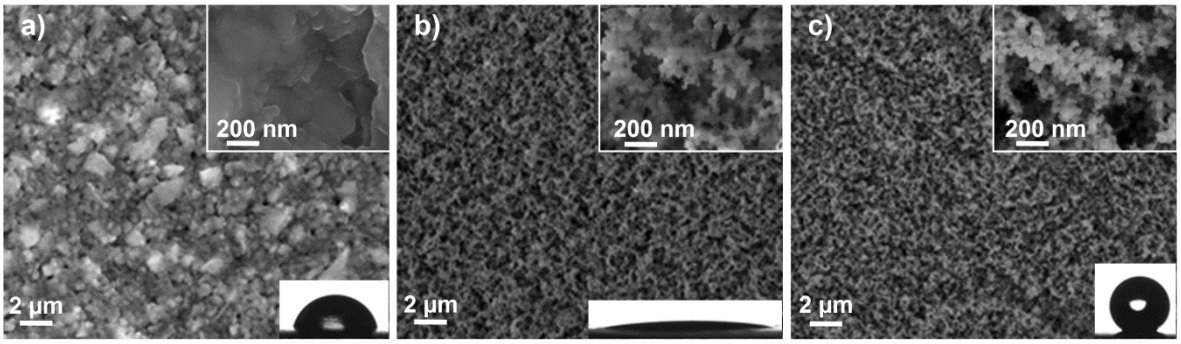

Figure 25. SEM micrographs of the pigment coated paperboard (a) before and after the (b) SiO_2 and (c) TiO_2 nanoparticle coating (parameter set 1). Water CAs on the corresponding surfaces were 77°, 12°, and 156°, respectively (insets show shapes of water droplets on the surfaces) [P2].

Figure 26 demonstrates how the coating deposition on rough paper substrate can be controlled by altering the distance between the burner face and substrate: with 15 cm burner-to-substrate distance (parameter set 2) it is possible to deposit nanoparticles mainly on topmost fibers of the paper surface (Figure 26b,e), while 6 cm burner-to-substrate distance (parameter set 3) contributes to nanoparticle deposition also in the cavities between the topmost fibers (Figure 26c,f) [P2].

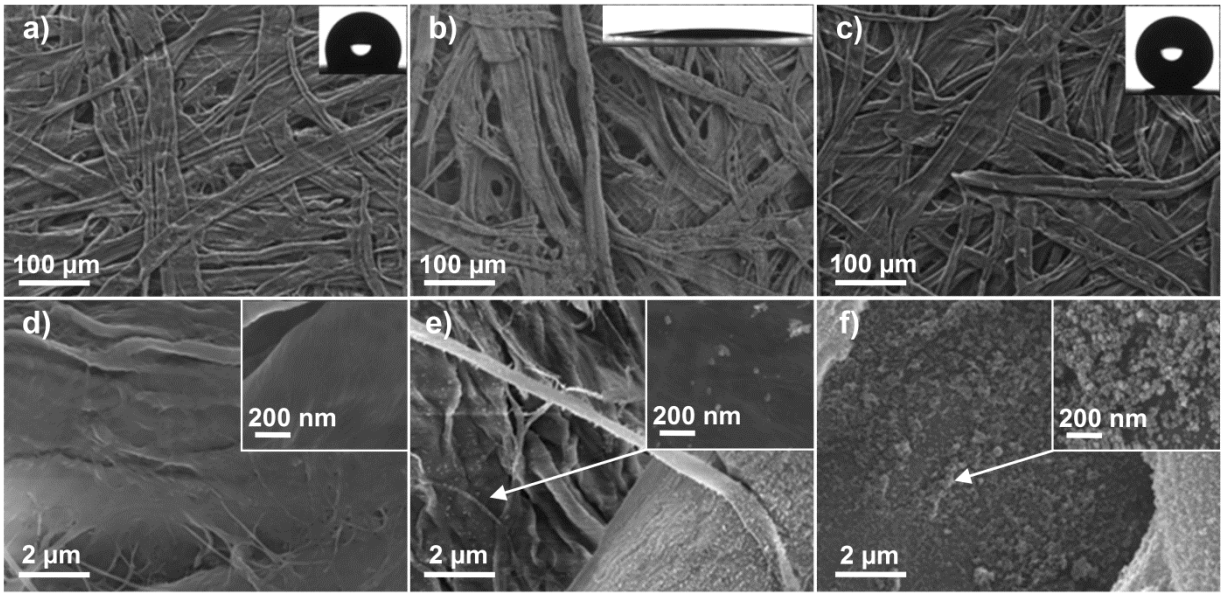

Figure 26. SEM micrographs of the paper surface (a, d) before and after the (b, e) SiO_2 and (c, f) TiO_2 nanoparticle coating (parameter set 2 for the SiO_2 and parameter set 3 for the TiO_2 coating). Water CAs on the corresponding surfaces were 120°, 7°, and 164°, respectively (insets show shapes of water droplets on the surfaces) [P2].

In case of polymer laminate substrates such as LDPE or PET coated paper, the polymer surface can slightly melt and deform due to heat of the flame, which can result to partial penetration of particles into the polymer and uneven coating layer [P2]. However, relatively homogeneous coating layer of nanoparticles with decent coverage of the substrate can be deposited also on polymer laminates by selecting suitable processing parameters (Figure 27) [P2, P3]. Coverage of a polymer surface by nanoparticle coating can further be improved by increasing the number of the coating layers and, for example, by double coating the substrate both superhydrophilic and superhydrophobic surfaces with water CAs lower than 10° and greater than 150°, respectively, can be fabricated on polymers such as LDPE and PET.

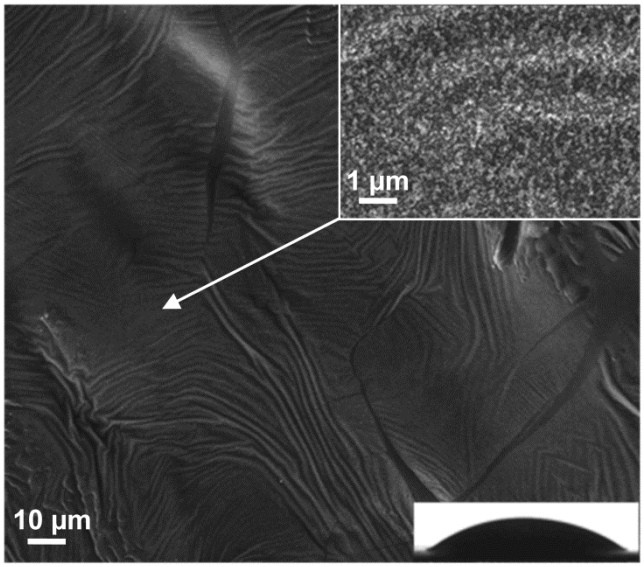

Figure 27. SEM micrographs of LDPE surface after coating with SiO_2 nanoparticles (parameter set 2). Water CA on the corresponding surface was 33° (inset shows shape of water droplet on the surface) [P2].

4.2. Surface chemistry of the coatings

The different wettability of the SiO_2 and TiO_2 coatings is mainly due to differences in the surface chemistry of the two coating materials. XPS experiments revealed that the amount of carbonaceous material, which spontaneously accumulates on the high surface energy oxides during the coating process, is much lower on the SiO_2 coating than on the TiO_2 coating [P2, R4]. The relative numbers of carbon (C) atoms on the SiO_2 and TiO_2 coatings (parameter set 1) were ~28% and ~46%, respectively (Figure 28). Surface coverage of the oxide coatings by the carbonaceous material can be evaluated by comparing the relative number of carbon atoms to the relative number of silicon (Si) and titanium (Ti) atoms detected on the coatings. The C/Si ratio on the SiO_2 coating was 1.5, while the C/Ti ratio on the TiO_2 coating was as high as 3.9. Consequently, the surface of the SiO_2 coating remains hydrophilic, while accumulation of the carbonaceous low surface energy material on the TiO_2 coating turns the surface hydrophobic.

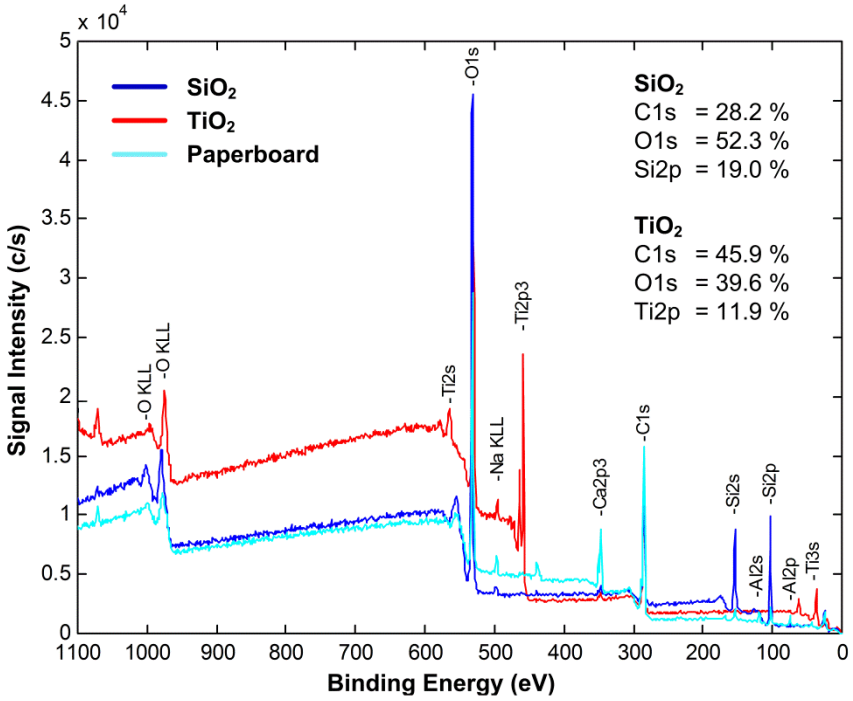

Figure 28. XPS survey spectra of the SiO_2 and TiO_2 nanoparticle coatings on pigment coated paperboard substrate (parameter set 1) and relative concentrations of the most common elements on the surfaces [P2].

Accumulation of carbonaceous material such as hydrocarbons on SiO_2 and TiO_2 cannot be avoided in ambient conditions. In fact, Kanta *et al.* [54] demonstrated that TiO_2 surface suffered a noticeable contamination by hydrocarbons even in vacuum. In the LFS coating process, possible origin of the carbonaceous material on the oxide coatings include precursor materials, evaporating compounds from the substrate material, and atmospheric compounds [P5, R5]. It seems reasonable that the different accumulation rate of the carbonaceous material on SiO_2 and TiO_2, and thus the different wettability of the SiO_2 and TiO_2 nanoparticle coatings, is because of the fundamental differences between the oxide materials as was first proposed by Takeda *et al.* [128]. That is, the number of OH-groups, which are known to act as good adsorption sites for organic compounds [129-133], is greater on TiO_2 than on SiO_2.

As it is clear by now, surface roughness is a necessary condition for superhydrophobicity, because water CAs greater than ~120° cannot be reached on any known smooth solids. Instead, surface roughness is not a necessary condition for superhydrophilicity, but water CAs close to 0° can be reached on carefully cleaned smooth surfaces of high surface energy materials such as SiO_2 and TiO_2 [54, 128]. However, surface roughness is a vital characteristic for permanent superhydrophilicity. On smooth solids, superhydrophilicity is only a temporary condition because of the surface contamination by atmospheric low surface energy compounds. Both the superhydrophilic and superhydrophobic properties of the nanostructured LFS-made SiO_2 and TiO_2 coatings, respectively, were permanent during a storage period of 6 months in the dark in ambient conditions of 23°C/50% RH [P5, R7].

4.3. Functional superhydrophobicity

High- and low-adhesive superhydrophobicity

Structure and properties of the superhydrophobic TiO_2 coatings can be altered by the processing parameters and selection of the substrate material [P3, P4]. The final coating structure depends on the particle size, formation of aggregates, and nature of the substrate material, *e.g.* roughness. By adjusting the hierarchical structure of the coatings (Figure 29), their adhesion and hysteresis properties can be altered between the high- and low-adhesive superhydrophobic states (Figures 30 and 31) familiar from natural surfaces of rose petals [28][R1] and lotus leaves [36], respectively. On the high-adhesive superhydrophobic TiO_2 coating on pigment coated board (parameter set 1), CA of 159° was measured for 10 µl droplets, which were able to remain on the surface even when tilted upside down. CAH on the coating varied from > 100° to 37°, depending on the setup of the hysteresis experiment. On the low-adhesive superhydrophobic coating on paper (parameter set 3), CA and SA for 10 µl water droplets were 168° and 10°, respectively, and the measured CAH varied between 31° and 6° [P3, P4].

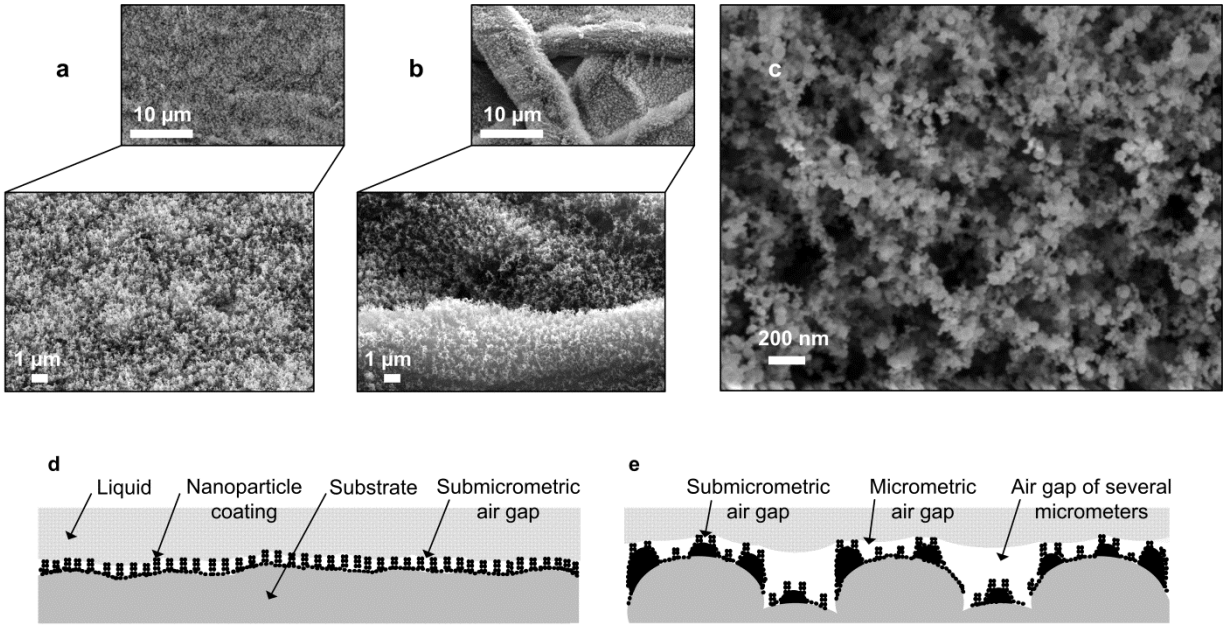

Figure 29. SEM images of superhydrophobic TiO_2 coatings on pigment coated board (parameter set 1) and paper (parameter set 3) substrates and schematic drawings of the proposed wetting states on the surfaces. (a, c, d) Dual-scale hierarchical coating structure on pigment coated board contributes to large liquid–solid contact area and high-adhesive superhydrophobicity. (b, e) Multi-scale hierarchical coating structure on paper contributes to low liquid–solid contact area and low-adhesive superhydrophobicity [P3, P4].

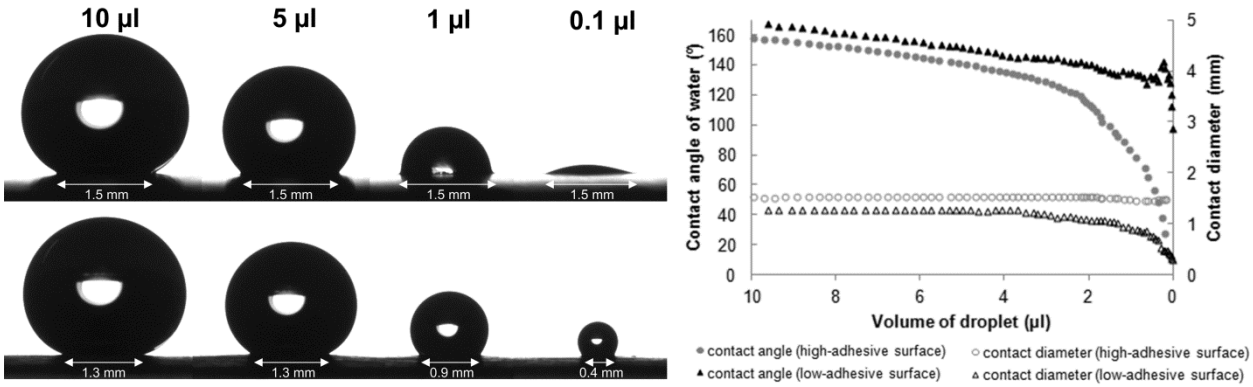

Figure 30. Shape, CA, and contact diameter of evaporating water droplets on the high- and low-adhesive superhydrophobic TiO_2 coatings on pigment coated board (parameter set 1) and paper (parameter set 3), respectively. The droplet is tightly pinned to the high-adhesive surface and the contact diameter remains constant at 1.5 mm. Consequently, at the end of the evaporation the droplet is clearly in a hydrophilic state possessing a very low CA. On the low-adhesive surface the contact diameter decreases with the decreasing droplet volume, and thus the droplet maintains its spherical shape and high CA [P3].

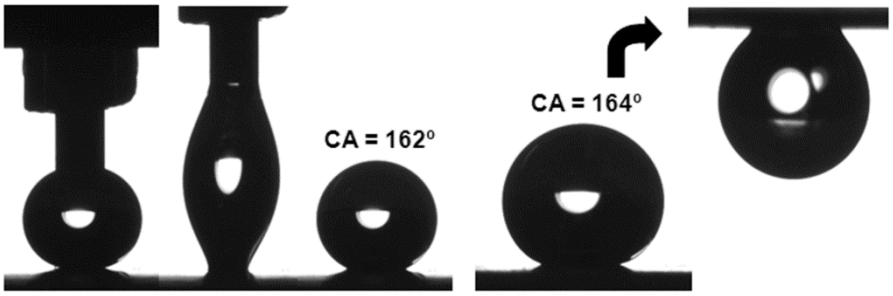

Figure 31. A set of images from the CA measurement illustrates the high adhesion between the water droplet and the superhydrophobic TiO_2 coating on pigment coated board substrate (parameter set 1, line speed 30 m/min). A 5 µl water droplet is able to remain on the flipped surface [P1].

The high water adhesion on the superhydrophobic TiO_2 coating demonstrated in Figures 30 and 31 can be explained by water penetration into the porous coating structure. That is, water is capable of penetrating in the nanoscale structure of the coating, which can contribute to exceptionally large liquid–solid contact area and strong water adhesion governed by different types of interactions, *e.g.* van der Waals forces, at the liquid–solid interface. In other words, on the topmost areas of the porous nanoparticle coating, the nanoscale gaps between the individual particles are in the Wenzel wetting state, while the larger submicrometer and micrometer scale gaps, for example between the particle aggregates, entrap air and are thus in the Cassie wetting state. So far, the Wenzel wetting state around nanoscale structures, and its effect on water droplet adhesion on superhydrophobic surfaces, has not been fully recognized [P3]. The effect of nanostructures on surface wetting was further studied on TiO_2 coated LDPE surface (parameter set 2). Smooth LDPE substrate together with the chosen coating parameters contributed to reduced hierarchical roughness of the coating (Figure 32). Because of the smooth substrate and small size of the particle aggregates, the coating was rather purely nanostructured.

As a result, the coating did not possess superhydrophobic properties, but water CA for 10 µl droplets was measured to be only 91°. Instead, the coating showed large CAH of 83° and low receding CA around 18°, which is demonstrated in Figure 32.

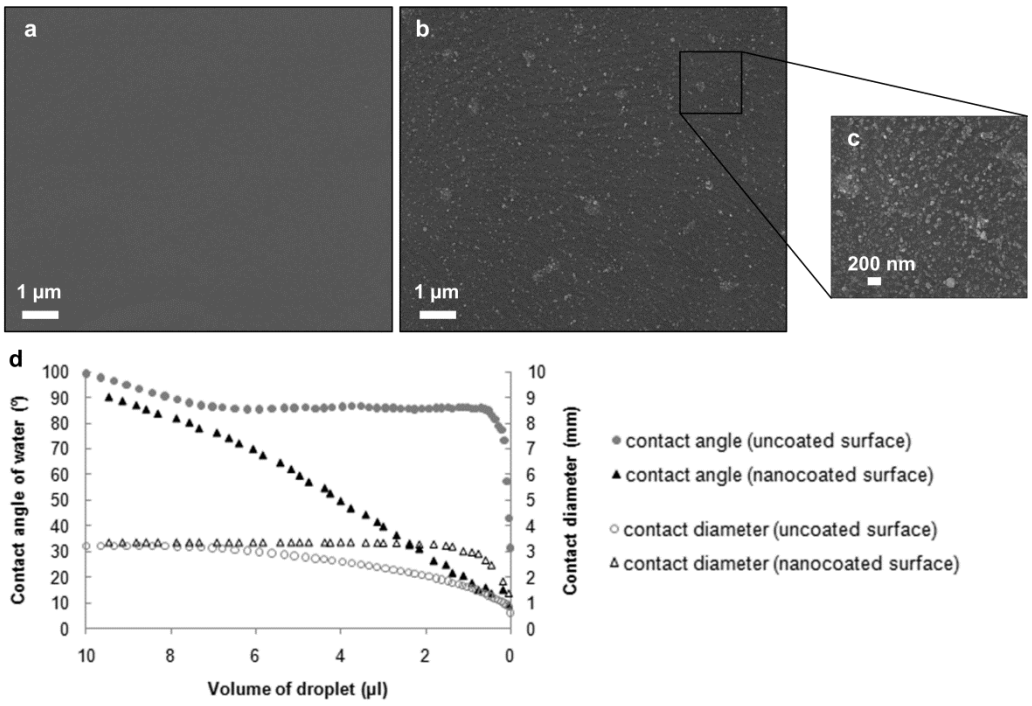

Figure 32. SEM images of LDPE surface (a) before and (b, c) after the TiO_2 coating (parameter set 2), and (d) CA and contact diameter of evaporating water droplets on the corresponding surfaces. CA of the evaporating droplet remains high on the uncoated surface because the contact diameter decreases quite freely with the decreasing droplet volume. In contrast, CA decreases rapidly on the nanostructured TiO_2 coated surface due to water pinning to the solid [P3].

Repellency of the superhydrophobic TiO_2 coatings against liquids of lower surface tension than water was studied using water–ethanol solution as a probe liquid. High CAs of > 150° were measured on the TiO_2 coated board (parameter set 1) up to ethanol concentrations of 15 wt% in the probe liquid. Further increment in the ethanol concentration resulted in collapse of the air pockets at the liquid–solid–air composite interface and drastic decrement in the CA. Because the paper substrate has much more irregular surface structure at micrometer scale compared to the pigment coated board substrate, liquid collapse in the largest micrometer scale air gaps and CA decrement on the TiO_2 coated paper (parameter set 3) began already with ethanol concentrations of 5 and 10wt% [P4]. That is, a wetting transition to so called Cassie impregnating wetting state, which earlier was believed to exist on superhydrophobic high-adhesive rose petals, occurred on the TiO_2 coated paper with the increment of ethanol in the probe liquid. The effect of wetting transition on the CAH and droplet adhesion to the surface is shown in Table 2 and Figure 33. The high stability of submicrometer scale air gaps in comparison with micrometer scale air gaps was recently utilized by Verho *et al.* [134], who demonstrated reversible and localized pressure-induced wetting transitions between the “micro-Cassie” and “nano-Cassie” states that allow

writing, erasing, rewriting, and storing of optically displayed information on the dual-scale topography of superhydrophobic surface.

Table 2. The effect of ethanol concentration on CAH on the superhydrophobic TiO_2 coatings on pigment coated board (parameter set 1) and paper (parameter set 3) substrates [P4].

substrate	0 wt%	5 wt%	10 wt%	15 wt%
pigment coated board	44 ± 5°	39 ± 5°	54 ± 6°	n/a
paper	28 ± 6°	62 ± 7°	n/a	n/a

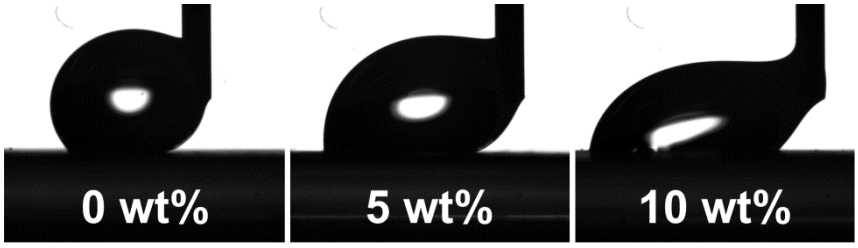

Figure 33. Droplet images during CAH measurement on the TiO_2 coated paper surface (parameter set 3) with ethanol concentrations of 0, 5, and 10 wt%. With 10 wt% ethanol, the droplet attached to the moving substrate, and thus the hysteresis could not be determined. The corresponding image was captured right before the droplet detached from the needle tip [P4].

The physical structure of the TiO_2 coating has proven itself to be well-suitable for liquid super-repellency, because the surface shows good superhydrophobic properties without any fluorochemical modification. In fact, the hierarchical topography of the TiO_2 coating resembles much the fluorosilane modified silica coating fabricated by Deng *et al.* [59] (Figure 13), which was capable of repelling variety of low surface tension liquids and showed good superamphiphobic properties with CAs greater than 150° for, for example, water (surface tension of 72.1 mN/m), diiodomethane (50.9 mN/m), ethylene glycol (47.3 mN/m), olive oil (32.0 mN/m), and hexadecane (27.5 mN/m). However, because the superhydrophobic TiO_2 coating has only moderately low energy surface chemistry, it cannot resist wetting by liquids of low surface tension such as high concentration alcohol solutions [P4] and oils. For example, although the TiO_2 coated board (parameter set 3) shows good water repellency with CA as high as 159°, the droplets of diiodomethane, ethylene glycol, olive oil, and hexadecane readily spread over the surface, and the corresponding CAs were measured to be 9°, 74°, 23°, and 8°, respectively.

With the liquids of low surface tension, the roughness of the TiO_2 coating can actually support surface wetting instead of liquid repellency. Such an effect is well demonstrated by the Kao experiment shown in Figure 3. Therefore, the oleophilic properties of the TiO_2 coating were expected. To date, any fluorine-free coatings with superoleophobic properties have not been reported. For example, the famous superhydrophobic leaves of lotus plant get perfectly wetted by low surface tension liquids such as hexadecane [57], because chemistry of the waxy plant surface is not sufficient to repel wetting by liquids of low surface tension. In order to achieve oleophobic properties for the superhydrophobic TiO_2 coating, its surface chemistry needs to be modified. Potential methods for the surface modification include several wet-chemical methods,

CVD, and plasma coatings. One of the potential candidates for solvent-free roll-to-roll surface modification of the superhydrophobic TiO_2 coating is atmospheric plasma deposition.

Self-cleaning effects

The self-cleaning effect on superhydrophobic surfaces, *i.e.*, the lotus-effect, is based on easy mobility of water droplets on the substrate. Rolling droplets, *e.g.* rain drops, can collect dirt particles with them and clean the surface without leaving any residue behind. Self-cleaning surfaces are among the most frequently suggested applications for superhydrophobic coatings. The famous self-cleaning effect by rolling water droplet is demonstrated on the superhydrophobic TiO_2 coating (parameter set 1) on pigment coated board substrate in Figure 34.

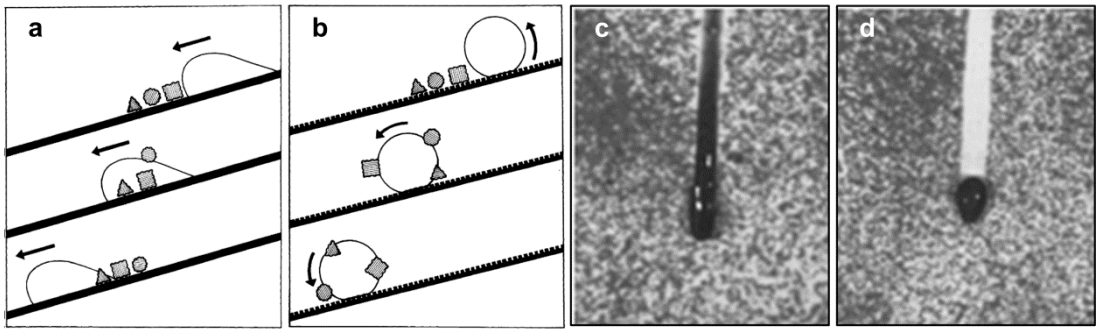

Figure 34. The lotus-effect. Schematic drawings of (a) sliding water droplet on a smooth surface and (b) rolling water droplet on a self-cleaning superhydrophobic surface [36], and the corresponding practical examples demonstrated on contaminated surfaces of (c) pigment coated board and (d) the superhydrophobic TiO_2 coated board (parameter set 1).

In addition to the lotus-effect, the superhydrophobic TiO_2 coating possesses also chemical self-cleaning ability through photocatalytic oxidation of organic compounds from its surface. The photocatalytic activity of TiO_2 is based on its band gap energy around 3.0–3.2 eV, which enables generation of photo-induced electron–hole pairs in TiO_2 and thus formation of highly reactive species such as superoxides, hydroxyl radicals, and hydrogen peroxides on the semiconductor surface [135-138]. For example, during UV-illumination period of 30 min (365 nm, 50 mW/cm^2), the relative amount of carbonaceous material on the TiO_2 coated board (parameter set 3) decreased from ~44% to ~30% and the C/Ti ratio decreased from 2.6 to 1.5. However, it is not necessary to use high-intensity UV-illumination to initiate the photocatalytic activity and the related self-cleaning phenomena on the superhydrophobic TiO_2 coating, as the reactions occur effectively also under natural daylight illumination even in the shade [P5].

Wettability switching/patterning

Related to the photocatalytic decomposition of the low surface energy carbonaceous material from the TiO_2 coating, the surface experiences a drastic wettability change from superhydrophobic to superhydrophilic upon illumination. That is, because of the illumination-induced changes in the surface chemistry, the coating roughness starts to support hydrophilicity, and thus the illuminated TiO_2 coating appears with similar wetting properties to the superhydrophilic SiO_2 coating. By controlling the illumination time, surface wettability of the

TiO_2 coating can be adjusted to any desired level in a wide range between water CAs of > 160° and < 10° [P5, R6]. Wettability of the coating can therefore be adjusted to optimal level considering, for example, ink properties in printing applications. In addition to the illumination, wettability of the TiO_2 coating can be adjusted by several other treatments [139] which are more suitable for large-scale roll-to-roll processing of materials, *e.g.* traditional surface treatments such as flame and corona which are typically used in industrial-scale paper converting processes [7][R7].

By illuminating the superhydrophobic TiO_2 coating through a photomask, it is possible to create surface energy patterns on the coating, and thus to create superhydrophilic channels and patterns on otherwise superhydrophobic surface (Figure 35). Surface energy patterning can be useful in wide range of applications. For example, Zhang *et al.* [55] utilized surface energy patterning to deposit PS microspheres on specific regions on the substrate (Figure 11), while Sirringhaus *et al.* [56] used surface energy patterning to guide the flow of water-based conducting polymer ink-jet droplets in fabrication of integrated circuits.

A liquid-repellent base coating for printed electronics, by which line widths and ink penetration into the substrate material can be controlled, or paper-based microfluidic devices [70, 114] could be among the most potential applications for the patterned superhydrophobic TiO_2 coatings. In the present paper-based devices, which are used in, for example, point-of-care diagnostics, typically only half of the sample volume dosed into a device reaches the detection zone because of fluid retention in capillaries in paper. This may be unacceptable in applications where sample and reagent volumes are precious. On the other hand, many hydrophobization treatments, *e.g.* wax treatments, cannot form barriers strong enough to repel leakage of low surface tension liquids from the sample transportation channels [70]. Superhydrophobic coatings could address many of the common problems the paper-based microfluidic devices encounter. For example, in the case that sample capillary flow takes place in a thin nanostructured coating layer on a paper-based substrate instead of traditional capillary action in bulk paper, significant savings in the sample and reagent volumes can be achieved. Moreover, fluorinated superhydrophobic coatings can possess good amphiphobic properties and are capable of forming strong barriers against liquids of low surface tension preventing their leakage from the channels of the device.

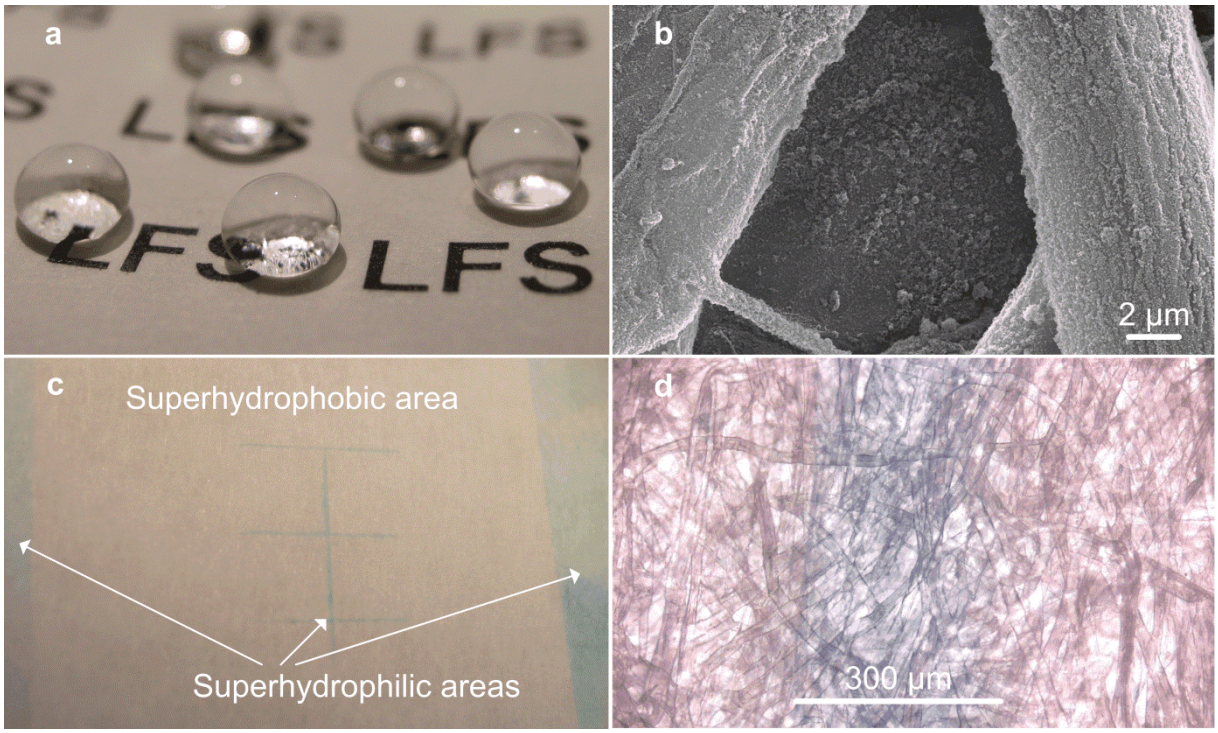

Figure 35. (a) Spherical water droplets on transparent superhydrophobic TiO_2 coating (parameter set 3) on printed paper and (b) SEM micrograph of the corresponding surface. (c) A figure formed on the photo-patterned TiO_2 coated paper after rod-coating with methylene blue colored water: the hydrophilic areas guided the fluid setting and figure formation on the intelligent substrate. (d) An optical microscope image of the photo-patterned figure shows the line width to be approximately 300 µm [P5].

Robustness and self-healing effect

Simple tape and abrasion experiments were executed on the superhydrophobic TiO_2 coating to examine its physical robustness. The experiments revealed that the surface structure of the coating is fragile and can be destroyed relatively easily by mechanical stress. However, several repeated tape and abrasion cycles could only partially destroy the hydrophobic effect of the coating. After 20 cycles of abrasion or taping/releasing sets, the surface of the TiO_2 coated board (parameter set 1, line speed 30 m/min) remained clearly hydrophobic with water CAs around 110–130° [P1].

Although the coating could be partially destroyed by mechanical stress, it showed good thermal stability and could maintain its superhydrophobic properties after high temperature treatments. Curing in an oven induced surface chemical changes on the TiO_2 coated board (parameter set 3), which drastically prolonged the time required for the photo-induced hydrophilicity conversion: after 7 days of artificial daylight illumination, water CA on the pristine TiO_2 coating was measured to be as low as 6°, while on the coating cured in an oven for 30 min at 150°C prior to the illumination, the hydrophobic properties remained after the illumination period of 7 days and the coating showed good water repellency with water CA of 138° [P5].

After the hydrophobic chemistry of the TiO_2 coating is destroyed by illumination and the surface has lost its superhydrophobicity, the coating starts to heal itself by gathering low surface

energy material from atmosphere [P5]. Consequently, the superhydrophobic properties of the coating are slowly restored in ambient conditions. For example, during 30 min of UV-illumination (365 nm, 50 mW/cm^2) the relative amount of carbon on the TiO_2 coated board (parameter set 3) decreased from ~44% to ~30% and water CA on the surface decreased from 163° to 7°. After 1 month of storage in the dark in ambient conditions at room temperature and relative humidity of 50%, the relative amount of carbon on the coating surface had increased from ~30% to ~35%, the C/Ti ratio had increased from 1.5 to 1.9, and water CA had increased from 7° to 146° as a result of the self-healing process.

The healing process of the TiO_2 coating can be significantly speeded up by heat treatment in an oven, as shown in Figure 36. At room temperature the self-healing and hydrophobicity recovery takes several days, but in an oven at temperatures above 100°C the healing process occurs within minutes. The self-healing effect after UV-illumination is a common and well-documented phenomenon on various types of TiO_2 surfaces. However, a collective understanding for the fundamental mechanisms of the self-healing process has been missing [P5]. Our experiments revealed that on the TiO_2 coated board, accumulation of the carbonaceous material on the coating surface is one of the most important factors explaining both the self-healing process at room temperature and the accelerated healing process at higher temperatures in the oven [P5].

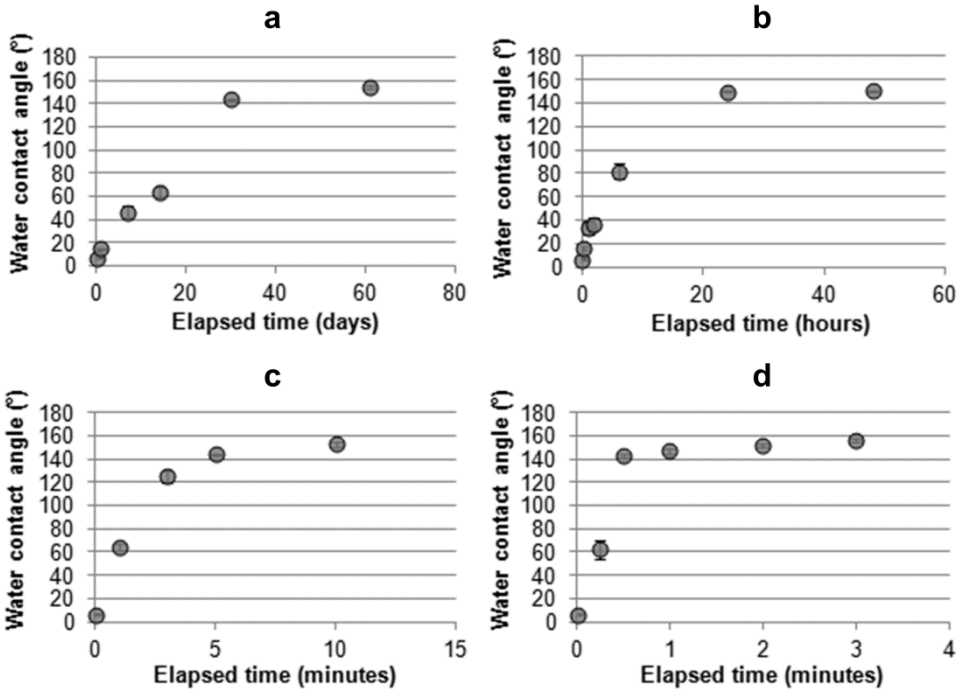

Figure 36. The self-healing effect and hydrophobicity recovery on illuminated (7 days of artificial daylight illumination) TiO_2 coated board (parameter set 3) in different conditions. (a) In the dark room in ambient conditions at 23°C the self-healing and hydrophobicity recovery occurs in several days, (b) in the oven at 50°C in hours, and (c) at 100°C and (d) at 150°C in minutes [P5].

Because of the self-healing effect, surface wetting of the TiO_2 coating adjusted by UV-illumination is not a permanent state. However, as it was discussed, wetting of the LFS-made TiO_2 coating can be adjusted by several other methods suitable for roll-to-roll processing of materials. Therefore, wettability of the coating can be adjusted *in-situ* on-line for, for example, printing and coating purposes. In addition, there are several heat treatment and other methods which are suitable for on-line healing of the TiO_2 coating [139], *e.g.* IR-dryers and atmospheric plasma deposition.

5. Conclusions

In this thesis work, feasibility of the LFS nanoparticle synthetization method in roll-to-roll coating of cellulose-based materials such as paper, pigment coated board, and extrusion-coated paper was studied. In addition to the examination of suitable processing parameters in coating of various cellulose-based substrates, properties and functionalities of the novel nanoparticle coatings were studied with focus on surface wettability, especially on superhydrophobicity. LFS proved itself simple, versatile, and straightforward one-step method to fabricate multifunctional nanoparticle coatings on various types of cellulose-based substrates in roll-to-roll coating procedure. LFS is among the most potential methods for large-scale fabrication of superhydrophobic coatings on affordable cellulose-based materials such as paper and board, because any type of additional chemical modification, drying, or curing steps are not needed.

Various metal and oxide nanoparticle coatings with hierarchical surface structure can be fabricated by LFS to introduce functionality to a material surface such as permanent superhydrophilicity and superhydrophobicity, self-cleaning, and self-healing ability. By altering the hierarchical coating structure, it is possible to affect water hysteresis and adhesion to fabricate both high- and low-adhesive superhydrophobic surfaces familiar from natural surfaces of rose petals and lotus leaves, respectively. Hierarchical structure of the coating determines many properties of the surface. For example, it was shown that the nanoscale structures on the coating reside in the Wenzel wetting state and thus increase water droplet adhesion and hysteresis on the surface. Also, the hierarchical structure of the coating has an important role in determining to what extent the surface is capable of repelling liquids of lower surface tension than water. The experiments with water–ethanol solution revealed that the small submicrometer scale air gaps at the liquid–solid–air composite interface were relatively stable with ethanol increment in the probe liquid, while the large micrometer scale air gaps collapsed at the early stage with the ethanol increment resulting to a wetting transition to so called Cassie impregnating wetting state. The experiments revealed high photocatalytic activity of the superhydrophobic TiO_2 coating, on which a stepless and reversible wettability conversion related to the self-cleaning effect and accumulation of carbonaceous material on the surface can be executed. The wettability conversion enables fabrication of local surface energy/wettability patterns on the coating surface, for example, by illuminating the sample through a photomask.

Overall, the pioneering studies on application of LFS method in roll-to-roll coating of cellulose-based substrates executed in this work produced novel information on the technological aspect of the LFS coating process. On the general aspect, the work provided relevant information on the wetting phenomena on superhydrophilic and superhydrophobic nanoparticle coatings. Particularly, the work provided new information and insights related to wetting phenomena around nanoscale structures on superhydrophobic surfaces and photo-induced wettability changes on TiO_2.

While this work was mainly focused on fabrication of SiO_2 and TiO_2 nanoparticle coatings on various substrates and on exploring and understanding the coating properties and the related phenomena, future work will increasingly focus on finding the most suitable practical

applications for the LFS-coated materials. In terms of wettability, which was the focus of this work, potential applications for the LFS coatings include tailored wetting properties for, for example, improved printability and adhesion of inks and coatings. In addition, other potential applications for LFS-coated cellulose-based materials include filters for oil/water separation and cheap and disposable products designed for short-term use, for example, water-repellent and gas permeable packaging materials. Especially, one emerging and globally important field of applications for cellulose-based materials is low-cost point-of-care diagnostic devices, where utilization potential of superhydrophobic coatings is yet largely unexplored.

References

1. Ostrikov, K., Colloquium: Reactive plasmas as a versatile nanofabrication tool. *Rev. Mod. Phys.* **2005,** 77, 489-511.
2. Choy, K. L., Chemical vapour deposition of coatings. *Prog. Mater. Sci.* **2003,** 48, 57-170.
3. Kemell, M.; Pore, V.; Ritala, M.; Leskelä, M.; Lindén, M., Atomic Layer Deposition in Nanometer-Level Replication of Cellulosic Substances and Preparation of Photocatalytic TiO2/Cellulose Composites. *J. Am. Chem. Soc.* **2005,** 127, 14178-14179.
4. Rao, N. P.; Tymiak, N.; Blum, J.; Neuman, A.; Lee, H. J.; Girshick, S. L.; McMurry, P. H.; Heberlein, J., Hypersonic plasma particle deposition of nanostructured silicon and silicon carbide. *J. Aerosol Sci.* **1998,** 29, 707-720.
5. Brinker, C. J.; Harrington, M. S., Sol-gel derived antireflective coatings for silicon. *Sol. Energy Mater.* **1981,** 5, 159-172.
6. Lu, Y.; Ganguli, R.; Drewien, C. A.; Anderson, M. T.; Brinker, C. J.; Gong, W.; Guo, Y.; Soyez, H.; Dunn, B.; Huang, M. H.; Zink, J. I., Continuous formation of supported cubic and hexagonalmesoporous films by sol–gel dip-coating. *Nature* **1997,** 389, 364-368.
7. Kuusipalo, J. (ed.), *Paper and Paperboard Converting*. 2nd ed.; Paperi ja Puu Oy: Jyväskylä, 2008; p 346.
8. Young, T., An essay on the cohesion of fluids. *Philos. Trans. R. Soc. London, Ser. A* **1805,** 95, 65-87.
9. Wenzel, R. N., Resistance of solid surfaces to wetting by water. *Ind. Eng. Chem.* **1936,** 28, 988-994.
10. Cassie, A. B. D.; Baxter, S., Wettability of porous surfaces. *Trans. Faraday Soc.* **1944,** 40, 546-551.
11. Onda, T.; Shibuichi, S.; Satoh, N.; Tsujii, K., Super-Water-Repellent Fractal Surfaces. *Langmuir* **1996,** 12, 2125-2127.
12. Shibuichi, S.; Onda, T.; Satoh, N.; Tsujii, K., Super Water-Repellent Surfaces Resulting from Fractal Structure. *J. Phys. Chem.* **1996,** 100, 19512-19517.
13. Roach, P.; Shirtcliffe, N. J.; Newton, M. I., Progess in superhydrophobic surface development. *Soft Matter* **2008,** 4, (2), 224.
14. Balu, B.; Kim, J. S.; Breedveld, V.; Hess, D. W., Tunability of the Adhesion of Water Drops on a Superhydrophobic Paper Surface via Selective Plasma Etching. *J. Adhes. Sci. Technol.* **2009,** 23, (2), 361-380.
15. Ma, M.; Hill, R. M., Superhydrophobic surfaces. *Curr. Opin. Colloid Interface Sci.* **2006,** 11, (4), 193-202.
16. Quéré, D., Wetting and Roughness. *Annu. Rev. Mater. Res.* **2008,** 38, (1), 71-99.
17. Carré, A.; Mittal, K. L. (eds.), *Superhydrophobic Surfaces*. VSP/Brill: Leiden, 2009; p 495.
18. Patankar, N. A., On the Modeling of Hydrophobic Contact Angles on Rough Surfaces. *Langmuir* **2003,** 19, 1249-1253.
19. Marmur, A., The Lotus Effect: Superhydrophobicity and Metastability. *Langmuir* **2004,** 20, 3517-3519.

20. Li, W.; Amirfazli, A., A thermodynamic approach for determining the contact angle hysteresis for superhydrophobic surfaces. *J. Colloid Interface Sci.* **2005,** 292, (1), 195-201.
21. Whyman, G.; Bormashenko, E.; Stein, T., The rigorous derivation of Young, Cassie–Baxter and Wenzel equations and the analysis of the contact angle hysteresis phenomenon. *Chem. Phys. Lett.* **2008,** 450, (4-6), 355-359.
22. Patankar, N. A., Consolidation of hydrophobic transition criteria by using an approximate energy minimization approach. *Langmuir* **2010,** 26, (11), 8941-5.
23. Bormashenko, E.; Musin, A.; Whyman, G.; Zinigrad, M., Wetting transitions and depinning of the triple line. *Langmuir* **2012,** 28, (7), 3460-4.
24. Bittoun, E.; Marmur, A., The role of multiscale roughness in the lotus effect: is it essential for super-hydrophobicity? *Langmuir* **2012,** 28, (39), 13933-42.
25. Korhonen, J. T.; Huhtamaki, T.; Ikkala, O.; Ras, R. H. A., Reliable measurement of the receding contact angle. *Langmuir* **2013,** 29, (12), 3858-63.
26. Balu, B.; Breedveld, V.; Hess, D. W., Fabrication of "Roll-off" and "Sticky" Superhydrophobic Cellulose Surfaces via Plasma Processing. *Langmuir* **2008,** 24, 4785-4790.
27. Jin, M.; Feng, X.; Feng, L.; Sun, T.; Zhai, J.; Li, T.; Jiang, L., Superhydrophobic Aligned Polystyrene Nanotube Films with High Adhesive Force. *Adv. Mater.* **2005,** 17, 1977-1981.
28. Feng, L.; Zhang, Y.; Xi, J.; Zhu, Y.; Wang, N.; Xia, F.; Jiang, L., Petal Effect: A Superhydrophobic State with High Adhesive Force. *Langmuir* **2008,** 24, 4114-4119.
29. Marmur, A., Hydro- hygro- oleo- omni-phobic? Terminology of wettability classification. *Soft Matter* **2012,** 8, (26), 6867.
30. Feng, L.; Li, S.; Li, Y.; Li, H.; Zhang, L.; Zhai, J.; Song, Y.; Liu, B.; Jiang, L.; Zhu, D., Super-Hydrophobic Surfaces: From Natural to Artificial. *Adv. Mater.* **2002,** 14, 1857-1860.
31. Sun, T.; Feng, L.; Gao, X.; Jiang, L., Bioinspired Surfaces with Special Wettability. *Acc. Chem. Res.* **2005,** 38, 644-652.
32. Zheng, Y.; Gao, X.; Jiang, L., Directional adhesion of superhydrophobic butterfly wings. *Soft Matter* **2007,** 3, (2), 178.
33. Koch, K.; Bhushan, B.; Barthlott, W., Multifunctional surface structures of plants: An inspiration for biomimetics. *Prog. Mater. Sci.* **2009,** 54, (2), 137-178.
34. Watson, G. S.; Cribb, B. W.; Watson, J. A., How Micro/Nanoarchitecture Facilitates Anti-Wetting: An Elegant Hierarchical Design on the Termite Wing. *ACS Nano* **2010,** 4, 129-136.
35. Liu, K.; Jiang, L., Bio-inspired design of multiscale structures for function integration. *Nano Today* **2011,** 6, (2), 155-175.
36. Barthlott, W.; Neinhuis, C., Purity of the sacred lotus, or escape from contamination in biological surfaces. *Planta* **1997,** 202, 1-8.
37. Gao, X.; Jiang, L., Water-repellent legs of water striders. *Nature* **2004,** 432, 36.
38. Neinhuis, C.; Barthlott, W., Characterization and Distribution of Water-repellent, Self-cleaning Plant Surfaces. *Ann. Bot.* **1997,** 79, 667-677.

39. Zhang, X.; Jin, M.; Liu, Z.; Nishimoto, S.; Saito, H.; Murakami, T.; Fujishima, A., Preparation and Photocatalytic Wettability Conversion of TiO2-Based Superhydrophobic Surfaces. *Langmuir* **2006,** 22, 9477-9479.
40. Gao, X.; Yao, X.; Jiang, L., Effects of Rugged Nanoprotrusions on the Surface Hydrophobicity and Water Adhesion of Anisotropic Micropatterns. *Langmuir* **2007,** 23, 4886-4891.
41. Öner, D.; McCarthy, T. J., Ultrahydrophobic Surfaces. Effects of Topography Length Scales on Wettability. *Langmuir* **2000,** 16, 7777-7782.
42. Sun, M.; Luo, C.; Xu, L.; Ji, H.; Ouyang, Q.; Yu, D.; Chen, Y., Artificial Lotus Leaf by Nanocasting. *Langmuir* **2005,** 21, 8978-8981.
43. Zhu, Y.; Zhang, J.; Zheng, Y.; Huang, Z.; Feng, L.; Jiang, L., Stable, Superhydrophobic, and Conductive Polyaniline/Polystyrene Films for Corrosive Environments. *Adv. Funct. Mater.* **2006,** 16, (4), 568-574.
44. Erbil, H. Y.; Demirel, A. L.; Avci, Y.; Mert, O., Transformation of a simple plastic into a superhydrophobic surface. *Science* **2003,** 299, (5611), 1377-80.
45. Lu, X.; Zhang, C.; Han, Y., Low-Density Polyethylene Superhydrophobic Surface by Control of Its Crystallization Behavior. *Macromol. Rapid Commun.* **2004,** 25, (18), 1606-1610.
46. Shirtcliffe, N. J.; McHale, G.; Newton, M. I.; Perry, C. C., Intrinsically Superhydrophobic Organosilica Sol-Gel Foams. *Langmuir* **2003,** 19, 5626-5631.
47. Kulinich, S. A.; Farzaneh, M., Effect of contact angle hysteresis on water droplet evaporation from super-hydrophobic surfaces. *Appl. Surf. Sci.* **2009,** 255, (7), 4056-4060.
48. Zhang, J.; Li, J.; Han, Y., Superhydrophobic PTFE Surfaces by Extension. *Macromol. Rapid Commun.* **2004,** 25, (11), 1105-1108.
49. Xu, Q. F.; Mondal, B.; Lyons, A. M., Fabricating superhydrophobic polymer surfaces with excellent abrasion resistance by a simple lamination templating method. *ACS Appl. Mater. Interfaces* **2011,** 3, (9), 3508-14.
50. Feng, X. J.; Jiang, L., Design and Creation of Superwetting/Antiwetting Surfaces. *Adv. Mater.* **2006,** 18, (23), 3063-3078.
51. Verplanck, N.; Coffinier, Y.; Thomy, V.; Boukherroub, R., Wettability Switching Techniques on Superhydrophobic Surfaces. *Nanoscale Res. Lett.* **2007,** 2, (12), 577-596.
52. Wang, R.; Hashimoto, K.; Fujishima, A.; Chikuni, M.; Kojima, E.; Kitamura, A.; Shimohigoshi, M.; Watanabe, T., Light-induced amphiphilic surfaces. *Nature* **1997,** 388, 431-432.
53. Miyauchi, M.; Nakajima, A.; Watanabe, T.; Hashimoto, K., Photocatalysis and Photoinduced Hydrophilicity of Various Metal Oxide Thin Films. *Chem. Mater.* **2002,** 14, 2812-2816.
54. Kanta, A.; Sedev, R.; Ralston, J., Thermally- and Photoinduced Changes in the Water Wettability of Low-Surface-Area Silica and Titania. *Langmuir* **2005,** 21, 2400-2407.
55. Zhang, X.; Jin, M.; Liu, Z.; Tryk, D. A.; Nishimoto, S.; Murakami, T.; Fujishima, A., Superhydrophobic TiO2 Surfaces: Preparation, Photocatalytic Wettability Conversion, and Superhydrophobic-Superhydrophilic Patterning. *J. Phys. Chem. C* **2007,** 111, 14521-14529.

56. Sirringhaus, H., High-Resolution Inkjet Printing of All-Polymer Transistor Circuits. *Science* **2000,** 290, (5499), 2123-2126.
57. Tuteja, A.; Choi, W.; Ma, M.; Mabry, J. M.; Mazzella, S. A.; Rutledge, G. C.; McKinley, G. H.; Cohen, R. E., Designing superoleophobic surfaces. *Science* **2007,** 318, (5856), 1618-22.
58. Tuteja, A.; Choi, W.; Mabry, J. M.; McKinley, G. H.; Cohen, R. E., Robust omniphobic surfaces. *Proc. Natl. Acad. Sci. U.S.A.* **2008,** 105, (47), 18200-5.
59. Deng, X.; Mammen, L.; Butt, H. J.; Vollmer, D., Candle soot as a template for a transparent robust superamphiphobic coating. *Science* **2012,** 335, (6064), 67-70.
60. Wong, T. S.; Kang, S. H.; Tang, S. K.; Smythe, E. J.; Hatton, B. D.; Grinthal, A.; Aizenberg, J., Bioinspired self-repairing slippery surfaces with pressure-stable omniphobicity. *Nature* **2011,** 477, (7365), 443-7.
61. Bohn, H. F.; Federle, W., Insect aquaplaning: Nepenthes pitcher plants capture prey with the peristome, a fully wettable water-lubricated anisotropic surface. *Proc. Natl. Acad. Sci. U.S.A.* **2004,** 101, (39), 14138-43.
62. Zhao, H.; Law, K. Y., Directional self-cleaning superoleophobic surface. *Langmuir* **2012,** 28, (32), 11812-8.
63. Zhou, H.; Wang, H.; Niu, H.; Gestos, A.; Wang, X.; Lin, T., Fluoroalkyl silane modified silicone rubber/nanoparticle composite: a super durable, robust superhydrophobic fabric coating. *Adv. Mater.* **2012,** 24, (18), 2409-12.
64. Li, Y.; Li, L.; Sun, J., Bioinspired self-healing superhydrophobic coatings. *Angew. Chem. Int. Ed.* **2010,** 49, (35), 6129-33.
65. Wang, H.; Xue, Y.; Ding, J.; Feng, L.; Wang, X.; Lin, T., Durable, self-healing superhydrophobic and superoleophobic surfaces from fluorinated-decyl polyhedral oligomeric silsesquioxane and hydrolyzed fluorinated alkyl silane. *Angew. Chem. Int. Ed.* **2011,** 50, (48), 11433-6.
66. Zhou, H.; Wang, H.; Niu, H.; Gestos, A.; Lin, T., Robust, Self-Healing Superamphiphobic Fabrics Prepared by Two-Step Coating of Fluoro-Containing Polymer, Fluoroalkyl Silane, and Modified Silica Nanoparticles. *Adv. Funct. Mater.* **2012,** 23, (13), 1664-1670.
67. Verho, T.; Bower, C.; Andrew, P.; Franssila, S.; Ikkala, O.; Ras, R. H. A., Mechanically durable superhydrophobic surfaces. *Adv. Mater.* **2011,** 23, (5), 673-8.
68. Eriksson, M.; Notley, S. M.; Wågberg, L., Cellulose Thin Films: Degree of Cellulose Ordering and Its Influence on Adhesion. *Biomacromolecules* **2007,** 8, 912-919.
69. Kontturi, E.; Suchy, M.; Penttilä, P.; Jean, B.; Pirkkalainen, K.; Torkkeli, M.; Serimaa, R., Amorphous characteristics of an ultrathin cellulose film. *Biomacromolecules* **2011,** 12, (3), 770-7.
70. Ballerini, D. R.; Li, X.; Shen, W., Patterned paper and alternative materials as substrates for low-cost microfluidic diagnostics. *Microfluid. Nanofluid.* **2012,** 13, (5), 769-787.
71. Mukhopadhyay, S. M.; Joshi, P.; Datta, S.; Macdaniel, J., Plasma assisted surface coating of porous solids. *Appl. Surf. Sci.* **2002,** 201, 219-226.
72. Lin, T.-S.; Wu, C.-F.; Hsieh, C.-T., Enhancement of water-repellent performance on functional coating by using the Taguchi method. *Surf. Coat. Technol.* **2006,** 200, (18-19), 5253-5258.

73. Nyström, D.; Lindqvist, J.; Östmark, E.; Hult, A.; Malmström, E., Superhydrophobic bio-fibre surfaces via tailored grafting architecture. *Chem. Commun.* **2006**, (34), 3594-6.
74. Li, Z.; Xing, Y.; Dai, J., Superhydrophobic surfaces prepared from water glass and non-fluorinated alkylsilane on cotton substrates. *Appl. Surf. Sci.* **2008,** 254, (7), 2131-2135.
75. Wang, H.; Fang, J.; Cheng, T.; Ding, J.; Qu, L.; Dai, L.; Wang, X.; Lin, T., One-step coating of fluoro-containing silica nanoparticles for universal generation of surface superhydrophobicity. *Chem. Commun.* **2008**, (7), 877-9.
76. Arbatan, T.; Zhang, L.; Fang, X.-Y.; Shen, W., Cellulose nanofibers as binder for fabrication of superhydrophobic paper. *Chem. Eng. J.* **2012,** 210, 74-79.
77. Gao, Q.; Zhu, Q.; Guo, Y., Formation of Highly Hydrophobic Surfaces on Cotton and Polyester Fabrics Using Silica Sol Nanoparticles and Nonfluorinated Alkylsilane. *Ind. Eng. Chem. Res.* **2009,** 48, 9797-9803.
78. Wang, H.; Ding, J.; Xue, Y.; Wang, X.; Lin, T., Superhydrophobic fabrics from hybrid silica sol-gel coatings: Structural effect of precursors on wettability and washing durability. *J. Mater. Res.* **2011,** 25, (07), 1336-1343.
79. Duan, W.; Xie, A.; Shen, Y.; Wang, X.; Wang, F.; Zhang, Y.; Li, J., Fabrication of Superhydrophobic Cotton Fabrics with UV Protection Based on CeO2Particles. *Ind. Eng. Chem. Res.* **2011,** 50, (8), 4441-4445.
80. Li, S.; Zhang, S.; Wang, X., Fabrication of Superhydrophobic Cellulose-Based Materials through a Solution-Immersion Process. *Langmuir* **2008,** 24, 5585-5590.
81. Wang, S.; Li, M.; Lu, Q., Filter paper with selective absorption and separation of liquids that differ in surface tension. *ACS Appl. Mater. Interfaces* **2010,** 2, (3), 677-83.
82. Bayer, I. S.; Fragouli, D.; Attanasio, A.; Sorce, B.; Bertoni, G.; Brescia, R.; Di Corato, R.; Pellegrino, T.; Kalyva, M.; Sabella, S.; Pompa, P. P.; Cingolani, R.; Athanassiou, A., Water-repellent cellulose fiber networks with multifunctional properties. *ACS Appl. Mater. Interfaces* **2011,** 3, (10), 4024-31.
83. Huang, X.; Wen, X.; Cheng, J.; Yang, Z., Sticky superhydrophobic filter paper developed by dip-coating of fluorinated waterborne epoxy emulsion. *Appl. Surf. Sci.* **2012,** 258, (22), 8739-8746.
84. Bayer, I. S.; Biswas, A.; Ellialtioglu, G., Fabrication of super water repellent silver flake/copolymer blend films and their potential as smart fabrics. *Polym. Compos.* **2011,** 32, (4), 576-585.
85. Ogihara, H.; Xie, J.; Okagaki, J.; Saji, T., Simple method for preparing superhydrophobic paper: spray-deposited hydrophobic silica nanoparticle coatings exhibit high water-repellency and transparency. *Langmuir* **2012,** 28, (10), 4605-8.
86. Mertaniemi, H.; Laukkanen, A.; Teirfolk, J.-E.; Ikkala, O.; Ras, R. H. A., Functionalized porous microparticles of nanofibrillated cellulose for biomimetic hierarchically structured superhydrophobic surfaces. *RSC Adv.* **2012,** 2, (7), 2882.
87. Barona, D.; Amirfazli, A., Producing a superhydrophobic paper and altering its repellency through ink-jet printing. *Lab Chip* **2011,** 11, (5), 936-40.
88. Li, J.; Wan, H.; Ye, Y.; Zhou, H.; Chen, J., One-step process to fabrication of transparent superhydrophobic SiO2 paper. *Appl. Surf. Sci.* **2012,** 261, 470-472.

89. Nyström, D.; Lindqvist, J.; Östmark, E.; Antoni, P.; Carlmark, A.; Hult, A.; Malmström, E., Superhydrophobic and self-cleaning bio-fiber surfaces via ATRP and subsequent postfunctionalization. *ACS Appl. Mater. Interfaces* **2009,** 1, (4), 816-23.
90. Deng, B.; Cai, R.; Yu, Y.; Jiang, H.; Wang, C.; Li, J.; Li, L.; Yu, M.; Li, J.; Xie, L.; Huang, Q.; Fan, C., Laundering durability of superhydrophobic cotton fabric. *Adv. Mater.* **2010,** 22, (48), 5473-7.
91. Hoefnagels, H. F.; Wu, D.; de With, G.; Ming, W., Biomimetic Superhydrophobic and Highly Oleophobic Cotton Textiles. *Langmuir* **2007,** 23, 13158-13163.
92. Xu, B.; Cai, Z., Fabrication of a superhydrophobic ZnO nanorod array film on cotton fabrics via a wet chemical route and hydrophobic modification. *Appl. Surf. Sci.* **2008,** 254, (18), 5899-5904.
93. Leng, B.; Shao, Z.; de With, G.; Ming, W., Superoleophobic Cotton Textiles. *Langmuir* **2009,** 25, 2456-2460.
94. Kivotidi, S.; Tsioptsias, C.; Pavlidou, E.; Panayiotou, C., Flame-retarded hydrophobic cellulose through impregnation with aqueous solutions and supercritical CO2. *J. Therm. Anal. Calorim.* **2012,** 111, (1), 475-482.
95. Shateri-Khalilabad, M.; Yazdanshenas, M. E., Preparation of superhydrophobic electroconductive graphene-coated cotton cellulose. *Cellulose* **2013,** 20, (2), 963-972.
96. Goncalves, G.; Marques, P. A.; Trindade, T.; Neto, C. P.; Gandini, A., Superhydrophobic cellulose nanocomposites. *J. Colloid Interface Sci.* **2008,** 324, (1-2), 42-6.
97. Georgakilas, V.; Bourlinos, A. B.; Zboril, R.; Trapalis, C., Synthesis, Characterization and Aspects of Superhydrophobic Functionalized Carbon Nanotubes. *Chem. Mater.* **2008,** 20, 2884-2886.
98. Yang, H.; Deng, Y., Preparation and physical properties of superhydrophobic papers. *J. Colloid Interface Sci.* **2008,** 325, (2), 588-93.
99. Hu, Z.; Zen, X.; Gong, J.; Deng, Y., Water resistance improvement of paper by superhydrophobic modification with microsized CaCO3 and fatty acid coating. *Colloids Surf. A* **2009,** 351, (1-3), 65-70.
100. Huang, L.; Chen, K.; Lin, C.; Yang, R.; Gerhardt, R. A., Fabrication and characterization of superhydrophobic high opacity paper with titanium dioxide nanoparticles. *J. Mater. Sci.* **2010,** 46, (8), 2600-2605.
101. Stanssens, D.; Van den Abbeele, H.; Vonck, L.; Schoukens, G.; Deconinck, M.; Samyn, P., Creating water-repellent and super-hydrophobic cellulose substrates by deposition of organic nanoparticles. *Mater. Lett.* **2011,** 65, (12), 1781-1784.
102. Fang, J.; Wang, H.; Xue, Y.; Wang, X.; Lin, T., Magnet-induced temporary superhydrophobic coatings from one-pot synthesized hydrophobic magnetic nanoparticles. *ACS Appl. Mater. Interfaces* **2010,** 2, (5), 1449-55.
103. Zhao, Y.; Xu, Z.; Wang, X.; Lin, T., Photoreactive azido-containing silica nanoparticle/polycation multilayers: durable superhydrophobic coating on cotton fabrics. *Langmuir* **2012,** 28, (15), 6328-35.
104. Zhang, M.; Wang, C.; Wang, S.; Shi, Y.; Li, J., Fabrication of coral-like superhydrophobic coating on filter paper for water–oil separation. *Appl. Surf. Sci.* **2012,** 261, 764-769.

105. Cho, S. C.; Hong, Y. C.; Cho, S. G.; Ji, Y. Y.; Han, C. S.; Uhm, H. S., Surface modification of polyimide films, filter papers, and cotton clothes by HMDSO/toluene plasma at low pressure and its wettability. *Curr. Appl. Phys.* **2009,** 9, (6), 1223-1226.
106. Artus, G. R. J.; Jung, S.; Zimmermann, J.; Gautschi, H. P.; Marquardt, K.; Seeger, S., Silicone Nanofilaments and Their Application as Superhydrophobic Coatings. *Adv. Mater.* **2006,** 18, (20), 2758-2762.
107. Zimmermann, J.; Reifler, F. A.; Fortunato, G.; Gerhardt, L.-C.; Seeger, S., A Simple, One-Step Approach to Durable and Robust Superhydrophobic Textiles. *Adv. Funct. Mater.* **2008,** 18, (22), 3662-3669.
108. Jin, H.; Kettunen, M.; Laiho, A.; Pynnönen, H.; Paltakari, J.; Marmur, A.; Ikkala, O.; Ras, R. H. A., Superhydrophobic and superoleophobic nanocellulose aerogel membranes as bioinspired cargo carriers on water and oil. *Langmuir* **2011,** 27, (5), 1930-4.
109. Cervin, N. T.; Aulin, C.; Larsson, P. T.; Wågberg, L., Ultra porous nanocellulose aerogels as separation medium for mixtures of oil/water liquids. *Cellulose* **2011,** 19, (2), 401-410.
110. Daoud, W. A.; Xin, J. H.; Zhang, Y. H.; Mak, C. L., Pulsed laser deposition of superhydrophobic thin Teflon films on cellulosic fibers. *Thin Solid Films* **2006,** 515, (2), 835-837.
111. Quan, C.; Werner, O.; Wågberg, L.; Turner, C., Generation of superhydrophobic paper surfaces by a rapidly expanding supercritical carbon dioxide–alkyl ketene dimer solution. *J. Supercrit. Fluids* **2009,** 49, (1), 117-124.
112. Werner, O.; Quan, C.; Turner, C.; Pettersson, B.; Wågberg, L., Properties of superhydrophobic paper treated with rapid expansion of supercritical CO2 containing a crystallizing wax. *Cellulose* **2009,** 17, (1), 187-198.
113. Zhang, Y. L.; Wang, J. N.; He, Y.; He, Y.; Xu, B. B.; Wei, S.; Xiao, F. S., Solvothermal synthesis of nanoporous polymer chalk for painting superhydrophobic surfaces. *Langmuir* **2011,** 27, (20), 12585-90.
114. Yager, P.; Domingo, G. J.; Gerdes, J., Point-of-care diagnostics for global health. *Annu. Rev. Biomed. Eng.* **2008,** 10, 107-44.
115. Balu, B.; Berry, A. D.; Hess, D. W.; Breedveld, V., Patterning of superhydrophobic paper to control the mobility of micro-liter drops for two-dimensional lab-on-paper applications. *Lab Chip* **2009,** 9, (21), 3066-75.
116. Li, L.; Breedveld, V.; Hess, D. W., Hysteresis controlled water droplet splitting on superhydrophobic paper. *Colloid Polym. Sci.* **2012**.
117. Keskinen, H.; Mäkelä, J. M.; Aromaa, M.; Ristimäki, J.; Kanerva, T.; Levänen, E.; Mäntylä, T.; Keskinen, J., Effect of silver addition on the formation and deposition of titania nanoparticles produced by liquid flame spray. *J. Nanopart. Res.* **2006,** 9, (4), 569-588.
118. Tikkanen, J.; Gross, K. A.; Berndt, C. C.; Pitkänen, V.; Keskinen, J.; Raghu, S.; Rajala, M.; Karthikeyan, J., Characteristics of the liquid flame spray process. *Surf. Coat. Technol.* **1997,** 90, 210-216.
119. Mäkelä, J. M.; Keskinen, H.; Forsblom, T.; Keskinen, J., Generation of metal and metal oxide nanoparticles by liquid flame spray process. *J. Mater. Sci.* **2004,** 39, 2783-2788.

120. Mäkelä, J. M.; Hellstén, S.; Silvonen, J.; Vippola, M.; Levänen, E.; Mäntylä, T., Collection of liquid flame spray generated TiO2 nanoparticles on stainless steel surface. *Mater. Lett.* **2006,** 60, (4), 530-534.
121. Aromaa, M.; Keskinen, H.; Mäkelä, J. M., The effect of process parameters on the Liquid Flame Spray generated titania nanoparticles. *Biomol. Eng.* **2007,** 24, (5), 543-8.
122. Keskinen, H.; Mäkelä, J. M.; Aromaa, M.; Keskinen, J.; Areva, S.; Teixeira, C. V.; Rosenholm, J. B.; Pore, V.; Ritala, M.; Leskelä, M.; Raulio, M.; Salkinoja-Salonen, M. S.; Levänen, E.; Mäntylä, T., Titania and titania-silver nanoparticle deposits made by Liquid Flame Spray and their functionality as photocatalyst for organic- and biofilm removal. *Catal. Lett.* **2006,** 111, (3-4), 127-132.
123. Awitor, K. O.; Rivaton, A.; Gardette, J. L.; Down, A. J.; Johnson, M. B., Photo-protection and photo-catalytic activity of crystalline anatase titanium dioxide sputter-coated on polymer films. *Thin Solid Films* **2008,** 516, (8), 2286-2291.
124. Calcagnile, P.; Fragouli, D.; Bayer, I. S.; Anyfantis, G. C.; Martiradonna, L.; Davide Cozzoli, P.; Cingolani, R.; Athanassiou, A., Magnetically Driven Floating Foams for the Removal of Oil Contaminants from Water. *ACS Nano* **2012,** 6, 5413-5419.
125. Valden, M., Onset of Catalytic Activity of Gold Clusters on Titania with the Appearance of Nonmetallic Properties. *Science* **1998,** 281, (5383), 1647-1650.
126. Cho, S.; Choi, W., Solid-phase photocatalytic degradation of PVC–TiO2 polymer composites. *J. Photochem. Photobiol. A* **2001,** 143, 221-228.
127. Keskinen, H.; Mäkelä, J. M.; Heikkinen, R.; Suopanki, A.; Keskinen, J., Synthesis of Pd–alumina and Pd–lanthana Suspension for Catalytic Applications by One-step Liquid Flame Spray. *Catal. Lett.* **2007,** 119, (1-2), 172-178.
128. Takeda, S.; Fukawa, M.; Hayashi, Y.; Matsumoto, K., Surface OH group governing adsorption properties of metal oxide films. *Thin Solid Films* **1999,** 339, 220-224.
129. Wang, C.-y.; Groenzin, H.; Shultz, M. J., Molecular Species on Nanoparticulate Anatase TiO2 Film Detected by Sum Frequency Generation: Trace Hydrocarbons and Hydroxyl Groups. *Langmuir* **2003,** 19, 7330-7334.
130. Tilocca, A.; Selloni, A., Methanol Adsorption and Reactivity on Clean and Hydroxylated Anatase(101) Surfaces. *J. Phys. Chem. B* **2004,** 108, 19314-19319.
131. Wang, C.-y.; Groenzin, H.; Shultz, M. J., Surface Characterization of Nanoscale TiO2 Film by Sum Frequency Generation Using Methanol as a Molecular Probe. *J. Phys. Chem. B* **2004,** 108, 265-272.
132. Wang, C.-y.; Groenzin, H.; Shultz, M. J., Direct Observation of Competitive Adsorption between Methanol and Water on TiO2: An in Situ Sum-Frequency Generation Study. *J. Am. Chem. Soc.* **2004,** 126, 8094-8095.
133. Gong, X.-Q.; Selloni, A., Reactivity of Anatase TiO2 Nanoparticles: The Role of the Minority (001) Surface. *J. Phys. Chem. B* **2005,** 109, 19560-19562.
134. Verho, T.; Korhonen, J. T.; Sainiemi, L.; Jokinen, V.; Bower, C.; Franze, K.; Franssila, S.; Andrew, P.; Ikkala, O.; Ras, R. H. A., Reversible switching between superhydrophobic states on a hierarchically structured surface. *PNAS* **2012,** 109, (26), 10210-10213.
135. Diebold, U., The surface science of titanium dioxide. *Surf. Sci. Rep.* **2003,** 48, 53-229.
136. Fujishima, A.; Rao, T. N.; Tryk, D. A., Titanium dioxide photocatalysis. *J. Photochem. Photobiol. C* **2000,** 1, 1-21.

137. Carp, O., Photoinduced reactivity of titanium dioxide. *Prog. Solid State Chem.* **2004,** 32, (1-2), 33-177.
138. Fujishima, A.; Zhang, X.; Tryk, D., TiO2 photocatalysis and related surface phenomena. *Surf. Sci. Rep.* **2008,** 63, (12), 515-582.
139. Tuominen, M., Multifunctional nanoparticle coatings on cellulose-based substrates using liquid flame spray (LFS) technique. In: *Ekmandagarna*, Stockholm, Sweden, 2013.

Appendices

Publication 1

Teisala, H.; Tuominen, M.; Aromaa, M.; Mäkelä, J. M.; Stepien, M.; Saarinen, J. J.; Toivakka, M.; Kuusipalo, J.

Development of superhydrophobic coating on paperboard surface using the Liquid Flame Spray

Surface and Coatings Technology **2010**, 205, 436–445, DOI: 10.1016/j.surfcoat.2010.07.003

Development of Superhydrophobic Coating on Paperboard Surface Using the Liquid Flame Spray

H. Teisala[a,*], M. Tuominen[a], M. Aromaa[b], J.M. Mäkelä[b], M. Stepien[c], J.J. Saarinen[c], M. Toivakka[c] and J. Kuusipalo[a]

[a]Paper Converting and Packaging Technology, Department of Energy and Process Engineering, Tampere University of Technology, P.O. Box 541, FI-33101 Tampere, Finland
[b]Aerosol Physics Laboratory, Department of Physics, Tampere University of Technology, P.O. Box 692, FI-33101 Tampere, Finland
[c]Laboratory of Paper Coating and Converting, Center for Functional Materials, Åbo Akademi University, Porthansgatan 3, FI-20500 Åbo / Turku, Finland
*Corresponding author: hannu.teisala@tut.fi, tel. +358414461662, fax. +358331153781

Abstract

This paper introduces a new method for generating nanoscale coatings in continuous roll-to-roll process at normal pressure. Nanostructured and transparent coating, based on titanium dioxide nanoparticles, was successfully deposited on-line at atmospheric conditions on pigment coated paperboard using a thermal spray method called the Liquid Flame Spray (LFS). The LFS coating process is described and the influences of process parameters on coating quality are discussed. Nanocoating was investigated by field emission gun scanning electron microscope (FEG-SEM), atomic force microscope (AFM), X-ray photoelectron spectroscopy (XPS) and water contact angle measurement.

The highest measured water contact angles on the nanocoated paperboard surface were over 160°. Falling water droplets were able to bounce off the surface, which is illustrated by high speed video system images. Regardless of the high hydrophobicity, the coating showed sticky nature, creating a high adhesion to water droplets immediately as the motion of the droplets stopped. Nanocoating with full coverage of the substrate was produced at line speeds up to 150 m/min. Therefore, the LFS coating has scale up potential to industrial level as an affordable and efficient method for coating large volumes at high line speeds.

Keywords: superhydrophobic, paperboard coating, on-line process, titanium dioxide nanoparticle, Liquid Flame Spray

1. Introduction

Paperboard is a highly versatile material with various favourable properties, e.g. biodegradability, renewability, mechanical flexibility and affordability. The complete utilisation of the versatility of paperboard requires the ability to control its surface properties. Comprehensive control of surface properties of paperboard, e.g. hydrophilicity and hydrophobicity, can benefit in the various converting processes of paperboard, including printing, extrusion coating, lamination, etc. [1]. The wettability (hydrophilicity) of paperboard surface can be increased with several industrial (roll-to-roll) surface modification techniques, like flame, corona discharge or atmospheric plasma treatments. These well-established surface modification techniques improve printability properties of paper [2] and enhance adhesion between polymers and paperboard or paper [3,4]. Generation of hydrophobic surface on cellulose based materials, e.g. on paperboard or paper, is more complicated, although several plasma and wet chemical techniques have been reported. Superhydrophobic surfaces have been created by fluorinating the paper using grafting and post-functionalisation [5] or by silane coating the paper through solution immersion process [6]. Plasma-assisted deposition of thin fluorocarbon [7−9], organosilicon [9] and hydrocarbon coatings [9] has also resulted in hydrophobic paper surfaces. Balu et al. [10] obtained superhydrophobic paper surface by combining plasma etching with PECVD (plasma enhanced chemical vapour deposition) of fluorocarbon film. However, for the paper or paperboard substrate, the plasma techniques are not yet utilised in large scale in packaging industry. The main limitation for the utilisation of plasma techniques in packaging industry is often the operating costs, because plasma deposition at vacuum or low pressure requires expensive vacuum chambers and pumps in order to create and contain the plasma process. Another drawback for vacuum or low-pressure systems and most of the wet chemical processes is that they are usually batch operations, which is not favoured in paper coating and lamination due to high-volume continuous roll-to-roll processes. Furthermore, fluoropolymers are widely used in superhydrophobic surfaces, but because of health issues they cannot be applied for example in food packaging.

Liquid Flame Spraying (LFS) is a thermal spraying method for generating and depositing nano-sized (less than 100 nanometres) metal and metal oxide particles. Initially the LFS was developed as a method for glass colouring [11]. Nowadays the LFS is also utilised in fibre doping [12] and for coating various substrates, for example ceramic tiles [13] or metal surfaces [14]. The continuous nature of the LFS process and the operating conditions at normal atmospheric pressure enable on-line roll-to-roll coating procedure to be used.

In the LFS process the precursors are in liquid form, diluted in water or alcohol, and are fed together with the combustion gases into a special designed spray gun. Instantly after exiting the burner nozzle the precursor solution is atomised to micron-sized droplets by the high-velocity gas flow. Liquid droplets evaporate in a hot and turbulent flame and subsequent reactions of the precursor vapour lead to formation of nanoparticles of desired material [15]. Afterwards nanoparticles grow larger in the flame by condensation, coagulation, coalescence and

agglomeration [16−18]. The final particle size can be controlled, e.g. via total mass flow rate of the precursor (product of the precursor solution feed rate and its concentration) or by adjusting the collecting or depositing distance [19−22]. The main exhaust gases formed as by-products in the LFS process are normally water vapour and carbon dioxide. Low waste flows combined with relatively simple and inexpensive equipment make the LFS process comparatively cheap and environmentally friendly.

LFS coatings consisting of nanoparticles have large fraction of surface molecules and hence high reactivity [16,23,24]. Added to this, the nanoscale roughness of the surface creates unique topography for the nanocoating and enlarges its effective surface area. The properties of the LFS-made coatings may therefore vary remarkably from the properties of homogeneous coatings made of bulk materials. LFS coatings have potential to improve properties traditionally demanded for example from packaging materials, such as barrier and adhesion, but these coatings may also introduce totally new functional properties for the materials, including antibacterial, self-cleaning, non-sticking, non-wetting, superwetting, light protection, heat and wear resistance and electrical properties for example.

The range of suitable LFS precursors, i.e., metal salts and alkoxides in water or alcohol solution, is wide. Thus a large number of various coatings with unique properties can be produced using the LFS. Iron and manganese oxide, alumina, silica, titania, silver and palladium nanoparticles have been successfully produced in laboratory scale using the LFS [13−15,19−22]. Multi-component materials can also be produced by mixing different precursors together [25−28].

The LFS coating parameters (i.e. concentration and feed rate of the precursor solution, gas flows, burner distance and line speed) must be carefully adjusted in order to obtain the desired coating quality. For instance, the properties of nanoparticles are strongly related to particle size [16,23,24], thus incorrect coating parameters may change the coating composition and properties dramatically. It is widely known that both the chemistry and the topography of a surface affect water contact angle (CA) [29−34]. By adjusting the surface roughness in micro- or nanoscale the hydrophobicity of the surface can be enhanced. Furthermore, the combination of micro- and nanoroughness (hierarchical roughness) is an effective way to increase surface hydrophobicity. On flat surfaces the highest CAs achieved are normally around 120°, but proper roughness of the surface can raise the CA close to 180°. Even materials which are inherently hydrophilic (CA < 90°) on a flat surface may show CAs of over 150°, if the surface is appropriately patterned [35,36]. Surfaces which have extraordinary high CA are often called superhydrophobic, and the widely accepted criterion for superhydrophobicity is the CA value of over 150°.

Superhydrophobic surfaces have raised much interest during the last decade, and many research groups have dedicated themselves to the development and manufacturing of such surfaces [33−43]. Quite often, guidance and inspiration for producing superhydrophobic surfaces can be found from the nature, for example leaves of lotus plant [44]. There are numerous ways to prepare superhydrophobic surfaces, e.g. plasma, laser and chemical etching, sol-gel methods,

lithographical means, replicate templates, electrochemical methods and various spraying methods [33,45−47]. Usually superhydrophobic surfaces are prepared by patterning low-surface-energy material or by inducing low-surface-energy layer on patterned surface afterwards. Almost any substance can be used as a substrate for superhydrophobic surfaces, including fluorocarbons, silicones, hydrocarbons and metal oxides [33]. In recent years even fibre-based materials, such as paper, have been successfully modified to produce superhydrophobic surfaces [5,6,10,48], as mentioned above. Most of the artificially made superhydrophobic surfaces exhibit the lotus-effect, i.e., water droplets roll off easily from the surface. However, studying and manufacturing of sticky superhydrophobic surfaces has recently attracted increasing interest [10,45,48−51].

The main purpose of this work is to demonstrate the creation of superhydrophobic surface on paperboard using a LFS on-line coating process. In addition, a goal is to understand the influences of various process parameters on the coating quality. Wettability of the nanocoated surface was studied by CA measurement and the behaviour of water droplets on the nanocoating was observed using high speed video system. The structure of the coating was investigated by field emission gun scanning electron microscope (FEG-SEM) and atomic force microscope (AFM). Chemical composition of paperboard and nanocoated surfaces was investigated by X-ray photoelectron spectroscopy (XPS). The nanocoating wear resistance and adhesion to paperboard surface were evaluated using simple abrasion and tape tests.

2. Materials and Methods

Titanium dioxide (TiO_2) nanoparticles were generated and deposited directly on the pigment coated paperboard (200 g/m^2, Natura, Stora Enso, Skoghall mill Sweden) surface using the LFS. TiO_2 was selected as a coating material because it is well known from earlier studies [21,27], but also because of its non-toxicity. Precursor for the nanocoating was titanium tetraisopropoxide (TTIP, 97 % pure, Aldrich). TTIP was diluted in isopropyl alcohol (IPA), so that two precursor solutions of separate concentrations (low concentration, LC ≈ 11.5 mg of pure Ti/ml and high concentration, HC ≈ 50 mg of pure Ti/ml) were obtained. The combustion gases used in this study were hydrogen (H_2) and oxygen (O_2). Reaction product of hydrogen-oxygen combustion is pure water, and the temperature in the flame is high enough to evaporate most of the precursor materials.

The LFS coating procedure was performed at Tampere University of Technology (TUT) on the Paper Converting and Packaging Technology (PCPT) pilot line. At this stage of examinations only one burner was used, and hence the width of the highly hydrophobic coating was relatively narrow, ca. 50 mm. The LFS burner was installed inside a hood which was equipped with an air exhaust duct for purging unattached particles. The flame was pointed downwards and the web was running below the burner. A schematic picture of the experimental set-up is presented in Fig. 1.

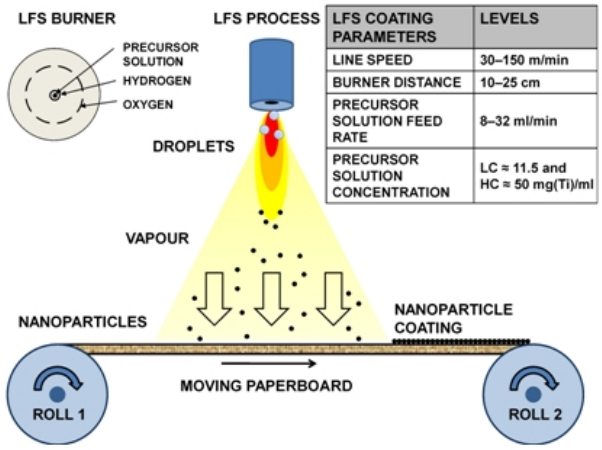

LFS COATING PARAMETERS	LEVELS
LINE SPEED	30–150 m/min
BURNER DISTANCE	10–25 cm
PRECURSOR SOLUTION FEED RATE	8–32 ml/min
PRECURSOR SOLUTION CONCENTRATION	LC ≈ 11.5 and HC ≈ 50 mg(Ti)/ml

Fig. 1. The LFS coating process (on-line) and the parameters.

The coating parameters which were varied were the concentration and the feed rate of the precursor solution, the burner distance and the line speed (Fig. 1). All the parameters affect the characteristics of the nanocoating, thus the desired end-use properties of the final coating must be taken into consideration when adjusting the coating parameters. Simultaneously, the type of the substrate and its limitations must also be taken into account. Furthermore, the volume and the ratio of the gas flows (H_2 and O_2) must be correctly chosen to obtain proper quality of the nanocoating.

The precursor solution was fed into a capillary needle in the middle of the burner by an infusion pump at a constant feed rate. Hydrogen was used as a combustion gas and an atomising gas, and it was fed into the flame through a circular channel immediately next to the precursor needle (Fig. 1). The other combustion gas, oxygen, was fed through the outer ducts, which form a circular ring around the precursor needle and the hydrogen flow channel. The volume flows for hydrogen and oxygen were 50 and 15 l/min respectively. The flow rates of the gases were controlled by Alicat Scientific mass flowmeters.

The nanocoating was examined by FEG-SEM (Zeiss ULTRAplus), AFM (NT-MDT NTEGRA Prima), XPS (PHI Quantum 2000) and CA measurement (KSV CAM200 and Pocket goniometer PG3). Due to resistive nature of paperboard the samples were sputter coated twice by thin carbon film prior to the FEG-SEM imaging. XPS instrument was equipped with a monochromatic Al K α X-ray source and operated at 25 W, where the charge compensation was enhanced by a combination of electron flood and ion bombarding. High resolution spectra were recorded with pass energy of 29.35 eV of oxygen O1s peak and titanium Ti2p peak. The CA measurement was done by distilled water and the CA value was taken approximately 3 seconds after the droplet placement (volume of 2 µl), unless mentioned otherwise. In 3 seconds the vibration of the droplet has settled down, but water evaporation and penetration to the substrate have not dramatically decreased the droplet volume and the CA yet. At least 3 parallel droplets were used in all the CA measurements. If additional information has not been given, the CA announced represents the

centre line of the coating stripe. A falling water droplet dynamics on the nanocoated surface was investigated by Memrecam fx K5 high speed video system (1000 frames per second).

Abrasion and tape tests were performed in order to evaluate the wear resistance and adhesion of the nanocoating. The tape test was carried out by gluing and releasing the tape (Scotch Crystal) 1, 10 and 20 times on the nanocoating surface. The abrasion test was carried out by wiping the nanocoated surface 1, 10 and 20 times with dry microfibre tissue. Metal cylinder (1.0 kg, contact area of 50 cm^2) was kept as a weight on the tissue to ensure constant wiping pressure. After the wear tests, the CA measurement was used for evaluating the stability of the nanocoating on the paperboard surface.

3. Results and Discussion

3.1. The Process Parameters

3.1.1. The Feed Rate of the Precursor Solution

The LFS coating procedure has always dual effect on the substrate: the formation of the nanocoating and the effect of the flame. Traditional flame treatment is relatively simple and well established method for increasing the surface energy (CA decreases) of various substrates. However, the LFS flame differs significantly from the traditional surface treatment flame, e.g. the oxygen content of traditional flame is much higher and the burner distance is much shorter [1,3].

When the burner distance is short (15 cm) and the line speed is slow (30 m/min), the pure LFS flame treatment (only IPA without any actual precursor) increases the CA on paperboard surface from the initial level of 54° (Fig. 2). This might be caused by various occurrences on the surface, like reduction of hydrophilic material from the surface, deposition of carbon containing hydrophobic material to the surface and changes in surface roughness for instance. Similar, but stronger effect can be observed when actual precursors are used, thus highly hydrophobic nanocoating with CAs of ~ 140° can be produced on paperboard surface. The higher the feed rate of the precursor solution, the higher the hydrophobicity of the final coating. The increase in hydrophobicity can be related to chemical and structural changes of the surface, which will be discussed in detail later on in this chapter (3.1). Furthermore, the nanocoating becomes wider when higher concentration of the precursor solution is used, i.e., the coating strip widens when more nanoparticles are produced.

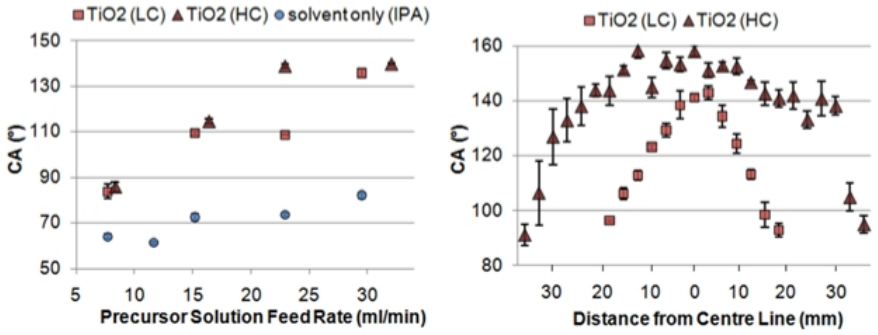

Fig. 2. The effect of the precursor solution feed rate and concentration on the CA of the nanocoated paperboard (left) and on the width of the nanocoating (right). Error bars indicate standard deviation. Feed rates for TiO_2 LC and HC were 30 and 32 ml/min respectively (burner distance 15 cm, line speed 30 m/min).

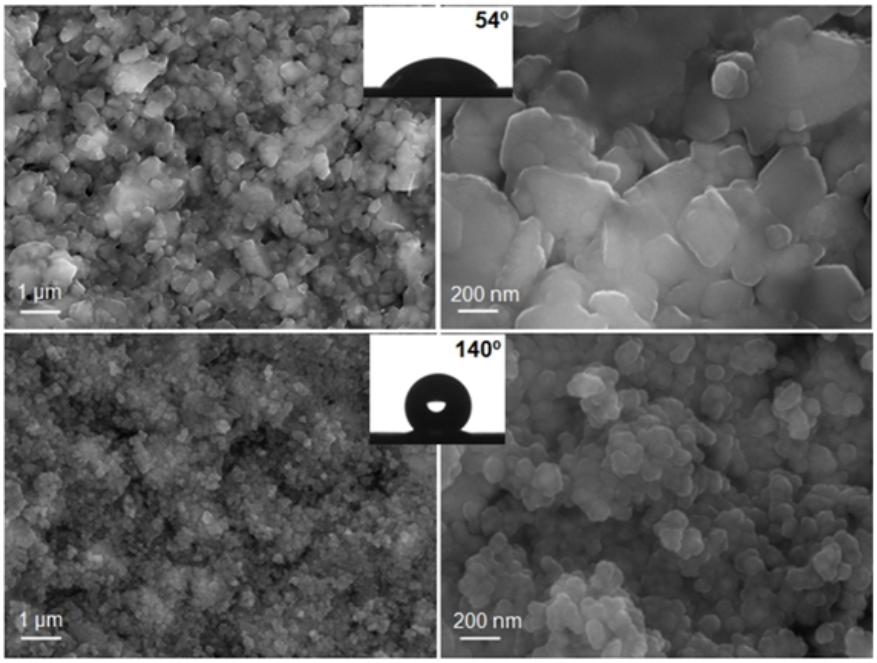

Fig. 3. FEG-SEM images of the pigment coated paperboard surface before (above) and after (below) the nanocoating (HC, feed rate 32 ml/min, burner distance 15 cm, line speed 30 m/min).

The LFS coated paperboard surface seems to be fully covered with highly sintered nanoparticles, which form a porous coating structure (Fig. 3). For human eye the nanocoating looks transparent. The size range for synthesised nanoparticles varies between ~ 20−80 nanometres depending on the coating parameters, thus the nanoparticles themselves and the interfacial gaps between the particles provide the nanoscale roughness for the surface. The larger scale roughness arises from the agglomerates of nanoparticles and microroughness of the substrate. The specific structure and roughness of the surface increases the hydrophobicity of the nanocoating.

Mäkelä et al. [52] made chemical analysis in order to quantify the mass of deposited nanoparticles. According these analyses, the deposited TiO_2 mass on the paperboard substrate should be in order of tens mg/m^2 at the maximum. The accurate thickness of the coating is very challenging to measure, but on the basis of the chemical analysis and FEG-SEM images, it can be estimated that the coating thickness should be less than one micrometre.

3.1.2. The Burner Distance

The number of attached nanoparticles on the paperboard surface reduces significantly as the distance between the burner face and the substrate is increased, leading to a drastic decrease in the CA on the surface. An increased burner distance (from 15 to 20 cm) can still be used to produce a hydrophobic surface, but it requires high concentration of the precursor solution. (Fig. 4)

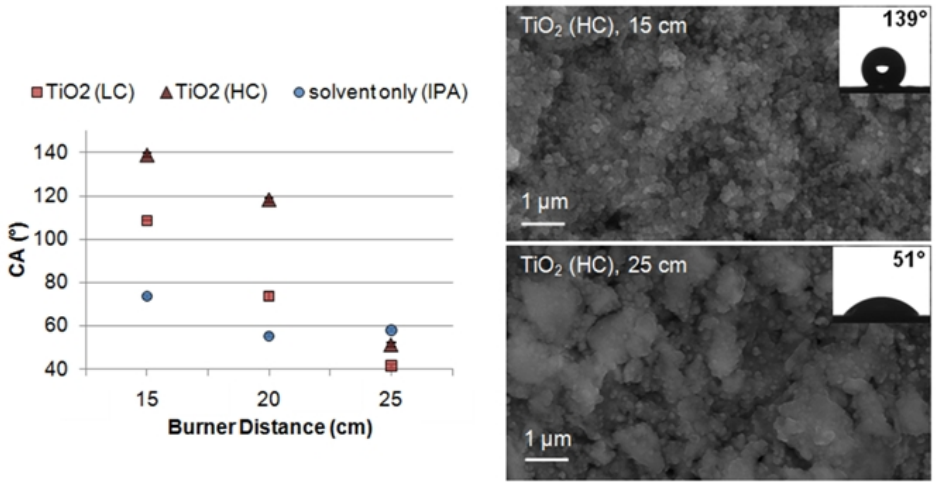

Fig. 4. CAs and FEG-SEM images of the nanocoating produced by variable burner distances (feed rate 23 ml/min, line speed 30 m/min). Error bars indicate standard deviation.

There are several reasons for weak nanocoating deposition on the paperboard surface as a result of the long burner distance usage (Fig. 4). First of all, the number density of nanoparticles in the aerosol decreases, i.e., the aerosol dilutes as the distance from the burner face increases. This is due to enlargement of the aerosol in horizontal direction, which occurs because of particle transportation by gas flows, diffusion and thermophoresis (particle transport from hot to cold temperature) [16−18]. Furthermore, before reaching the substrate, nanoparticles must migrate through a thin boundary layer of air which moves with the paperboard, immediately above its surface. The most important particle transportation mechanisms through the layer of air are diffusion and thermophoresis. The effect of both mechanisms is reduced when the burner distance is increased because the gradients in particle content and temperature decrease, and hence the number of particles passing the boundary layer of air decreases. The attachment efficiency of nanoparticles to the paperboard surface may also weaken as a result of increased burner distance. This could happen due to changed conditions, e.g. temperature and pressure, on the paperboard surface. Mäkelä et al. [52] carried out temperature measurements in the flame (at

distance of 10–25 cm from the burner face) and on the paperboard surface with various IPA feeding rates. They measured temperatures ranging from 450 ºC to over 2000 ºC in the flame and temperatures between 72–115 ºC on the paperboard surface and discussed the boundary layer issue in detail.

3.1.3. The Line Speed

As a result of the increased line speed, both the amount of the nanocoating and the CA on the surface decrease (Fig. 5). Higher concentration of the precursor solution allows faster line speeds, still ensuring enough nanocoating on the surface to maintain its hydrophobicity. Shortening the burner distance to less than 15 cm also enables faster line speeds and improves the efficiency of the coating process significantly. Usage of low concentration at 10 cm burner distance results almost similar CAs as the usage of high concentration at 15 cm distance, pointing out that shortening of the burner distance leads to much more efficient particle deposition onto the substrate. This important fact was also observed in Fig. 4. Hence, the usage of short burner distances is reasonable for minimising precursor consumption and thus making the process more economical. Furthermore, short burner distance together with small mass flow rate of the precursor result in smaller particle size, which is often favourable. However, if the total mass flow rate of the precursor is very high, the liquid evaporation and the particle formation take more time. As a consequence, some of the precursor may deposit on the substrate as liquid or vapour if too short burner distances are used. This may naturally change the coating structure and properties significantly.

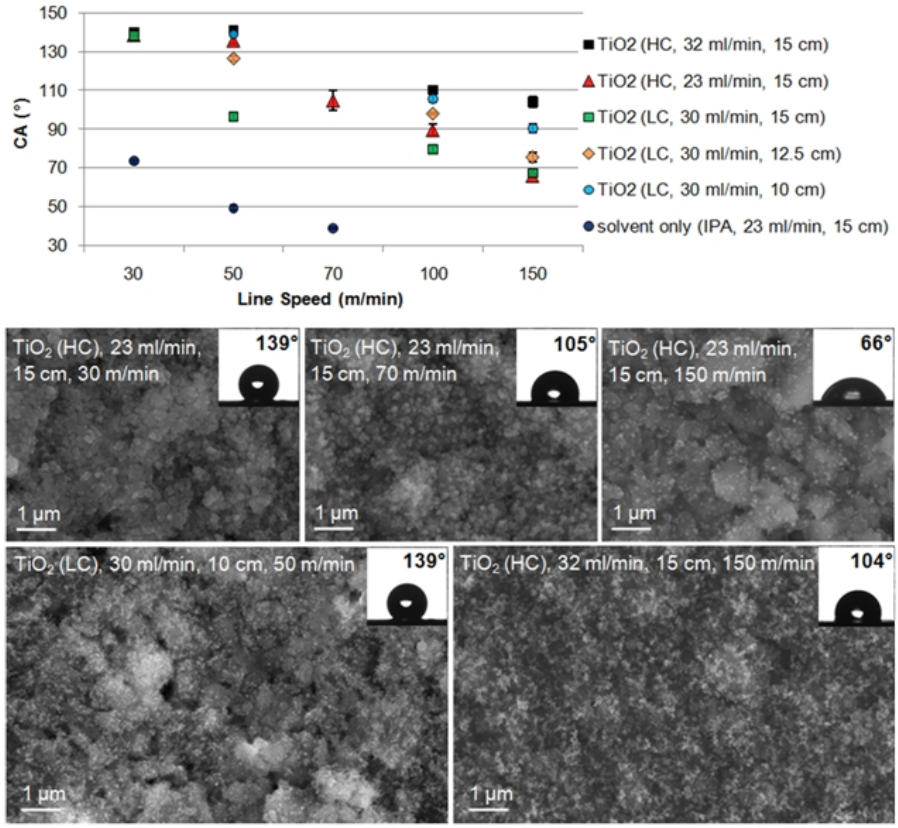

Fig. 5. CAs on the nanocoated paperboard surface as a function of line speed and FEG-SEM images of nanocoatings produced with various sets of parameters. Error bars indicate standard deviation.

CA on the nanocoated paperboard surface decreases with increasing line speed, even if the substrate was still fully covered with nanoparticles (Fig. 5). The main reason for the CA decrease on the surface seems to be the structural changes of the nanocoating. Although the nanosized roughness still exists on the surface, on the grounds of several FEG-SEM images, the larger scale roughness seems to have remarkably reduced so that the micron or submicron structure of the surface has rounded and the height differences between the highest and the lowest points of the surface have reduced. One reason for the decrement of larger scale structure is the reduced amount of deposited nanoparticles, which is a natural consequence of increased line speed, and leads to smaller aggregates of particles on the substrate. However, there are also several other factors that are involved with transportation and deposition of nanosized particles, which were discussed earlier in section 3.1.2.

At low line speeds the paperboard surface is exposed to the flame for relatively long time, and hence the particle growth and sintering may still continue on the surface or immediately above it [52]. However, considering the high hydrophobicity of the nanocoating, the existence of micron or submicron sized roughness on the surface seems to be much more important than the actual particle size, because hierarchically structured nanocoating surface which composes of small

particles of ~ 40 nanometres in diameter (studied by FEG-SEM) also possesses high hydrophobicity (Fig. 5 bottom left, LC, 30 ml/min, 10 cm, 50 m/min).

3.1.4. XPS Analysis of the Deposited Nanoparticles

The surface chemical analysis of the LFS nanocoated surface is performed using XPS. From the binding energy of a photoelectron peak the elemental identity, chemical state, and semiquantity of an element are determined and presented in Fig. 6. The low-resolution survey spectra show the chemical composition of the reference surface in Fig. 6 a) and nanocoated surface in Fig. 6 b). The presence of calcium (Ca), silicon (Si), and aluminium (Al) peaks indicate that both calcium carbonate (Ca) and kaolin (Si, Al) pigments were used in coating colour of the paperboard. For nanocoated sample titanium (Ti) peak with much higher intensity than in the reference sample is found. From high resolution Ti2p spectra it is possible to determine the types of titanium-oxygen bonding formed during nanoparticle deposition, and the results are presented in Fig. 6 c). The binding energies of Ti2p at 458.2 eV and 464.0 eV may be identified as titanium-oxygen bonds corresponding to TiO_2 [53]. XPS analysis gives chemical information approximately from 10 nm depths of the substrate, while fabricated nanocoatings with present parameters according to the deposition model described by Mäkelä et al. [52] leads to the deposition mass of 12.7 mg/m^2 and a coverage of 16% for titanium dioxide. Here, we are aware that more surface sensitive techniques would be desirable in order to reach an analysis only on the level of nanoparticle deposition despite a complex background resulting from the paperboard substrate.

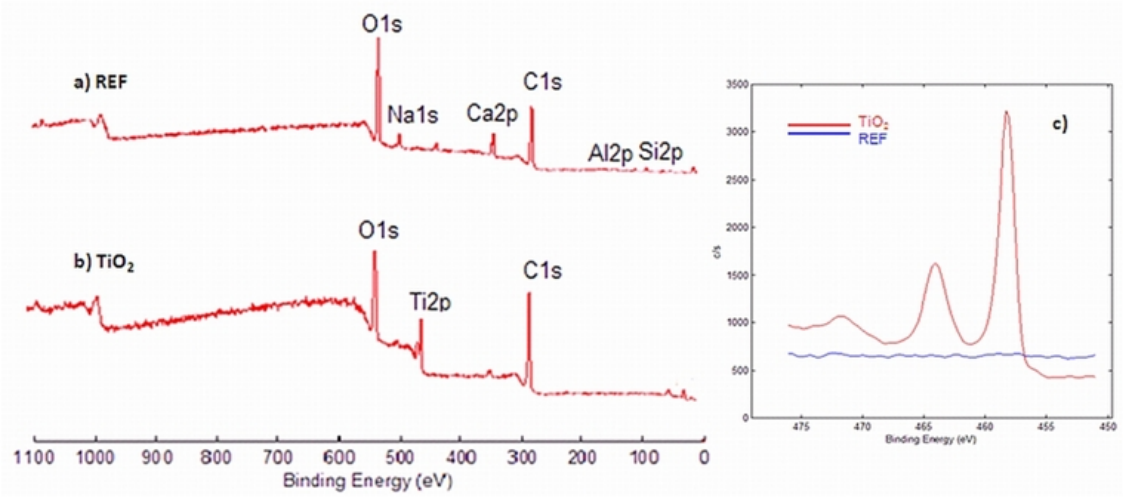

Fig. 6. Comparison of XPS survey of reference paperboard a) to TiO_2 nanocoated sample b), and a comparison of high resolution Ti2p spectra c) to the reference sample.

It is known that hydroxyl groups play important role in the surface properties of metal oxides, for example in the adsorption efficiency of organic substances [54,55]. In addition to the topographical changes, variation in the LFS coating process parameters may also cause changes in the surface chemistry of the nanocoating. Therefore, the variation in the CA of the nanocoating

cannot be strictly related only to the topographical changes of the surface. A more detailed chemical analysis of the nanocoating will be carried out in future examinations.

The FEG-SEM images show that full coating coverage of the paperboard combined with relatively smooth microstructural topography of the coating was obtained even at line speed of 150 m/min (Fig. 5 bottom right, HC, 32 ml/min, 15 cm). Therefore, it can be concluded that particle deposition onto the substrate occurs effectively also with high line speeds, which is obviously a positive observation considering the ambition for higher line speeds and larger coating volumes used in industrial processes.

3.2. Water Droplet Behaviour on the Nanocoating Surface

3.2.1. Spreading of the Droplet

Normally water droplets spread on the surface of pigment coated paperboard. As a result, the surface wets more efficiently as time passes and the CA of the droplet decreases. The decrease in the CA is rapid at first but slows down afterwards (Fig. 7).

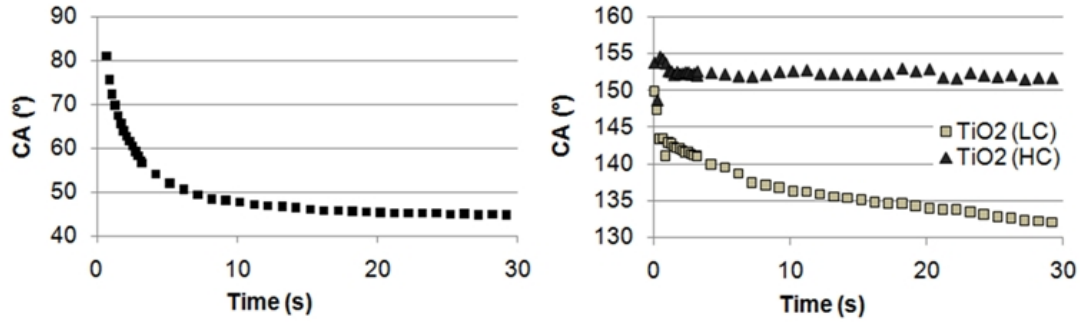

Fig. 7. The water droplet spreading as a function of time on the paperboard (left) and on the nanocoated paperboard (right). Feed rates for TiO_2 LC and HC were 30 and 32 ml/min respectively (burner distance 15 cm, line speed 30 m/min).

Although the initial CA on both nanocoating surfaces (LC and HC) is very high, a clear difference on the droplet spreading can be observed. The higher concentration of the precursor solution leads to a stable state on the nanocoating surface, on which the water droplet remains spherical showing a CA of over 150°, whereas on the surface created by the lower precursor concentration the CA starts to decrease slowly (Fig. 7). Differences in the thickness and the structure (e.g. depth of the pores) of the nanocoating could explain the droplet spreading on thinner (LC) coating layer. Some of the water is absorbed into the paperboard and may promote the droplet spreading in the case of the thin nanocoating.

3.2.2. Adhesion Between the Surface and the Droplet

Despite the high hydrophobicity of the nanocoating, the droplets placed on the surface adhered to it strongly. Due to high adhesion, water droplets remained easily on the surface without rolling off, even though the surface was tilted upside down. A set of images from the CA measurement clearly illustrates how strong the adhesive force actually is (Fig. 8). As the water droplet gets in contact with the nanocoating, it adheres to the surface very strongly. When the needle tip is pulled up the droplet starts to stretch between the needle tip and the nanocoating. After detaching from the needle tip the droplet heavily shakes on the surface for a while. Due to rough droplet placement the maximum CA that can be measured usually varies between ~ 140−155°. Thus, the highest CAs presented in this paper would be even higher if the droplet placement was done more gently, e.g. by using a thinner needle. By setting larger droplets (~ 11 µl) manually by using a thin needle, the CA on nanocoating (Fig. 3, HC, 32 ml/min, 15 cm, 30 m/min) was measured as high as 166.6 ± 1.7°.

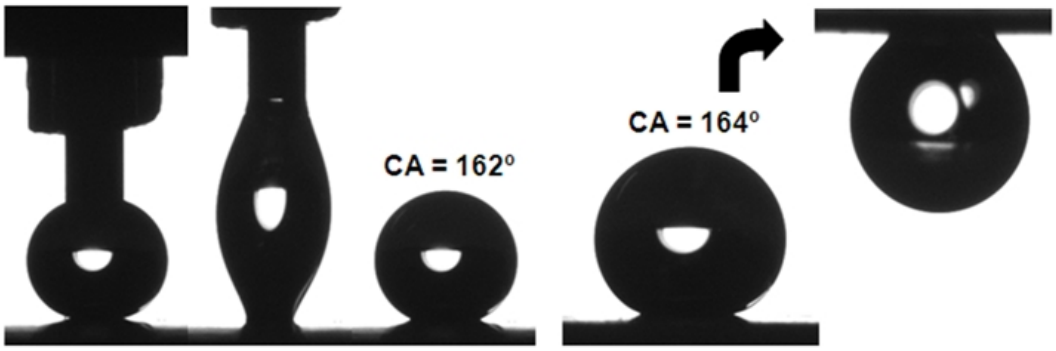

Fig. 8. A set of images from the CA measurement illustrates the high adhesion between the water droplet and the nanocoating surface (left). 5 µl droplet is able to remain on the flipped surface (right). (HC, feed rate 32 ml/min, burner distance 15 cm, line speed 30 m/min).

Similar surfaces, exhibiting extremely high CA and high adhesive force, occurs on rose petals [45] and gecko feet [56] for example, which Feng et al. [45] and Jin et al. [51] have mimicked respectively, preparing similarly structured polystyrene surfaces. Some other researchers have also reported of artificially made highly hydrophobic sticky surfaces [10,48−50]. The high adhesive force is usually explained by the capillary effect and van der Waals forces. The roughness of the LFS nanocoated surface provides a large amount of grooves and gaps which water may penetrate and thus the droplet adheres strongly to the surface.

Stepien and co-workers [57] applied an AFM for the surface topography studies of the LFS nanocoating. The AFM images clearly illustrate the increased nanoscale roughness of the nanocoated paperboard surface (Fig. 9), which was also observed from the FEG-SEM images (Fig. 3). The AFM imaging of LFS-coated paperboard is very challenging because of its complex surface structure. Therefore, for detailed AFM imaging of nanoparticles Stepien et al. also studied LFS nanocoated aluminium foil. These images show that coating process parameters and actual nanocoating material have effect on the sintering rate of nanoparticles in the final coating.

In addition, because of variation in thermal conductivities of different materials, also the substrate may have a role in the sintering of nanoparticles [52].

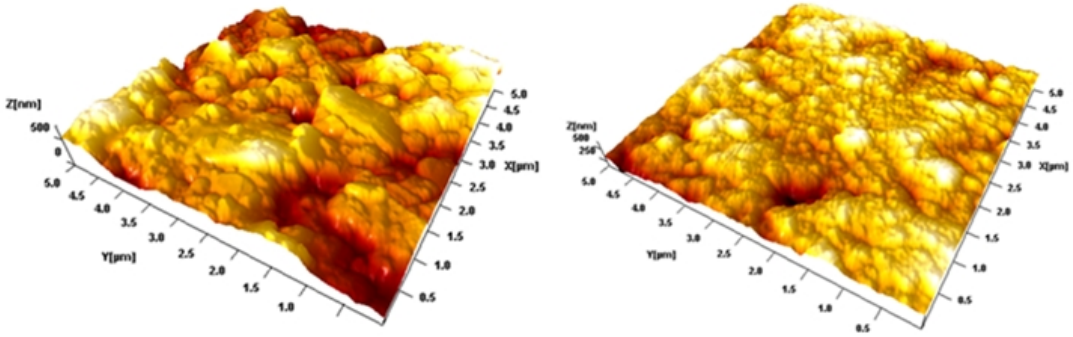

Fig. 9. The AFM images of paperboard surface (left) and TiO_2 nanoparticle coated (LC, feed rate 30 ml/min, burner distance 15 cm, line speed 30 m/min) paperboard surface (right). The z-scales of the paperboard and the TiO_2 nanocoating images are 813 and 491 nm respectively. AFM images (1024 × 1024 pixels, pixel size ~ 5 nm) were captured in ambient conditions (RT 24ºC ± 1ºC and RH 38 ± 5 %) using the tapping mode [57].

The definition of hydrophobic surface (CA > 90°) is clear, but the widely used criterion for superhydrophobicity (CA > 150°) needs specification due to large variation in the adhesion of droplets on different surfaces. Balu et al. [10] listed a large variety of descriptions that has been used for surfaces having high CA but variation in the adhesion level. They categorised highly hydrophobic (CA > 150°) low-adhesive surfaces as “roll-off” superhydrophobic surfaces and the highly hydrophobic high-adhesive ones as “sticky” superhydrophobic surfaces. According to this categorisation, the LFS nanocoating surface could be called “sticky” superhydrophobic surface. Still, many scientists [58−61] have the opinion that in addition to CA of over 150°, truly superhydrophobic surfaces should always have extremely low adhesion to water droplets. Therefore, if the term “superhydrophobic” should be avoided in the case of this highly adhesive LFS nanocoating surface, it could alternatively be called highly hydrophobic adhesive surface.

3.2.3. Dynamics of Falling Droplet on the Nanocoating Surface

Despite the sticky nature of the LFS nanocoating, water droplets can slide, roll or even jump on the surface. Fig. 10 illustrates the dynamics of falling droplets on the surfaces. Due to kinetic energy the falling droplet flattens as it collides with both the paperboard and the nanocoated paperboard. However, on the highly hydrophobic nanocoating the surface tension of water is able to gather the droplet up again, and hence the droplet is able to bounce off the surface, whereas on the paperboard surface the droplet remains flat.

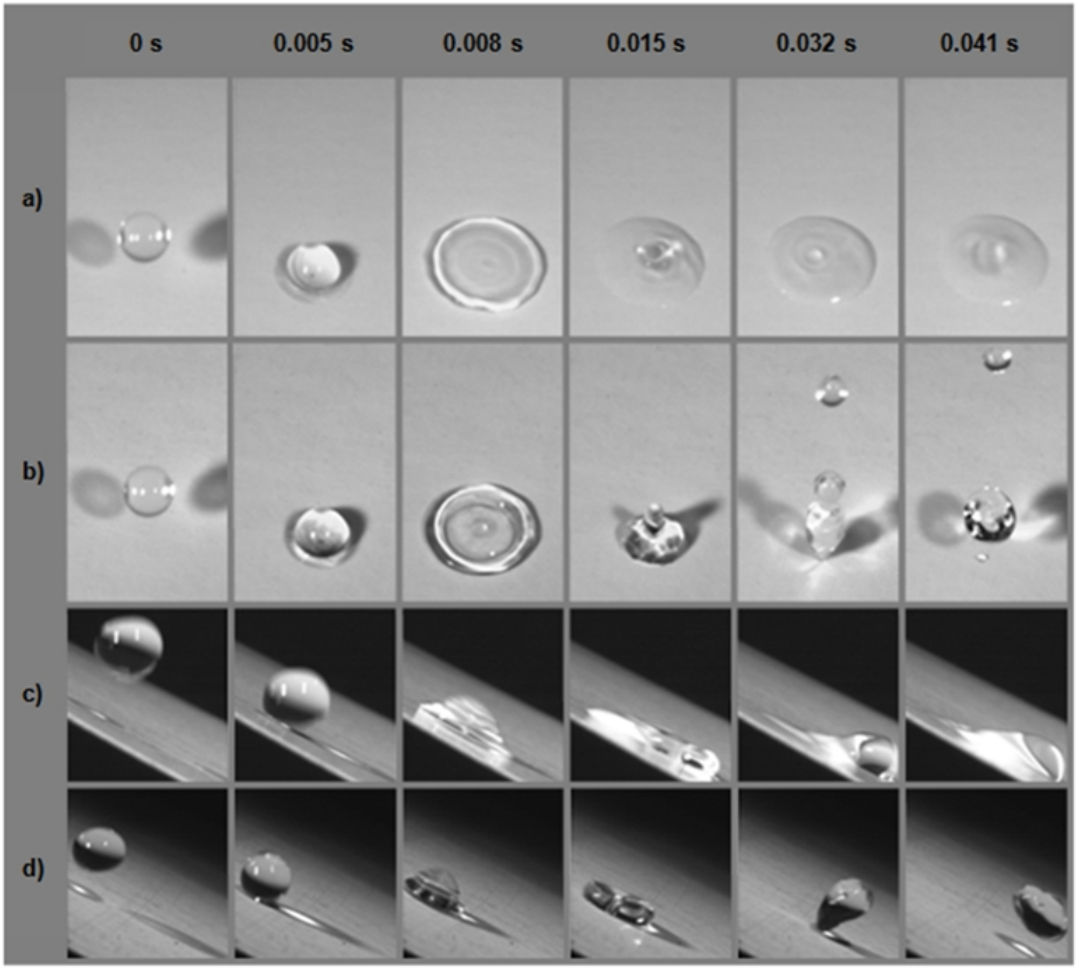

Fig. 10. Dynamics of the falling water droplet on the paperboard (a and c) and on the nanocoated paperboard (b and d). The droplet is able to bounce off the nanocoated surface (HC, feed rate 32 ml/min, burner distance 15 cm, line speed 30 m/min).

When the surface is not tilted (Fig. 10, b), the water droplet does not slide while being flattened, and adheres to the nanocoating within a few milliseconds during which the droplet is in contact with the surface. The pinning occurs in the middle point of the droplet (the point that first touches the surface) where the flow of the water is the lowest, and the local pressure caused by the impact highest. Despite of the rapid pinning, the main part of the droplet is able to bounce off the nanocoated surface. If the surface is tilted (Fig. 10, d) the water droplet slides while being in contact with the nanocoating, thus the forward motion of the droplet remains continuous preventing the droplet from adhering to the surface. In conclusion, as long as the droplet moves it will not attach to the nanocoating surface, but as soon as the motion of the droplet stops the highly adhesive forces take effect. It is also noteworthy that the highly hydrophobic state of the nanocoating will not collapse, even though the impact of the falling droplet creates additional pressure and causes forced wetting of the surface.

3.3. Adhesion of the Nanocoating to the Paperboard Surface

Adhesion of the nanocoating, or more precisely stability of the specific structure of the coating, that highly determines the CA on the surface, was studied by rough wear tests and the CA measurement. The results of the tape and the abrasion tests are presented in Fig. 11. The CA on the nanocoated surface remains significantly higher compared to the CA on the paperboard surface, thus the wear tests indicate that the nanocoating adhesion to the paperboard surface is relatively good.

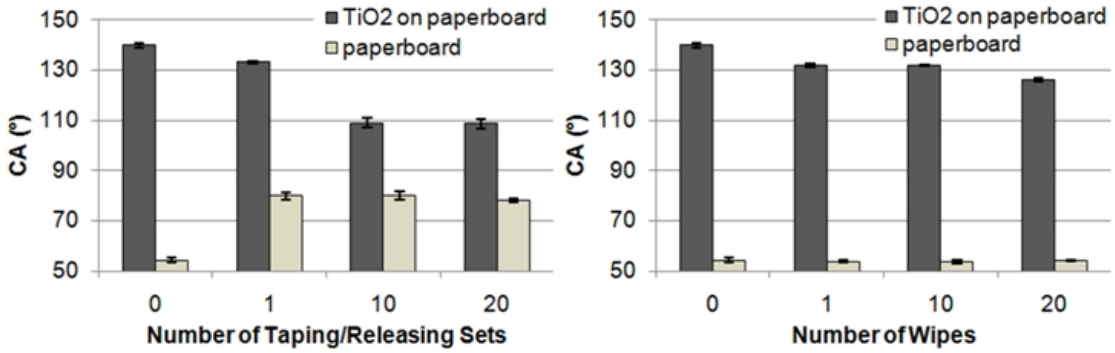

Fig. 11. CA on the nanocoating (HC, feed rate 32 ml/min, burner distance 15 cm, line speed 30 m/min) as a function of taping/releasing sets (left) and after the abrasion test (right). Error bars indicate standard deviation.

The wear tests roughly indicate the adhesion of the nanocoating to the paperboard surface, but in great extent the CA lowering as a result of the wear tests is likely due to destruction or blocking of the specific roughness of the nanocoating surface. Especially the glue of the tape remaining on the surface may block the porous nanocoating or change the surface chemistry (Fig. 11).

The ability to resist wear and contamination is a universal problem among artificial superhydrophobic surfaces. This is because of the fragility of the micro- or nanoscale structure that is needed to increase the hydrophobicity [61,62]. In nature the superhydrophobicity of plants and insects remains under wearing and contaminating conditions because of their ability to renew and maintain the surfaces.

4. Conclusions

A new method for generating nanoscale coatings on-line at atmospheric conditions was introduced. Nanostructured coating based on titanium dioxide nanoparticles was successfully deposited directly on pigment coated paperboard surface in a roll-to-roll process up to 150 m/min by utilising the Liquid Flame Spray. The main parameters of the coating process, besides the type of precursor, are the precursor solution feed rate and concentration, the burner distance and the line speed. The parameters do not affect only the thickness of the nanocoating, but also the topography of it.

Nanoparticles synthesised in this work had a size range of ca. 20−80 nanometres in diameter. The LFS coated surface is hierarchically rough, possessing both micro- and nanoscale roughness. Individual nanoparticles create the nanoscale roughness for the coating, whereas the larger scale roughness arises from the agglomerated nanoparticles and microroughness of the substrate. Prepared nanocoating is transparent and shows hydrophobic nature. The highest measured water contact angle on the nanocoated paperboard surface was 166.6 ± 1.7°. It seems that relatively smooth layer of nanoparticles is not enough to make the surface very hydrophobic, but larger scale roughness is needed in order to obtain the extreme hydrophobicity. A falling water droplet was able to bounce off the nanocoated surface, which indicates that the highly hydrophobic state of the surface did not collapse despite the external pressure and forced wetting. Regardless of the extremely high hydrophobicity of the nanocoating, the water droplets adhered strongly to the surface as soon as their motion stopped. The grooves and gaps of the rough nanocoating surface, which water can penetrate, were deduced to cause the strong adhesion of water droplets. Wear tests indicated that the nanocoating stability on the paperboard surface was relatively good.

The benefits of the LFS coating are affordability and continuous nature of the process. The LFS equipment is relatively simple, inexpensive and reliable, and the coating is carried out roll-to-roll at normal pressure. Therefore, it is likely that the LFS coating can be scaled up to industrial level for coating large volumes at high line speeds.

Acknowledgements

Tekes (Finnish Funding Agency for Technology and Innovation) is acknowledged for the financial support of this study. The work was done in Functional Materials 2007−2013 programme, under the project called Liquid flame spray nanocoating for flexible roll-to-roll web materials. The authors would also like to thank Mrs. Mari Honkanen (TUT, Department of Materials Science) for the FEG-SEM images and Mr. Jari Rämö (TUT, Department of Materials Science) for the high speed video system images.

References

1. J. Kuusipalo (Ed.), Paper and Paperboard Converting, second ed., Paperi ja Puu Oy, Jyväskylä, 2008.

2. M. Pykönen, H. Sundqvist, J. Järnström, O.V. Kaukoniemi, M. Tuominen, J. Lahti, J. Peltonen, P. Fardim, M. Toivakka, Appl. Surf. Sci. 255 (2008) 3217-3229.

3. M. Tuominen, J. Kuusipalo, R. Bothor, T. Lankinen, TAPPI European PLACE Conference, Vienna, 25. May 2005.

4. M. Tuominen, J. Lavonen, J. Kuusipalo, CAPPSA 2009 - 4th International Congress on Cold Atmospheric Pressure Plasmas: Sources and Applications, Ghent, 22.-24. June 2009.

5. D. Nyström, J. Lindqvist, E. Östmark, A. Hult, E. Malmström, Chem. Commun. (2006) 3594-3596.

6. S. Li, S. Zhang, X. Wang, Langmuir 24 (2008) 5585-5590.

7. S.M. Mukhopadhyay, P. Joshi, S. Datta, J. Macdaniel, Appl. Surf. Sci. 201 (2002) 219-226.

8. S. Vaswani, J. Koskinen, D.W. Hess, Surf. Coat. Technol. 195 (2005) 121-129.

9. M. Pykönen, K. Johansson, M. Dubreuil, D. Vangeneugden, G. Ström, P. Fardim, M. Toivakka, J. Adhesion Sci. Technol. 24 (2010) 511-537.

10. B. Balu, J.S. Kim, V. Breedveld, D.W. Hess, J. Adhesion Sci. Technol. 23 (2009) 361-380.

11. K.A. Gross, J. Tikkanen, J. Keskinen, V. Pitkänen, M. Eerola, R. Siikamäki, M. Rajala, J. Therm. Spray Technol. 8 (1999) 583-589.

12. S. Tammela, M. Söderlund, J. Koponen, V. Philippov, P. Stenius, SPIE Photonics West Conference 6116-16, San Jose, 23. January 2006.

13. J.A. Pimenoff, A.K. Hovinen, M.J. Rajala, Thin Solid Films 517 (2009) 3057-3060.

14. J.M. Mäkelä, S. Hellstén, J. Silvonen, M. Vippola, E. Levänen, T. Mäntylä, Mater. Lett. 60 (2006) 530-534.

15. J. Tikkanen, K.A. Gross, C.C. Berndt, V. Pitkänen, J. Keskinen, S. Raghu, M. Rajala, J. Karthikeyan, Surf. Coat. Technol. 90 (1997) 210-216.

16. A.S. Edelstein, R.C. Cammarata (Eds.), Nanomaterials: Synthesis, Properties and Applications, Institute of Physics Publishing, Bristol, 1996.

17. A. Gurav, T. Kodas, T. Pluym, Y. Xiong, Aerosol Sci. Technol. 19 (1993) 411-452.

18. S.E. Pratsinis, Prog. Energy Combust. Sci. 24 (1998) 197-219.

19. J.M. Mäkelä, H. Keskinen, T. Forsblom, J. Keskinen, J. Mater. Sci. 39 (2004) 2783-2788.

20. H. Keskinen, J.M. Mäkelä, S. Hellstén, M. Aromaa, E. Levänen, T. Mäntylä, Electrochem. Soc. 19 (2005) 491-498.

21. M. Aromaa, H. Keskinen, J.M. Mäkelä, Biomol. Eng. 24 (2007) 543-548.

22. A. Pitkänen, J.M. Mäkelä, M. Nurminen, A. Oksanen, K. Janka, J. Keskinen, H. Keskinen, J.K. Liimatainen, S. Hellstén, T. Määttä, IFRF Combust. J. (2005) 200509.

23. M. Hosokawa, K. Nogi, M. Naito, T. Yokoyama (Eds.), Nanoparticle Technology Handbook, Elsevier, Amsterdam, 2007.

24. S.C. Tjong, H. Chen, Mater. Sci. Eng. R. 45 (2004) 1-88.

25. H. Keskinen, J.M. Mäkelä, M. Vippola, M. Nurminen, J. Liimatainen, T. Lepistö, J. Keskinen, Mater. Res. Soc. 19 (2004) 1544-1550.

26. H. Keskinen, J.M. Mäkelä, M. Aromaa, J. Ristimäki, T. Kanerva, E. Levänen, T. Mäntylä, J. Keskinen, J. Nanopart. Res. 9 (2007) 569-588.

27. H. Keskinen, J.M. Mäkelä, M. Aromaa, J. Keskinen, S. Areva, C.V. Teixeira, J.B. Rosenholm, V. Pore, M. Ritala, M. Leskelä, M. Raulio, M.S. Salkinoja-Salonen, E. Levänen, T. Mäntylä, Catal. Lett. 111 (2006) 127-132.

28. H. Keskinen, J.M. Mäkelä, R. Heikkinen, A. Suopanki, J. Keskinen, Catal. Lett. 119 (2007) 172-178.

29. R.N. Wenzel, Ind. Eng. Chem. 28 (1936) 988-994.

30. A.B.D. Cassie, S. Baxter, Trans. Faraday Soc. 40 (1944) 546-551.

31. G. Whyman, E. Bormashenko, T. Stein, Chem. Phys. Lett. 450 (2008) 355-359.

32. C. Ran, G. Ding, W. Liu, Y. Deng, W. Hou, Langmuir 24 (2008) 9952-9955.

33. M. Ma, R.M. Hill, Curr. Opin. Colloid Interface Sci. 11 (2006) 193-202.

34. B. Bhushan, Y.C. Jung, J. Phys.: Condens. Matter 20 (2008) 225010.

35. J. Wang, F. Liu, H. Chen, D. Chen, Appl. Phys. Lett. 95 (2009) 084104.

36. L. Cao, H.-H. Hu, D. Gao, Langmuir 23 (2007) 4310-4314.

37. T. Sun, L. Feng, X. Gao, L. Jiang, Acc. Chem. Res. 38 (2005) 644-652.

38. H. Liu, J. Zhai, L. Jiang, Soft Matter 2 (2006) 811-821.

39. Z. Guo, W. Liu, Plant Sci. 172 (2007) 1103-1112.

40. R. Fürstner, W. Barthlott, Langmuir 21 (2005) 956-961.

41. N.A. Patankar, Langmuir 20 (2004) 8209-8213.

42. B. Bhushan, M. Nosonovsky, Y.C. Jung, J. R. Soc. Interface 4 (2007) 643-648.

43. D. Öner, T.J. McCarthy, Langmuir 16 (2000) 7777-7782.

44. W. Barthlott, C. Neinhuis, Planta 202 (1997) 1-8.

45. L. Feng, Y. Zhang, J. Xi, Y. Zhu, N. Wang, F. Xia, L. Jiang, Langmuir 24 (2008) 4114-4119.

46. E. Burkarter, C.K. Saul, F. Thomazi, N.C. Cruz, S.M. Zanata, L.S. Roman, W.H. Schreiner, J. Phys. D: Appl. Phys. 40 (2007) 7778-7781.

47. T.-S. Lin, C.-F. Wu, C.-T. Hsieh, Surf. Coat. Technol. 200 (2006) 5253-5258.

48. B. Balu, V. Breedveld, D.W. Hess, Langmuir 24 (2008) 4785-4790.

49. Z. Guo, W. Liu, Appl. Phys. Lett. 90 (2007) 223111.

50. J. Xi, L. Jiang, Ind. Eng. Chem. Res. 47 (2008) 6354-6357.

51. M. Jin, X. Feng, L. Feng, T. Sun, J. Zhai, T. Li, L. Jiang, Adv. Mater. 17 (2005) 1977-1981.

52. J.M. Mäkelä, M. Aromaa, H. Teisala, M. Tuominen, M. Stepien, J.J. Saarinen, M. Toivakka, J. Kuusipalo, submitted (18.03.2010) to Aerosol Sci. Technol.

53. C.D. Wagner, W.M. Riggs, L.E. Davis, J.F. Moulder, G.E. Muilenberg, Handbook of X-Ray Photoelectron Spectroscopy, Perkin-Elmer, Eden Prairie, 1979.

54. E. McCafferty, J.P. Wightman, Surf. Interface Anal. 26 (1998) 549-564.

55. S. Takeda, M. Fukawa, Y. Hayashi, K. Matsumoto, Thin Solid Films 339 (1999) 220-224.

56. K. Autumn, A.M. Peattie, Integr. Comp. Biol. 42 (2002) 1081-1090.

57. M. Stepien, J.J. Saarinen, H. Teisala, M. Tuominen, M. Aromaa, J. Kuusipalo, J.M. Mäkelä, M. Toivakka, submitted (18.03.2010) to Appl. Surf. Sci.

58. R. Taurino, E. Fabbri, M. Messori, F. Pilati, D. Pospiech, A. Synytska, J. Colloid Interface Sci. 325 (2008) 149-156.

59. M. Nosonovsky, B. Bhushan, Ultramicroscopy 107 (2007) 969-979.

60. W. Li, A. Amirfazli, J. Colloid Interface Sci. 292 (2005) 195-201.

61. P. Roach, N.J. Shirtcliffe, M.I. Newton, Soft Matter 4 (2008) 224-240.

62. D. Quéré, Annu. Rev. Mater. Res. 38 (2008) 71-99.

Publication 2

Teisala, H.; Tuominen, M.; Aromaa, M.; Stepien, M.; Mäkelä, J. M.; Saarinen, J. J.; Toivakka, M.; Kuusipalo, J.

Nanoparticle Deposition on Packaging Materials by Liquid Flame Spray – Generation of Superhydrophilic and Superhydrophobic Coatings

In: Gutowski, W. and Dodiuk, H. (eds.) *Recent Advances in Adhesion Science and Technology in Honor of Dr. Kash Mittal*, Taylor & Francis, In press.

Publication 3

Teisala, H.; Tuominen, M.; Aromaa, M.; Stepien, M.; Mäkelä, J. M.; Saarinen, J. J.; Toivakka, M.; Kuusipalo, J.

Nanostructures Increase Water Droplet Adhesion on Hierarchically Rough Superhydrophobic Surfaces

Langmuir **2012**, 28, 3138–3145, DOI: dx.doi.org/10.1021/la203155d

Langmuir

Article

pubs.acs.org/Langmuir

Nanostructures Increase Water Droplet Adhesion on Hierarchically Rough Superhydrophobic Surfaces

Hannu Teisala,*[,†] Mikko Tuominen,[†] Mikko Aromaa,[‡] Milena Stepien,[§] Jyrki M. Mäkelä,[‡] Jarkko J. Saarinen,[§] Martti Toivakka,[§] and Jurkka Kuusipalo[†]

[†]Paper Converting and Packaging Technology, Department of Energy and Process Engineering, Tampere University of Technology, P.O. Box 589, FI-33101 Tampere, Finland

[‡]Aerosol Physics Laboratory, Department of Physics, Tampere University of Technology, P.O. Box 692, FI-33101 Tampere, Finland

[§]Laboratory of Paper Coating and Converting, Center for Functional Materials, Abo Akademi University, Porthansgatan 3, FI-20500 Abo/Turku, Finland

ABSTRACT: Hierarchical roughness is known to effectively reduce the liquid−solid contact area and water droplet adhesion on superhydrophobic surfaces, which can be seen for example in the combination of submicrometer and micrometer scale structures on the lotus leaf. The submicrometer scale fine structures, which are often referred to as nanostructures in the literature, have an important role in the phenomenon of superhydrophobicity and low water droplet adhesion. Although the fine structures are generally termed as nanostructures, their actual dimensions are often at the submicrometer scale of hundreds of nanometers. Here we demonstrate that small nanometric structures can have very different effect on surface wetting compared to the large submicrometer scale structures. Hierarchically rough superhydrophobic TiO_2 nanoparticle surfaces generated by the liquid flame spray (LFS) on board and paper substrates revealed that the nanoscale surface structures have the opposite effect on the droplet adhesion compared to the larger submicrometer and micrometer scale structures. Variation in the hierarchical structure of the nanoparticle surfaces contributed to varying droplet adhesion between the high- and low-adhesive superhydrophobic states. Nanoscale structures did not contribute to superhydrophobicity, and there was no evidence of the formation of the liquid−solid−air composite interface around the nanostructures. Therefore, larger submicrometer and micrometer scale structures were needed to decrease the liquid−solid contact area and to cause the superhydrophobicity. Our study suggests that a drastic wetting transition occurs on superhydrophobic surfaces at the nanometre scale; i.e., the transition between the Cassie−Baxter and Wenzel wetting states will occur as the liquid−solid−air composite interface collapses around nanoscale structures. Consequently, water adheres tightly to the surface by penetrating into the nanostructure. The droplet adhesion mechanism presented in this paper gives valuable insight into a phenomenon of simultaneous superhydrophobicity and high water droplet adhesion and contributes to a more detailed comprehension of superhydrophobicity overall.

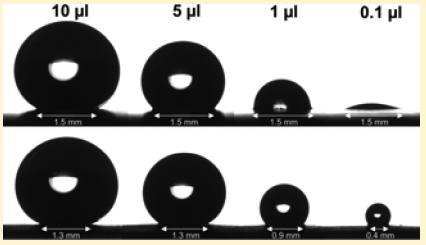

1. INTRODUCTION

Extremely water-repellent surfaces, on which water droplets sit in a spherical shape with contact angles higher than 150°, are often called superhydrophobic. These surfaces have attracted considerable scientific interest in the past decade, which becomes evident in the huge number of research papers published on superhydrophobicity. The phenomenon of superhydrophobicity and related mechanisms are attractive scientifically, but also from the industrial point of view, because extreme water repellency is desired in several applications. Superhydrophobicity can potentially be exploited for example in nonwetting, nonfogging, nonicing, and self-cleaning surfaces or in droplet transportation and in micro- and macrofluidic devices.[1−6] Recent development in the field of superhydrophobicity has contributed to significant advances also in other areas, for example in oleophobicity.[7,8]

The highest water contact angles reported on smooth low-energetic surfaces, such as fluoropolymers, are usually around 120°.[3−5] Surface roughness can further increase the hydrophobicity significantly, and therefore, it is essential for superhydrophobicity. Nature has guided us to understand the mechanisms of superhydrophobicity by introducing a wide range of topography variations that exist on superhydrophobic surfaces of plants[4,9−11] and insects.[4,5,12] The waxy surface of superhydrophobic plants composes mainly of hydrocarbon derivatives, and contains predominantly CH_2 groups.[1,11,13,14] Therefore, extremely low surface energy is not necessary for superhydrophobicity. Even today, after the extensive study of superhydrophobic surfaces, the pioneering work of Wenzel[15] (complete wetting state) and Cassie and Baxter[16] (partial wetting state) provide the basis for understanding the wetting phenomena on rough surfaces.

The most well-known example of superhydrophobicity is the leaf of lotus plant,[9] which has hierarchically rough dual-scale surface structure. The micrometric nubs on the lotus surface (epidermal cells) are decorated with the submicrometer tubular

Received: August 12, 2011
Revised: December 29, 2011
Published: January 20, 2012

   dx.doi.org/10.1021/la203155d | Langmuir 2012, 28, 3138−3145

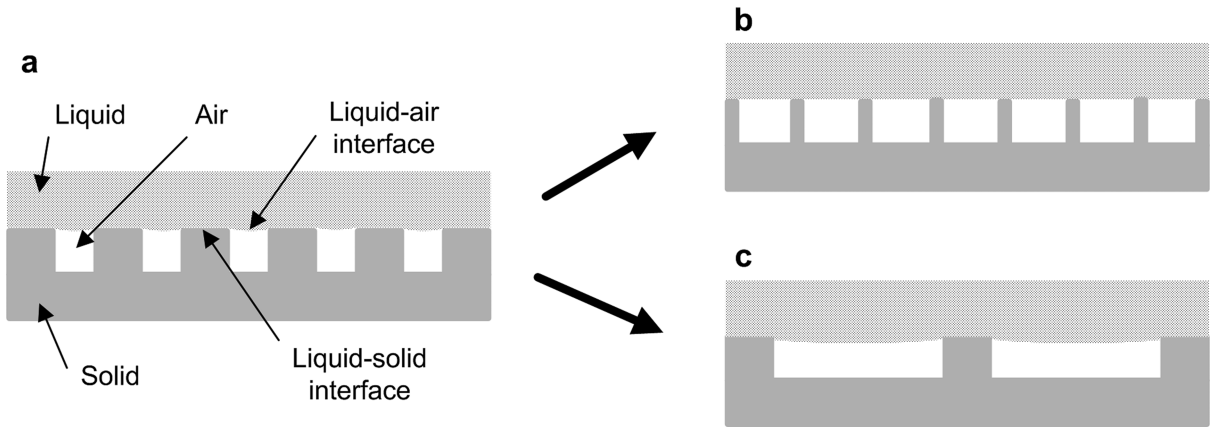

Figure 1. Illustration of phase interfaces on superhydrophobic surfaces. Entrapped air between water and rough surface causes the formation of the liquid–solid–air composite interface (a). Liquid–solid contact area and droplet adhesion can be reduced by decreasing the structural dimensions of the surface (b) or by increasing the air gaps between the structures (c).

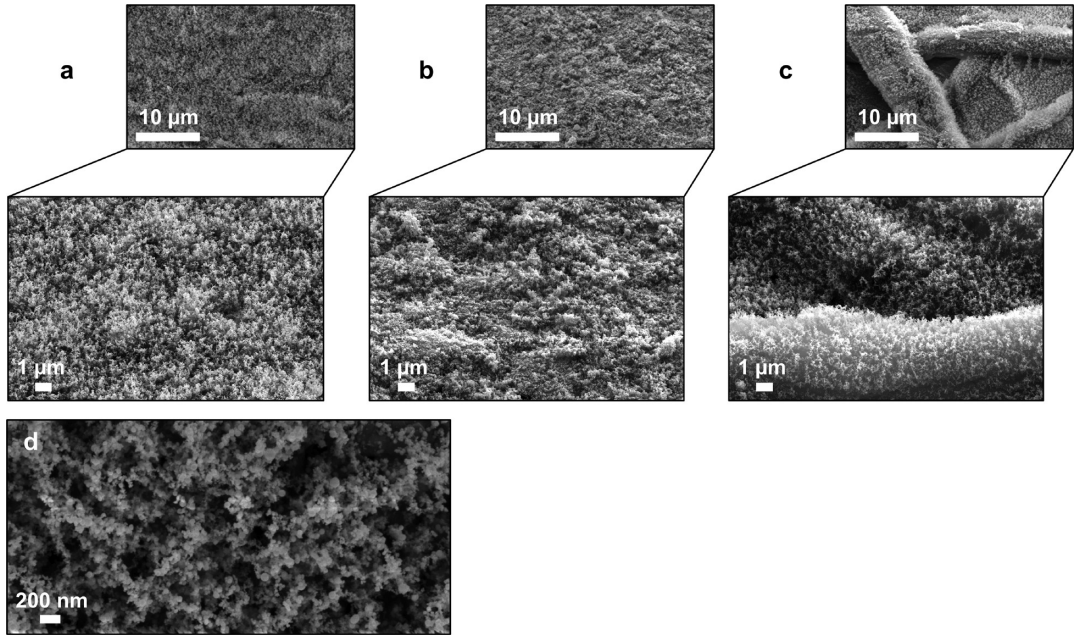

Figure 2. FEG-SEM images of hierarchically rough superhydrophobic TiO_2 nanoparticle surfaces. The low-resolution images (a–c) were captured at the angle of 45°. The high-resolution image (d) was taken from above. The high-adhesive surface on the pigment-coated board substrate (a, d) is hierarchically rough predominantly at two scales: the particles create the nano- and their aggregates the submicrometer scale structures to the surface. In addition to the nanometric and submicrometer structures, the medium-adhesive surface on the pigment-coated board substrate (b) possesses micrometric structures, which originate from large aggregates of particles (see processing details in Methods section). On the low-adhesive surface (c) the fibrous structure of the paper substrate adds one more level to the hierarchical roughness.

fine structure (epicuticular waxes). Spherical water droplets sit on the lotus surface, leaving air trapped between the liquid and rough solid. Because of the small liquid–solid contact area, the droplet adhesion to the surface is minimal and the droplets roll off easily.

Contact angle hysteresis is commonly used to evaluate water droplet adhesion to superhydrophobic surfaces.[5,6,14,17] The hysteresis is determined as a difference between advancing and receding contact angle of a droplet. However, because there is no single way to measure the hysteresis, the reported results always depend, for example, on the method used or the droplet volume. The hysteresis describes the ability of a surface to resist the movement of a droplet. Both chemical and physical heterogeneities of the surface can increase the hysteresis. Particularly, when the liquid penetrates into a rough surface, the receding contact angle may become very low, and thus the hysteresis can rise significantly high. High hysteresis therefore indicates large liquid–solid contact area and high adhesion of water droplets to the surface. On the other hand, low hysteresis on a superhydrophobic surface means that the liquid does not penetrate into the surface structure at large extent, but water droplets sit on the asperities of the surface with a small liquid–solid contact area and low adhesion. In such case, droplets are able to roll off the surface very easily (e.g., the lotus surface).

Generally, superhydrophobic surfaces possessing purely submicrometer scale structures or a combination of submicrometer and micrometer scale structures (hierarchical roughness) have smaller water droplet adhesion compared to surfaces possessing purely micrometric structures.[1,4,5,10,11,14] This is easy to comprehend because for the low water droplet adhesion the

dx.doi.org/10.1021/la203155d | *Langmuir* 2012, 28, 3138–3145

liquid−solid contact area must be minimized, and usually, it decreases with the decreasing structural dimensions of the surface (Figure 1a,b). It is not unusual that the fine structure of a superhydrophobic surface, for example the lotus leaf, is referred to as nanostructure. However, the dimensions of the fine structures on low-adhesive superhydrophobic surfaces, whether artificial or natural, are often at the scale of hundreds of nanometers. Therefore, the structural dimensions on those surfaces can be considered to be rather in a submicrometer size range than in a nanometric range. This also applies to the lotus surface, on which the outer diameter of the tubular fine structure is typically around 100 nm, and the gaps between the randomly distributed tubules are often in the range of hundreds of nanometers.[10,11,13,14]

Another way to reduce the liquid−solid contact area is to increase the gaps between the structures on the surface (Figure 1a,c). However, this may lead to a metastable superhydrophobicity,[5,6,11,18−20] where the droplet initially sitting on the asperities of the surface can collapse into the structure. The collapse of superhydrophobicity can be caused for example by increased internal Laplace pressure of the droplet or by some external pressure, such as impaction. As a consequence of the collapse, the liquid−solid contact area and droplet adhesion to the surface increase drastically.

Water droplet adhesion to superhydrophobic surfaces is usually at least moderately low because the surface structures tend to decrease the liquid−solid contact area, as was already discussed. Nevertheless, this does not apply to all superhydrophobic surfaces because there are several examples of surfaces on which spherical water droplets are able to remain even when the surface is tilted upside down.[21−25] It is known that high water droplet adhesion on superhydrophobic surfaces is related to large liquid−solid contact area,[5,11,14,21−23,26,27] but the exact wetting mechanisms and the role of hierarchical roughness in the phenomenon are not yet completely understood.

Here we present one of the water droplet adhesion mechanisms on superhydrophobic surfaces. Our studies on hierarchically rough superhydrophobic nanoparticle surfaces on board and paper substrates demonstrate that the nanoscale surface structure has the opposite effect on the droplet adhesion in comparison with the submicrometer and micrometer scale structures. That is, water adheres tightly to the surface by penetrating into the nanostructure of the solid. The nanostructure by itself does not cause superhydrophobicity.

2. RESULTS AND DISCUSSION

Nanoparticle surfaces are suitable for studying the effect of hierarchical roughness on superhydrophobicity and droplet adhesion because they can possess hierarchical structures at multiple scales. We generated three differently structured superhydrophobic titanium dioxide (TiO_2) nanoparticle surfaces (Figure 2) on pigment-coated board and paper substrates by the liquid flame spray (LFS). Water droplet adhesion to the surfaces varied between a sticky behavior observed on the high-adhesive surface and an easy roll-off effect observed on the low-adhesive surface. The generation of the superhydrophobic TiO_2 nanoparticle surfaces by the LFS is discussed in detail in our previous studies.[23,28,29]

The nanosized particles (typically smaller than 50 nm in diameter) create the nanoscale structure for the surfaces. The particle structure is highly porous, and the effective surface area is therefore significantly large, as is shown by the high-resolution SEM image in Figure 2. The larger structures at submicrometer and micrometer scale originate from aggregates of the particles and from roughness of the substrates. Size of the particle aggregates and the gaps between them typically vary from hundreds of nanometers up to some micrometers. In addition, roughness of a substrate can significantly increase the structural dimension on the nanoparticle-coated surface. This becomes apparent when the high- and medium-adhesive surfaces on the pigment-coated board substrate (Figure 2a,b) are compared with the low-adhesive surface on the paper substrate (Figure 2c), where the fibrous structure is still clearly visible below the nanoparticle coating. Because of the fibrous substrate structure, the low-adhesive surface is highly irregular, possessing large-scale structures and gaps up to tens of micrometers. Detailed information on the substrate materials (e.g., SEM, AFM, and XPS analyses) can be found in earlier works.[29−32] The particle growth and aggregate formation in aerosol processes is discussed in detail by e.g. Gurav et al.[33] and Pratsinis.[34] Because of nature of the substrate materials and aggregate formation in the LFS process, the nanoparticle surfaces are highly irregular at several different scales. However, the dominating structural dimensions on the surfaces can be characterized as follows: the high-adhesive surface possesses structures predominantly at two scales: nano- and submicrometer scale (Figure 2a,d); the medium-adhesive surface at three scales: nanometer, submicrometer, and micrometer scale (Figure 2b); and the low-adhesive surface at four scales: nanometer, submicrometer, micrometer, and tens of micrometers scale (Figure 2c).

The advancing and receding water contact angles for the surfaces were measured using the increment−decrement method (Table 1), but to get a wider perspective, the hysteresis was also measured from moving droplets (Table 2). With both methods the trend is clear: the more levels of hierarchical roughness on the surface, the lower the hysteresis. The advancing contact angle is almost the same for all the surfaces (Tables 1 and 2) because on each of the surfaces the advancing edge of the droplet must jump over the air gaps existing on the rough solid. The variation in the contact angle hysteresis is therefore mainly due to the different receding contact angles.

The receding contact angle decreased continuously close to nil on the high-adhesive surface (Figures 3 and 4), and the real

Table 1. Contact Angles and Hysteresis (in deg) of the Superhydrophobic Surfaces Measured by the Increment−Decrement Method

surface	static angle	adv angle	rec angle	hysteresis
high-adhesive surface	159 ± 2	169 ± 1	<60	>100
medium-adhesive surface	169 ± 1	169 ± 1	114 ± 2	55
low-adhesive surface	168 ± 1	169 ± 1	138 ± 3	31

Table 2. Contact Angles and Hysteresis (in deg) of the Superhydrophobic Surfaces Measured from the Moving Droplets

surface	adv angle	rec angle	hysteresis
high-adhesive surface	161 ± 2	124 ± 7	37
medium-adhesive surface	164 ± 4	156 ± 3	8
low-adhesive surface	160 ± 2	154 ± 2	6

dx.doi.org/10.1021/la203155d | Langmuir 2012, 28, 3138−3145

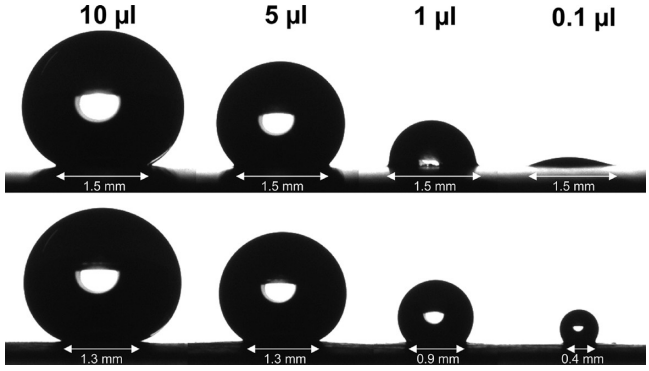

Figure 3. Shape and contact diameter of evaporating water droplets on the high- (above) and low-adhesive (below) superhydrophobic surfaces. The droplet is tightly pinned to the high-adhesive surface, and therefore the contact diameter remains constant at 1.5 mm. Consequently, at the end of the evaporation the droplet is clearly in a hydrophilic state possessing a very low contact angle. On the low-adhesive surface the contact diameter decreases with the decreasing droplet volume, and thus the droplet maintains its spherical shape and high contact angle.

hysteresis measured by the increment−decrement method could therefore be even higher than 150°. Nevertheless, we only declare the receding contact angle to be less than 60° and the hysteresis over 100° because at the late stage of the evaporation the receding contact angle cannot be determined reliably. The remarkably low receding contact angle on the high-adhesive surface indicates water penetration between the nanoparticles in a large extent and thus formation of significantly large liquid−solid contact area and high water droplet adhesion.

When the contact angle hysteresis results from the moving droplets (Table 2) are compared with the results from the increment−decrement method (Table 1), it can be seen that the hysteresis values are lower and the differences between the surfaces are therefore smaller. From the moving droplets the extremely low hysteresis of 8° and 6° were measured for the medium- and low-adhesive surfaces, respectively. The droplets were able to move even on the high-adhesive surface, which we observed already in our previous study.[23] We conclude the liquid−solid contact time of the moving droplets was too short for proper water penetration into the nanostructure of the surfaces.

Tilt angles where 10 μL water droplets rolled off the superhydrophobic surfaces and contact angle hysteresis in a static state right before the roll-off are shown in Table 3. The

Table 3. Tilt Angles Where Water Droplets Rolled off the Superhydrophobic Surfaces and the Contact Angles and Hysteresis in a Static State Right before the Roll-Off (All Values in deg)

surface	tilt angle	adv angle	rec angle	hysteresis
high-adhesive surface				
medium-adhesive surface	28 ± 7	168 ± 2	117 ± 4	51
low-adhesive surface	10 ± 2	168 ± 2	134 ± 4	34

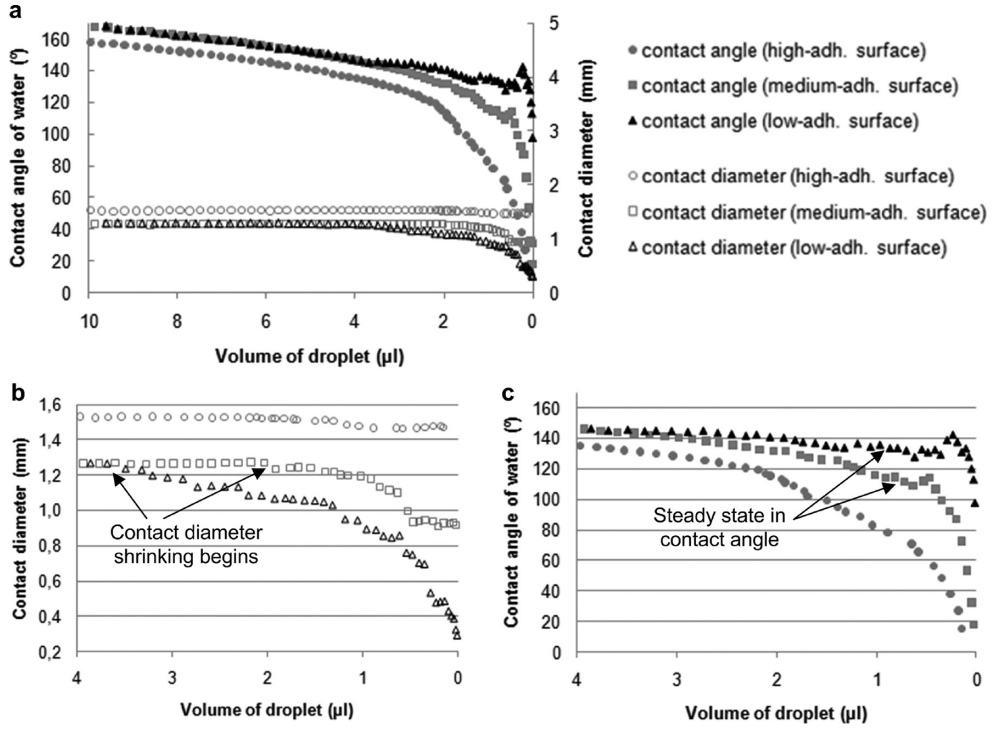

Figure 4. Contact angle and contact diameter of evaporating water droplets on the high-, medium-, and low-adhesive superhydrophobic surfaces. When the contact diameter decreases with the decreasing droplet volume, the contact angle remains high, and conversely, pinning of the contact diameter causes a rapid decrease in the contact angle (a). The contact diameter remains almost unchanged throughout the evaporation on the high-adhesive surface but starts to decrease around the droplet volumes of 2 and 3.7 μL on the medium- and low-adhesive surfaces, respectively (b). Consequently, the contact angle decreases continuously on the high-adhesive surface but remains high on the medium-, and especially, on the low-adhesive surface. Variation in the receding contact angle at the steady states can be attributed to water pinning at the liquid−solid contact sites and to sudden jumps over the air gaps (c). Complete evaporation of the 10 μL droplets took approximately 60 min on the high-adhesive surface and 65 min on the medium- and low-adhesive surfaces.

dx.doi.org/10.1021/la203155d | *Langmuir* 2012, 28, 3138−3145

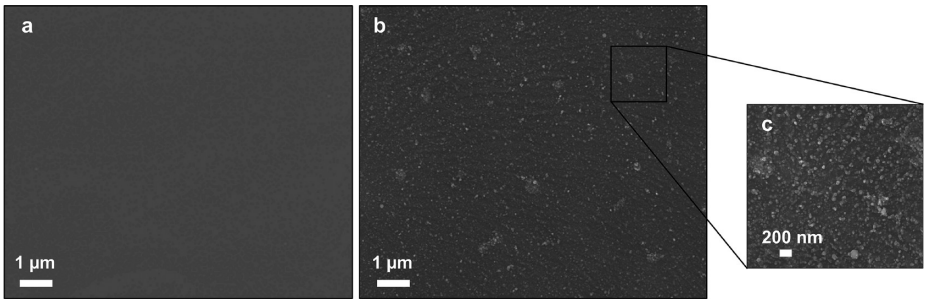

Figure 5. FEG-SEM images of the LDPE surface before (a) and after the nanocoating (b, c).

droplets did not roll off the high-adhesive surface even when tilted upside down. In contrast, on the low-adhesive surface the roll-off occurred already at the tilt angle of 10°. The hysteresis values measured right before the roll-off are quite similar to the values measured by the increment–decrement method (Table 1). In both cases, the droplets were practically in a static state, which explains the similarity of the results.

We followed the contact angle and contact diameter of evaporating water droplets in order to obtain more detailed information on the liquid–solid contact line pinning and droplet shape on the surfaces (Figures 3 and 4). On the high-adhesive surface the droplet contact diameter remained pinned and almost unchanged during the evaporation, and therefore, the contact angle decreased constantly close to nil. An opposite phenomenon was observed on the low-adhesive surface, where the contact diameter decreased quite freely with the decreasing droplet volume. Consequently, the contact angle remained high and the droplet maintained its spherical shape (Figure 3). Although there was a steady state in the contact angle (determined as the receding contact angle in Table 1) on the medium- and low-adhesive surfaces, at the end of the evaporation the contact angle decreased rapidly (Figure 4). Internal Laplace pressure of the droplet increases constantly with the decreasing droplet volume, which may disturb the equilibrium state of the evaporating droplets at the end of the evaporation. In addition, e.g. concentration of impurities in the droplet could affect the receding contact angle at the late stage of the evaporation.

In order to approach the hydrophobicity and droplet adhesion from another perspective, we studied nanoparticle-coated low-density polyethylene (LDPE) surface (Figure 5), which did not practically possess any hierarchical roughness. Contact angle hysteresis of the nanocoated surface was measured to be as high as 83° (Table 4). The high hysteresis

Table 4. Contact Angles and Hysteresis (in deg) of the Uncoated and Nanocoated LDPE Surfaces Measured by the Increment–Decrement Method

surface	static angle	adv angle	rec angle	hysteresis
uncoated surface	99 ± 0	108 ± 1	86 ± 0	22
nanocoated surface	91 ± 2	101 ± 1	18 ± 1	83

does not occur because of high advancing contact angle that would indicate the formation of the liquid–solid–air composite interface but because of the low receding contact angle (18°) that indicates the liquid penetration into the nanostructure of the surface. For comparison, because the uncoated LDPE surface has relatively homogeneous physical and chemical structure, its contact angle hysteresis is only 22°.

A detailed observation of the evaporating droplets (Figure 6) shows that there was only a weak pinning on the liquid–solid contact line on the uncoated LDPE surface, and thus the contact diameter decreased comparatively freely with the decreasing droplet volume. Consequently, the receding contact angle remained in a steady state close to the static contact angle for a long period of time, until it rapidly decreased at the end of the evaporation in the similar manner as it did with the superhydrophobic surfaces. The nanostructure does not cause superhydrophobicity because the static contact angle on the nanocoated surface is only 91°. Instead, the nanostructure is responsible for the droplet pinning to the surface.

In conclusion, our study demonstrates that the nanoscale structure of the LFS-generated surfaces does not cause superhydrophobicity. Instead, water can adhere tightly to the surface by penetrating into the nanostructure, where intermolecular forces, such as van der Waals interactions, cause the liquid–solid adhesion. Structures at submicrometer and micrometer scale are required to entrap air below water droplets and thus reduce the liquid–solid contact and cause superhydrophobicity. Therefore, after the nanoscale structure, each level in the hierarchical roughness of the surfaces decreases the liquid–solid contact area and water droplet adhesion. The results indicate that wetting transition between the Cassie–Baxter and Wenzel states will occur when the surface structures get small enough at nanometer scale; that is, water will penetrate into the nanostructure either partially or fully.

Usually, the liquid–solid contact area and water droplet adhesion on superhydrophobic surfaces decrease with the decreasing structural dimensions of the surface, as was discussed in the Introduction. However, this is not always the case because for example on the superhydrophobic rose petal surface the submicrometer cuticular folding on the micrometer scale epidermal cells causes the high water droplet adhesion.[21] As we have shown here, also nanoscale structures can increase water droplet adhesion on superhydrophobic surfaces. With the decreasing structural dimensions, at certain point, air pockets no longer form onto the liquid–solid interface and superhydrophobicity will be lost. Smooth solids for example, which can never be superhydrophobic regardless of their chemistry, practically always possess at least atomic scale roughness. The critical point where the liquid–solid–air composite interface will collapse depends on the shape and chemistry of the surface structures. After the collapse the roughness of the solid no longer reduces the liquid–solid contact area. Instead, when the liquid penetrates into the structure, the real contact area and droplet adhesion may become much larger compared to a smooth surface. This observation, on the other hand, gives us a tool to create high-adhesive superhydrophobic surfaces by

dx.doi.org/10.1021/la203155d | Langmuir 2012, 28, 3138–3145

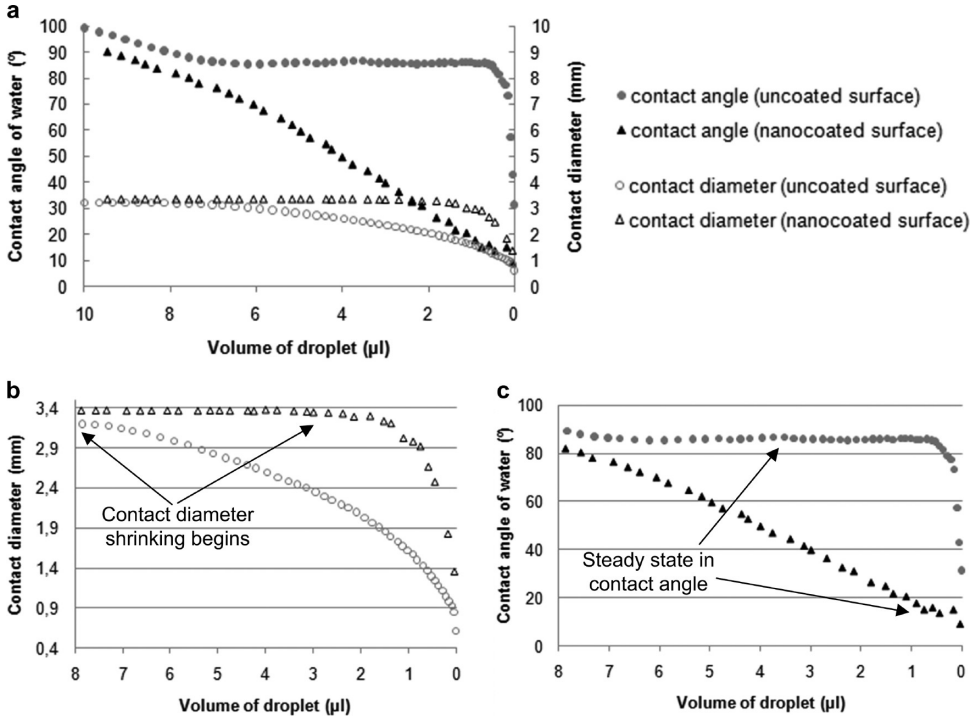

Figure 6. Contact angle and contact diameter of evaporating water droplets on the uncoated and nanocoated LDPE surfaces. Contact angle of the evaporating droplet remains high on the uncoated surface because the contact diameter decreases quite freely with the decreasing droplet volume. In contrast, contact angle decreases rapidly on the nanocoated surface due to water pinning to the solid (a). On the uncoated surface the contact diameter decrement begins already at the droplet volume of 8 μL, whereas on the nanocoated surface the decrement does not begin until the droplet volume is less than 3 μL (b). In consequence, on the uncoated surface the receding contact angle stays in a steady state close to the static contact angle for a long period of time, but on the nanocoated surface the contact angle decreases almost linearly, and only a short steady state can be observed at the end of the evaporation (c). Complete evaporation of the 10 μL droplets took approximately 55 min on the uncoated surface and 40 min on the nanocoated surface.

combining the nanoscale structure with a larger, air-entrapping structure, as we have done in this study. That is, the large-scale structure causes superhydrophobicity, and the overlaying nanoscale structure causes water adhesion.

It is typical that surface phenomena and characteristics of micro- and nanometric materials may vary significantly from bulk materials. Quite often drastic changes in material properties, even a turn over, occur when the particle or grain size decreases to nanometer scale, below 10−20 nm.[35,36] From that point of view, it is not surprising that the above-discussed superhydrophobicity and adhesion phenomena occur on surfaces decorated with micro- and nanometric structures, but not on smooth surfaces. Detailed discussion of water interactions around nanometric structures can be found from the literature, but so far this discussion has been generally ignored in practical superhydrophobicity studies. For example, several research groups have suggested that so-called drying transition of water occurs around small scale hydrophobic objects.[37−40] That is, water molecules recede from hydrophobic surfaces, and thus the density of water decreases close to the hydrophobic objects, leading to a formation of thin vapor layer between the liquid and solid. If two or more hydrophobic objects are close enough to each other, the vapor layers unite to form one larger bubble covering the interfacial area of the structures. This is in good agreement with the well-documented observations on superhydrophobic surfaces: submicrometer and micrometer scale surface structures can entrap air and create the liquid−solid−air composite interface. However, Lum et al.[38] carried out theoretical calculations suggesting that density fluctuations in the liquid−vapor interface may lead to vanishing of the metastable vapor bubble if the interfacial distances between the hydrophobic structures decrease small enough at nanometer scale. Later studies[39−41] have confirmed that water really can fill hydrophobic nanometric pores, and Hummer et al.[40] even simulated a density fluctuations driven conduction of water molecules through a hydrophobic carbon nanotube channel of less than 1 nm (10 Å) in diameter. The above discussion is in strong consensus with the observations of our study. That is, although the decreasing structural dimensions on superhydrophobic surfaces can reduce the liquid−solid contact area and increase hydrophobicity to a certain point, indeed, there will be a critical turn over limit, after which the liquid will collapse into the nanostructure. If the turn over takes place, it will have a drastic effect on the hydrophobicity, liquid−solid contact area, and droplet adhesion of the surface.

In recent years, a number of practical studies on superhydrophobic paper surfaces have been published. Cellulose fibers of paper are inherently highly irregular, possessing a variety of structures at several scales. There are lots of pinning sites for water, for example grooves[21] or nanoscale structures, and thus e.g. deposition of a thin fluorocarbon film typically results in a highly hydrophobic and high-adhesive surface.[42,43] Balu et al.,[42,43] among others,[44,45] have done thorough study with superhydrophobic paper surfaces. They successfully modified the hierarchical structure of paper surface by plasma etching, which shifted the surface wetting from the high-adhesive state to the low-adhesive state. More precisely, after

dx.doi.org/10.1021/la203155d | Langmuir 2012, 28, 3138−3145

the plasma etching the initially highly irregular fiber surface appeared with rather well-defined submicrometer scale structures. Although our approach is quite different from many other superhydrophobicity studies on paper substrates, i.e., instead of a film-type coating we generate hierarchically structured particle coatings, the results of the earlier studies on paper substrates are in consensus with the conclusions of this study.

An overview of superhydrophobicity in general, based on the findings of our study, shows that although the materials, fabrication methods, and chemical and physical structure of the high-adhesive superhydrophobic surfaces can vary significantly, a combining factor for several of them[17,23−25,42,43,46−49] is the hierarchical roughness where the smallest structures, for example pores or gaps, are at the nanometre scale. On the basis of that observation and the discussion in this paper, there is a reason to presume that the droplet adhesion mechanism demonstrated in this study applies not only to the LFS-generated surfaces, but is relevant to different types of surfaces in general, and has therefore a great scientific impact in the field of wetting and superhydrophobicity.

3. CONCLUSIONS

We have shown that hierarchically rough superhydrophobic TiO_2 nanoparticle surfaces with varying water droplet adhesion can be generated onto board and paper substrates by the LFS. Spherical water droplets were not able to roll off the high-adhesive surface, and the contact angle hysteresis on the surface was even higher than 100°. In contrast, on the low-adhesive surface the droplet roll-off occurred at the tilt angle of 10°, and the contact angle hysteresis was as low as 6°. The submicrometer and micrometer scale structures on the hierarchically rough surfaces entrap air below water droplets and thus create the liquid−solid−air composite interface that is required for superhydrophobicity. The nanoscale structure of the surfaces does not contribute to superhydrophobicity. Instead, water droplets can adhere tightly to the surface by penetrating into the nanostructure. Droplet adhesion is therefore dependent on the hierarchical structure of the surfaces.

Our results suggest that a drastic wetting transition occurs on superhydrophobic surfaces at the nanometer scale. At certain point with the decreasing structural dimensions, which is determined by the physical and chemical structure of the surface, the transition between the Cassie−Baxter and Wenzel wetting states will occur as the liquid−solid−air composite interface collapses. Consequently, water adheres tightly to the surface by penetrating into the nanoscale structure. The water droplet adhesion mechanism presented in this paper gives valuable insight into a phenomenon of simultaneous superhydrophobicity and high water droplet adhesion and contributes to a more detailed comprehension of superhydrophobicity overall.

4. METHODS

Hierarchically rough superhydrophobic titanium dioxide (TiO_2) nanoparticle surfaces were generated onto pigment coated (PC) board and machine glossed (MG) paper in a continuous roll-to-roll process by the liquid flame spray (LFS). A detailed description of the LFS coating process and materials are given in our previous publications.[23,28,29] Hierarchical structure of the superhydrophobic surfaces was controlled by the processing parameters and substrate material. Three superhydrophobic surfaces with varying water droplet adhesion (high, medium, and low) were generated using the processing parameters shown in Table 5. In addition, low-density polyethylene (LDPE) surface was TiO_2 nanocoated in order to obtain nanostructured surface without hierarchical roughness. Uncoated LDPE was studied as a "smooth" reference surface.

Table 5. Substrate Materials and LFS Processing Parameters Used in the Surface Preparation

surface description	substrate	concn (mg atomic Ti/mL)	feed rate (mL/min)	burner distance (cm)	line speed (m/min)
high-adhesive surface	PC board	50	32	15	50
medium-adhesive surface	PC board	50	12	6	50
low-adhesive surface	MG paper	50	12	6	50
nanocoated surface	LDPE	50	12	15	50

A field emission gun scanning electron microscope (FEG-SEM), Zeiss ULTRAplus, was used for imaging the nanoparticle surfaces. Because of resistive nature of the surfaces, they were sputter-coated with thin gold (board and paper substrates) or carbon (LDPE substrates) films prior to the FEG-SEM imaging.

All the contact angle measurements were performed at ambient conditions of 23 °C/50% relative humidity using distilled water and KSV CAM200 equipment. Three parallel droplets were used for each measurement, and standard deviation was used to evaluate the error. Advancing and receding contact angles were measured by increasing and decreasing the droplet volume (increment−decrement method), respectively, and from moving droplets.

In the increment−decrement method droplet volume was increased up to 10 μL with 0.2 μL increments. The droplet was imaged after each increment to determine the advancing contact angle. The receding contact angle was studied by imaging an evaporating droplet (initially 10 μL) every 60 s. An average value was calculated from the points where the droplet was in a steady state where the contact angle decrement had stopped (see Figures 4 and 6). Droplet volumes under 0.5 μL were not considered for the receding contact angle because the experiments did show that the receding contact angle cannot be determined reliably with small droplet volumes.

Contact angle hysteresis from moving droplets was measured by setting a substrate to the tilt angle of 9°, after which 10 μL droplets were gently deposited onto the surface from which they instantly rolled off. The rolling droplets were then imaged to determine the advancing and receding contact angles from the front and rear of the droplets, respectively. Tilt angles where 10 μL droplets rolled off the surfaces were obtained by tilting the substrate slowly until the droplet started to move. Contact angle hysteresis "in a static state" was measured right before the droplet started to move.

AUTHOR INFORMATION

Corresponding Author

*E-mail: hannu.teisala@tut.fi; tel: +358414461662.

ACKNOWLEDGMENTS

Tekes (Finnish Funding Agency for Technology and Innovation) is acknowledged for the financial support of this study. The work was carried out in the Functional Materials 2007−2013 program, under the project called Liquid flame spray nanocoating for flexible roll-to-roll web materials. The authors also thank Mrs. Mari Honkanen (TUT, Department of Materials Science) for the FEG-SEM images.

REFERENCES

(1) Ma, M.; Hill, R. M. Superhydrophobic surfaces. *Curr. Opin. Colloid Interface Sci.* **2006**, *11*, 193−202.
(2) Erbil, H. Y.; Demirel, A. L.; Avci, Y.; Mert, O. Transformation of a simple plastic into a superhydrophobic surface. *Science* **2003**, *299*, 1377−1380.
(3) Roach, P.; Shirtcliffe, N. J.; Newton, M. I. Progress in superhydrophobic surface development. *Soft Matter* **2008**, *4*, 224−240.
(4) Carré, A., Mittal, K. L., Eds.; *Superhydrophobic Surfaces*; Brill: Leiden, The Netherlands, 2009; 495 pp.
(5) Quéré, D. Wetting and Roughness. *Annu. Rev. Mater. Res.* **2008**, *38*, 71−99.
(6) Callies, M.; Quéré, D. On water repellency. *Soft Matter* **2005**, *1*, 55−61.
(7) Tuteja, A.; Choi, W.; Ma, M.; Mabry, J. M.; Mazzella, S. A.; Rutledge, G. C.; McKinley, G. H.; Cohen, R. E. Designing superoleophobic surfaces. *Science* **2007**, *318*, 1618−1622.
(8) Han, D.; Steckl, A. J. Superhydrophobic and Oleophobic Fibers by Coaxial Electrospinning. *Langmuir* **2009**, *25*, 9454−9462.
(9) Barthlott, W.; Neinhuis, C. Purity of the sacred lotus, or escape from contamination in biological surfaces. *Planta* **1997**, *202*, 1−8.
(10) Koch, K.; Bhushan, B.; Barthlott, W. Multifunctional surface structures of plants: an inspiration for biomimetics. *Prog. Mater. Sci.* **2009**, *54*, 137−178.
(11) Bhushan, B.; Jung, Y. C.; Koch, K. Micro-, nano- and hierarchical structures for superhydrophobicity, self-cleaning and low adhesion. *Philos. Trans. R. Soc. London, A* **2009**, *367*, 1631−1672.
(12) Gao, X.; Jiang, L. Water-repellent legs of water striders. *Nature* **2004**, *432*, 36.
(13) Koch, K.; Dommisse, A.; Barthlott, W. Chemistry and Crystal Growth of Plant Wax Tubules of Lotus (*Nelumbo nucifera*) and Nasturtium (*Tropaeolum majus*) Leaves on Technical Substrates. *Cryst. Growth Des.* **2006**, *6*, 2571−2578.
(14) Bhushan, B.; Jung, Y. C.; Koch, K. Self-cleaning efficiency of artificial superhydrophobic surfaces. *Langmuir* **2009**, *25*, 3240−3248.
(15) Wenzel, R. N. Resistance of solid surfaces to wetting by water. *Ind. Eng. Chem.* **1936**, *28*, 988−994.
(16) Cassie, A. B. D.; Baxter, S. Wettability of porous surfaces. *Trans. Faraday Soc.* **1944**, *40*, 546−551.
(17) Kulinich, S. A.; Farzaneh, M. Effect of contact angle hysteresis on water droplet evaporation from super-hydrophobic surfaces. *Appl. Surf. Sci.* **2009**, *255*, 4056−4060.
(18) Varanasi, K. K.; Deng, T.; Hsu, M. F.; Bhate, N. Wetting hysteresis, metastability, and droplet impact on superhydrophobic surfaces. Proceedings of IPACK2009, InterPACK09, July 19−23, 2009, San Francisco, CA.
(19) Jung, Y. C.; Bhushan, B. Wetting transition of water droplets on superhydrophobic patterned surfaces. *Scr. Mater.* **2007**, *57*, 1057−1060.
(20) Luo, C.; Xiang, M.; Liu, X.; Wang, H. Transition from Cassie-Baxter to Wenzel states on microline-formed PDMS surfaces induced by evaporation or pressing of water droplets. *Microfluid. Nanofluid.* **2011**, *10*, 831−842.
(21) Teisala, H.; Tuominen, M.; Kuusipalo, J. Adhesion mechanism of water droplets on hierarchically rough superhydrophobic rose petal surface. *J. Nanomater.* **2011**, DOI: 10.1155/2011/818707.
(22) Jin, M.; Feng, X.; Feng, L.; Sun, T.; Zhai, J.; Li, T.; Jiang, L. Superhydrophobic aligned polystyrene nanotube films with high adhesive force. *Adv. Mater.* **2005**, *17*, 1977−1981.
(23) Teisala, H.; Tuominen, M.; Aromaa, M.; Mäkelä, J. M.; Stepien, M.; Saarinen, J. J.; Toivakka, M.; Kuusipalo, J. Development of superhydrophobic coating on paperboard surface using the liquid flame spray. *Surf. Coat. Technol.* **2010**, *205*, 436−445.
(24) Guo, Z.-G.; Liu, W.-M. Sticky superhydrophobic surface. *Appl. Phys. Lett.* **2007**, *90* (223111), 1−3.
(25) Wu, J.; Bai, H.-J.; Zhang, X.-B.; Xu, J.-J.; Chen, H.-Y. Thermal/Plasma-Driven Reversible Wettability Switching of a Bare Gold Film on a Poly(dimethylsiloxane) Surface by Electroless Plating. *Langmuir* **2010**, *26*, 1191−1198.
(26) Marmur, A. The lotus effect: superhydrophobicity and metastability. *Langmuir* **2004**, *20*, 3517−3519.
(27) Nosonovsky, M.; Bhushan, B. Hierarchical roughness makes superhydrophobic states stable. *Microelectron. Eng.* **2007**, *84*, 382−386.
(28) Mäkelä, J. M.; Aromaa, M.; Teisala, H.; Tuominen, M.; Stepien, M.; Saarinen, J. J.; Toivakka, M.; Kuusipalo, J. Nanoparticle deposition from liquid flame spray onto moving roll-to-roll paperboard material. *Aerosol Sci. Technol.* **2011**, *45*, 827−837.
(29) Teisala, H.; Tuominen, M.; Aromaa, M.; Stepien, M.; Mäkelä, J. M.; Saarinen, J. J.; Toivakka, M.; Kuusipalo, J. *J. Adhes. Sci. Technol.* **2012**.
(30) Tuominen, M.; Teisala, H.; Aromaa, M.; Stepien, M.; Mäkelä, J. M.; Saarinen, J. J.; Toivakka, M.; Kuusipalo, J. *J. Adhes. Sci. Technol.* **2012**.
(31) Stepien, M.; Saarinen, J. J.; Teisala, H.; Tuominen, M.; Aromaa, M.; Kuusipalo, J.; Mäkelä, J. M.; Toivakka, M. Adjustable wettability of paperboard by liquid flame spray nanoparticle deposition. *Appl. Surf. Sci.* **2011**, *257*, 1911−1917.
(32) Kuusipalo, J., Ed.; *Paper and Paperboard Converting*, 2nd ed.; Paperi ja Puu Oy: Jyväskylä, Finland, 2008; 346 pp.
(33) Gurav, A.; Kodas, T.; Pluym, T.; Xiong, Y. Aerosol Processing of Materials. *Aerosol Sci. Technol.* **1993**, *19*, 411−452.
(34) Pratsinis, S. E. Flame aerosol synthesis of ceramic powders. *Prog. Energy Combust. Sci.* **1998**, *24*, 197−219.
(35) Tjong, S. C.; Chen, H. Nanocrystalline materials and coatings. *Mater. Sci. Eng., R* **2004**, *45*, 1−88.
(36) Valden, M.; Lai, X.; Goodman, D. W. Onset of Catalytic Activity of Gold Clusters on Titania with the Appearance of Nonmetallic Properties. *Science* **1998**, *281*, 1647−1650.
(37) Singh, S.; Houston, J.; van Swol, F.; Brinker, C. J. Drying transition of confined water. *Nature* **2006**, *442*, 526.
(38) Lum, K.; Chandler, D.; Weeks, J. D. Hydrophobicity at Small and Large Length Scales. *J. Phys. Chem. B* **1999**, *103*, 4570−4577.
(39) Rasaiah, J. C.; Garde, S.; Hummer, G. Water in Nonpolar Confinement: From Nanotubes to Proteins and Beyond. *Annu. Rev. Phys. Chem.* **2008**, *59*, 713−740.
(40) Hummer, G.; Rasaiah, J. C.; Noworyta, J. P. Water conduction through the hydrophobic channel of a carbon nanotube. *Nature* **2001**, *414*, 188−190.
(41) Sansom, M. S. P.; Biggin, P. C. Water at the nanoscale. *Nature* **2001**, *414*, 156−158.
(42) Balu, B.; Breedveld, V.; Hess, D. W. Fabrication of "Roll-off" and "Sticky" Superhydrophobic Cellulose Surfaces via Plasma Processing. *Langmuir* **2008**, *24*, 4785−4790.
(43) Balu, B.; Kim, J. S.; Breedveld, V.; Hess, D. W. Tunability of the Adhesion of Water Drops on a Superhydrophobic Paper Surface via Selective Plasma Etching. *J. Adhes. Sci. Technol.* **2009**, *23*, 361−380.
(44) Nyström, D.; Lindqvist, J.; Östmark, E.; Hult, A.; Malmström, E. Superhydrophobic bio-fibre surfaces via tailored grafting architecture. *Chem. Commun.* **2006**, 3594−3596.
(45) Li, S.; Zhang, S.; Wang, X. Fabrication of Superhydrophobic Cellulose-Based Materials through a Solution-Immersion Process. *Langmuir* **2008**, *24*, 5585−5590.
(46) Zhao, Y.; Lu, Q.; Chen, D.; Wei, Y. Superhydrophobic modification of polyimide films based on gold-coated porous silver nanostructures and self-assembled monolayers. *J. Mater. Chem.* **2006**, *16*, 4504−4509.
(47) Khalil-Abad, M. S.; Yazdanshenas, M. E. Superhydrophobic antibacterial cotton textiles. *J. Colloid Interface Sci.* **2010**, *351*, 293−298.
(48) Peng, J.; Yu, P.; Zeng, S.; Liu, X.; Chen, J.; Xu, W. Application of Click Chemistry in the Fabrication of Cactus-Like Hierarchical Particulates for Sticky Superhydrophobic Surfaces. *J. Phys. Chem. C* **2010**, *114*, 5926−5931.
(49) Du, X.; Li, X.; He, J. Facile Fabrication of Hierarchically Structured Silica Coatings from Hierarchically Mesoporous Silica Nanoparticles and Their Excellent Superhydrophilicity and Superhydrophobicity. *ACS Appl. Mater. Interfaces* **2010**, *2*, 2365−2372.

Publication 4

Teisala, H.; Tuominen, M.; Aromaa, M.; Stepien, M.; Mäkelä, J. M.; Saarinen, J. J.; Toivakka, M.; Kuusipalo, J.

High- and low-adhesive superhydrophobicity on the liquid flame spray-coated board and paper: structural effects on surface wetting and transition between the low- and high-adhesive states

Colloid and Polymer Science **2013**, 291, 447–455, DOI: 10.1007/s00396-012-2833-5

High- and low-adhesive superhydrophobicity on the liquid flame spray-coated board and paper: structural effects on surface wetting and transition between the low- and high-adhesive states

Hannu Teisala[a,*], Mikko Tuominen[a], Mikko Aromaa[b], Milena Stepien[c], Jyrki M. Mäkelä[b], Jarkko J. Saarinen[c], Martti Toivakka[c] and Jurkka Kuusipalo[a]

[a]Paper Converting and Packaging Technology, Department of Energy and Process Engineering, Tampere University of Technology, P.O. Box 589, FI-33101 Tampere, Finland

[b]Aerosol Physics Laboratory, Department of Physics, Tampere University of Technology, P.O. Box 692, FI-33101 Tampere, Finland

[c]Laboratory of Paper Coating and Converting, Center for Functional Materials, Abo Akademi University, Porthansgatan 3, FI-20500 Turku, Finland

*Corresponding author: hannu.teisala@tut.fi, tel. +358414461662

Abstract

Surface wetting is an important and relevant phenomenon in several different fields. Scientists have introduced a large number of applications where special surface wetting could be exploited. Here we study wetting phenomena on high- and low-adhesive superhydrophobic Liquid Flame Spray (LFS) generated TiO_2 coatings on paper and pigment coated board substrates using water-ethanol solution as a probe liquid. Submicrometer scale air gaps, which exist on superhydrophobic surfaces below the liquid droplets, were more stable with the ethanol increment than the larger scale micrometric air gaps. With the droplet ethanol concentration of 15 wt%, static contact angle as high as 155 ± 2° was measured on the LFS-TiO_2 coated board. Transition from the low-adhesive wetting state to the high-adhesive state was demonstrated on the LFS-TiO_2 coated paper. The LFS method enables efficient roll-to-roll production of surfaces with special wetting properties on economically viable board and paper substrate materials.

Keywords: superhydrophobic, wetting, hierarchical roughness, contact angle hysteresis, paper, roll-to-roll process

1. Introduction

Spreading of a liquid on a solid surface, i.e. surface wetting, is a phenomenon that is strongly related to our daily life. Consider, for example, washing the dishes: detergents are needed to lower the surface tension of water and thus to enable its penetration below the dirt. Or imagine a rainy day, when water droplets on a window may hinder the view. Nature has resolved wetting problems by creating an impressive and broad range of surfaces with special wettability [1−3]. Water-repellent leaves of lotus plant [4], wings of butterflies [5, 6] or legs of water striders [7], as well as high-adhesive water repellency of rose petals [8, 9], are just few examples. Surface wetting is a very interesting topic from industrial point of view, because it is often related to manufacturing or functioning of materials and products. For example, special wettability is exploited in offset printing [10], self-cleaning [4, 11, 12], anti-fogging surfaces [12, 13] and microfluidic devices [14, 15], among others.

One simple and widely used method to evaluate surface wettability is the contact angle measurement. That is, a liquid droplet is placed on a solid surface and the angle between the liquid and solid is measured in a static state. Water-repellent surfaces, where droplets stay in a spherical shape, result in high contact angles, whereas on hydrophilic surfaces droplet spreading results in low contact angles. Surface wetting is fundamentally governed by two factors: chemistry and physical structure of the surface. Extremely water-repellent surfaces, where contact angle is higher than 150°, are usually called superhydrophobic. These surfaces always possess special physical structure or roughness at the scale from tens of micrometers to a few nanometers [16−18]. Wetting of rough surfaces has attracted appreciable attention of scientists ever since Wenzel [19] and Cassie and Baxter [20] introduced their wetting theories for rough surfaces. These two idealistic theories

describe opposite wetting states, i.e., the state where a surface is completely wetted by a liquid (Wenzel state) and the state where only top areas of a surface are wetted (Cassie-Baxter state). Although wetting of real surfaces is often a combination of the Wenzel and Cassie-Baxter states, these two theories are still useful and help us perceive the wetting phenomenon on rough surfaces.

More detailed information on surface wetting properties can be obtained by measuring dynamic contact angles in addition to the static contact angle. Advancing contact angle in front of the moving liquid phase is always higher than the receding one in the rear. The difference between the advancing and receding contact angles is called contact angle hysteresis. Hysteresis gives information on the chemical heterogeneity of a surface. For example, in the case of water, hydrophobic surface areas increase the advancing contact angle, whereas hydrophilic areas decrease the receding contact angle, and thus the hysteresis increases. Hysteresis can also provide valuable information on wetting of rough surfaces, because liquid penetration into the solid affects particularly the receding contact angle by decreasing it [21−23]. On superhydrophobic surfaces, the advancing contact angle is always very high (> 150°). Even though all superhydrophobic surfaces have the high static and high advancing contact angles in common, there can be large variation in the receding contact angles on the differently structured surfaces. Therefore, contact angle hysteresis and droplet adhesion on superhydrophobic surfaces can vary significantly. When the receding contact angle on a superhydrophobic surface is close to the advancing contact angle, i.e. the hysteresis is low, the droplet is in Cassie-Baxter state sitting on top of the surface asperities. On this type of surfaces, e.g. on lotus leaf, the droplet adhesion is very low because of the small contact area between the liquid and solid substrate. In contrast, when the receding contact angle is considerably low in comparison with the advancing one, i.e. the hysteresis is high, the droplet is typically at least partially in the Wenzel state. That is, the liquid partially penetrates into the surface texture, and thus the real liquid-solid contact area can be significantly larger than the projected contact area. Therefore, high hysteresis indicates high droplet adhesion on a surface.

Paper and board are economically viable and cheap substrate materials made of renewable, recyclable and biodegradable cellulose fibers. The ability to control wetting properties of paper and board, for example by creating a superhydrophobic surface, can be an advantage in various converting processes of the materials, e.g. in printing, coating and lamination. Moreover, controlled surface wetting of paper and board can broaden their exploitation potential in other fields as well. As an example, superhydrophobic paper or board could potentially be utilized as a cheap and disposable substrate for microfluidic devices or as a lab-on-paper (LOP) platform as was demonstrated by Balu et al. [24]. In the past few years researchers have introduced a variety of methods to generate superhydrophobic paper surfaces with varying liquid adhesion properties [25−32]. Typically, the fibrous surface of paper is utilized as a base for the hierarchical structure that can provide superhydrophobicity after chemical modification, e.g. by plasma coating. This was the approach e.g. in the earlier work of Balu et al. [29], where fluorocarbon coated paper surface did show superhydrophobicity with high droplet adhesion and high contact angle hysteresis. In the same study, it was demonstrated how plasma etching of the paper surface generated submicrometer structures on the cellulose fibers, which effectively reduced the water droplet adhesion and hysteresis.

In this study we have investigated wetting and hysteresis phenomena on superhydrophobic Liquid Flame Spray (LFS) [33, 34] generated TiO_2 nanoparticle coatings on paper and pigment coated board substrates. In particular, surface wetting by water-ethanol solution and ethanol effect on the contact angle hysteresis are studied. Our approach is quite different from many other superhydrophobicity studies on paper materials because of the atmospheric and continuous nature of the roll-to-roll LFS coating procedure. Another distinctive feature of the present study is that the pigment coating on the board substrate eliminates the micrometric roughness of the cellulose fibers. In the case of the pigment coated substrate the surface roughness needed for superhydrophobicity is mainly caused by the submicrometric nanoparticle aggregates of the LFS coating. As we will demonstrate, the smoothening effect caused by the pigment layer can be a benefit when generating superhydrophobic paper and board surfaces, which are repellent to liquids other than just pure water.

2. Materials and methods

Hierarchically rough superhydrophobic TiO_2 nanoparticle coatings were generated onto commercial pigment coated board (Natura 200 g/m^2, Stora Enso, Skoghall mill, Sweden) and machine glossed paper (SwanWhite 83 g/m^2, UPM Kymmene, Valkeakoski mill, Finland) in a continuous roll-to-roll process by the LFS method. Titanium tetraisopropoxide (97 % pure, Aldrich) dissolved in isopropanol with a concentration of 50 mg (atomic metal)/ml was used as a precursor liquid for the nanoparticle synthesis. The pigment coated board substrate was LFS coated with the following parameters: precursor feed rate 32 ml/min, burner distance 15 cm and line speed 50 m/min. The paper substrate was coated with the following parameters: precursor feed rate 12 ml/min, burner distance 6 cm and line speed 50 m/min.

In the LFS process the liquid precursor is fed together with the combustion gases (hydrogen and oxygen) into a special designed spray gun. Instantly after exiting the burner nozzle, the precursor solution is atomized to micrometer-sized droplets by the high-velocity gas flow. Liquid droplets evaporate in a hot and turbulent flame and subsequent reactions of the precursor vapor lead to formation of nanoparticles. Afterwards nanoparticles grow larger in the flame by condensation, coagulation, coalescence and agglomeration, and deposit onto a moving substrate to form a highly porous nanoparticle coating. A detailed description of the LFS coating process, equipment and materials are given in our previous publications [23, 35−38].

All the contact angle measurements were performed in a conditioned room at 23ºC / 50% relative humidity using distilled water and ethanol (Altia Oyj, Rajamäki, Finland). Water-ethanol solutions were prepared by weight (ethanol concentration is given in wt%) using Precisa 240A scale (Oy Teo-Pal Ab, Espoo, Finland). Liquid proportions (10 g in total) were measured into a glass vessel with an accuracy of ± 0.02 g. Instantly after preparation and stirring of the water-ethanol solution it was sucked into microsyringe to avoid ethanol evaporation. The droplets were carefully placed onto the substrates with the microsyringe and the droplet imaging was done with KSV CAM200 equipment (KSV Instruments Oy, Helsinki, Finland) three seconds after the droplet placement. The droplet volume of 10 µl was used in the study and the given static contact angles are average values measured from three to five droplets.

Advancing and receding contact angles for the contact angle hysteresis were obtained by moving the substrate below the liquid droplets that were attached to the microsyringe needle tip (see Fig. 5). The microsyringe was mounted to the dispenser system of the CAM200 equipment so that the needle tip was fixed at 0.8 mm above the substrate. A motorised stage and constant speed of 2 mm/s were used to move the substrate, and droplet imaging was done every 0.2 s. Droplet size of 25 µl was used in the hysteresis measurements. Despite the gentle droplet placement onto the moving substrate, in some cases the droplet always detached from the needle tip and thus the advancing and receding contact angles/hysteresis could not be measured (see Table 1). The receding contact angle and liquid-solid contact diameter of evaporating droplets were studied by imaging the droplet every 60 seconds.

3. Results and discussion

3.1. Surface wetting by water

In our previous study [23] we generated high- and low-adhesive superhydrophobic TiO_2 nanoparticle coatings on board and paper substrates using the LFS method. Hierarchical structure of the LFS-TiO_2 surfaces, shown in Fig. 1, governs the superhydrophobicity, but in addition, it establishes the droplet adhesion and contact angle hysteresis on the surfaces. Nanoscale structures on the surfaces increase water droplet adhesion since water can penetrate between the nanoparticles. In contrast, submicrometer and micrometer scale structures entrap air below water droplets and thus decrease the liquid-solid contact area and droplet adhesion. On the high-adhesive LFS-TiO_2 coated board (Fig. 1a) there is not much micrometric structure because the pigment layer on the board levels the substrate irregularity significantly [36, 39]. The surface is still highly irregular due to the submicrometer scale structure caused by the particle aggregates, which can entrap air and produce superhydrophobicity. However, despite the air-entrapping submicrometer structure, the liquid-solid contact area on the surface is large due to the surface nanostructures. On the LFS-TiO_2 coated paper (Fig. 1b) the fibrous structure of the substrate makes the surface highly irregular also at micrometer scale, which reduces the liquid-solid contact area and thus governs the low-adhesive behavior of the surface.

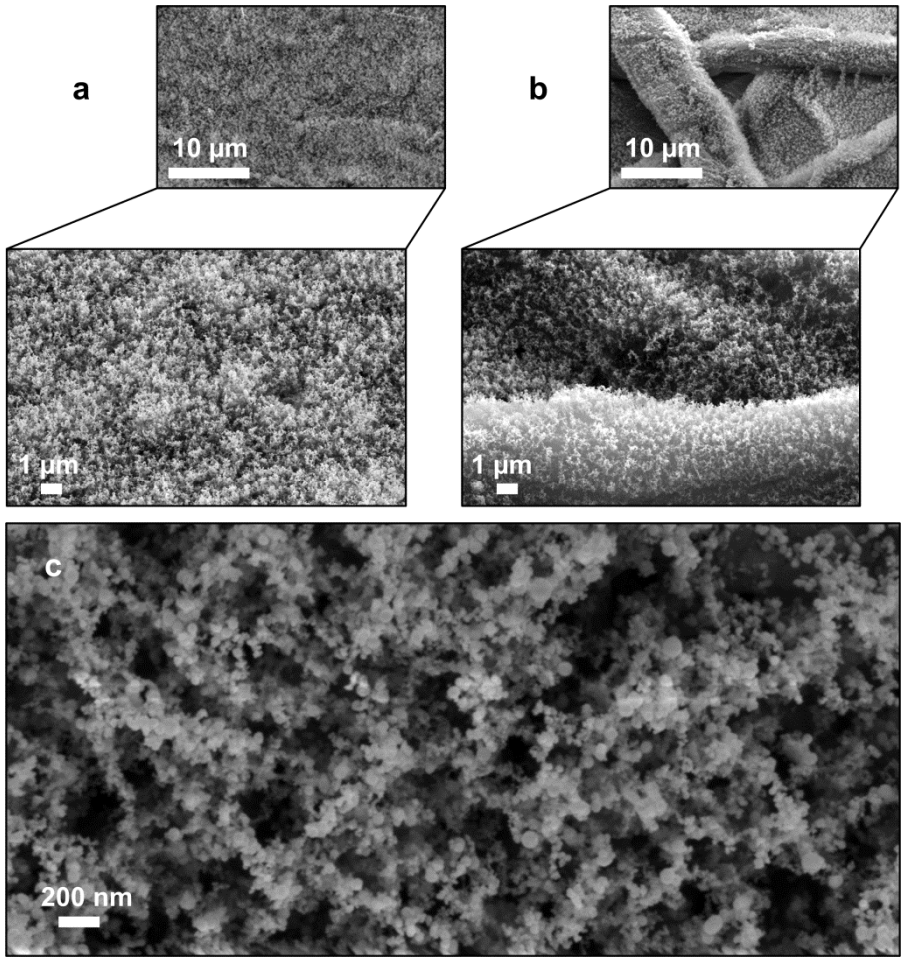

Fig. 1 Scanning electron microscope images of high- and low-adhesive superhydrophobic LFS-TiO_2 coated surfaces. The high-adhesive surface on pigment coated board (a) is significantly smoother at the micrometric scale compared to the low-adhesive surface on paper (b). The high-resolution image (c) reveals the hierarchical structure of the high-adhesive surface at the submicrometer and nanoscale. Reprinted (adapted) with permission from [23] Teisala et al. (2012) Langmuir 28:3138─3145. Copyright 2012 American Chemical Society

In our previous study [23] the contact angle hysteresis on the superhydrophobic surfaces was measured in two ways: from the rolling droplets and by the increment-decrement method. In the latter one, the receding contact angle was evaluated from evaporating droplets. The hysteresis measured from rolling droplets was relatively low on both surfaces: 37° on the high-adhesive surface and 6° on the low-adhesive surface. However, when water droplets evaporated freely from the surfaces, the liquid was able to penetrate into the nanostructure and the difference between the surfaces became more evident. On the high-adhesive surface water was tightly pinned to the surface, i.e. contact diameter of the droplet did not shrink with the decreasing droplet volume, and thus the receding contact angle decreased constantly close to zero, which indicates a hysteresis of over 150°. In contrast, on the low-adhesive surface the contact diameter decreased with the decreasing droplet volume. Thus, the droplet maintained its spherical shape during the evaporation and the receding contact angle remained comparatively high, around 140° (Fig. 2).

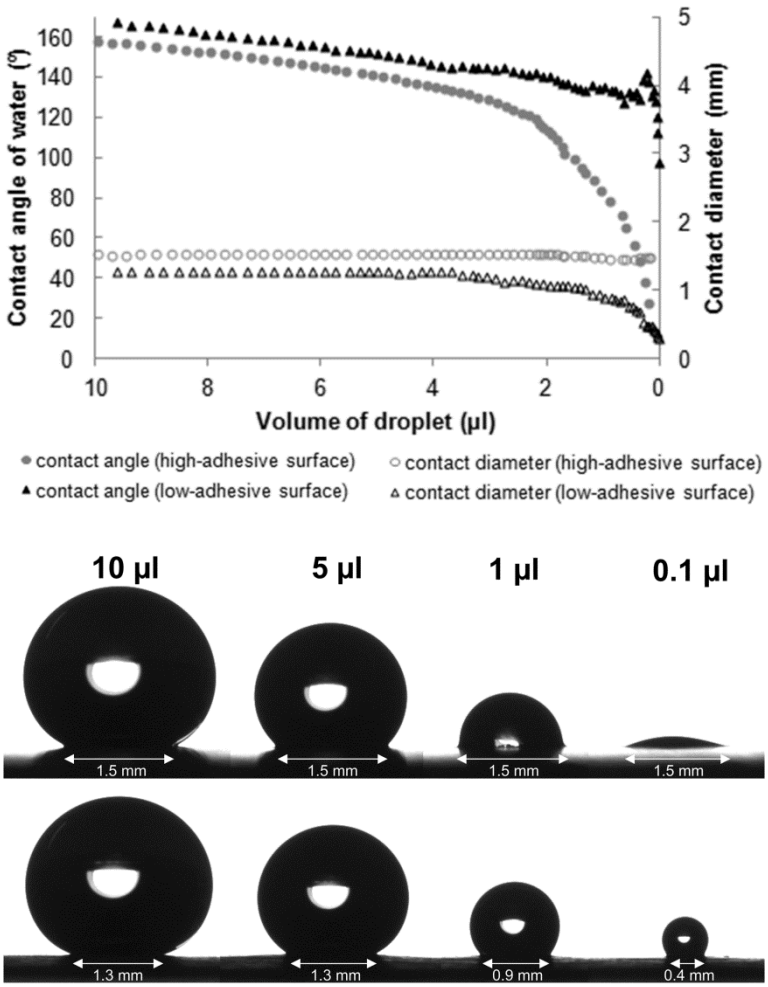

Fig. 2 Contact angle, contact diameter and shape of evaporating water droplets on the high- and low-adhesive superhydrophobic LFS-TiO_2 surfaces. The droplet is tightly pinned to the nanostructures of the high-adhesive surface and therefore the contact diameter remains constant at 1.5 mm. Consequently, at the end of the evaporation the droplet is clearly in a hydrophilic state possessing a very low contact angle. On the low-adhesive surface the contact diameter decreases with the decreasing droplet volume, and thus the droplet maintains its spherical shape and high contact angle. Reprinted (adapted) with permission from [23] Teisala et al. (2012) Langmuir 28:3138─3145. Copyright 2012 American Chemical Society

3.2. Surface wetting by water-ethanol solution

Water is a special liquid because of its high surface tension, which is caused by the hydrogen bonds between H_2O molecules. For this reason it is comparatively easy to prevent water spreading on a surface, for example in the case of superhydrophobic surfaces. Many other liquids, e.g. alcohols, possess much lower surface tension than water, and thus they spread more easily on a solid surface. For example, surface tensions for water and ethanol at 20°C have been reported to be 72.8 and 22.3 mN/m, respectively [40]. Here we study wettability of the high- and low-adhesive superhydrophobic LFS-TiO_2 surfaces using water-ethanol solution as a probe liquid. Fig. 3 shows contact angles on both superhydrophobic surfaces as a function of increasing ethanol concentration in the liquid. The high-adhesive surface can resist spreading of water-ethanol solution clearly better

than the low-adhesive surface. The contact angle as high as 155 ± 2° was measured on the high-adhesive surface when the ethanol concentration in the probe liquid was 15 wt%. On the low-adhesive surface the contact angle had decreased already below 150° at the ethanol concentration of 10 wt%, and at the concentration of 15 wt% it was no higher than 87 ± 1°. According to Vázquez et al. [40], who provide extensive information on different water-alcohol solutions, surface tensions for the 10 and 15 wt% water-ethanol solutions at 20°C are 48.1 and 42.7 mN/m, respectively.

On the high-adhesive surface the contact angle decrement as a function of increasing ethanol concentration has clearly three stages (Fig. 3). At the first stage, which lasts approximately until 15 wt% of ethanol concentration, the contact angle decrement is quite linear. At the second stage between the ethanol concentrations of 15 and 20 wt%, there is a rapid decrement in the contact angle. We assume that during the second stage most of the entrapped air is replaced by the liquid. That is, the air pockets below the liquid droplets collapse, which decreases the contact angle rapidly. After the collapse, at the third stage, the contact angle decrement continues again rather linearly. On the low-adhesive surface the contact angle decrement occurs rather in a similar manner as with the high-adhesive surface. However, the three stages are not as clear as on the high-adhesive surface, the contact angle decrement is steeper already at the first stage, and the rapid decrement occurs earlier. On the reference substrates, i.e. pigment coated board and paper without the LFS-TiO_2 coating, the contact angle decrement always appears to be linear.

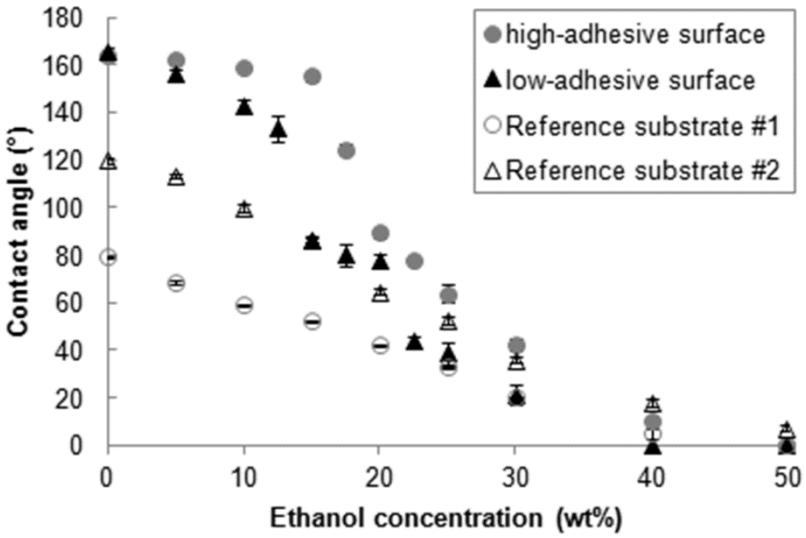

Fig. 3 Contact angles on the high- and low-adhesive superhydrophobic LFS-TiO_2 surfaces as a function of increasing ethanol concentration in the probe liquid. Reference substrates number 1 and 2 refer to pigment coated board and paper without the LFS coating, respectively. The error bars represent standard deviation

With the increasing ethanol concentration the non-wetting state on the superhydrophobic LFS-TiO_2 surfaces converted to complete wetting state, where all the air pockets were considered to be filled by the liquid (Fig. 3). In general, it is typical for superhydrophobic surfaces that pure water can also be forced to penetrate into the surface structure by internal Laplace pressure of the droplet or some external pressure, such as impaction [11, 21, 41, 42]. It is also well known that the smaller the

structures on a superhydrophobic surface, the higher the surface resistance against the water collapse, until a specific limit at the nanoscale is reached where the collapse will occur [23, 43].

The different wetting behaviors by water-ethanol solution on the high- and low-adhesive LFS-TiO_2 surfaces observed in Fig. 3 can be attributed to the structural differences between the surfaces. Fig. 4 shows a schematic illustration of water wetting states on the hierarchically structured high- and low-adhesive LFS-TiO_2 surfaces. According to the findings in our previous study [23], water penetrates into the nanostructure of the surfaces, but entrapped air remains in the submicrometer and micrometer scale structures. The high-adhesive surface is predominantly composed of nano- and submicrometer scale structure, and thus the liquid-solid contact area on the surface is large. In contrast, the low-adhesive surface possesses much microstructure, even at the scale of tens of micrometers, which contributes to a small liquid-solid contact area. The wetting results shown in Fig. 3 indicate that the submicrometer scale surface structure prevents the liquid collapse more effectively than the micrometer scale structure when the surface tension of the probe liquid is decreased by adding ethanol. In other words, with the ethanol addition the collapse will occur first at the largest air entrapping gaps, i.e. at the gaps at the scale of tens of micrometers, and only after that at the smaller micrometer and submicrometer scale gaps (Figs. 1 & 4). Recent study by Boreyko et al. [44] on silicon micropillar surface decorated by carbon nanotubes showed similar wetting results as our present study on nanoparticle coated paper and board surfaces. Their superhydrophobic two-tier surface exhibited a two-stage wetting transition when ethanol concentration of the solution was increased. That is, at the first stage there was a collapse in the contact angle as the liquid filled the micrometric structure of the surface, and after that, at the second stage there was another collapse when the liquid penetrated into the submicrometer structure. In fact, the same type of two-stage wetting transition can be distinguished also on the low-adhesive LFS-TiO_2 surface: the first collapse occurs between the ethanol concentrations of 12.5 and 15 wt% and the second one between the concentrations of 20 and 22.5 wt%.

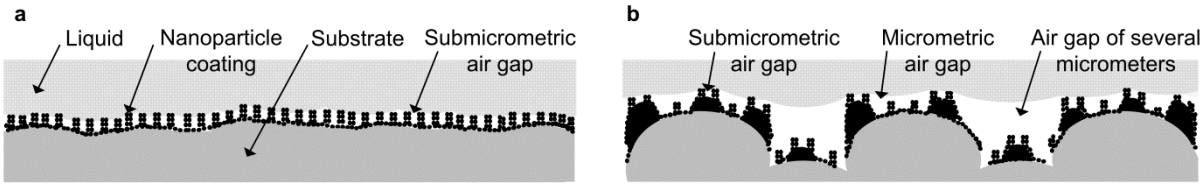

Fig. 4 Schematic illustration of water wetting states on the high- (a) and low-adhesive (b) superhydrophobic LFS-TiO_2 surfaces. The nanoscale structures increase the liquid-solid contact area, whereas the submicrometer and micrometer scale structures entrap air and reduce the liquid-solid contact. On the high-adhesive surface the liquid-solid contact area is larger and the amount of entrapped air is smaller than on the low-adhesive surface

The wettability results shown in Fig. 3 are well in agreement with the physical structure of the surfaces. Because of the submicrometric scale and narrow size distribution of the air gaps, the high-adhesive surface (Figs. 1 & 4) can resist the spreading of water-ethanol solution well until a rapid collapse occurs when majority of the air gaps presumably get replaced by the liquid. On the low-adhesive surface the largest air gaps are much larger than the average size of the air gaps.

Considering this and the results shown in Fig. 3, i.e. the contact angle decreases comparatively fast already at the first linear stage, it seems that although most of the entrapped air still remains on the surface with the small ethanol concentrations of 5 and 10 wt%, the largest air gaps already start to collapse. Moreover, because of the larger average size of the air gaps on the low-adhesive surface compared to the high-adhesive surface, majority of the entrapped air will vanish at lower ethanol concentration, and thus the rapid collapse in the contact angle occurs earlier.

The altered wetting state on the low-adhesive surface as a result of the ethanol increment, i.e. partial liquid penetration into the microstructure, affects not only the static contact angle but also the droplet adhesion and contact angle hysteresis. As shown in Table 1, there was an increment of 34° in the hysteresis already when the ethanol concentration in the droplet was increased from 0 to 5 wt%. The hysteresis values were determined by moving the substrate below the liquid droplets which were attached to the microsyringe needle tip. With 10 wt% of ethanol the hysteresis could not be measured, because the increased liquid adhesion to the surface caused droplet detachment from the needle tip, as illustrated in Fig. 5. Because the high-adhesive superhydrophobic surface on the pigment coated board substrate is more regular and does not possess as large micrometric structures as the low-adhesive surface on the fibrous paper substrate, the effect of ethanol addition on the contact angle hysteresis is not as drastic (Table 1). With the droplet ethanol concentration of 10 wt% the contact angle hysteresis on the high-adhesive surface was still close to that of pure water. When the ethanol concentration of the droplet was increased to 15 wt%, the liquid adhesion reached the level where the droplet detachment from the needle tip occurred also on the high-adhesive surface.

Table 1 The effect of ethanol concentration on the contact angle hysteresis on the superhydrophobic LFS-TiO_2 surfaces

	0 wt%	5 wt%	10 wt%	15 wt%
high-adhesive surface	44 ± 5°	39 ± 5°	54 ± 6°	n/a
low-adhesive surface	28 ± 6°	62 ± 7°	n/a	n/a

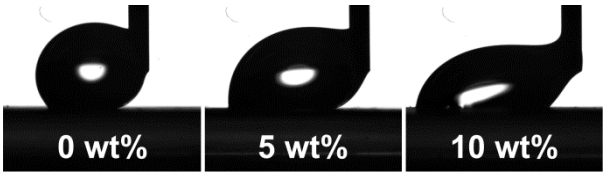

Fig. 5 Droplet images during contact angle hysteresis measurement on the low-adhesive LFS-TiO_2 surface with ethanol concentrations of 0, 5 and 10 wt%. With 10 wt% ethanol, the droplet attached to the surface, and thus the hysteresis could not be determined. The corresponding image was captured right before the droplet detached from the needle tip

To study the wetting behavior of the low-adhesive superhydrophobic LFS-TiO_2 surface further, we followed contact angle and contact diameter of evaporating water-ethanol droplets as a function of decreasing droplet volume. The static contact angle of the droplets remained comparatively high when the ethanol concentrations were 5 and 10 wt%, but the partial replacement of the entrapped air by the liquid started to decrease the receding contact angle more significantly, as shown in Fig. 6. In other words, a shift from the low-adhesive state to the high-adhesive state occurred with the

increasing ethanol concentration. The high-adhesive state was caused by the liquid collapse into the largest air gaps, whereas the smallest gaps still remained below the liquid and prevented the droplet from spreading effectively. This can be seen well in Fig. 6: even with ethanol concentration of 10 wt% contact diameter of the droplet did not increase with time.

Because the evaporation rate of ethanol is much faster than that of water the ethanol concentration decreases during the evaporation experiment, and thus in the end the liquid composition will be close to that of pure water. Still, the droplets with the initial ethanol concentration of 5 and 10 wt% did not start to behave like pure water droplet. This was an expected result, because it is unlikely that the liquid could rise up from the microstructure of the surface where it once penetrated at the initial wetting state after the droplet placement.

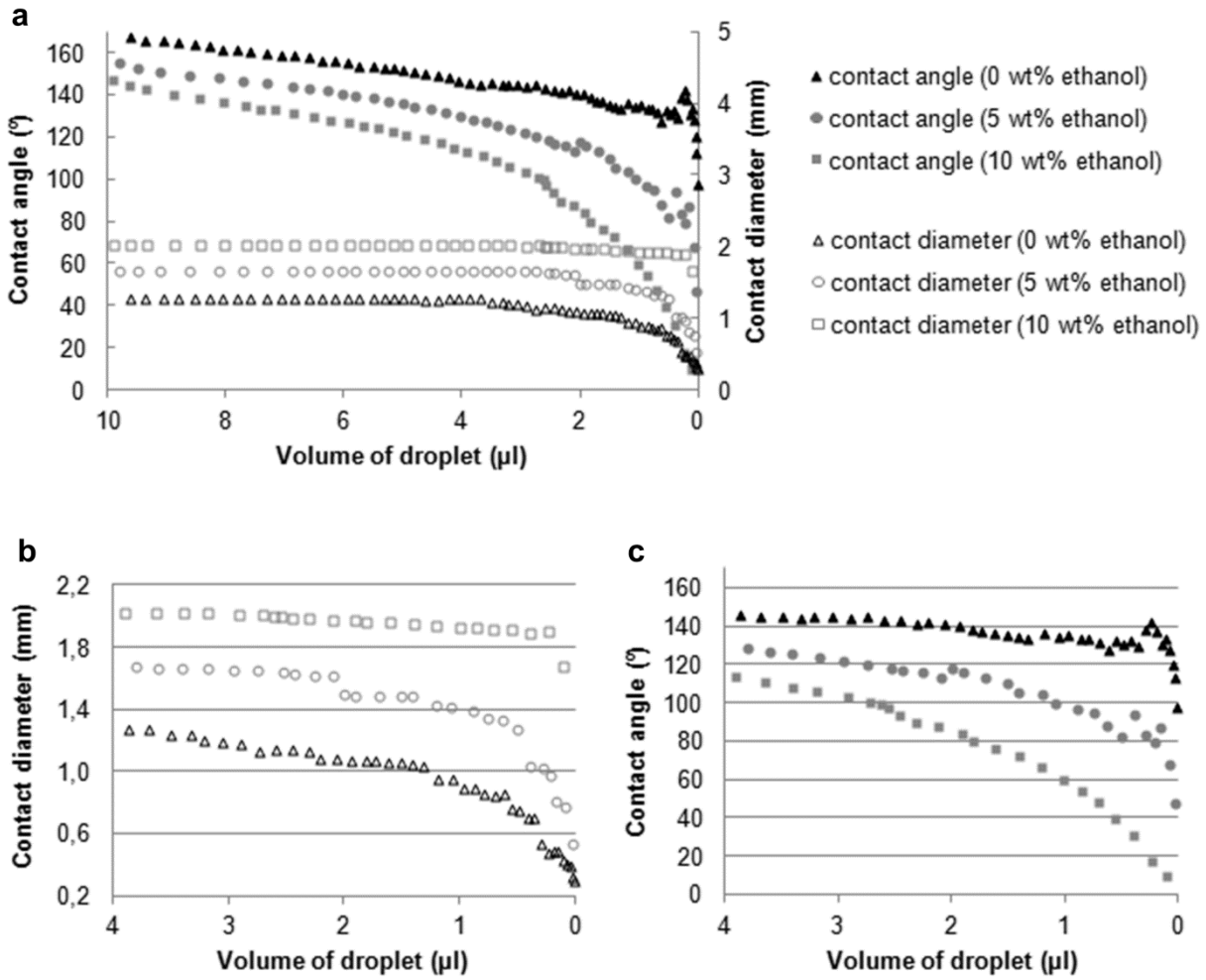

Fig. 6 Contact angle and contact diameter of evaporating water-ethanol droplets on the low-adhesive superhydrophobic LFS-TiO_2 surface (a). Increment in the ethanol concentration in the probe liquid shifts the droplet from the low-adhesive state towards the high-adhesive state, which is indicated by the contact diameter pinning (b) and by the receding contact angle decrement (c)

Comparing artificial and natural superhydrophobic surfaces is always interesting. We compared the water-ethanol wettability of the superhydrophobic LFS-TiO_2 surfaces with the high-adhesive superhydrophobic rose petal surface, which we studied recently [9]. On the petal surface, the

superhydrophobic structure is based on the epidermal cells at the scale of several micrometers, whereas the droplet adhesion on a fresh petal is caused by the cuticular folding on top of the epidermal cells. Because the superhydrophobicity on the petal is based on the air gaps at the scale of several micrometers, the contact angle on the surface decreased quite rapidly even with a small ethanol concentration. This phenomenon occurred both with the fresh, high-adhesive petal and dried, low-adhesive petal. With the ethanol concentration of 10 wt%, the contact angle on the fresh petal decreased from 151 to 125° and on the dried petal from 163 to 149°. Fang et al. [6] observed similar wetting behavior on hierarchically structured superhydrophobic butterfly wings, i.e., already a small alcohol portion of 5 % decreased the contact angle below 150°.

Surface wetting is an important and relevant phenomenon in several different fields. Thus, there are a large number of applications where for example superhydrophobicity can be exploited [11, 14−18]. Advantage of the LFS method is its continuous nature. Single-step roll-to-roll LFS coating procedure enables efficient mass production of superhydrophobic surfaces at high line speeds. In addition, the LFS coating itself, i.e. the particle aggregates, can form a suitable structure for superhydrophobicity. Thus, the complex fiber structure of paper surface can be smoothened by pigment layer prior to application of superhydrophobic LFS coating. As we have demonstrated in this study, more well-defined surface structure at submicrometer scale can stabilize liquid behavior on a surface, which can be an advantage in preparation of inexpensive paper surfaces with special wetting properties for, for example, printed electronics and microfluidic devices. A drawback of the superhydrophobic LFS coating is its relatively poor stability against physical wear [35]. However, this is an issue with superhydrophobic surfaces in general because of the fragile micrometer or submicrometer scale structure that is needed to build up superhydrophobicity.

4. Conclusions

Wetting of the superhydrophobic LFS-TiO_2 nanoparticle coated board and paper surfaces was studied using water-ethanol solution as a probe liquid. It was found that the submicrometer scale air gaps on the surfaces were more stable with the ethanol increment than the larger air gaps at the scale of several micrometers. Because of the smoothening pigment layer below the nanoparticle coating, the LFS-TiO_2 coated board had the air entrapping surface structure predominantly at the submicrometer scale, and thus the surface had high resistance against wetting by water-ethanol solution. Contact angle of 155 ± 2° was measured on the LFS-TiO_2 coated board with the ethanol concentration of 15 wt%. The LFS-TiO_2 coated paper experienced partial replacement of the entrapped air by the liquid when the ethanol concentration was increased. As a consequence, wetting of the surface shifted from the low-adhesive state to the high-adhesive state.

Acknowledgements

Tekes (Finnish Funding Agency for Technology and Innovation) is acknowledged for the financial support of this study. The work was carried out in the Functional Materials 2007−2013 programme, under the project called Liquid Flame Spray nanocoating for flexible roll-to-roll web materials.

References

1. Koch K, Bhushan B, Barthlott W (2009) Multifunctional surface structures of plants: an inspiration for biomimetics. Prog Mater Sci 54:137─178

2. Liu M, Zheng Y, Zhai J, Jiang L (2010) Bioinspired Super-antiwetting Interfaces with Special Liquid─Solid Adhesion. Acc Chem Res 43:368─377

3. Byun D, Hong J, Saputra, Ko JH, Lee YJ, Park HC, Byun B-K, Lukes JR (2009) Wetting Characteristics of Insect Wing Surfaces. J Bionic Eng 6:63─70

4. Barthlott W, Neinhuis C (1997) Purity of the sacred lotus, or escape from contamination in biological surfaces. Planta 202:1─8

5. Zheng Y, Gao X, Jiang L (2007) Directional adhesion of superhydrophobic butterfly wings. Soft Matter 3:178─182

6. Fang Y, Sun G, Cong Q, Chen G-h, Ren L-q (2008) Effects of Methanol on Wettability of the Non-Smooth Surface on Butterfly Wing. J Bionic Eng 5:127─133

7. Gao X, Jiang L (2004) Water-repellent legs of water striders. Nature 432:36

8. Feng L, Zhang Y, Xi J, Zhu Y, Wang N, Xia F, Jiang L (2008) Petal effect: a superhydrophobic state with high adhesive force. Langmuir 24:4114─4119

9. Teisala H, Tuominen M, Kuusipalo J (2011) Adhesion mechanism of water droplets on hierarchically rough superhydrophobic rose petal surface. J Nanomaterials. doi:10.1155/2011/818707

10. Kuusipalo J (2008) Paper and Paperboard Converting, 2nd ed. Paperi ja Puu Oy, Jyväskylä

11. Bhushan B, Jung YC, Koch K (2009) Self-cleaning efficiency of artificial superhydrophobic surfaces. Langmuir 25:3240─3248

12. Fujishima A, Rao TN, Tryk DA (2000) Titanium dioxide photocatalysis. J Photochem Photobiol C: Photochem Rev 1:1─21

13. Schmidt H (1994) Multifunctional inorganic─organic composite sol─gel coatings for glass surfaces. J Non-Cryst Solids 178:302─312

14. Ahn CH, Choi J-W, Beaucage G, Nevin JH, Lee J-B, Puntambekar A, Lee JY (2004) Disposable Smart Lab on a Chip for Point-of-Care Clinical Diagnostics. In: Proceedings of the IEEE 92:154─173

15. Londe G, Chunder A, Wesser A, Zhai L, Cho HJ (2008) Microfluidic valves based on superhydrophobic nanostructures and switchable thermosensitive surface for lab-on-a-chip (LOC) systems. Sensors Actuators, B 132:431─438

16. Ma M, Hill RM (2006) Superhydrophobic surfaces. Curr Opin Colloid Interface Sci 11:193─202

17. Roach P, Shirtcliffe NJ, Newton MI (2008) Progress in superhydrophobic surface development. Soft Matter 4:224─240

18. Carré A, Mittal KL (2009) Superhydrophobic Surfaces. VSP/Brill, Leiden

19. Wenzel RN (1936) Resistance of solid surfaces to wetting by water. Ind Eng Chem 28:988─994

20. Cassie ABD, Baxter S (1944) Wettability of porous surfaces. Trans Faraday Soc 40:546─551

21. Quéré D (2008) Wetting and Roughness. Annu Rev Mater Res 38:71─99

22. Kulinich SA, Farzaneh M (2009) Effect of contact angle hysteresis on water droplet evaporation from super-hydrophobic surfaces. Appl Surf Sci 255:4056─4060

23. Teisala H, Tuominen M, Aromaa M, Stepien M, Mäkelä JM, Saarinen JJ, Toivakka M, Kuusipalo J (2012) Nanostructures increase water droplet adhesion on hierarchically rough superhydrophobic surfaces. Langmuir 28:3138─3145. doi:10.1021/la203155d

24. Balu B, Berry AD, Hess DW, Breedveld V (2009) Patterning of superhydrophobic paper to control the mobility of micro-liter drops for two-dimensional lab-on-paper applications. Lab Chip 9:3066─3075

25. Nyström D, Lindqvist J, Östmark E, Hult A, Malmström E (2006) Superhydrophobic bio-fibre surfaces via tailored grafting architecture. Chem Commun 3594─3596

26. Li S, Zhang S, Wang X (2008) Fabrication of Superhydrophobic Cellulose-Based Materials through a Solution-Immersion Process. Langmuir 24:5585─5590

27. Balu B, Breedveld V, Hess DW (2008) Fabrication of “Roll-off” and “Sticky” Superhydrophobic Cellulose Surfaces via Plasma Processing. Langmuir 24:4785─4790

28. Yang H, Deng Y (2008) Preparation and physical properties of superhydrophobic papers. J Colloid Interface Sci 325:588─593

29. Balu B, Kim JS, Breedveld V, Hess DW (2009) Tunability of the Adhesion of Water Drops on a Superhydrophobic Paper Surface via Selective Plasma Etching. J Adhesion Sci Technol 23:361─380

30. Quan C, Werner O, Wågberg L, Turner C (2009) Generation of superhydrophobic paper surfaces by a rapidly expanding supercritical carbon dioxide-alkyl ketene dimer solution. J Supercrit Fluids 49:117─124

31. Werner O, Quan C, Turner C, Pettersson B, Wågberg L (2010) Properties of superhydrophobic paper treated with rapid expansion of supercritical CO_2 containing a crystallizing wax. Cellulose 17:187─198

32. Wang S, Li M, Lu Q (2010) Filter paper with selective absorption and separation of liquids that differ in surface tension. ACS Appl Mater Interfaces 2:677─683

33. Tikkanen J, Gross KA, Berndt CC, Pitkänen V, Keskinen J, Raghu S, Rajala M, Karthikeyan J (1997) Characteristics of the liquid flame spray process. Surf Coat Technol 90:210─216

34. Aromaa M, Keskinen H, Mäkelä JM (2007) The effect of process parameters on the Liquid Flame Spray generated titania nanoparticles. Biomol Eng 24:543─548

35. Teisala H, Tuominen M, Aromaa M, Mäkelä JM, Stepien M, Saarinen JJ, Toivakka M, Kuusipalo J (2010) Development of superhydrophobic coating on paperboard surface using the liquid flame spray. Surf Coat Technol 205:436─445

36. Teisala H, Tuominen M, Aromaa M, Stepien M, Mäkelä JM, Saarinen JJ, Toivakka M, Kuusipalo J (2012) Nanoparticle Deposition on Packaging Materials by Liquid Flame Spray ─ Generation of Superhydrophilic and Superhydrophobic Coatings. In: Proceedings of the Special Symposium on Recent Advances in Adhesion Science and Technology, 240th ACS National Meeting, August 22 ─ 26, 2010, Boston, Accepted.

37. Stepien M, Saarinen JJ, Teisala H, Tuominen M, Aromaa M, Kuusipalo J, Mäkelä JM, Toivakka M (2011) Adjustable wettability of paperboard by liquid flame spray nanoparticle deposition. Appl Surf Sci 257:1911─1917

38. Mäkelä JM, Aromaa M, Teisala H, Tuominen M, Stepien M, Saarinen JJ, Toivakka M, Kuusipalo J (2011) Nanoparticle deposition from liquid flame spray onto moving roll-to-roll paperboard material. Aerosol Sci Technol 45:827─837

39. Tuominen M, Teisala H, Aromaa M, Stepien M, Mäkelä JM, Saarinen JJ, Toivakka M, Kuusipalo J (2012) Creation of superhydrophilic surfaces of paper and board. J Adhesion Sci Technol. doi:10.1080/01694243.2012.697744

40. Vázquez G, Alvarez E, Navaza JM (1995) Surface Tension of Alcohol + Water from 20 to 50 ºC. J Chem Eng Data 40:611─614

41. Jung YC, Bhushan B (2007) Wetting transition of water droplets on superhydrophobic patterned surfaces. Scripta Materialia 57:1057─1060

42. Varanasi KK, Deng T, Hsu MF, Bhate N (2009) Wetting hysteresis, metastability, and droplet impact on superhydrophobic surfaces. In: Proceedings of IPACK2009, InterPACK´09, 2009, San Francisco, California, USA

43. Callies M, Quéré D (2005) On water repellency. Soft Matter 1:55─61

44. Boreyko JB, Baker CH, Poley CR, Chen C-H (2011) Wetting and Dewetting Transitions on Hierarchical Superhydrophobic Surfaces. Langmuir 27:7502─7509

Publication 5

Teisala, H.; Tuominen, M.; Stepien, M.; Haapanen, J.; Mäkelä, J. M.; Saarinen, J. J.; Toivakka, M.; Kuusipalo, J.

Wettability conversion on the liquid flame spray generated superhydrophobic TiO_2 nanoparticle coating on paper and board by photocatalytic decomposition of spontaneously accumulated carbonaceous overlayer

Cellulose **2013**, 20, 391–408, DOI: 10.1007/s10570-012-9825-y

Wettability Conversion on the Liquid Flame Spray Generated Superhydrophobic TiO_2 Nanoparticle Coating on Paper and Board by Photocatalytic Decomposition of Spontaneously Accumulated Carbonaceous Overlayer

Hannu Teisala,[a,*] Mikko Tuominen,[a] Milena Stepien,[c] Janne Haapanen,[b] Jyrki M. Mäkelä,[b] Jarkko J. Saarinen,[c] Martti Toivakka,[c] and Jurkka Kuusipalo[a]

[a]Paper Converting and Packaging Technology, Department of Energy and Process Engineering, Tampere University of Technology, P.O. Box 589, FI-33101 Tampere, Finland

[b]Aerosol Physics Laboratory, Department of Physics, Tampere University of Technology, P.O. Box 692, FI-33101 Tampere, Finland

[c]Laboratory of Paper Coating and Converting, Center for Functional Materials, Abo Akademi University, Porthansgatan 3, FI-20500 Abo / Turku, Finland

*Corresponding author: hannu.teisala@tut.fi, tel. +358414461662

Abstract

Titanium dioxide (TiO_2) is a photoactive material with various interesting and useful properties. One of those is the perfect wettability of TiO_2 surface after ultraviolet (UV) illumination. Wettability of a solid surface plays an important role in the field of printing, coating, and adhesion among others. Here we report on a superhydrophobic and photoactive liquid flame spray (LFS) generated TiO_2 nanoparticle coating that can be applied on web-like materials such as paper and board in one-step roll-to-roll process. The LFS TiO_2 nanoparticle coated paper and board were superhydrophobic instantly after the coating procedure because of spontaneously accumulated carbonaceous overlayer on TiO_2, and thus there was no need for any type of separate hydrophobization treatment. The highly photoactive LFS TiO_2 nanoparticle coating could be converted steplessly from superhydrophobic to superhydrophilic by UV-illumination, and the coating gave strong response to natural daylight illumination even in the shade. The superhydrophobic LFS TiO_2 coated surface can be used as an intelligent substrate, where photo-generated hydrophilic patterns guide the fluid setting and figure formation. Our study reveals that the wettability changes on the LFS TiO_2 surface were primarily caused by the photocatalytic removal of the carbonaceous material from TiO_2 during the UV-illumination and spontaneous accumulation of the carbonaceous material on the surface of the metal oxide during storage in the dark. The latter mechanism was found to be a temperature activated process which could be significantly speeded up by heat treatment. If other mechanisms such as surface

oxidization, increment of hydroxyl groups, or charge separation played a role in the wetting phenomena on TiO_2, their effect was rather secondary as the removal and accumulation of the carbonaceous material dominated the wettability changes on the surface. Our study gives valuable information on the complex issue of photo-induced wettability changes on TiO_2.

Keywords: interface wetting, patterning, titanium, photocatalysis, cellulose, roll-to-roll

1. Introduction

In recent years various techniques based on plasma deposition (Ostrikov 2005), chemical vapor deposition (CVD) (Choy 2003), atomic layer deposition (ALD) (Kemell et al. 2005), nanoparticle deposition (Rao et al. 1998; Teisala et al. 2010), and sol-gels (Brinker and Harrington 1981; Lu et al. 1997) among others, have been introduced to create nanoscale coatings that can improve material properties and bring functionality for the surfaces. One of the important material properties is wettability of a solid surface by a liquid. Surface wetting is a relevant characteristic for various cellulose-based substrates as it plays an important role in the field of printing, coating, and adhesion among others. Chemistry of a solid surface determines whether the surface has a tendency to repel or get wetted by the liquid. In addition, surface roughness can have a significant effect on wettability (Wenzel 1936; Cassie and Baxter 1944) and liquid adhesion (Teisala et al. 2012a), as natural water repellent surfaces such as lotus leaves (Barthlott and Neinhuis 1997) and rose petals (Teisala et al. 2011) have shown.

One of the most studied materials worldwide in different fields is titanium dioxide (TiO_2). It is a photoactive semiconductor, which makes it highly attractive for several applications. TiO_2 also has many other advantageous properties such as non-toxicity and high refractive index, and thus it is used in a wide range of different applications including toothpastes, variety of coatings, and highly developed solar cell applications. One of the fascinating properties of TiO_2 is its self-cleaning ability, that is, TiO_2 has a strong photo-induced oxidizing capability to decompose organic substances from its surface. The self-cleaning phenomenon is based on the low band gap energy of TiO_2 around 3.0 ─ 3.2 eV, which enables generation of photo-induced electron-hole pairs in TiO_2. The photo-generated electrons and holes can react directly with organic substances, or alternatively, they can create highly reactive species such as superoxides ($O_2^{\bullet-}$), hydroxyl radicals ($^{\bullet}OH$), and hydrogen peroxides (H_2O_2), which then react with the organic substances on TiO_2 to form for example water (H_2O) and carbon dioxide (CO_2) (Fujishima et al. 2000; Diebold 2003; Carp et al. 2004; Fujishima et al. 2008).

It is well-documented by several studies that photoactive TiO_2 surface can experience a hydrophilicity conversion under ultraviolet (UV) illumination. However, there has been a debate of the fundamental mechanism of the photo-induced hydrophilicity conversion on TiO_2. One theory suggests that the wetting conversion is entirely related to removal of contaminating hydrocarbon layer from TiO_2, that is, clean TiO_2 surface is always superhydrophilic (water contact angle < 10°). A strong argument for this theory is that the amount of carbonaceous substances on TiO_2 has been shown to correlate well with surface wetting (Takeda et al. 1999; Wang et al. 2003; White et al. 2003; Kanta et al. 2005; Stepien et al. 2012a). The other theory suggests that UV-illumination generates oxygen vacancies on TiO_2, and that dissociative water adsorption at the vacancy sites contributes to increased number of hydroxyl groups (OH) on TiO_2, which then promote water spreading on the surface making it superhydrophilic (Wang et al. 1997; Fujishima et al. 2000; Miyauchi et al. 2002; Fujishima et al. 2008). In this theory TiO_2 surface is considered to be free from contaminants. It is well known that after illumination the superhydrophilicity of TiO_2 surface will be lost during storage in the dark. The former theory explains the hydrophilicity decay by adsorption of hydrocarbons from atmosphere, which leads to re-formation of the thin organic layer on TiO_2. According to the latter theory, the photo-induced hydroxyl groups get replaced by oxygen in the dark, and thus the surface wettability reverts back to its initial state.

Fabrication of extremely water-repellent surfaces on cellulose-based substrates has recently gathered considerable attention because of the broad range of potential applications (Ma and Hill 2006; Carré and Mittal 2009). Both chemical and physical structure of a surface affect its wettability, and thus so-called superhydrophobic surfaces, where water contact angle is greater than 150°, must fulfill certain criteria from both aspects. That is, in addition to the appropriate low-energy surface chemistry, a superhydrophobic surface needs to have physical roughness at micrometer and submicrometer scale. Although cellulose fibers on paper surface create hierarchical roughness at micrometer scale and below, which is a good basis for the structure needed for superhydrophobicity, it is typical that even fluorinated papers are not superhydrophobic without additional roughening of the surface (Mukhopadhyay et al. 2002; Balu et al. 2008; Thorvaldsson et al. 2012). If a superhydrophobic coating is made of TiO_2, after creating a suitable structure for the surface, further treatment is needed to obtain the hydrophobic chemistry because TiO_2 itself is a hydrophilic material (Takeda et al. 1999; Kanta et al. 2005; Zhang et al. 2007; Kim et al. 2011). All together, fabrication of superhydrophobic surface on a cellulose-based material is often a multi-step and time-consuming procedure which requires vacuum equipment if plasma processing is used and drying steps if wet-chemical methods are used.

In our earlier studies we have shown that a nanoparticle deposition method called the liquid flame spray (LFS) can be used to generate superhydrophobic TiO_2 coating

on cellulose-based flexible materials such as paper and board in one-step roll-to-roll process (Teisala et al. 2010; Mäkelä et al. 2011; Stepien et al. 2011; Teisala et al. 2012a; Teisala et al. 2012b). The earlier studies (Teisala et al. 2010; Stepien et al. 2012a; Teisala et al. 2012b; Stepien et al. 2012b; Aromaa et al. 2012) revealed that LFS synthesized TiO_2 particles deposited on board substrate were covered by carbonaceous material. Most likely, the carbonaceous material on TiO_2 contains a variety of compounds such as hydrocarbons, soot, and elemental carbon. Because of the carbonaceous overlayer, which spontaneously accumulates on hierarchically structured TiO_2 coating during the atmospheric and high-temperature coating process, the LFS TiO_2 coated paper and board are superhydrophobic instantly after the coating procedure. Paper and board as substrate materials play a role in the hydrophobicity of the LFS TiO_2 coating. For example, some carbonaceous substances can evaporate from those materials when exposed to high temperatures (Aromaa et al. 2012).

In this study we show that photocatalytic decomposition of the carbonaceous overlayer on TiO_2 converts the surface from superhydrophobic to superhydrophilic. Our study indicates that the accumulation of the carbonaceous overlayer on the LFS TiO_2 coated board and the related hydrophobicity conversion are activated processes, and thus their speed is dependent on the surrounding temperature. Stimuli-responsive, intelligent TiO_2 coating can broaden exploitation potential of economically viable cellulose-based materials in different fields.

2. Experimental Section

LFS Coating Procedure

Machine glossed paper (83 g/m^2, UPM) and pigment coated board (200 g/m^2, Stora Enso) were coated with TiO_2 nanoparticles using the LFS method. The coating procedure was carried out on-line at the Tampere University of Technology (TUT) on the Paper Converting and Packaging Technology (PCPT) pilot line at ambient conditions using the line speed of 50 m/min, precursor feed rate of 12 ml/min, and burner-to-substrate distance of 6 cm. Titanium tetraisopropoxide (TTIP, 97 % pure, Aldrich) was used as a precursor for the LFS TiO_2 coating. The precursor was diluted in isopropanol with the Ti concentration of 50 mg (atomic metal)/ml. Hydrogen and oxygen with the ratio of 50/15 l/min were used as combustion gases in the process. The aerosol synthesized TiO_2 nanoparticles made by the LFS are mainly of anatase crystal structure (Keskinen et al. 2007; Aromaa et al. 2012), aggregated, and they form a highly porous coating layer. With the current processing parameters, the mean particle size is smaller than 20 nm in diameter, as shown in Fig. 1. Detailed description and more information of the LFS on-line coating procedure can be found from our previous studies (Teisala et al. 2010; Mäkelä et al. 2011; Stepien et al. 2011; Teisala et al. 2012a; Teisala et al. 2012b).

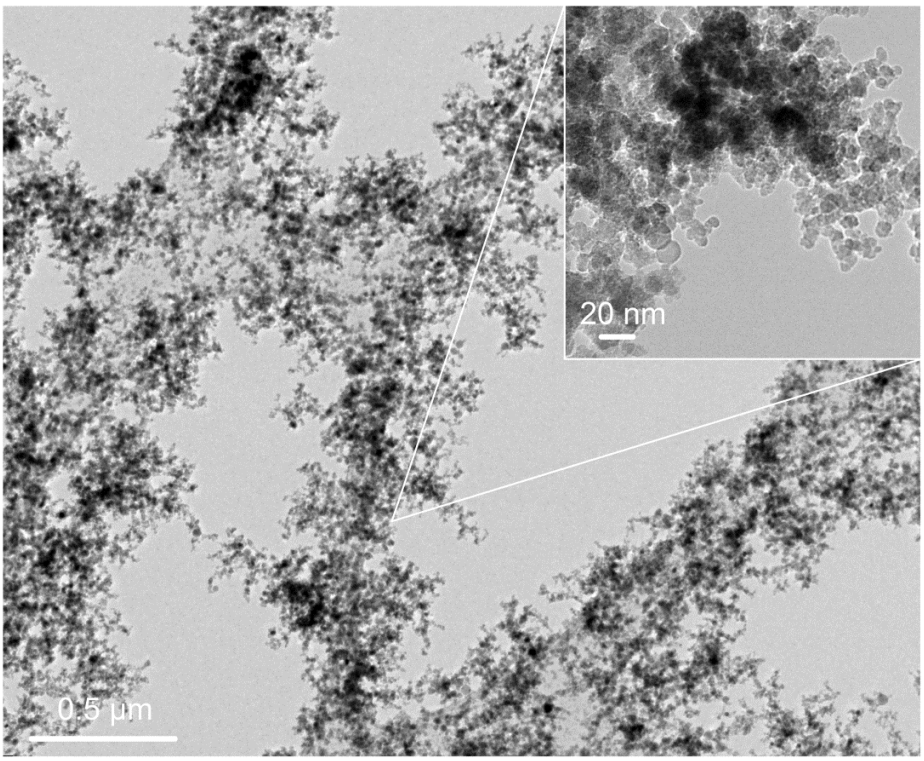

Fig. 1 TEM micrographs of the LFS TiO_2 nanoparticles collected during the on-line coating procedure

Water Contact Angle

Water contact angle measurements were performed in a conditioned room at ambient conditions of 23 ºC / 50 % relative humidity (RH) using distilled water and KSV CAM200 equipment (KSV Instruments Oy, Finland). Contact angle was always determined 3 seconds after the droplet placement on the sample. However, any rapid changes did not occur in the contact angle after the droplets were placed on the samples, because droplets did not start to spread even during a long-term follow-up period of 60 min, as was demonstrated in our previous study (Teisala et al. 2012a). The droplet volume of 2 µl was used in this study, and the given contact angles are average values measured from 5 droplets. The given error margins indicate standard deviation. During ageing the samples were stored in the dark in the conditioned room at 23 ºC / 50 % RH.

UV-illumination

UV-illumination was carried out with a lamp (Bluepoint 4 ecocure, Hönle UV Technology, Germany) providing the central wavelength of 365 nm with the filter of 320 ─ 390 nm. Illumination intensity was 50 mW/cm^2. The artificial daylight illumination was accomplished by GTI MiniMatcher illumination system (model MM-1UV/65, GTI Graphic Technology Inc., USA). Both illuminations were carried out at ambient conditions. The subsequent XPS and contact angle experiments were performed instantly after removing the samples from the illumination to minimize

the surface contamination and other possible changes occurring after the illumination.

Photopatterning

Hydrophilic pattern on the superhydrophobic LFS TiO_2 coating was made by illuminating the surface through a photomask. The photomask was made of pigment coated board, on which the pattern was fabricated by knife. After the photopatterning, the sample was rod coated with methylene blue colored water using a smooth rod made of stainless steel. The superhydrophobic coating rejected the liquid, while the hydrophilic pattern got wetted by the liquid and became visible. The colored sample was set between laboratory glass plates and the pattern was imaged using Zeiss Axioskop 40 optical microscope.

XPS

X-ray photoelectron spectroscopy (XPS) experiments were performed by PHI Quantum 2000 instrument (Physical Electronics Instruments, USA) equipped with a monochromatic Al Kα X-ray source and operated at 25 W. The charge compensation was enhanced by combination of electron flood and ion bombarding. The take-off angle was 45º in relation to the sample surface. The survey spectra were recorded with the pass energy of 184 eV from 3 different points with diameter of approximately 100 µm. The high-resolution spectra for the C 1s, O 1s, and Ti 2p photopeaks were recorded with the pass energy of 29.35 eV from 3 different points. The given error margins indicate standard deviation. Mixed Gaussian-Lorentzian character and Shirley background were used for curve fitting. The pressure in the main chamber was maintained at 2×10^{-7} Torr during spectra acquisition. The carbon photopeak with the binding energy of 285.0 eV was associated with the bindings labeled as group C1 (C-C, C-H), and the relative chemical shifts were associated as follows: 1.7 ± 0.2 eV with group C2 (C-O, C-OH, C-O-C); 3.1 ± 0.3 eV with group C3 (C=O, O-C-O); 4.6 ± 0.3 eV with group C4 (O-C=O); and 5.0 eV with group C5 (CO_3^{2-}). The oxygen photopeak with the binding energy of 530.0 eV was associated with the bindings labeled as group O1 (O^{2-}), and the relative chemical shifts of 1.4 ± 0.2 eV and 3.1 ± 0.2 eV were associated with groups O2 (-OH, C-O) and O3 (O-C=O, H_2O), respectively (Moulder et al. 1992; Beamson and Briggs 1992; Ström and Carlsson 1993; NIST 2003).

TEM

Transmission electron microscopy (TEM) of TiO_2 nanoparticles was performed with JEOL JEM-2010 instrument. TEM grid (lacey carbon film on copper grid, Agar) was attached on the board substrate with a staple aligned with the moving direction of the web, and the TiO_2 particles were collected on the grid during the normal on-line coating procedure of the board substrate.

FEG-SEM

Zeiss ULTRAplus field emission gun scanning electron microscope (FEG-SEM) was used for imaging the LFS coatings. The samples were sputter coated with thin gold film prior to the FEG-SEM imaging to obtain conductivity.

Heat Treatment

Heat treatment of the samples (Fig. 5 and Table 1) was carried out in Firlabo Air Concept oven equipped with fan circulation. After placing the samples in the oven the real temperature in the oven decreased momentarily below the set value, but was rapidly restored within approximately 1 min. The contact angle measurements on the heat treated samples were carried out as soon as the sample had cooled down to the room temperature.

Surface Roughness

Parker Print-Surf (PPS) roughness measurements were carried out from 5 different points of each sample using H.E. Messmer Ltd., model MK 2, equipment. The measurements were carried out according to ISO 8791-4:1992 and SCAN-P 21:67 standards.

3. Results

3.1. Superhydrophobicity of the LFS TiO_2 Coating

Water contact angles as high as 163.6 ± 1.4º and 162.5 ± 1.0º were measured on the LFS TiO_2 coated paper and board, respectively. Any additional hydrophobization treatment is not required to obtain superhydrophobicity on the LFS TiO_2 coating. Hydrophobicity of the coating is a permanent characteristic: any decrement in the hydrophobicity of the LFS TiO_2 coated paper or board was not observed during a storage period of 6 months in the dark room. Water contact angles of 162.4 ± 1.8º and 162.0 ± 1.2º were measured on the LFS TiO_2 coated paper and board after the ageing in the dark, respectively.

3.2. Superhydrophilicity Conversion by UV-illumination

The LFS TiO_2 surface is not an exception to other TiO_2 surfaces: it possesses the self-cleaning ability and experiences the related hydrophilicity conversion under UV-illumination. Because of the surface chemical changes caused by the illumination, the initially superhydrophobic LFS TiO_2 coating turns to superhydrophilic. The wettability conversion enables creation of hydrophilic patterns on hydrophobic surface, which allow the control of printability and line widths when aqueous inks or dyes are used. Thus, for example the dye can be applied with a very robust and simple method such as rod coating as shown on the LFS TiO_2 coated paper in Fig. 2.

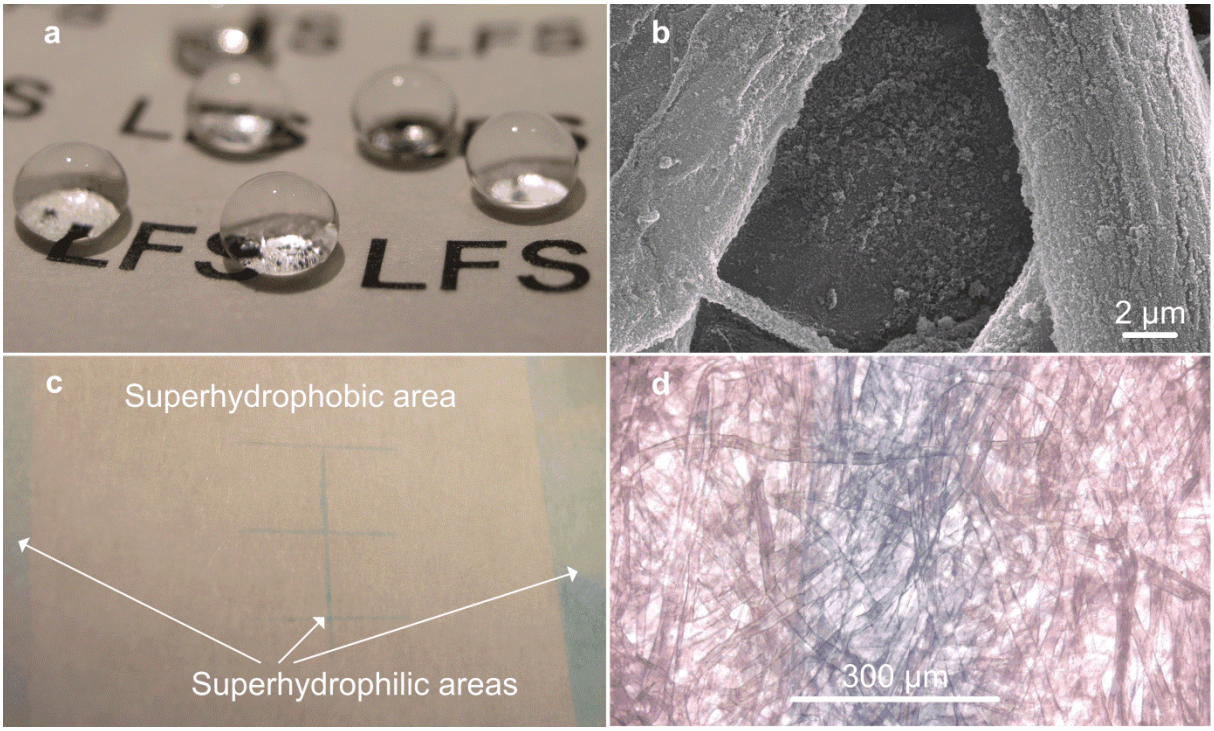

Fig. 2 Spherical water drops on transparent superhydrophobic LFS TiO_2 coating on printed paper (a) and FEG-SEM micrograph of the corresponding surface (b). A figure formed on the photo-patterned LFS TiO_2 coated paper after rod coating with methylene blue colored water (c). The hydrophilic areas guide the fluid setting and figure formation on the intelligent substrate. An optical microscope image of the photo-patterned figure shows the line width to be approximately 300 µm (d)

The chemical changes related to the UV-induced hydrophilicity conversion were studied on the LFS TiO_2 coated board. After 30 min of UV-illumination (365 nm, 50 mW/cm^2), water contact angle on the surface was measured to be 7°. As shown in Fig. 3, during the illumination the relative number of carbon atoms (C) on the surface decreased from 43.9 ± 0.6 % to 29.6 ± 0.9 % as a result of the photodegradation of the carbonaceous overlayer on TiO_2. Prior to the illumination the C/Ti ratio was 2.6 while after the illumination it was 1.5, which indicate the changes in the coverage of TiO_2 by the carbonaceous material. Most of the carbon decrement occurred from carbon-to-hydrogen or carbon-to-carbon bindings (group C1). In addition, small decrement in the number of carbon-to-oxygen bindings (groups C2 ─ C5) can be observed after the UV-illumination. As a result of the photodegradation of the carbonaceous overlayer, the larger number of titanium (Ti) and oxygen (O) atoms originating from the underlaying TiO_2 structure became detectable by XPS (information depth is ~ 10 nm in vertical direction). However, after the UV-illumination, the total increment of oxygen in relation to the total increment of titanium was greater than is characteristic for TiO_2, which means that all the oxygen increment did not arise from TiO_2 structure.

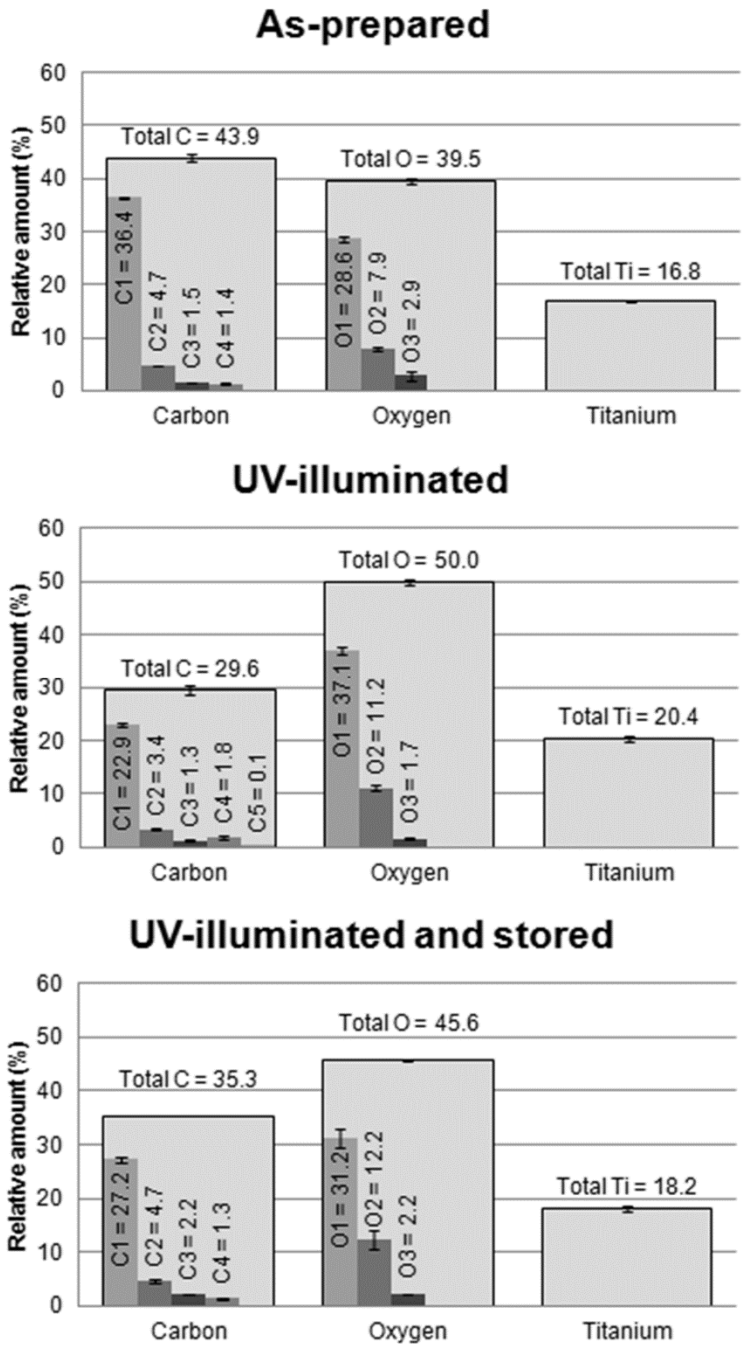

Fig. 3 Atomic concentrations and the corresponding bindings for carbon (C), oxygen (O), and titanium (Ti) on the LFS TiO_2 coated board before and after UV-illumination (365 nm, 50 mW/cm^2), and after the illuminated sample was stored in the dark (at 23 °C and 50 % RH) for 1 month. Groups C1 ─ C5 and O1 ─ O3 correspond to the bindings of carbon and oxygen as follows: C1 (C-C, C-H); C2 (C-O, C-OH, C-O-C); C3 (C=O, O-C-O); C4 (O-C=O); C5 (CO_3^{2-}); O1 (O^{2-}); O2 (-OH, C-O), and O3 (O-C=O, H_2O). All the titanium bindings correspond to TiO_2

The UV-illumination was not extended any longer than it was necessary to obtain the superhydrophilicity. Thus, the self-cleaning process on the UV-illuminated superhydrophilic LFS TiO_2 surface was not complete, which is indicated by the

relatively high total amount of carbon observed on the surface after the illumination (~ 30 %). In connection with our earlier study on photo-induced hydrophilicity on LFS TiO_2 coating (Stepien et al. 2012a), we verified that even though superhydrophilicity on the LFS TiO_2 coated board was obtained already after 30 min of UV-illumination (365 nm, 50 mW/cm^2), after which water contact angle on the surface no longer substantially decreased with the extended UV-exposure, the self-cleaning process and related decrement of carbon still continued.

3.3. Hydrophobicity Recovery in the Dark

After placing the UV-illuminated superhydrophilic LFS TiO_2 surface in the dark, its wettability started to return back to the initial superhydrophobic state. After storage of 1 month in the dark the water contact angle on the UV-illuminated LFS TiO_2 surface had increased from 7° to 146°. There is no evidence that the wettability change on TiO_2 would have been caused by the surface hydroxyl group replacement by oxygen in the dark, but the results are rather opposite: there was not any indication that the number of surface hydroxyls would have decreased (group O2: after illumination 11.2 ± 0.4 % and after subsequent storage 12.2 ± 1.7 %), instead, the number of oxide species (group O1) decreased from 37.1 % to 31.2 % during the storage in the dark (Fig. 3). In the dark the relative amount of total carbon increased from 29.6 % to 35.3 %. Correspondingly, the relative amount of total oxygen decreased from 50.0 % to 45.6 % and the relative amount of titanium decreased from 20.4 % to 18.2 %. The decrement of oxygen in relation to the decrement of titanium was characteristic for TiO_2 structure, which indicates that most of the oxygen decrement was related to masking of TiO_2 by the spontaneously accumulated carbonaceous overlayer. After the storage of 1 month in the dark, the C/Ti ratio on the surface had increased to 1.9 while it was 1.5 instantly after the UV-illumination. In conclusion, the result strongly indicates that the hydrophilicity ─ hydrophobicity conversion on the UV-illuminated LFS TiO_2 coated board occurs because organic atmospheric substances, such as hydrocarbons, spontaneously accumulate on TiO_2 during the storage in the dark.

3.4. Superhydrophilicity Conversion by Daylight Illumination

As was recently shown by Stepien et al. (2012a), the UV-induced hydrophilicity conversion on LFS TiO_2 coated board is not an on-off type switchable reaction with instant response. The self-cleaning phenomenon and related hydrophilicity conversion are time-consuming processes, where the reaction rate is dependent for example on the illumination intensity and wavelength, but also on the nature and thickness of the carbonaceous layer to be decomposed. Consequently, wettability of the LFS TiO_2 coating can be steplessly adjusted to any level between superhydrophobicity and superhydrophilicity for example by controlling the time and intensity of illumination. In this study, the superhydrophilicity conversion

before the XPS experiment was accomplished by illuminating the LFS TiO_2 surface for 30 min with light intensity of 50 mW/cm^2 and wavelength of 365 nm. With short-wave UV-irradiation of 245 nm (43 mW/cm^2) the hydrophilicity conversion on the LFS TiO_2 coated board could be accomplished already in few minutes: water contact angle of 15° was measured on initially superhydrophobic LFS TiO_2 coated board after 5 min of illumination, and the relative number of carbon atoms detected on the surface by XPS decreased from 47.6 % to 41.6 %. Alternatively, the wettability conversion can occur very slowly within several days when weak illumination is used. As shown in Fig. 4, when the illumination corresponding to natural daylight was used, the superhydrophobicity ─ superhydrophilicity conversion on the LFS TiO_2 coated board took approximately 7 days. On the board substrate without the LFS coating (reference) the surface wettability did not substantially change during the 7 days of illumination.

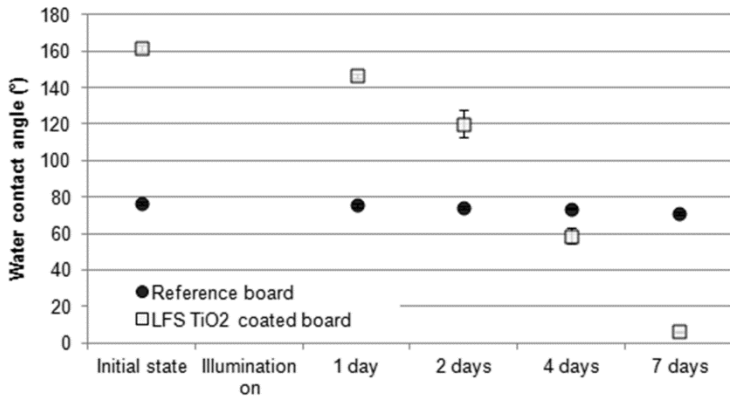

Fig. 4 Wettability conversion on the LFS TiO_2 coated board induced by artificial daylight illumination

Reactivity of the LFS TiO_2 surface was also verified under natural daylight illumination. The LFS TiO_2 coated board samples were placed outside on a sunny day (Tampere, Finland, May 23th, clear sky, 18 °C in the afternoon): one sample was placed in direct sunlight, while the other sample was placed in the shade. After 6 h of exposure (9 a.m. ─ 3 p.m.), water contact angle of 9.7 ± 1.0º was measured on the sample placed in direct sunlight. Even in the shade the contact angle on the LFS TiO_2 coated board had decreased to 94.2 ± 5.7º, which further evidences the high photocatalytic activity of the surface.

3.5. Long-Lasting Hydrophilicity and Temperature Dependent Hydrophobicity Conversion

Time scale for the hydrophilicity ─ hydrophobicity conversion on the illuminated LFS TiO_2 surface (artificial daylight, Fig. 4) stored in the dark at ambient conditions (23 °C and 50 % RH) is shown in Fig. 5a. After 1 day of storage, water contact angle on the surface had increased from 6 ± 1° to 14 ± 1°, after 1 week to 46 ± 5°, and after 2 months the contact angle was as high as 154 ± 2°. It is noteworthy that

after the illumination, the wettability recovery close to the natural level takes much longer on the nanostructured LFS TiO_2 surface than is typically reported on smooth TiO_2 surfaces (Takeda et al. 1999; Kanta et al. 2005).

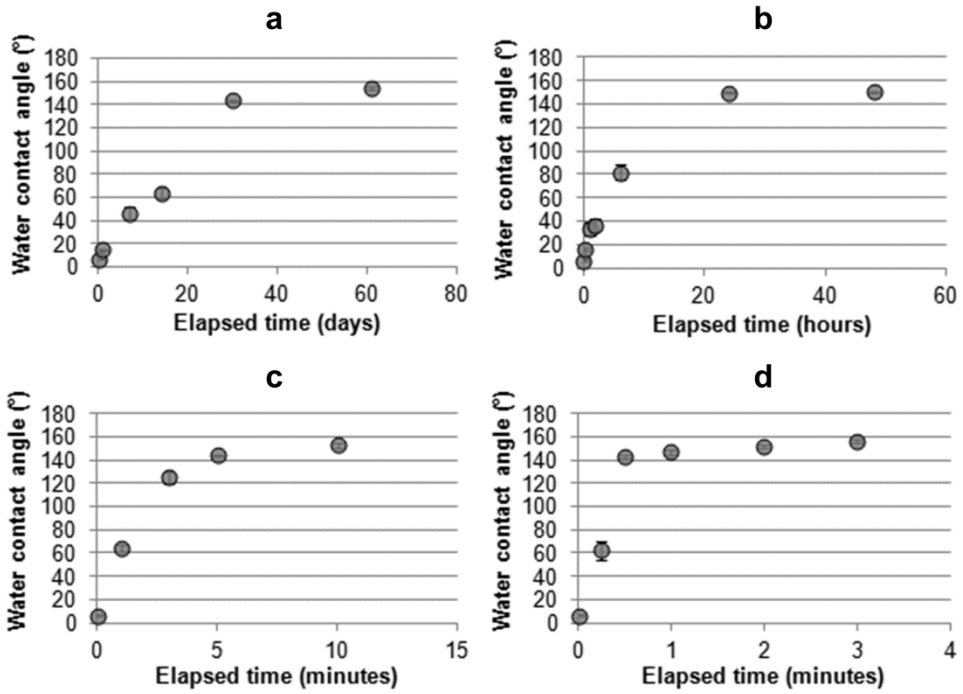

Fig. 5 Hydrophobicity recovery on artificial daylight illuminated LFS TiO_2 coated board at different conditions. In the dark room at 23 °C the hydrophobicity recovery occurs in several days (a), in the oven at 50 °C in hours (b), and at 100 °C (c) and at 150 °C (d) in minutes

In the dark, exposed to ambient conditions at the temperature of 23 °C, the hydrophobicity recovery on the illuminated LFS TiO_2 surface is relatively slow and takes several days, as was already discussed. However, recovery of the hydrophobicity can be significantly speeded up by heat treatment in the oven. As shown in Fig. 5, the recovery rate is strongly dependent on the surrounding temperature. In the oven at 50 °C the hydrophobicity recovery of the surface occurs in hours, and at higher temperatures of 100 °C and 150 °C it takes only few minutes.

3.6. Extended Hydrophilicity Conversion Time Caused by the Heat Treatment

As a natural outcome of the high-temperature LFS coating process, the freshly prepared LFS TiO_2 surface already has the spontaneously accumulated carbonaceous overlayer that fundamentally governs the surface hydrophobicity. Due to the high photoactivity of the LFS TiO_2 nanoparticles, the superhydrophobic surface can be easily converted to superhydrophilic using weak illumination corresponding to natural daylight, as was shown in Fig. 4. However, the surface resistance to hydrophilicity conversion can be increased when heat treatment in the oven is applied prior to the illumination. As shown in Table 1, after 7 days of

artificial daylight illumination most of the pre-heat treated samples (5 ─ 60 min at 150 °C) were still clearly hydrophobic. On the sample without any pre-heat treatment the water contact angle decrement during the 7 days of illumination was significant, more than 150º. In contrast, the samples which were kept in the oven (at 150 °C) for 30 and 60 min prior to the illumination suffered only minor contact angle decrement of less than 20º. The longer the heat treatment time, the slower the hydrophilicity conversion, although there is a saturation point between 15 min and 30 min, after which the extended heat treatment does no longer significantly affect the rate of the hydrophilicity conversion. Even after 16 days of illumination the samples kept in the oven for 30 min and 60 min were rather hydrophobic with water contact angles of 87 ± 4° and 91 ± 4°, respectively.

Table 1 Water Contact Angle (in deg) on LFS TiO_2 Coated Board After Heat Treatment of Varying Periods in the Oven at 150 °C and After Subsequent Illumination of 7 Days With Light Corresponding to Natural Daylight

	0 min	5 min	10 min	15 min	30 min	60 min
Before illumination	163 ± 1	162 ± 0	159 ± 2	158 ± 2	154 ± 1	152 ± 1
After illumination	6 ± 1	27 ± 1	91 ± 2	127 ± 4	138 ± 2	134 ± 2

The pre-heat treatment at 150 ºC has a significant effect on the speed of the hydrophilicity conversion on the LFS TiO_2 surface as shown in Table 1. The heat treatment also increases the amount of carbonaceous material on the surface (Stepien et al. 2012a). However, after the heat treatment of 30 min the relative amount of carbon on the LFS TiO_2 surface was still the same, 57 ─ 58 %, which was observed already after 3 min of heat treatment. Therefore, the higher amount of carbonaceous material to be decomposed on TiO_2 is not the main factor explaining the extended time required for the hydrophilicity conversion on the heat treated surfaces. Because the temperature of 150 ºC is far too low to induce any phase transformations or other changes in TiO_2 that might affect its reactivity (Li et al. 2003; Yang et al. 2005; Koparde and Cummings 2008; Naceur et al. 2012), the changes occurring on the surface due to the heat treatment seem to take place in the spontaneously accumulated carbonaceous overlayer on TiO_2. That is, during the heat treatment the carbonaceous overlayer on TiO_2 experiences chemical transformations and thus becomes more difficult to decompose photocatalytically.

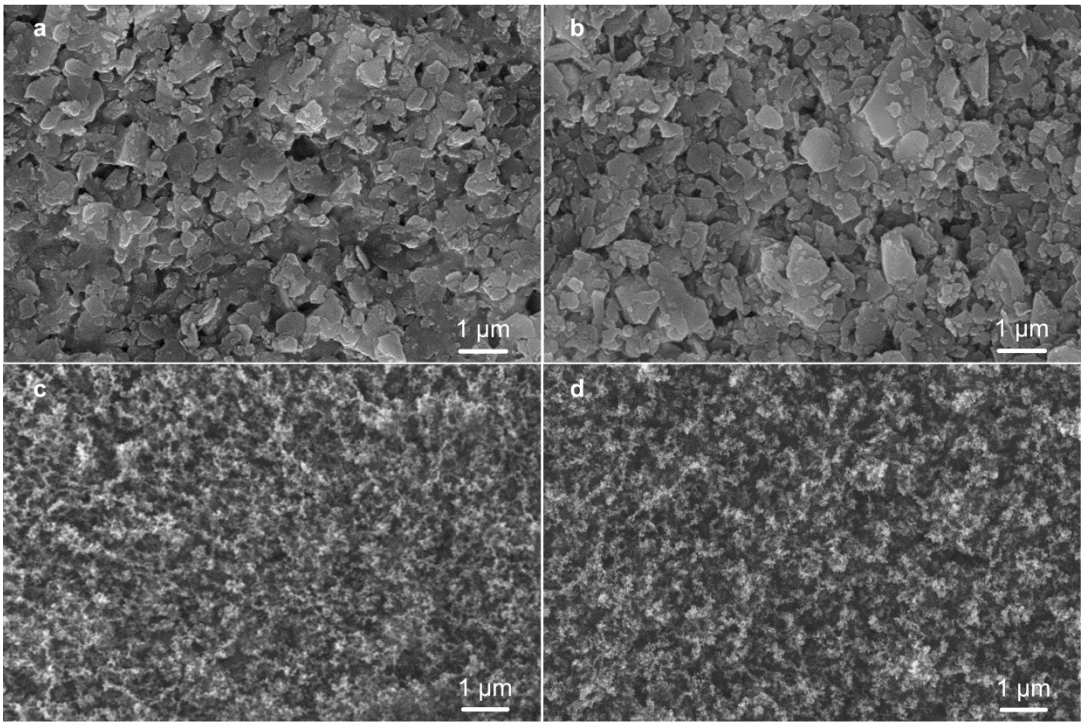

Fig. 6 FEG-SEM micrographs of board (a, b) and LFS TiO_2 nanoparticle coated board (c, d) before (a, c) and after (b, d) the heat treatment in the oven (60 min at 150 ºC)

In addition to the extended hydrophilicity conversion time, another outcome of the heat treatment is that the hydrophobicity of the LFS TiO_2 surface slightly decreases as shown in Table 1. During the heat treatment of 60 min the water contact angle on the surface decreased from 163° to 152°. We conclude that the decrement in the contact angle is mostly due to the chemical changes occurring in the carbonaceous overlayer on TiO_2 during the heat treatment. In addition, structural changes in the substrate material, which then affect the overlaying LFS TiO_2 nanoparticle coating, could be related to the contact angle decrement. For example, moisture content of the board decreases during the high-temperature heat treatment, and cellulose fibers, kaolin plates, and the binders in the pigment layer experience reorientation. Any structural changes on the pigment coated board substrate or on the LFS TiO_2 coating could not be detected from the FEG-SEM micrographs (Fig. 6), but PPS roughness measurements revealed increment in the micrometric roughness of the surfaces. The PPS roughness values measured from the pigment coated board substrate before and after the heat treatment of 60 min at 150 ºC were 2.1 µm and 2.4 µm, respectively, whereas the corresponding values for the LFS TiO_2 coated surface were 1.3 µm and 1.7 µm, respectively.

4. Discussion

As it was discussed in the introduction, the photo-induced hydrophilicity conversion on TiO_2 surfaces is a well-known and intensively studied phenomenon. However,

the mechanisms that actually cause the wettability conversion are not completely resolved even today. Our recent study (Tuominen et al. 2012) concerning superhydrophilic surfaces revealed that wettability of the corresponding LFS SiO_2 surfaces was completely different from the LFS TiO_2 surfaces. Water contact angles measured on the LFS SiO_2 coated paper and board were as low as 3.4 ± 2.3^{o} and 10.6 ± 1.4^{o}, respectively. Moreover, the LFS SiO_2 surfaces were able to maintain their superior wettability throughout a storage period of 6 months, which is not typical for TiO_2 surfaces converted to superhydrophilic by UV-illumination. The different wettability of the LFS-generated SiO_2 and TiO_2 coatings originates from the differences in their surface chemistry. For example, the studies of Takeda et al. (1999) and Kanta et al. (2005) have shown that TiO_2 is more prone to gather low-energetic organic substances onto its surface than SiO_2, when exposed to ambient conditions. Those studies also revealed that on SiO_2 and TiO_2 the level of surface contamination by carbonaceous material from atmosphere correlates well with the surface wettability. Similar tendency have been shown to occur also with the atmospheric and high-temperature LFS coating process (Stepien et al. 2012b; Teisala et al. 2012b). That is, neither of the LFS SiO_2 or TiO_2 coatings are entirely clean metal oxides. There is a certain amount of carbonaceous material on both surfaces. However, the amount of the carbonaceous material is lower on the hydrophilic LFS SiO_2 coating than on the hydrophobic LFS TiO_2 coating. Most likely, the carbonaceous layer on TiO_2 originates from variety of sources such as precursor materials, evaporating compounds from the substrate material, and atmospheric compounds. Because of the different surface chemistry between the LFS SiO_2 and TiO_2 coatings, the hierarchical roughness of the surface (Teisala et al. 2010; Teisala et al. 2012a; Teisala et al. 2012c) promotes hydrophilicity on the LFS SiO_2 coating and hydrophobicity on the LFS TiO_2 coating. After altering the surface chemistry of LFS TiO_2 coating by UV-illumination, the coating roughness changes to promote hydrophilicity. Hydrophilic patterns on superhydrophobic surface, e.g. on LFS TiO_2 coated paper and board, enable new-type of applications, where intelligent substrate guides the fluid setting and figure formation. Sirringhaus et al. (2000) demonstrated that the use of substrate surface energy patterning to direct the flow of water-based conducting polymer inkjet droplets enabled fabrication of integrated circuits with the practical channel lengths of 5 μm on glass substrate. More recently, surface energy patterning on cellulose-based substrates such as paper and fabrics has attracted considerable attention (Ballerini et al. 2012).

It is typical that after UV-illumination both the decrement of organic substances and increment of hydroxyl groups on TiO_2 are detected. Our XPS measurements show similar results (Fig. 3): the decrement of carbon and increment of oxygen in group O2 indicate removal of carbonaceous overlayer from TiO_2 and increment of surface hydroxyls, respectively. There is still some carbonaceous material left on the LFS TiO_2 surface after the UV-illumination, and thus we cannot distinguish in what extent the increment of hydroxyls occurs on the carbonaceous overlayer and in what

extent it occurs on bare TiO_2. From wettability point of view, the question is not whether there occur structural changes such as increment of hydroxyl groups on TiO_2. The question is how much these possible changes affect wettability of TiO_2 surface.

In general, the exact role of surface hydroxyl groups in the hydrophilicity conversion on TiO_2 is challenging to evaluate, but the effect of organic contaminants on the surface wetting is indisputable and can never be ignored, because at molecular level there are always some surface contaminants. It is well known that a number of organic species exist in the atmosphere (Seinfeld and Pandis 2006). Many of the atmospheric organic compounds are released from natural sources, for example from vegetation. Atmospheric chemistry includes, among others, a variety of hydrocarbons, oxygenated hydrocarbons, and alcohols. Therefore, it is obvious that perfectly clean surfaces do not exist at atmospheric conditions. In fact, Kanta et al. (2005) did show that even in vacuum chamber UV-cleaned TiO_2 surface suffered a noticeable contamination by hydrocarbons. Their ToF-SIMS study on UV-treated TiO_2 samples revealed a strong correlation between hydrocarbon contamination and surface hydroxyl groups. They concluded that the observed increment in the hydroxyl groups was due to removal of the contaminating hydrocarbon layer that masked the hydroxyls on TiO_2, and that the UV-induced wettability changes on TiO_2 are entirely related to the amount of surface contaminants: the cleaner the surface, the closer the water contact angle to the intrinsic value of 0°. The results of Kanta et al. (2005) give strong support to the earlier conclusion of Takeda et al. (1999), according which surface hydroxyl groups act as adsorptive sites for organic substances. It is well-documented, and also shown in the present study, that the photo-induced hydrophilicity on TiO_2 is not a permanent state. As soon as TiO_2 surface is removed from illumination, adsorption of organic substances from atmosphere contributes to formation of hydrophobic hydrocarbon overlayer on TiO_2. Kanta et al. (2005) observed a significant hydrocarbon contamination on UV-illuminated TiO_2 surface already after storage of 1 h at laboratory atmosphere, no matter whether the sample was kept in the dark or exposed to visible light (λ = 450 nm). Consequently, water contact angle on both samples increased from 0º to above 60º. Wang et al. (2003) stated that hydrocarbon layer responsible for the hydrophobicity of TiO_2 is regenerated upon exposure of the surface for ambient conditions for about a day. Small amount of organic contaminants on TiO_2, for example one molecule layer of hydrocarbons, is challenging to detect by XPS or other surface sensitive methods. However, the contaminant layer is the topmost layer on the surface and is therefore in direct contact with a liquid applied on the surface. Therefore, even one molecule layer of contaminants on the surface does have a drastic effect on the surface wettability. In that sense, simple contact angle measurement is the most surface sensitive experiment available.

It has been shown that after re-contamination of the UV-cleaned TiO_2 surface the amount of organic substances detected on the surface can be higher than it was initially prior to the illumination (Wang et al. 2003; Kanta et al. 2005). Wang et al. (2003) concluded that the high amount of hydrocarbon contamination on the UV pre-treated surface was due to the UV-induced structural changes on TiO_2, namely formation of oxygen vacancies and increment of hydroxyl groups, which facilitate chemisorption of organic compounds on the surface. Nowadays it is well-known that surface hydroxyls play a central role in the adsorption phenomena on TiO_2 and are favorable sites for example chemisorption of organic compounds. This information further supports the conclusion made by Takeda et al. (1999), that the number of surface hydroxyl groups determines the adsorption rate of atmospheric organic substances on different metal oxides, and thus it also determines surface wettability of the oxides. Indeed, as we concluded in our earlier study (Teisala et al. 2012b), it seems reasonable that also with the LFS surfaces the tendency of SiO_2 to be hydrophilic, and on the other hand, the tendency of TiO_2 to be hydrophobic, is fundamentally because of the different number of hydroxyls on the metal oxide surfaces.

As was shown in Fig. 5, the hydrophobicity recovery on the LFS TiO_2 surface after photo-induced hydrophilicity conversion takes several days and is thus much slower than is typically reported on TiO_2. Similar long-lasting hydrophilicity was also reported by Spagnol et al. (2009) on nanostructured TiO_2 surface. It is obvious that the storage conditions affect the recovery rate of the wettability on illuminated TiO_2, but there are also several other factors which are related to the phenomenon, for example nature of the illumination and surface topography, crystal structure, particle size, or film thickness of TiO_2 (Koparde and Cummings 2008; Spagnol et al. 2009). Therefore, direct comparison between different studies and different surfaces is difficult, but it seems plausible that after the illumination, nanostructured TiO_2 surfaces can maintain the photo-induced activity and the related self-cleaning process for a longer period than smooth TiO_2 surfaces.

In a theoretical situation where TiO_2 surface is entirely clean from organic contaminants after purification by UV-illumination, there are still hydroxyl groups on the surface which are formed as a result of dissociative adsorption of water molecules on TiO_2. In addition, more weakly bound molecular water typically exists on TiO_2. Similar to water, adsorption of organic substances can occur both molecularly (physisorption) and dissociatively (chemisorption) on TiO_2 (Tanner et al. 2002; Diebold 2003; Wang et al. 2003; Tilocca and Selloni 2004; Gong and Selloni 2005). For example, adsorption of methanol (CH_3OH), which is a common compound in the atmosphere, has been extensively studied on TiO_2 surfaces. As a result of dissociative chemisorption of methanol at hydroxylated regions on TiO_2, stable methoxy groups (OCH_3) replace surface hydroxyl groups as illustrated in Scheme 1 (Wang et al. 2003; Tilocca and Selloni 2004; Wang et al. 2004).

Computational experiments carried out by Tilocca and Selloni (2004) revealed that dissociative adsorption of methanol is favorable also at oxygen vacancies present on defective TiO_2 surface. According to Gong and Selloni (2005), dissociative adsorption energy of methanol on TiO_2(001) surface is always larger than that of water, which implies that water replacement by methanol is energetically favored. Their conclusion based on computational simulations was later on supported by experimental study on competitive adsorption between methanol and water on anatase TiO_2 nanoparticles carried out by Wang et al. (2005).

Scheme 1 Proposed Mechanisms of Decomposition and Dissociative Adsorption of Organic Compounds on TiO_2 Based on Discussion and Experimental Observations Reported in the Present Study

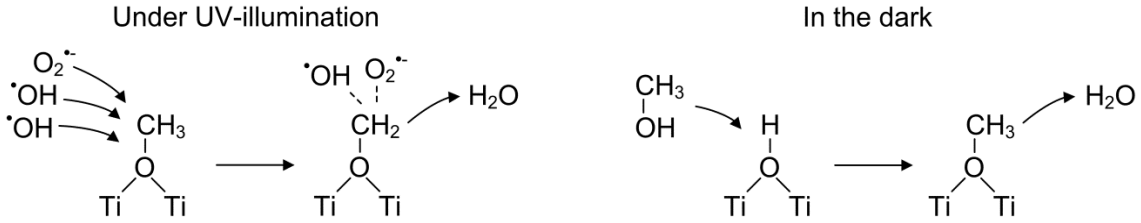

The excess increment of oxygen that we observed on the LFS TiO_2 coated board after the UV-illumination (Fig. 3) is likely related to oxidization of the topmost molecular layers of the surface during the self-cleaning process on TiO_2. That is, the additional oxygen arises from reactive compounds such as superoxides (group O1) and hydroxyl radicals (group O2) that have attached to the surface to decompose the carbonaceous overlayer on TiO_2 (Scheme 1). It is possible that the increased signal from group O2, which contains hydroxyl groups, originates partially from the UV-induced structural changes on bare TiO_2 (Wang et al. 1997). That is, dissociative water adsorption at the UV-generated oxygen vacancies contributes to increment in hydroxyl groups on TiO_2. Overall, the chemical changes observed on the LFS TiO_2 surface after the UV-illumination and after the subsequent storage in the dark (Fig. 3) well support the reactions presented in Scheme 1. The relative increment in the amount of oxygen in the top surface layer can be explained by the photodegradation process of the carbonaceous overlayer on TiO_2: (i) higher amount of oxygen originating from TiO_2 structure became detectable because of the removal of the carbonaceous overlayer, and (ii) the self-cleaning process on the surface was still unfinished, and thus there were oxygen containing species attached to the surface to decompose the carbonaceous overlayer on TiO_2. Although the total amount of oxygen in the top surface layer increased as a result of the UV-illumination, the number of carbon-to-oxygen bindings (groups C2 ─ C5) decreased. The decrement in the carbon-to-oxygen bindings can be associated with removal of chemisorbed organic species such as methyl groups (CH_3) from TiO_2. Because of the atmospheric and high-temperature nature of the LFS coating process, the carbonaceous overlayer rendering the hydrophobicity of the LFS TiO_2 coating contains most likely a variety

of carbonaceous compounds, and may contain some oxygen as well. Therefore, all the decrement in the carbon-to-oxygen bindings during the UV-illumination cannot be directly linked to removal of chemisorbed species from the LFS TiO_2 surface. During the storage period of 1 month in the dark, the UV-illuminated LFS TiO_2 coating gathered a considerable amount of low-energetic organic material on its surface, and thus the hydrophobicity of the surface was restored. Although the overall number of carbon atoms detected on the surface after the storage was not as high as it was before the UV-illumination, it is noticeable that the number of carbon-to-oxygen bindings (groups C2 ─ C5) had increased to higher level than it was before the UV-treatment. The increment in the carbon-to-oxygen bindings may be related to the possible UV-induced structural changes on TiO_2, and can be associated, among others, with dissociative chemisorption of organic substances, and thus to formation of, for example, methyl groups on TiO_2 as shown in Scheme 1.

From the results shown in the present study and in the earlier study by Stepien et al. (2012a), it is obvious that the LFS TiO_2 surface does not need to be entirely clean from low-energetic carbonaceous material to reach the superhydrophilicity. Similar observations have been made in other studies on smooth TiO_2 surfaces (Takeda et al. 1999; Kanta et al. 2005). It is well known that both chemistry and roughness affect wettability of a surface. In the case of a rough hydrophilic surface, for example the UV-illuminated LFS TiO_2 nanoparticle coating, surface roughness can promote hydrophilicity. This means that a rough surface can reach superhydrophilicity with a less hydrophilic chemistry than a smooth surface. In other words, a rough surface can withstand more contamination than a smooth surface without losing its superhydrophilicity. Moreover, in the case of a rough surface, if the carbonaceous material is concentrated for example on the bottom of the grooves, pores, or gaps, its effect on the surface wettability is likely not as significant as it is with the material located on top of the surface asperities, because the topmost areas of the surface dominate the wetting phenomenon.

In our previous study (Stepien et al. 2012a), it was confirmed that the rapid hydrophilicity − hydrophobicity conversion on LFS TiO_2 surface caused by the heat treatment in the oven is based on the spontaneous accumulation of carbonaceous overlayer on TiO_2 in a similar way to the slow-rate conversion at ambient conditions in the dark (Figs. 3 and 5). Already 3 min at 150 ºC in the oven increased the relative number of carbon atoms on the UV-illuminated LFS TiO_2 surface up to ~ 57 %, while it was only ~ 44 % on the freshly prepared surface without any treatments. In that study the wettability conversion was performed repeatedly using 30 min illumination periods and 3 min oven periods. Each time the hydrophilicity conversion was related to decrement of carbonaceous substances on the surface, while the hydrophobicity conversion was related to increment of carbonaceous substances on the surface.

The temperature dependency of the hydrophobicity recovery on the illuminated LFS TiO_2 surface (Fig. 5) and the observed increment in the carbonaceous material on the photocatalyst surface after the heat treatment indicate that the accumulation of the carbonaceous overlayer on TiO_2 is an activated process. Typically, for example dissociative chemisorption of organic compounds on catalyst surfaces is temperature dependent (Walker and King 1999; Hirsimäki et al. 2001; Egeberg et al. 2002; Nuhu et al. 2007). Increased surface temperature, or even more important, increased energy of incident molecules (translational, vibrational, and rotational energy) can easily thousandfold the initial sticking probability of a molecule to a surface, as was demonstrated by Hirsimäki et al. (2001) with methane (CH_4) adsorption on Pd(110) surface. In addition to the increased energy of incident molecules, also removal of molecular water from TiO_2 (Gong and Selloni 2005) during the heat treatment can facilitate the adsorption of organic substances and thus accelerate the hydrophobicity recovery on TiO_2. When a high-temperature heat treatment is used with the LFS TiO_2 coated board to return its hydrophobicity after the illumination, it is likely that all the carbonaceous material adsorbing on TiO_2 does not originate from atmospheric compounds, but some low-energetic substances such as latex can evaporate from the substrate and condense onto TiO_2 surface to further accelerate the hydrophobicity conversion. We will continue studies to find out to what extent the carbonaceous material on TiO_2 originates from the substrate materials, and what type of compounds it contains. The temperature dependency of the hydrophobicity recovery on TiO_2 which we report here, however, is not specific only for the LFS TiO_2 coating or is not a special feature related to the board substrate used in this study. Miyauchi et al. (2002) used strontium titanate and Borras et al. (2008) used silver as a substrate for TiO_2 coating, and in both studies the hydrophobicity recovery on the UV-illuminated TiO_2 could be drastically accelerated by heat treatment using visible light or hot plate at ~ 100 ºC. In those studies the authors did not discuss possible contamination of TiO_2 by organic compounds from atmosphere, but the observed wettability changes were explained by replacement of surface hydroxyls by oxygen.

Several studies have demonstrated the high photoactivity of TiO_2. Photo-induced phenomena on TiO_2 has been proven or suggested to include: (i) self-cleaning from organic contaminants, (ii) charge separation, and (iii) structural changes such as oxygen replacement by hydroxyl groups. Theoretically, all the above mentioned phenomena might contribute to the photo-induced hydrophilicity on TiO_2. It has been shown in this study and in many other studies, that TiO_2 is very prone to gather organic substances on its surface. When the organic substances are removed from TiO_2 by UV-illumination, the surface chemistry experiences a drastic change. Therefore, it is obvious that the removal of organic substances from TiO_2 has a major effect on the surface wettability. Moreover, the effect of photo-induced charge separation on TiO_2 (the photo-generated holes migrate to the surface and the

electrons to the bulk of TiO_2) cannot be ruled out when considering the phenomena responsible for the wettability conversion. In the case that the charge separation on TiO_2 is strong enough and has a detectable effect on the surface wettability, it might be relevant even in the presence of a thin organic overlayer on TiO_2. In such case the wettability changes on TiO_2 are related to both the amount of organic substances and the magnitude of the charge separation on the surface. As far as the effect of the possible structural changes on the wettability of TiO_2 is considered, the surface needs to remain entirely clean from organic contaminants. As soon as the organic substances adsorb on TiO_2, they will dominate the surface wettability over any structural changes occurring on the underlying TiO_2. Moreover, it has been shown that the number of hydroxyls groups or oxygen vacancies on clean TiO_2 does not detectably affect the surface wettability (White et al. 2003; Kanta et al. 2005). In the case that UV-illumination induces structural changes on TiO_2 as several studies suggest (Wang et al. 1997; Wang et al. 2003; White et al. 2003), it is plausible that their effect on surface wettability is rather indirect. That is, structural changes on TiO_2 can facilitate adsorption of organic substances on the surface, and therefore accelerate the hydrophobicity recovery after the UV-illumination. In addition to the above mentioned three mechanisms, the fourth mechanism that might play a role in the TiO_2 hydrophilicity conversion is the surface oxidization by reactive compounds which have attached to the surface to decompose the organic substances on TiO_2 (see Scheme 1).

Our study confirms that the photo-induced hydrophilicity on the LFS TiO_2 surface and the surface tendency to recover back to hydrophobic in the dark are strongly related to removal and spontaneous accumulation of carbonaceous overlayer on TiO_2, respectively. During the self-cleaning process, oxygen-containing species such as hydroxyl radicals attach to TiO_2 surface to decompose organic compounds, and therefore the overall amount of oxygen on the surface increases during illumination. The surface oxidization is a rapid phenomenon compared to the time required to complete the self-cleaning process. As we have shown, the photo-induced hydrophilicity conversion on the LFS TiO_2 surface can be a very slow process, and the time required for the conversion can be extended by modifying the chemical structure of the carbonaceous overlayer on TiO_2 by heat treatment in the oven. Therefore, in the case of the slow-rate hydrophilicity conversion on the LFS TiO_2 surface, it seems that the surface oxidization does not play a central role, but the wettability conversion is much more dependent on the removal of the carbonaceous overlayer from TiO_2. In addition, the result indicates that the photo-induced charge separation or possible structural changes on TiO_2, which are rather rapid phenomena as well, do not have any significant role in the wettability changes on the LFS TiO_2 surface, but the removal and spontaneous accumulation of carbonaceous substances on the surface dominate the wettability changes over any other mechanisms. In different case, for example when high-energy UV-illumination is used, the mechanisms of wettability conversion can be different. For

example, surface oxidization can become increasingly important, because other high-energy treatments such as corona and other plasmas (Kuusipalo 2008; Tuominen et al. 2012) can improve wettability of variety of materials by oxidizing the topmost surface layer.

In general, the wettability changes on TiO_2 cannot be explained simply by photo-induced increment in surface hydroxyl groups and their replacement by atmospheric oxygen in the dark, as some earlier studies have suggested. Even though the above mechanism has suffered a harsh criticism (Kanta et al. 2005) and several studies have reported the existence of hydrocarbon layer on TiO_2 (Takeda et al. 1999; Wang et al. 2003; White et al. 2003; Kanta et al. 2005), Spagnol et al. (2009) and Denison and Boxall (2007) stated that it is well-admitted and accepted mechanism to explain the wettability changes on TiO_2. In those studies the authors did not discuss the possibility of organic contaminants on TiO_2 and their possible effect on the wettability changes during UV-illumination and storage in the dark. The fact is that typically studies attempting to explain the photo-induced wettability changes on TiO_2 by the structural changes ignore the possibility of surface contamination, and do not show any results that reveal the changes in the amount of organic substances on TiO_2. This is a serious concern. We are not aware of any studies where TiO_2 surface would not be extremely hydrophilic if it has been convincingly proven to be free from organic contaminants. As we have discussed in this study, several different phenomena may play a role in the photo-induced hydrophilicity conversion on TiO_2. When considering the most important single factor explaining the wettability conversion on TiO_2, surface contamination by low-energetic organic substances cannot be ignored, as in many cases, including the present study, it is the most significant factor explaining the wettability changes on TiO_2.

Wettability switching techniques of LFS TiO_2 coating are not limited to illumination and heat treatment in the oven. There are several surface stimulation methods, for example flame, corona, and other plasma treatments, which are also suitable for on-line processing of materials and are commonly used in industrial-scale paper converting processes (Kuusipalo 2008; Tuominen et al. 2012). We will return to the on-line wettability switching of LFS TiO_2 coating in detail in our future contributions.

5. Conclusions

Paper and pigment coated board were coated with photo-active TiO_2 nanoparticles using the LFS on-line coating procedure. Because of the spontaneously accumulated carbonaceous overlayer on TiO_2 which ensured the suitable chemistry, and the hierarchical roughness which further enhanced the hydrophobicity of the surface, the LFS TiO_2 coating was superhydrophobic instantly after the coating procedure. There was no need to apply any subsequent hydrophobization treatment on the LFS

TiO_2 coating to obtain the superhydrophobicity. The highly photoactive LFS TiO_2 nanoparticle coating can be converted steplessly from superhydrophobic to superhydrophilic by UV-illumination, low-intensity artificial daylight illumination, and natural daylight illumination. The photo-patterned superhydrophobic LFS TiO_2 coated paper and board can be used as an intelligent substrate, where superhydrophilic patterns on the superhydrophobic surface guide fluid setting and figure formation. Thus, dye can be applied with very robust and simple methods such as rod coating.

The LFS TiO_2 coating has a natural tendency to be superhydrophobic. In the dark the coating easily maintains its superhydrophobicity. Moreover, the illuminated superhydrophilic LFS TiO_2 surface starts to recover back to its natural superhydrophobic state in the dark. The hydrophobicity recovery is a relatively slow process, which indicates that the nanostructured LFS TiO_2 coating can maintain its photo-induced activity for a long period after the illumination. The hydrophobicity recovery on the illuminated LFS TiO_2 coated board is an activated process, and thus it can be significantly speeded up by heat treatment in the oven. Several different phenomena may be involved in the photo-induced wettability changes on the LFS TiO_2 surface. However, the wettability changes are mainly caused by the removal and spontaneous accumulation of the carbonaceous overlayer on TiO_2, while the other possible mechanisms seem to play only a minor role in the phenomenon.

Acknowledgements

Tekes (Finnish Funding Agency for Technology and Innovation) is acknowledged for the financial support of this study. The work was carried out in the Functional Materials 2007−2013 programme under the project called Liquid flame spray nanocoating for flexible roll-to-roll web materials. We also want to thank Mrs. Mari Honkanen (TUT, Department of Materials Science) for the TEM and SEM images.

References

Aromaa M, Arffman A, Suhonen H, Haapanen J, Keskinen J, Honkanen M, Nikkanen J-P, Levänen E, Messing ME, Deppert K, Teisala H, Tuominen M, Kuusipalo J, Stepien M, Saarinen JJ, Toivakka M, Mäkelä JM (2012) Atmospheric synthesis of superhydrophobic TiO_2 nanoparticle deposits in a single step using liquid flame spray. J Aerosol Sci 52:57─68

Ballerini DR, Li X, Shen W (2012) Patterned paper and alternative materials as substrates for low-cost microfluidic diagnostics. Microfluid Nanofluid. doi:10.1007/s10404-012-0999-2

Balu B, Breedveld V, Hess DW (2008) Fabrication of “Roll-off” and “Sticky” Superhydrophobic Cellulose Surfaces via Plasma Processing. Langmuir 24:4785─4790

Barthlott W, Neinhuis C (1997) Purity of the sacred lotus, or escape from contamination in biological surfaces. Planta 202:1─8

Beamson G, Briggs D (1992) High Resolution XPS of Organic Polymers: The Scienta ESCA300 Database. Wiley, New York

Borras A, Barranco A, González-Elipe AR (2008) Reversible Superhydrophobic to Superhydrophilic Conversion of Ag@TiO_2 Composite Nanofiber Surfaces. Langmuir 24:8021─8026

Brinker CJ, Harrington MS (1981) Sol-gel derived antireflective coatings for silicon. Sol Energy Mater 5:159─172

Carp O, Huisman CL, Reller A (2004) Photoinduced reactivity of titanium dioxide. Prog Solid State Chem 32:33─177

Carré A, Mittal KL (2009) Superhydrophobic Surfaces. VSP/Brill, Leiden

Cassie ABD, Baxter S (1944) Wettability of porous surfaces. Trans Faraday Soc 40:546─551

Choy KL (2003) Chemical vapour deposition of coatings. Prog Mater Sci 48:57─170

Denison KR, Boxall C (2007) Photoinduced “Stick─Slip” on Superhydrophilic Semiconductor Surfaces. Langmuir 23:4358─4366

Diebold U (2003) The surface science of titanium dioxide. Surf Sci Rep 48:53─229

Egeberg RC, Ullmann S, Alstrup I, Mullins CB, Chorkendorff I (2002) Dissociation of CH_4 on Ni(111) and Ru(0001). Surf Sci 497:183─193

Fujishima A, Rao TN, Tryk DA (2000) Titanium dioxide photocatalysis. J Photochem Photobiol C 1:1─21

Fujishima A, Zhang X, Tryk DA (2008) TiO_2 photocatalysis and related surface phenomena. Surf Sci Rep 63:515─582

911 Gong X-Q, Selloni A (2005) Reactivity of Anatase TiO_2 Nanoparticles: The Role of
912 the Minority (001) Surface. J Phys Chem B 109:19560─19562
913
914 Hirsimäki M, Paavilainen S, Nieminen JA, Valden M (2001) Role of translational
915 and vibrational energy in the dissociative chemisorption of methane on Pd{110}.
916 Surf Sci 482─485:171─176
917
918 Kanta A, Sedev R, Ralston J (2005) Thermally- and Photoinduced Changes in the
919 Water Wettability of Low-Surface-Area Silica and Titania. Langmuir
920 21:2400─2407
921
922 Kemell M, Pore V, Ritala M, Leskelä M, Lindén M (2005) Atomic Layer
923 Deposition in Nanometer-Level Replication of Cellulosic Substances and
924 Preparation of Photocatalytic TiO_2/Cellulose Composites. J Am Chem Soc
925 127:14178─14179
926
927 Keskinen H, Mäkelä JM, Aromaa M, Ristimäki J, Kanerva T, Levänen E, Mäntylä
928 T, Keskinen J (2007) Effect of silver addition on the formation and deposition of
929 titania nanoparticles produced by liquid flame spray. J Nanoparticle Res 9:569─588
930
931 Kim H, Noh K, Choi C, Khamwannah J, Villwock D, Jin S (2011) Extreme
932 Superomniphobicity of Multiwalled 8 nm TiO_2 Nanotubes. Langmuir
933 27:10191─10196
934
935 Koparde VN, Cummings PT (2008) Phase Transformations during Sintering of
936 Titania Nanoparticles. ACS Nano 2:1620─1624
937
938 Kuusipalo J (Ed.) (2008) Paper and Paperboard Converting, 2nd edition. Paperi ja
939 Puu Oy, Jyväskylä
940
941 Li Y, White T, Lim SH (2003) Structure control and its influence on photoactivity
942 and phase transformation of TiO_2 nano-particles. Rev Adv Mater Sci 5:211─215
943
944 Lu Y, Ganguli R, Drewien CA, Anderson MT, Brinker CJ, Gong W, Guo Y, Soyez
945 H, Dunn B, Huang MH, Zink JI (1997) Continuous formation of supported cubic
946 and hexagonal mesoporous films by sol-gel dip-coating. Nature 389:364─368
947
948 Ma M, Hill RM (2006) Superhydrophobic surfaces. Curr Opin Colloid Interface Sci
949 11:193─202
950
951 Mäkelä JM, Aromaa M, Teisala H, Tuominen M, Stepien M, Saarinen JJ, Toivakka
952 M, Kuusipalo J (2011) Nanoparticle deposition from liquid flame spray onto moving
953 roll-to-roll paperboard material. Aerosol Sci Technol 45:827─837

Miyauchi M, Kieda N, Hishita S, Mitsuhashi T, Nakajima A, Watanabe T, Hashimoto K (2002) Reversible wettability control of TiO_2 surface by light irradiation. Surf Sci 511:401─407

Moulder J, Stickle W, Sobol P, Bomben K (1992) Handbook of X-Ray Photoelectron Spectroscopy, 2nd edition. Perkin-Elmer Corp, Eden Prairie

Mukhopadhyay SM, Joshi P, Datta S, Macdaniel J (2002) Plasma assisted surface coating of porous solids. Appl Surf Sci 201:219─226

Naceur JB, Gaidi M, Bousbih F, Mechiakh R, Chtourou R (2012) Annealing effects on microstructural and optical properties of Nanostructured-TiO_2 thin films prepared by sol─gel technique. Curr Appl Phys 12:422─428

NIST (2003) X-ray Photoelectron Spectroscopy Database, Version 3.5. National Institute of Standards and Technology, Gaithersburg. http://srdata.nist.gov/xps/

Nuhu A, Soares J, Gonzalez-Herrera M, Watts A, Hussein G, Bowker M (2007) Methanol oxidation on Au/TiO_2 catalysts. Top Catal 44:293─297

Ostrikov K (2005) Reactive plasmas as a versatile nanofabrication tool. Rev Mod Phys 77:489─511

Rao NP, Tymiak N, Blum J, Neuman A, Lee HJ, Girshick SL, McMurry PH, Heberlein J (1998) Hypersonic plasma particle deposition of nanostructured silicon and silicon carbide. J Aerosol Sci 29:707─720

Seinfeld JH, Pandis SN (2006) Atmospheric chemistry and physics, 2nd edition. Wiley, New Jersey

Sirringhaus H, Kawase T, Friend RH, Shimoda T, Inbasekaran M, Wu W, Woo EP (2000) High-Resolution Inkjet Printing of All-Polymer Transistor Circuits. Science 290:2123─2126

Spagnol V, Cachet H, Baroux B, Sutter E (2009) Influence of Sub-Band-Gap States on Light Induced Long-Lasting Super-Hydrophilic Behavior of TiO_2. J Phys Chem C 113:3793─3799

Stepien M, Saarinen JJ, Teisala H, Tuominen M, Aromaa M, Kuusipalo J, Mäkelä JM, Toivakka M (2011) Adjustable wettability of paperboard by liquid flame spray nanoparticle deposition. Appl Surf Sci 257:1911─1917

997 Stepien M, Saarinen JJ, Teisala H, Tuominen M, Aromaa M, Kuusipalo J, Mäkelä
998 JM, Toivakka M (2012a) Surface chemical analysis of photocatalytic wettability
999 conversion of TiO_2 nanoparticle coating. Surf Coat Technol 208:73─79.
1000 doi:10.1016/j.surfcoat.2012.08.008
1001
1002 Stepien M, Saarinen JJ, Teisala H, Tuominen M, Aromaa M, Kuusipalo J, Mäkelä
1003 JM, Toivakka M (2012b) Surface chemical characterization of nanoparticle coated
1004 paperboard. Appl Surf Sci 258:3119─3125
1005
1006 Ström G, Carlsson G (1993) Chemical composition of coated paper surfaces
1007 determinated by means of esca. Nordic Pulp Pap Res J 1:105─112
1008
1009 Takeda S, Fukawa M, Hayashi Y, Matsumoto K (1999) Surface OH group
1010 governing adsorption properties of metal oxide films. Thin Solid Films
1011 339:220─224
1012
1013 Tanner RE, Liang Y, Altman EI (2002) Structure and chemical reactivity of
1014 adsorbed carboxylic acids on anatase TiO_2(001). Surf Sci 506:251─271
1015
1016 Teisala H, Tuominen M, Aromaa M, Mäkelä JM, Stepien M, Saarinen JJ, Toivakka
1017 M, Kuusipalo J (2010) Development of superhydrophobic coating on paperboard
1018 surface using the liquid flame spray. Surf Coat Technol 205:436─445
1019
1020 Teisala H, Tuominen M, Kuusipalo J (2011) Adhesion mechanism of water droplets
1021 on hierarchically rough superhydrophobic rose petal surface. J Nanomater.
1022 doi:10.1155/2011/818707
1023
1024 Teisala H, Tuominen M, Aromaa M, Stepien M, Mäkelä JM, Saarinen JJ, Toivakka
1025 M, Kuusipalo J (2012a) Nanostructures Increase Water Droplet Adhesion on
1026 Hierarchically Rough Superhydrophobic Surfaces. Langmuir 28:3138─3145
1027
1028 Teisala H, Tuominen M, Aromaa M, Stepien M, Mäkelä JM, Saarinen JJ, Toivakka
1029 M, Kuusipalo J (2012b) Nanoparticle Deposition on Packaging Materials by Liquid
1030 Flame Spray ─ Generation of Superhydrophilic and Superhydrophobic Coatings.
1031 Proceedings of the Special Symposium on Recent Advances in Adhesion Science
1032 and Technology, 240th ACS National Meeting, August 22 ─ 26, 2010, Boston,
1033 Accepted
1034
1035 Teisala H, Tuominen M, Aromaa M, Stepien M, Mäkelä JM, Saarinen JJ, Toivakka
1036 M, Kuusipalo J (2012c) High- and low-adhesive superhydrophobicity on the liquid
1037 flame spray-coated board and paper: structural effects on surface wetting and
1038 transition between the low- and high-adhesive states. Colloid Polym Sci.
1039 doi:10.1007/s00396-012-2833-5

Thorvaldsson A, Edvinsson P, Glantz A, Rodriguez K, Walkenström P, Gatenholm P (2012) Superhydrophobic behaviour of plasma modified electrospun cellulose nanofiber-coated microfibers. Cellulose 19:1743─1748

Tilocca A, Selloni A (2004) Methanol Adsorption and Reactivity on Clean and Hydroxylated Anatase(101) Surfaces. J Phys Chem B 108:19314─19319

Tuominen M, Teisala H, Aromaa M, Stepien M, Mäkelä JM, Saarinen JJ, Toivakka M, Kuusipalo J (2012) Superhydrophilic Surface for Paper and Board. J Adhes Sci Technol. doi:10.1080/01694243.2012.697744

Walker AV, King DA (1999) Dynamics of the Dissociative Adsorption of Methane on Pt{110}(1×2). Phys Rev Lett 82:5156─5159

Wang C-y, Groenzin H, Shultz MJ (2003) Molecular Species on Nanoparticulate Anatase TiO_2 Film Detected by Sum Frequency Generation: Trace Hydrocarbons and Hydroxyl Groups. Langmuir 19:7330─7334

Wang C-y, Groenzin H, Shultz MJ (2004) Surface Characterization of Nanoscale TiO_2 Film by Sum Frequency Generation Using Methanol as a Molecular Probe. J Phys Chem B 108:265─272

Wang C-y, Groenzin H, Shultz MJ (2005) Comparative Study of Acetic Acid, Methanol, and Water Adsorbed on Anatase TiO_2 Probed by Sum Frequency Generation Spectroscopy. J Am Chem Soc 127:9736─9744

Wang R, Hashimoto K, Fujishima A, Chikuni M, Kojima E, Kitamura A, Shimohigoshi M, Watanabe T (1997) Light-induced amphiphilic surfaces. Nature 388:431─432

Wenzel RN (1936) Resistance of solid surfaces to wetting by water. Ind Eng Chem 28:988─994

White JM, Szanyi J, Henderson MA (2003) The Photon-Driven Hydrophilicity of Titania: A Model Study Using TiO_2(110) and Adsorbed Trimethyl Acetate. J Phys Chem B 107:9029─9033

Yang G-J, Li C-J, Wang Y-Y (2005) Phase Formation of Nano-TiO_2 Particles during Flame Spraying with Liquid Feedstock. J Therm Spray Technol 14:480─486

Zhang X, Jin M, Liu Z, Tryk DA, Nishimoto S, Murakami T, Fujishima A (2007) Superhydrophobic TiO_2 Surfaces: Preparation, Photocatalytic Wettability

Conversion, and Superhydrophobic ─ Superhydrophilic Patterning. J Phys Chem C 111:14521─14529

Tampereen teknillinen yliopisto
PL 527
33101 Tampere

Tampere University of Technology
P.O.B. 527
FI-33101 Tampere, Finland

ISBN 978-952-15-3172-9
ISSN 1459-2045